wellcome trust

UNIVERSITY OF LIVERPOOL

Rapid removal of TACC3–ch-TOG–clathrin from kinetochore fibres during mitosis

Liam Patrick Cheeseman

This thesis was submitted in accordance with the requirements of the University of Liverpool for the degree of Doctor of Philosophy

September 2013

Abstract

The mitotic spindle is required to accurately separate the two duplicated copies of the genome between the two daughter cells. Errors that occur during this process can lead to aneuploidy, a hallmark of cancer. Some microtubules of the spindle are bundled by inter-microtubule bridges to form kinetochore fibres (K-fibres), which are responsible for pulling the sister chromatids apart. Previous work has identified one type of inter-microtubule bridge, composed of three proteins: TACC3, ch-TOG and clathrin. These TACC3–ch-TOG–clathrin crosslinkers are important for accurate mitosis and were found to contribute to K-fibre stability.

However, these studies used RNAi-mediated depletion to study the functions of these proteins at metaphase. RNAi-mediated depletion is slow, and it is therefore difficult to separate the roles of the proteins at early mitosis versus metaphase. For instance, the depletion phenotype at metaphase may have been due to the absence of the protein at metaphase, or to the assembly of a defective mitotic spindle in early mitosis.

Here, knocksideways (KS) was used to deplete TACC3 in under 5 minutes from fully assembled spindle at metaphase, and trap the protein on the external membrane of mitochondria. TACC3 KS also caused the rerouting of both ch-TOG and clathrin, without affecting other spindle proteins. This depletion was supported by a concomitant reduction of inter-microtubule bridge frequency in K-fibres. When TACC3 KS was performed at early mitosis, cells displayed severe delays in aligning chromosomes. When TACC3 KS was performed at metaphase following a normal prometaphase, anaphase onset was delayed. In these cells, Mad2 on a subset of kinetochores indicated that the spindle checkpoint was active, and K-fibre tension was reduced. However, both a cold-stable K-fibre assay and electron microscopy analysis of K-fibres indicated that there was no significant loss of K-fibre microtubules, even after prolonged removal at metaphase. Furthermore, TACC3 KS at metaphase significantly altered kinetochore microdynamics and reduced spindle length.

These results indicate that TACC3–ch-TOG–clathrin crosslinkers are important for mitotic spindle assembly, but not for K-fibre stability at metaphase. However, the complex is required for K-fibre function at metaphase, satisfaction of the spindle checkpoint, most likely by maintenance of K-fibre tension.

Pre-chapter contents

Table of contents

List of figures and tables

Chapter 1 - Introduction

Chapter 2: Materials and methods

Chapter 3: Implementing the knocksideways method for spindle proteins

Acknowledgements

"When you see a claim that a common drug or vitamin 'kills cancer cells in a Petri dish', keep in mind: so does a handgun." *– xkcd*

"[Science] is like sex: sure, it may give some practical results, but that's not why we do it." *– Richard Feynman*

First and foremost, I would like to thank my supervisors Steve Royle and Ian Prior. For three years, Steve has been supportive of my work both in the lab and as part of the Institute's Postgraduate Society. He has been unrelenting in demanding only the highest quality research, and most importantly, has always been enthusiastic and available to chat about science. Ian has been a great secondary supervisor and was always helpful in offering an external point of view on my project. He was also thoroughly supportive of my independent work in the lab after Steve moved to Warwick, for which I am truly grateful. A mention to Mike Clague and Sylvie Urbé for kindly hosting me in their lab and allowing me to continue experimenting over the past 6 months.

A huge thanks to members of the Royle lab who have helped me along the way, in particular Dan 'Smooth' Booth for spending time training me at EM, and Fiona Hood for her help with pretty much every other type of experiment. Thanks to Anna, Andrew, Faye, Sam and Maria for their help and friendship in the lab, and sharing tea and cake. Thanks to Alison Beckett for sharing many coffees, EM advice and generally helping me to avoid personal injury and total destruction of the lab.

A large number of people from the department and beyond must also be acknowledged for making my time in Liverpool enjoyable, a list so long it would vastly surpass the amount of data in this thesis. To name a few, Sylvain for being a great friend for over 15 years, Dave and Gyuri for fruitful science discussions in the pub, Hannah for many hangover cures, and Lally, Ryan, Jamie, Liz, Jack, Luke, Sully and Andy for making the hangovers happen. A thank you to Helen for the great times we shared and for making my last months in Liverpool so much more special (and also for the odd tip about using Illustrator "properly"). Also, Dayani, Martin and

Kelly for helping me bring to life my crazy ideas for the ITM PG Society (especially the symposium) and bearing some of the workload. Thanks also to ‘Dangerous’ Craig Mageean and Ewan MacDonald for being good friends, excellent scientists and average beer drinkers. My apologies to all those both here and in France that I have missed out and who have supported me in their own ways.

And last but not least, a thank you to my family for their support, in particular my mum who has always been supportive, loving and proud of me despite the distance.

The work in this thesis was generously funded by the Wellcome Trust.

List of abbreviations

2D	Two-dimensional
3D	Three-dimensional
4D	Four-dimensional
γ-TURC	gamma-tubulin ring complex
Aid	Auxin-inducible degron
ALK	Anaplastic lymphoma kinase
AMP-PNP	Adenylyl imidodiphosphate
ANOVA	Analysis of variance
AP-1	Adaptor protein 1
APC/C	Anaphase promoting complex/cyclosome
Ase1	Anaphase spindle elongation protein 1
ATP	Adenosine triphosphate
BSA	Bovine serum albumin
CCAN	Constitutive centromere-associated network
CCD	Charge-coupled device
CCP	Clathrin-coated pit
CCV	Clathrin-coated vesicle
CDK	Cyclin-dependent kinase
CENP-A	Centromere protein A
CHC	Clathrin heavy chain
ch-TOG	Colonic and hepatic tumour overexpressed protein

CIP	Calf intestinal phosphatase
CMV	Cytomegalovirus
CPEB	RNA-binding cytoplasmic polyadenylation element-binding
DAPI	4',6-diamidino-2-phenylindole
ddH_2O	Double-distilled water
DMEM	Dulbecco's modified eagle medium
DMSO	Dimethyl sulfoxide
DNA	Deoxyribonucleic acid
dNTP	Deoxyribonucleotide triphosphate
EDTA	Ethylenediaminetetraacetic acid
EGTA	Ethylene glycol tetraacetic acid
EM	Electron microscopy
ER	Endoplasmic reticulum
ET	Electron tomography
FBS	Foetal bovine serum
FGFR	Fibroblast growth factor receptor
FKBP	FK506-binding protein
FRB	FKBP and rapamycin-binding protein
G1	Gap phase 1
G2	Gap phase 2
GDP	Guanosine diphosphate
(E)GFP	(Enhanced) green fluorescent protein
GGA	Golgi-localised, γ-adaptin ear-containing, ARF-binding

GTP	Guanosine triphosphate
GTSE1	G2 and S phase expressed protein 1
H2B	Histone 2B
HeLa cell	Henrietta Lacks cell
HEPES	4-(2-hydroxyethyl)-1-piperazineethanesulfonic acid
HURP	Hepatoma upregulated protein
K-fibre	Kinetochore fibre
kb	Kilobase
KDP	Knockdown-proof
KMN	KNL-1/Mis12/Ndc80 complex
kMT	Kinetochore fibre microtubule
KS	Knocksideways
LB	Lysogeny broth
LCa	Clathrin light chain A
LGN	Leucine-Glycine-Asparagine repeat-enriched protein
M phase	Mitotic phase
Mad2	Mitotic arrest-deficient 2
MAP	Microtubule-associated protein
MCAK	Mitotic centromere-associated kinesin
MIA	Multiple image alignment
mRNA	Messenger RNA
Msps	Minispindles protein
MT	Microtubule

MTOC	Microtubule organising centre
mTOR	Mammalian target of rapamycin
NA	Numerical aperture
NEB	New England Biolabs
NEBD	Nuclear envelope breakdown
NuMA	Nuclear and mitotic apparatus protein
NuSAP	Nucleolar and spindle-associated protein
PBS	Phosphate buffered saline
PCM	Pericentriolar material
PCR	Polymerase chain reaction
Plk	Polo-like kinase
PNK	Poly nucleotide kinase
PRC1	Protein regulator of cytokinesis 1
RNA	Ribonucleic acid
RNAi	RNA interference
ROI	Region of interest
rpm	Revolutions per minute
S phase	Synthesis phase
S2 cell	*Drosophila* Schneider 2 cell
SAC	Spindle assembly checkpoint
s.e.m.	Standard error of the mean
SOB	Super optimal broth
TACC3	Transforming acidic coiled-coil protein 3

TFE3	Transcription factor binding to IGHM enhancer 3
TGN	Trans-Golgi network
TPX2	Targeting protein for Xklp2
TRF2	Telomeric repeat-binding factor 2
UV	Ultraviolet
XCTK2	*Xenopus* COOH-terminal kinesin 2
XMAP215	*Xenopus* microtubule-associated protein 215
YFP	Yellow fluorescent protein

1 Chapter 1 – Introduction

1.1 The cell cycle

The cell cycle is a regulated and coordinated sequence of cellular events, which lead to the production of two daughter cells from a single mother cell. The cell cycle includes cell growth, DNA synthesis and condensation, distribution of chromosomes between daughter cells, cell division and a number of other functional modifications in the cell. It is vital that the two identical copies of the genome should be equally shared between daughter cells, as any errors that happen during this process will lead to aneuploidy, a condition where cells contain an abnormal number of chromosomes (Boveri, 1902). Aneuploidy is a hallmark of cancer (Boveri, 1914; Lengauer *et al*., 1997; Kops *et al*., 2005; Hanahan and Weinberg, 2011) and also the cause of conditions such as Down syndrome during early development (Murray, 2011).

The cell cycle of eukaryotic cells can be broadly separated into two stages: interphase and mitosis. Interphase is a much longer process compared to the relatively short stage of mitosis, usually lasting approximately 23 hours compared to just 1 hour for mitosis in cultured human cells. Interphase comprises several sub-stages: G1 (Gap-1) phase, a period of cell growth, S (Synthesis) phase, a period of duplication of the genome, and G2 (Gap-2) phase, during which the cell continues to grow and synthesise proteins (Norbury and Nurse, 1992)(**Figure 1.1**). Mitosis also comprises a number of sub-stages (see **1.2**), which are more dynamic and short.

These cellular events are regulated by a number of key proteins called the cyclins and cyclin-dependent kinases (CDKs) (Nurse, 1975; Evans *et al*., 1983). The CDKs are kinases responsible for the temporal coordination of cellular events by phosphorylating substrates, and are themselves subject to regulated degradation (Murray *et al*., 1989; Glotzer *et al*., 1991; Hershko *et al*., 1991). Cyclins D and E, along with their interactors CDKs 4/5 and 2 respectively, are responsible

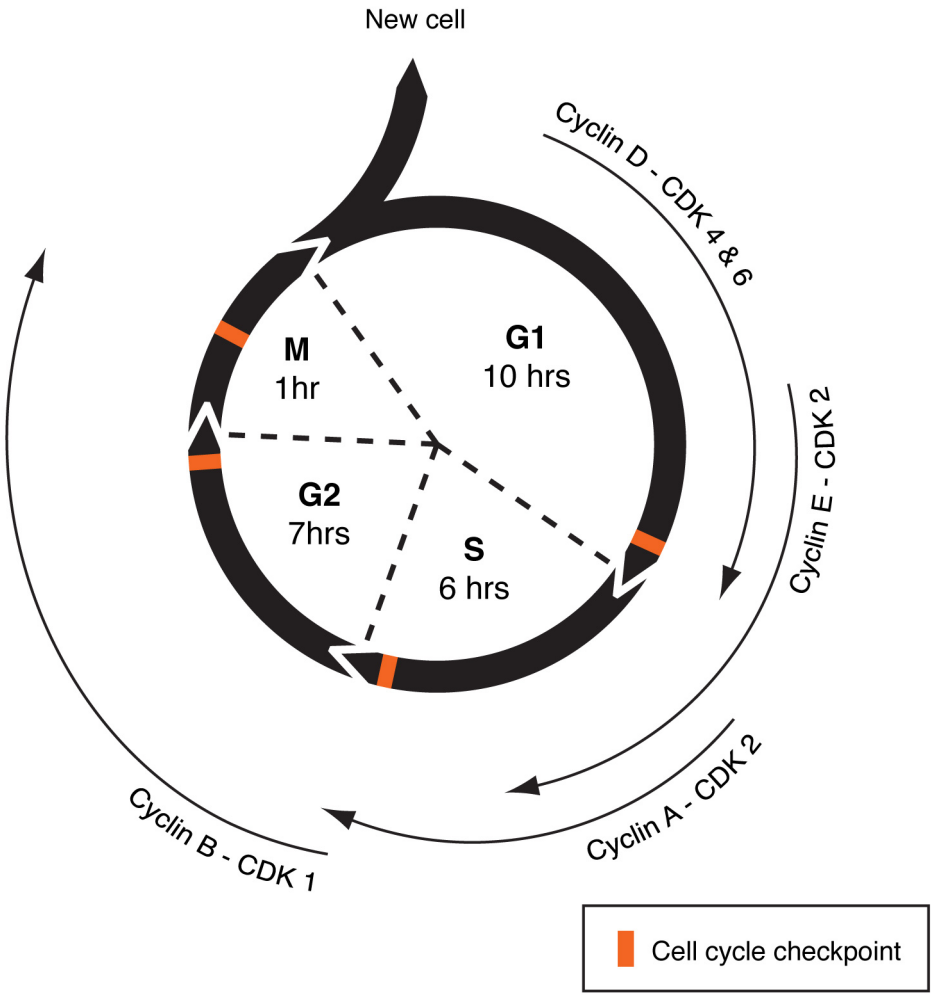

Figure 1.1: The cell cycle. Schematic diagram of the cell cycle and its phases, with their respective regulators and approximate durations. The cell cycle is under the control of proteins such as the cyclins, which are regulated by the cyclin-dependent kinases (CDKs). Progression of the cycle is regulated by their phosphorylation activity and degradation. Several checkpoints (orange) are present during the cycle, halting or allowing progression to the next stage. These checkpoints ensure the correct replication of the DNA, entry into mitosis, mitotic spindle assembly and separation of the chromosomes. Defects in checkpoint activity cause aberrant cell division and aneuploidy.

for guiding the cell through G1 phase and entry into S phase (Richardson *et al*., 1995; Sherr and Roberts, 1999). The genome must be fully and correctly duplicated in order for the cell to progress to G2 phase. This checkpoint control is regulated by the activity of cyclin A–CDK2 and causes the degradation of cyclin E–CDK2 upon the completion of DNA synthesis, thus allowing the progression of the cell cycle (Strausfeld *et al*., 1996; Hua *et al*., 1997; Hu *et al*., 2001). G2 phase and entry into mitosis are controlled by the activity of cyclin B–CDK1, which are later degraded during mitosis (Nurse, 1994; Taylor and Stark, 2001; Rieder, 2011)(**Figure 1.1**).

1.2 Stages of mitosis

1.2.1 Prophase

Prophase indicates the first stage of mitosis, at which point the cell is committed to division. At this stage, the duplicated chromosomes condense as the DNA is wrapped around nucleosomes under the control of condensin II (Kimura and Hirano, 1997). Each chromosome is formed by two identical sister chromatids, duplicated during S phase. The two centrosomes, which will form the spindle poles during mitosis, separate under the control of microtubule (MT) motor proteins, and migrate to opposite sides of the nucleus (Scholey *et al*., 2003). The centrosomes also increase their MT-nucleating abilities and dynamically unstable MTs start to polymerise outwards, creating the first buds of the mitotic spindle (Scholey *et al*., 2003)(**Figure 1.2**). Upon completion of prophase, nuclear envelope breakdown (NEBD) occurs, releasing the chromosomes into the cytosol (Scholey *et al*., 2003). Furthermore, endocytosis is shut down, the Golgi apparatus is broken down and the endoplasmic reticulum (ER) undergoes restructuring.

1.2.2 Prometaphase

Prometaphase primarily consists of the development of the mitotic spindle. MTs emanating from the centrosomes are believed to attach to the chromosomes through a 'search and capture' mechanism, where the capture of a chromosome by a MT stabilises the MT against disassembly (Kirschner and Mitchison, 1986; McIntosh *et al*., 2002)(**Figure 1.4C**). However, a separate model (named the 'self-organisation' model) suggests that MTs are nucleated in the vicinity of the chromosomes, and

become focused at the spindle poles by the action of MT motors and crosslinkers, particularly in acentrosomal cell division (McKim and Hawley, 1995; Heald *et al*., 1996)(**Figure 1.4C**). A final model indicates that both of the above mechanisms are involved in the formation of a mitotic spindle (Rusan *et al*., 2002; Khodjakov *et al*., 2003; Tulu *et al*., 2003)(**Figure 1.4C**).

The MTs bind a chromosome via the kinetochore, a large protein complex assembled on the centromere, which forms an interaction platform between the chromosome and the mitotic spindle (Cheeseman and Desai, 2008)(see **1.3.3**). The MTs reposition the chromosomes along the equator of the cell by the action of MT motor proteins (Wood *et al*., 1997; Kapoor *et al*., 2006; Cai *et al*., 2009a)(**Figure 1.2**).

At the same time, astral and interpolar fibres develop, extending from the centrosomes towards the cell cortex and the cell equator, respectively (Scholey *et al*., 2003)(**Figure 1.2)** Astral MTs form connections with the cell cortex, and these interactions have been found to play a critical role in spindle positioning and centrosome anchoring (Grill and Hyman, 2005). Interpolar fibres extend between the chromosomes and interact with interpolar MTs from the opposite pole (Mastronarde *et al*., 1993; Scholey *et al*., 2003).

Recently, two reports indicated that in both mitosis and meiosis, chromosomes formed a circular belt in early prometaphase, with the kinetochores pointing towards the spindle axis and the chromosome arms towards the cell cortex. This disposition facilitated the attachment of MTs to kinetochores, which would otherwise be shielded by the chromosome arms (Kitajima *et al*., 2011; Magidson *et al*., 2011). Prometaphase is considered to be complete once all chromosomes have become biorientated, that is to say that each of the kinetochores of a chromosome has formed a single attachment to opposite centrosomes, and have aligned along the cell equator forming the “metaphase plate” (Scholey *et al*., 2003)(**Figure 1.2)**.

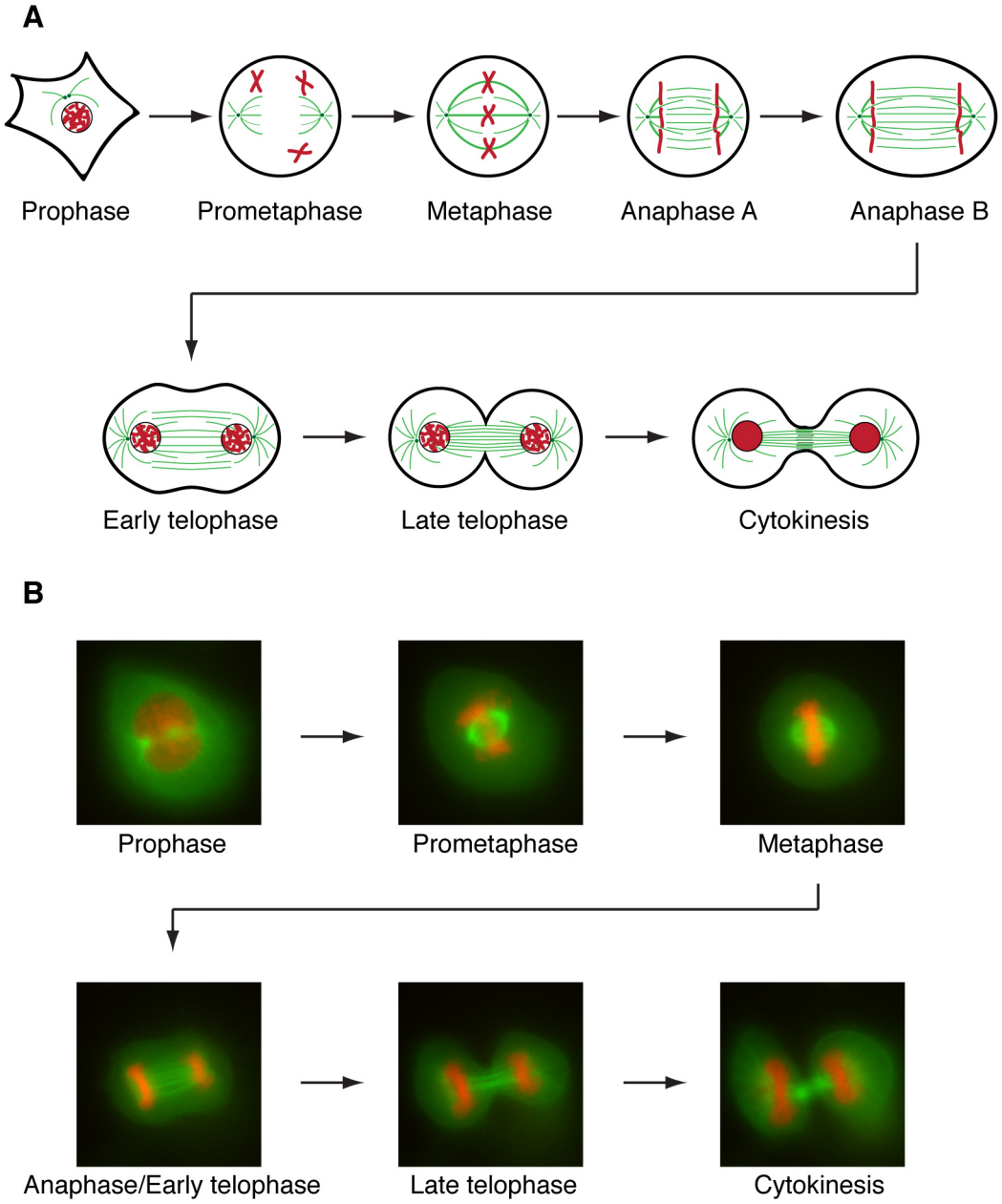
A
Prophase
Prometaphase
Metaphase
Anaphase A
Anaphase B
Early telophase
Late telophase
Cytokinesis
B
Prophase
Prometaphase
Metaphase
Anaphase/Early telophase
Late telophase
Cytokinesis

Figure 1.2: The stages of mitosis. **A.** Schematic diagram of the stages of mitosis, with microtubules in green, and DNA in red. Condensed chromosomes are released into the cytosol at NEBD (nuclear envelope breakdown; prophase-prometaphase) and aligned along the cell equator (metaphase). They are then separated by depolymerisation of the K-fibres (Anaphase A) and further separated by distancing of the centrosomes (Anaphase B), with formation of the central spindle. An ingression furrow forms and pinches the cell apart (telophase). The compressed microtubules of the central spindle become the midbody. The midbody is close to the location of abscission at cytokinesis. **B.** Video still images of a mitotic HeLa cell expressing YFP-tubulin (green) and H2B-mCherry (red) progressing through mitosis.

1.2.3 Metaphase

During metaphase, the mitotic spindle undergoes functional maturation until the satisfaction of the spindle assembly checkpoint (SAC), which prevents anaphase until all chromosomes have formed bipolar attachment, also called amphitelic attachment (Waters *et al*., 1998; Nicklas *et al*., 2001; Musacchio and Salmon, 2007).

The chromosomes are aligned along the cell equator, and each kinetochore is connected to its nearest centrosome by MTs, which will accumulate over time and form a bundle called a kinetochore fibre (K-fibre)(**Figure 1.2, Figure 1.5**). These fibres can then apply poleward tension on the kinetochores and undergo periods of lengthening and shorting, causing the sister kinetochores to oscillate along the spindle axis, and stretching of the centromeric DNA (Lampson and Cheeseman, 2011) and of the kinetochores themselves (Maresca and Salmon, 2009; Uchida *et al*., 2009). This stretching allows for the stabilisation of kinetochore-MT attachments, and satisfies the SAC (Li and Nicklas, 1995; Elowe *et al*., 2007; Lampson and Cheeseman, 2011). Checkpoint proteins such as Mad2 are consequentially released from the kinetochores and no longer inhibit the APC/C (anaphase-promoting complex/cyclosome)–Cdc20 complex. This allows the metaphase-to-anaphase transition in two ways: the degradation of cyclin B–CDK1 by the APC/C, and the release of separase, an enzyme that cleaves the sister chromatids apart, allowing their migration to opposite poles of the cell (Uhlmann *et al*., 1999).

1.2.4 Anaphase

Anaphase can be separated into two successive stages: anaphase A and anaphase B (**Figure 1.2**). Both stages involve the segregation of sister chromatids to opposite poles of the cell, but these happen in different manners.

During anaphase A, K-fibres depolymerise whilst maintaining their kinetochore-MT attachments, thus dragging the chromatids towards the spindle poles (Maddox *et al*., 2002; Scholey *et al*., 2003)(**Figure 1.2**). During anaphase B, the movement of the chromatids is not powered by shortening of K-fibres, but by the separation of the centrosomes themselves, which migrate further apart (Scholey *et al*., 2003; Brust-Mascher and Scholey, 2011)(**Figure 1.2**). This distancing is driven by MT motor proteins located at the cell equator, which slide antiparallel interpolar MTs towards

their centrosome of origin whilst the MTs elongate (Civelekoglu-Scholey and Scholey, 2010). These interpolar MTs form the central spindle.

1.2.5 Telophase

During telophase, a new nuclear membrane forms around each of the two groups of chromosomes, mainly derived from ER membrane (Larijani and Poccia, 2009)(**Figure 1.2**). In addition, the cell equator – newly vacated by the chromosomes – will start to constrict to allow for cell division, forming the cleavage plane. A cleavage furrow will start to form on the cell cortex, with the plasma membrane ingressing along the cell equator (Scholey *et al*., 2003; Lekomtsev *et al*., 2012)(**Figure 1.2**). This furrow is formed by an actomyosin contractile ring that 'pinches' the two new daughter cells apart (Scholey *et al*., 2003). This pinching of the equator causes the density of interpolar MTs to increase dramatically during this time. Their organisation is maintained and coordinated by proteins such as PRC1, which coordinate the MT bundling and sliding necessary to push the new cells apart (Zhu and Jiang, 2005; Bieling *et al*., 2010).

1.2.6 Cytokinesis

Cytokinesis, although not considered a stage of mitosis itself, is the ultimate step of cell division as it is the creation of the two separate daughter cells following mitosis. At this point, the two future cells are connected by a narrow structure of plasma membrane and dense MTs of the central spindle, which form the midbody (**Figure 1.2**). The plasma membrane continues to ingress until it presses against the central spindle. A recent paper indicated that centralspindlin, a spindle protein, is responsible for linking the plasma membrane to the mitotic spindle during this period (Lekomtsev *et al*., 2012).

The final cleavage stage, termed 'abscission', requires membrane trafficking and reorganisation in the midbody by the endosomal sorting complex required for transport III (ESCRT III) in order to take place (Carlton and Martin-Serrano, 2007). Once abscission has taken place, the two daughter cells are formed and are completely independent from each other.

1.3 The metaphase mitotic spindle

The mitotic spindle was described by Walther Flemming over 130 years ago (Flemming, 1882) and is a complex yet organised array of MTs, motor and non-motor proteins (Mandelkow and Mandelkow, 1995; Mack and Compton, 2001; Peterman and Scholey, 2009). Together, these elements are responsible for generating the forces needed to push and pull the chromosomes during mitosis.

1.3.1 Microtubules

Microtubules are polar macromolecular protein structures composed of α- and β-tubulin subunits (Borisy *et al*., 1972; Desai and Mitchison, 1997)(**Figure 1.3**). Each MT typically comprises 13 laterally assembled protofilaments of tubulin in mammals, forming cylindrical hollow tubes approximately 23 nm in diameter (Desai and Mitchison, 1997). They display highly dynamic remodelling through stochastic variations in length at the tip of individual MTs (Mitchison and Kirschner, 1984). This stochastic switching between phases of growth, pause and shrinkage is known as 'dynamic instability' (Mitchison and Kirschner, 1984). The transition from a period of growth to a period of shrinkage is known as 'catastrophe', whereas the opposite is known as 'rescue' (**Figure 1.3**).

During assembly, tubulin subunits form a sheet which then curves itself into a tubular shape as the 'seam' closes (Desai and Mitchison, 1997). However, during depolymerisation, individual tubulin protofilaments of a MT detach from each other and curve outwards, losing tubulin dimers at their tips (Desai and Mitchison, 1997)(**Figure 1.3**).

Whereas disassembly of the tubulin polymers is not an active process, their assembly is (Borisy *et al*., 1972; Desai and Mitchison, 1997). MT polymerisation requires the presence of energy in the form of guanosine-5'-triphosphate (GTP) which binds to α/β-tubulin dimers. Once GTP-tubulin binds to the tip of a MT, GTP is hydrolysed into guanosine-5'-diphosphate (GDP), and the tubulin subunit is added to the polymer via a non-covalent bond (Kobayashi, 1975; Desai and Mitchison, 1997; Kline-Smith and Walczak, 2004), (**Figure 1.3**).

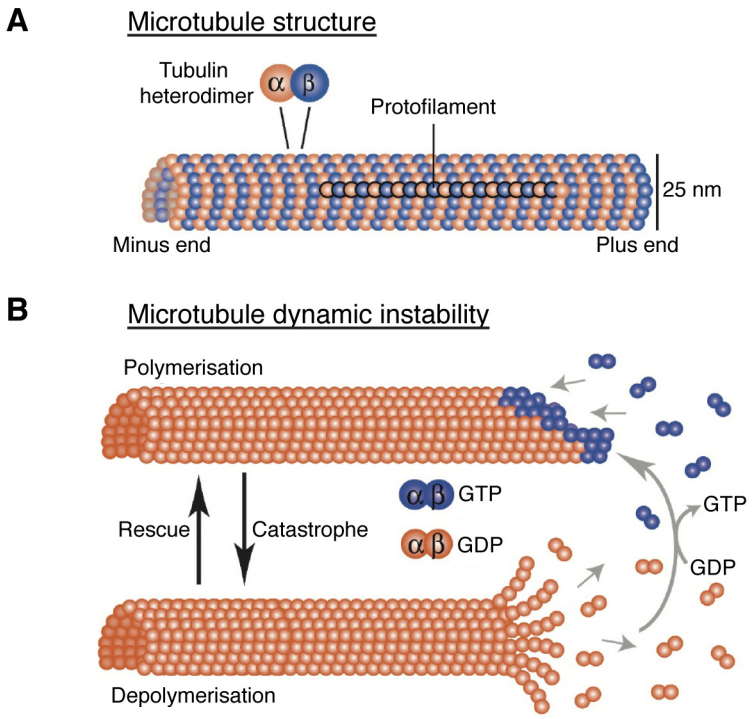

Figure 1.3: Microtubule structure and dynamics. A. Schematic diagram of the structure of microtubules. Dimers of α- and β-tubulin form 13 protofilaments bound along a seam. Microtubules possess a dynamic plus end, and a less dynamic minus end. **B.** Schematic diagram of the dynamic instability at the plus ends of microtubules. GTP-tubulin subunits are incorporated at the plus tip followed by hydrolysis of GTP into GDP, thus allowing the microtubule to grow. The transition from a period of growth to shrinkage is called a catastrophe, whereas the opposite is called a rescue. **A** and **B** are adapted from Kline-Smith and Walczak, 2004.

MTs are polar structures, and their extremities are designated as either a 'minus' end or a 'plus' end. The plus end of a MT is characterised by the presence of a 'GTP cap' (Desai and Mitchison, 1997; Schek *et al*., 2007), allowing it to undergo high rates of growth and shrinkage. On the other hand, the minus end, formed by GDP-tubulin, undergoes slower changes (Desai and Mitchison, 1997).

MTs are the binding platform for a high number of MT-associated proteins (MAPs). These MAPs have highly variable functions, and some are able to influence the dynamic instability of MTs and tilt the balance towards increased growth by promoting polymerisation or inhibiting catastrophe, or towards increased shrinkage by promoting depolymerisation or inhibiting rescue (Kinoshita *et al*., 2001).

During interphase, MTs are involved in a number of important cellular processes such as cell migration (Kaverina and Straube, 2011; Stehbens and Wittmann, 2012), intracellular trafficking (Saxton and Hollenbeck, 2012) and cell shape (Tilney and Porter, 1967). When compared to mitotic MTs, interphase MTs are fewer and much less dynamic, usually forming a near-stable cytoskeletal network. This difference is due to MAPs altering MT dynamics such as the upregulation of mitotic centromere–associated kinesin (MCAK), a strong ATP-dependent depolymerase which disassembles the interphase MTs during the G2/M transition (Holmfeldt *et al*., 2004; Kline-Smith and Walczak, 2004).

MTs form the backbone of the mitotic spindle and act as such by providing the structural engineering properties of a skeleton. In addition to linking the separate elements of the cell together (the chromosomes to the centrosomes, centrosomes to the cell cortex, etc.), they act as the vessel for the tensile forces generated during mitosis thanks to their structural integrity (Mizushimasugano *et al*., 1983; Gittes *et al*., 1993).

1.3.1.1 Astral fibres

Astral fibres strongly resemble the star-shaped asters of radial MTs that nucleate from the centrosomes during prophase. They extend from the centrosomes to the cell cortex and the equator, where they interact with the actin cytoskeleton (Scholey *et al*., 2003)(**Figure 1.4A,B**). Astral MTs are usually not bundled, and are instead single MTs (Vogel *et al*., 2007).

They serve to position the mitotic spindle within the cell by pulling the spindle poles into position via the synergistic activities of dynein, nuclear mitotic apparatus protein (NuMA) and LGN (Leucine-Glycine-Asparagine-enriched protein, also known as G-protein signal regulator 2) (Kiyomitsu and Cheeseman, 2012), and thus determine the cleavage plane. Once in place, they also serve to anchor the centrosomes in position, as pulling and pushing forces will be generated on the centrosomes by K-fibres and interpolar MTs.

1.3.1.2 Interpolar fibres

Interpolar fibres are MTs that polymerise towards the opposite pole of the spindle. However, rather than capturing and being stabilised by kinetochores, they sometimes contact interpolar MTs from the opposite pole and are crosslinked (Mastronarde *et al*., 1993)(**Figure 1.4A,B**). Interpolar MTs are thought to contribute to spindle assembly by positioning the spindle poles, and are also involved in the separation of the centrosomes during anaphase B (Civelekoglu-Scholey and Scholey, 2010).

Interpolar MTs are very diverse in length, with subpopulations terminating within the first half of the spindle, at the metaphase plate, in the second half of the spindle, or in contact with the opposite spindle pole (Mastronarde *et al*., 1993). Interpolar MTs emanating from the same centrosome will be in parallel conformation, therefore any that overlap at the metaphase plate are antiparallel (Mastronarde *et al*., 1993).

Interpolar MTs may bundle into fibres, but not to the same extent as K-fibres. Overlapping interpolar fibres usually consist of 2-6 MTs at the metaphase plate (Mastronarde *et al*., 1993). These bundles increase in number during anaphase and later form the central spindle and midbody during telophase and cytokinesis (Mastronarde *et al*., 1993).

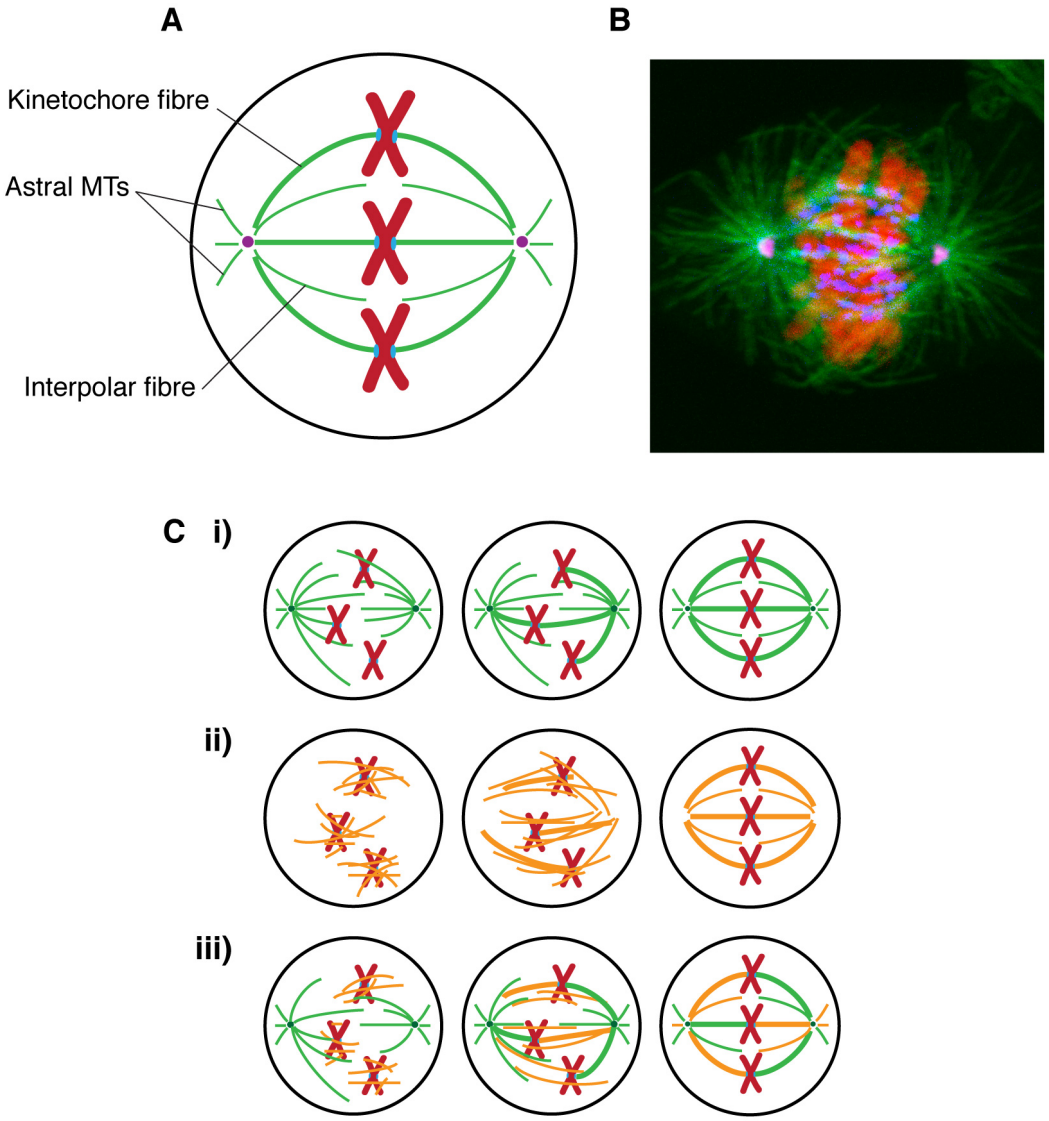
A
B
Kinetochore fibre
Astral MTs
Interpolar fibre
C i)
ii)
iii)

Figure 1.4: Formation and structure of the mammalian mitotic spindle. **A.** Schematic diagram of the mitotic spindle. The microtubules, DNA, kinetochores and centrosomes are depicted in green, red, blue and purple, respectively. **B.** Immunofluorescent micrograph of a mitotic mammalian cell. Microtubules are labelled in green, DNA in red, kinetochores in blue and centrosomes in purple. **C.** Schematic diagrams of the three different models of spindle assembly. Green depicts microtubules nucleated from centrosomes, and orange depicts microtubules nucleated from the kinetochores. Chromosomes are in red and kinetochores are in blue. **i)** The search-and-capture model. Microtubules are nucleated solely from the centrosomes and search for kinetochores in the cytoplasm before capturing them as they form an attachment. Chromosomes are then aligned on the metaphase plate. **ii)** The self-assembly model. Microtubules are solely nucleated from the kinetochores and chromosomes. This model of assembly is found in acentrosomal divisions. Microtubules are focussed at the poles by microtubule crosslinkers. **iii)** The combined model. Microtubules are nucleated from both centrosomes and kinetochores.

1.3.1.3 Kinetochore fibres

Kinetochore fibres are bundles of 20-40 MTs in mammals (**Table 1**) that extend from the centrosome and terminate at the kinetochore (**Figure 1.4A,B**, **Figure 1.5**). They are responsible for applying the forces needed to separate chromosomes during anaphase (Nicklas *et al*., 1982), and although they are not required for the congression of chromosomes to the metaphase plate, they are required for their maintenance at the equator (Cai *et al*., 2009a). K-fibres are able to both push and pull chromosomes (Mitchison and Kirschner, 1985), and are able to withstand considerably (~10,000 times) more force than is necessary to move chromosomes (Nicklas, 1983).

During prometaphase and metaphase, K-fibre MTs (kMTs) are stabilised against depolymerisation as they connect with the kinetochore, but remain dynamic nonetheless. Addition of tubulin subunits at the plus ends of kMTs at the kinetochore (**Figure 1.5A**), and removal of subunits at the minus ends near the centrosome, maintains a tubulin turnover in K-fibres despite maintaining a steady length, a phenomenon known as 'flux' (Sawin and Mitchison, 1991).

Microtubule flux may take part in SAC satisfaction by generating tension on the kinetochores (Sawin and Mitchison, 1991; Shimamoto *et al*., 2011). However, K-fibre activity also contributes to the oscillations of kinetochore during prometaphase and metaphase. This is supported by measurements of micromechanical properties of mitotic spindles assembled *in vitro*, which also approximated the force generated by flux in this system to 10–20 pN per μm per MT (Shimamoto *et al*., 2011).

During anaphase, K-fibres are able to pull sister chromatids towards the poles as they depolymerise from the plus tips. This interesting feature is still poorly understood, in particular, how are K-fibres able to maintain their connection with a kinetochore if the MTs are depolymerising (**Figure 1.5A**)? How does MT depolymerisation generate pulling force on a kinetochore? In yeast, it is believed that the Dam1

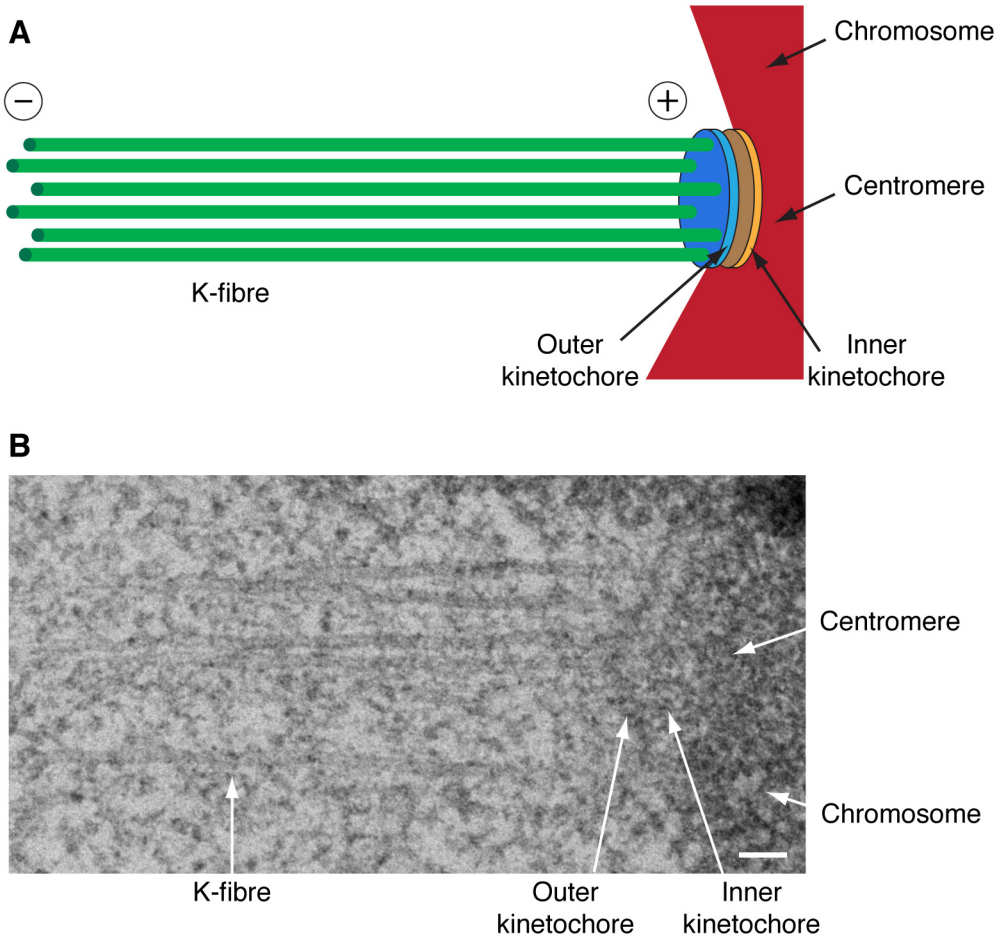

Figure 1.5: Structure of the mammalian kinetochore. A. Schematic diagram of a kinetochore and its attached K-fibre. The kinetochore is assembled on the centromere of a chromosome (red), and is formed by two plates: an outer plate (blue) and an inner plate (orange). The microtubules of a K-fibre (green) connect with the outer kinetochore by their plus ends. **B.** A representative electron micrograph of a longitudinal section of a HeLa kinetochore with attached K-fibre. The inner and outer kinetochore plates are visible, along with attached microtubules forming the K-fibre. Scale bar, 100 nm.

complex forms a closed ring around a MT, which becomes trapped when protofilaments curve outwards during MT disassembly, thus coupling kMT depolymerisation with kinetochore movement (Westermann *et al*., 2005; Westermann *et al*., 2006). However in mammals, no such complex has been found. Rather, it has been proposed that thin fibrils connect the outer kinetochore with the curved protofilaments of kMTs (McIntosh *et al*., 2008). It has been proposed that these fibrils are composed of centromere proteins (CENPs (McAinsh and Meraldi, 2011)) however, a recent study has shown that the Ska1 complex located on the kinetochore is able to bind and track depolymerising MT plus ends, suggesting that it may mediate this function (Schmidt *et al*., 2012).

Although the function of K-fibres deviates little between species, the number of kMTs that compose the fibres are variable (**Table 1**). This number is proportional to the surface area of the kinetochore rather than the size of the chromosome of each species (Nicklas *et al*., 1982; Cherry and Johnston, 1987; McEwen *et al*., 1998), which may explain the excess of tensile strength in K-fibres.

1.3.2 Centrosomes

Centrosomes form the poles of the spindle, and in mammals, act as the primary MT nucleation site for the mitotic spindle (**Figure 1.4A,B**), but also the centre of the MT network in interphase cells (Rusan and Rogers, 2009). As such, they are microtubule organising centres (MTOCs).

Two centrioles form a centrosome: a mother centriole and a daughter centriole (Duensing *et al*., 2007; Avidor-Reiss and Gopalakrishnan, 2013). The daughter centriole is synthesised from the mother during S/G2 phase under the control of proteins such as polo-like kinase 4 (Plk4) (Habedanck *et al*., 2005; Kleylein-Sohn *et al*., 2007). A centriole is a cylindrical protein polymer with a peculiar structure: it has a circular 9-fold symmetry around a cartwheel-like formation (Kitagawa *et al*., 2011). Attached to the 'spokes' of the cartwheel are 9 MT triplets; these MT are unusual compared to the rest of the cellular MT network, as they are composed of γ-tubulin (Zheng *et al*., 1995), and form the γ-tubulin ring complex (γ-TuRC). The γ-TuRC nucleates MTs formed of α- and β-tubulin and protects them against

Species/cell type	MT number/K-fibre	Reference
Saccharomyces cerevisiae	1	Peterson and Ris, 1976
Dictyostelium discoideum	1	Moens, 1976
Physarum polycephalum	1-2	Ryser, 1970
Thraustotheca clavata	1-2	Heath, 1974
Schizosaccharomyces pombe	2-4	Ding *et al*., 1993
Drosophila S2 cells	11±2	Maiato *et al*., 2006
Chinese hamster ovary cells	13	Witt *et al*., 1980
Locusta	21±4.6	Moens, 1979
Potorous tridactylis kidney cell	25.5±5.2	McDonald *et al*., 1992
HeLa	27.7±1.1	Booth *et al*., 2011
Neopodismopsis	33±9.2	Moens, 1979
Melanoplus spermatocyte	40	King and Nicklas, 2000
Haemanthus	120	Jensen and Bajer, 1973

Table 1: K-fibre MT number in different species. A comparison of kMT numbers of K-fibres in different species and cell types, varying from 1 to 120 MTs per fibre. Values are presented as mean ± standard deviation.

depolymerisation by capping their minus ends, allowing the plus ends to grow outwards. A pericentriolar material (PCM) surrounds the centrioles; the PCM is a matrix of proteins that promote MT polymerisation and focus the spindle poles (Avidor-Reiss and Gopalakrishnan, 2013).

In some species, certain types of cell division are acentriolar, such as during male meiosis in *Drosophila* (Bonaccorsi *et al*., 1998) where the chromosomes act as MTOCs (**Figure 1.4C**), or during mitosis in plant cells (Binarova *et al*., 2000). Furthermore, laser ablation experiments of centrosomes during animal mitosis can have little effect on cell division itself, suggesting redundant MTOC activities (Khodjakov *et al*., 2000; Basto *et al*., 2006; Mahoney *et al*., 2006). In support of this theory, MTs have been found to nucleate at non-centrosomal sites, even in cells containing centrosomes (Heald *et al*., 1997; Vorobjev *et al*., 1997; Yvon and Wadsworth, 1997).

1.3.3 Kinetochores

Kinetochores are complex protein structures that serve as the interaction platform between the K-fibres of the mitotic spindle and the chromosomes (**Figure 1.4A,B**). The MT-binding interface of kinetochores must fulfil 4 functions: (1) robust and dynamic kMT anchorage; (2) force generation coupled to kMT plus tip dynamics; (3) error-correction of erroneous kMT attachment; and (4) control of the SAC.

Kinetochores are assembled on specific DNA structures of the chromosomes called centromeres at mitotic entry (Gascoigne and Cheeseman, 2013), and are formed of two electron-dense plates – an inner plate and an outer plate (Lampert and Westermann, 2011)(**Figure 1.5**). MTs connect and attach to the outer plate, which is only assembled during cell division (Gascoigne and Cheeseman, 2011; Gascoigne and Cheeseman, 2013)(**Figure 1.5**). It is formed by the KMN protein network, which includes KNL1, Mis12 complex (Mis12, Nnf1, Nsl1, and Dsn1), and the Ndc80 complex (Ndc80, Nuf2, Spc24, and Spc25) (Cheeseman *et al*., 2004). The inner plate is closely associated with centromeric DNA and persists throughout the cell cycle (Perpelescu and Fukagawa, 2011), and is formed by the constitutive centromere-associated protein network (CCAN), composed of many proteins including several of the centromere proteins (CENPs) (Perpelescu and Fukagawa, 2011). The two plates

are linked by CENP-C and CENP-T (Przewloka *et al*., 2011; Screpanti *et al*., 2011; Nishino *et al*., 2013). Although many proteins have been found to form kinetochores in proteomics studies, it is thought that there are still many undiscovered (Sauer *et al*., 2005).

Kinetochores are not passive structures; they possess enzymatic activity important for the satisfaction of the SAC. In particular, they possess MT motor and depolymerising activities applied to the tips of K-fibres during metaphase and anaphase whilst maintaining a connection (Bajer, 1982; Nicklas, 1989; Schmidt *et al*., 2012). At metaphase, this causes the periodic stretching of centromeres, termed 'kinetochore breathing', distinct from kinetochore oscillations along the spindle axis (Jaqaman *et al*., 2010). Both kinetochore breathing and oscillations are thought to be signs of a functional metaphase spindle. During anaphase, this MT depolymerase activity becomes much more obvious, as the K-fibres are disassembled from their plus tips, thereby generating enough force to drag the chromosomes through the cytosol (Maddox *et al*., 2002; Scholey *et al*., 2003).

During prometaphase, incorrect MT-kinetochore attachments occur regularly (Kitajima *et al*., 2011). Several types of aberrant connections are possible: (1) monotelic, where only one out of a pair of sister kinetochores is attached to a centrosome (**Figure 1.6B**), (2) syntelic, where both sister kinetochores are attached to the same centrosome (**Figure 1.6D**), (3) and merotelic, where one kinetochore is attached to both centrosomes (Salmon *et al*., 2005)(**Figure 1.6E**). Merotelic attachments are particularly problematic as enough tension may still be generated for the SAC to be satisfied, and can lead to lagging chromosomes during anaphase and subsequent aneuploidy (Salmon *et al*., 2005).

The SAC is able to correct faulty MT-kinetochore attachments via the alteration of the phosphorylation state of various kinetochore proteins (Gorbsky and Ricketts, 1993), primarily under the control of Aurora B kinase (Cheeseman *et al*., 2002). Aurora B activity destabilises MT-kinetochore connections when little or no tension

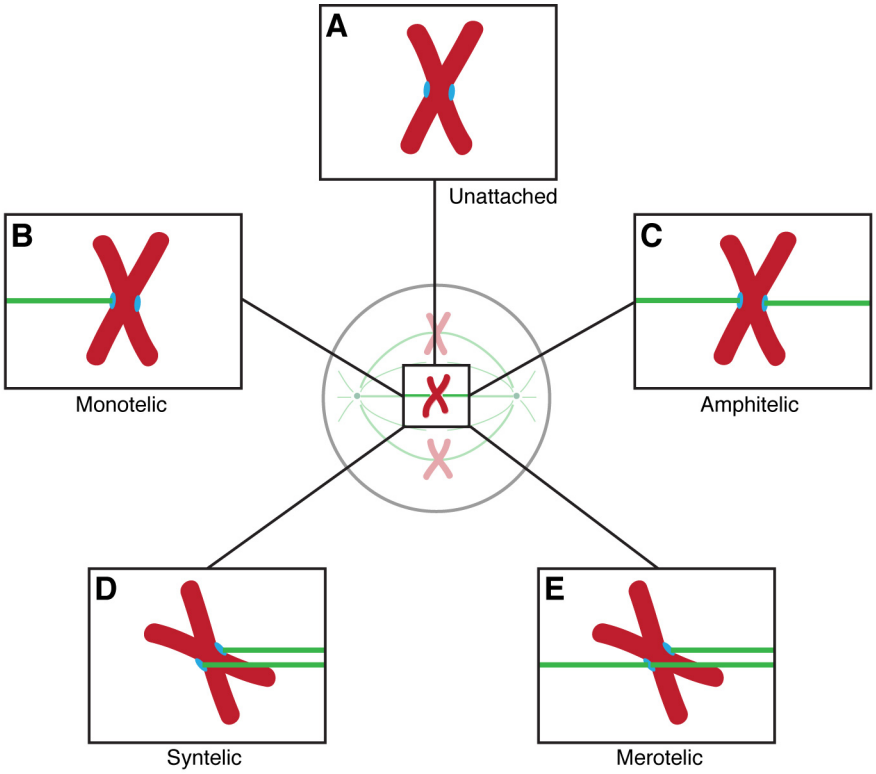

Figure 1.6: The different types of kinetochore attachments. A-E are schematic diagrams of chromosomes (red), with various types of attachments of microtubules (green) with kinetochores (blue). **A.** An unattached pair of sister kinetochores. Neither sister kinetochore is attached to a spindle pole by microtubules. **B.** A monotelic kinetochore attachment. Only one of the sister kinetochores is attached to a centrosome by microtubules. **A** and **B** are often observed during prometaphase. **C.** An amphitelic kinetochore attachment. Each sister kinetochore is attached to a centrosome via microtubules; this is the only correct type of attachment. **D.** A syntelic kinetochore attachment. Both sister kinetochores are attached to the same spindle pole, forming an aberrant attachment. **E.** A merotelic kinetochore attachment. In addition to an amphitelic attachment, one of the sister kinetochores is attached to both spindle poles.

is applied (Pinsky *et al*., 2006). When enough tension is generated, Aurora B is physically separated from its substrates (Welburn *et al*., 2010), and can no longer destabilise the MT-kinetochore attachment thus allowing recruitment of further kMTs and maturation of the K-fibre (Cheeseman *et al*., 2002; Pinsky *et al*., 2006), though it should be also noted that recent evidence suggests tension may stabilise kinetochore-MT interactions directly, independently of Aurora B (Akiyoshi *et al*., 2010). When sufficient tension is generated by the MT flux, kinetochore oscillations and kinetochore breathing to satisfy the SAC, anaphase onset can begin.

1.3.4 Microtubule crosslinkers

Many types of proteins compose the mitotic spindle, including kinases, MT dynamics modulators and structural proteins such as MT crosslinkers. Of this last type, some possess motor activity, called motor proteins, whilst non-motor proteins are devoid of it.

The first notable report focussing on MT crosslinkers, or inter-MT bridges, in the spindle apparatus was by Wilson in 1969, who studied electron micrographs of *Blastophysa* algae (Wilson, 1969). The author reported electron-dense 'bridges' between adjacent parallel MTs and between MTs and membranes. They were later further characterised in the human mitotic spindle (Hepler *et al*., 1970) and displayed very similar features. Since then, MT crosslinkers have been further reported in a number of organisms and species, including plants (Hepler *et al*., 1970; Witt *et al*., 1981; Tiwari *et al*., 1984), Chinese hamster ovary cells (Witt *et al*., 1981), crane fly (Bastmeyer and Fuge, 1986), *Cryptomonas* algae (Oakley and Heath, 1978) and have been reconstituted *in vitro* using carrot proteins (Chan *et al*., 1999). They have also been found in different cellular structures such as cilia (Warner, 1976).

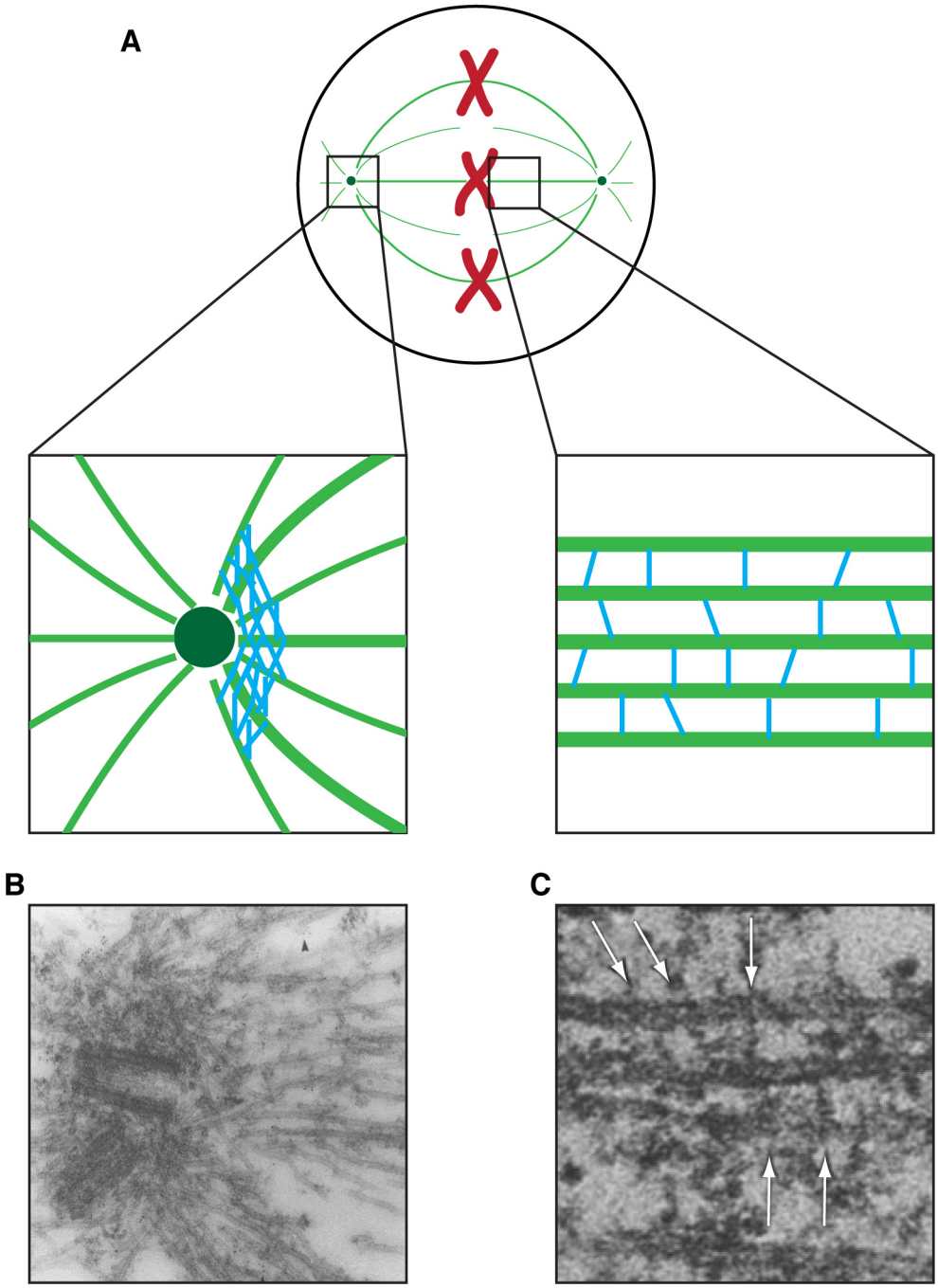
A
B
C

Figure 1.7: Microtubules crosslinkers in the mitotic spindle. **A.** Schematic diagram of microtubule crosslinkers in proximity to the centrosome (left) or on the K-fibre (right). Microtubules are in green, chromosomes in red, and crosslinkers in blue. **B.** Electron micrograph of the dense spindle pole matrix, composed of microtubule crosslinkers such as NuMA. The two centrioles of the centrosome are visible. Image adapted from Dionne *et al*., 1999. **C.** Electron micrograph of microtubules with crosslinkers indicated by arrows. Image adapted from Hepler *et al*.,1970.

Despite the diversity of species studied, inter-MT bridges possessed the same following criteria: (1) electron-dense under the electron microscope (EM), (2) linking neighbouring MTs, (3) 2-5 nm in width, (4) 20-40 nm in length (Hepler *et al*., 1970)(**Figure 1.7C**). EM currently remains the only method for visualising MT crosslinkers. It was also noted that whilst the majority of the bridges were straight and perpendicular to the MT, some were curved and at an angle between MTs. The regularity of bridges was also noticeable, as they appeared every 10, 20, 30 or 40 nm (Hepler *et al*., 1970). This periodicity suggests that crosslinkers attach at specific MT binding sites along the MT lattice.

When observed under the EM, it is impossible to distinguish motor from non-motor MT bridges. Therefore, their function(s) were hypothesised to bundle MTs and maintain their parallel conformation (Wilson, 1969), or increase structural rigidity of MT bundles by forming an elastic force providing MT-MT shear resistance (Warner, 1976) and distributing forces throughout kMTs of a fibre (Witt *et al*., 1981)(**Figure 1.7A, C**). The discovery that MAPs could affect the dynamic instability of MTs also led to considering crosslinkers as potential MT stabilisers. In the case of motor proteins, their potential involvement in MT-MT sliding to generate spindle elongation force was considered early on (Wilson, 1969), due to the prior identification and isolation of the MT motor protein dynein (Gibbons, 1963; Gibbons and Rowe, 1965). However, the identity of these inter-MT bridges remained mostly elusive until *in vitro* reconstruction studies (Chan *et al*., 1999) and the formal identification using immunogold staining *in vivo* of some subpopulations of crosslinkers (Mountain *et al*., 1999; Booth *et al*., 2011)(**Figure 1.7**).

More recently, *in silico* models for meiotic spindles required the presence of MT crosslinkers in order to recreate the MT parameters observed *in vitro* using *Xenopus* egg extract (Loughlin *et al*., 2010), suggesting their necessity *in vivo*. However, it is important to find out what functions MT crosslinkers achieve, particularly in K-fibres, and discover the identity of the different bridge populations.

1.3.4.1 Microtubule motor proteins

MT motor proteins are involved in force generation during the entire cell cycle. They attach to a cargo which varies in type from vesicles to entire organelles, and can

traffic them within the cell using the MTs as tracks (Saxton and Hollenbeck, 2012). Several MT-binding motor domains can be present on a single protein or protein complex, allowing it to crosslink parallel or antiparallel MTs and slide them relative to each other (Kapitein *et al*., 2005). This sliding is responsible for much of the forces generated in the mitotic spindle, from the resistance of the astral fibres holding the spindle poles in place (Kiyomitsu and Cheeseman, 2012), to sliding antiparallel interpolar fibres apart during prophase and anaphase B until cytokinesis (Scholey *et al*., 2003).

1.3.4.2 Non-motor microtubule crosslinkers

Non-motor MT crosslinkers are the focus of the present study. Since they have no MT sliding ability, their roles are thought to be exclusively structural with some possessing MT stabilisation activity. This potential influence on MT dynamics was shown using purified MAP2 in *Xenopus* egg extract (Gotoh *et al*., 1991). Their role in MT bundling, organisation and spacing was demonstrated in neuronal cells overexpressing the inter-MT bridges MAP2, MAP2C and tau (Chen *et al*., 1992).

More recently, it was proposed that non-motor MT bridges also act as passive resistance forces to MT sliding, helping to regulate the MT-MT movements by effectively acting as a brake (Janson *et al*., 2007; Braun *et al*., 2011). This was demonstrated using *Schizosaccharomyces pombe* anaphase spindle elongation protein 1 (Ase1), a protein that crosslinks antiparallel MTs at the central spindle during anaphase to cytokinesis. It is the homolog of human protein regulator of cytokinesis 1 (PRC1), one of the major MT bundling proteins necessary for cytokinesis (Kurasawa *et al*., 2004).

1.3.4.3 Identified microtubule crosslinkers and candidates

Since the first characterisation of MT crosslinkers, many have been identified or have strong evidence towards their identification. Some, such as the kinesin Eg5, a homo-tetrameric, plus end-directed MT motor protein, have been extensively studied (Sawin *et al*., 1992; Miyamoto *et al*., 2004; Kapitein *et al*., 2005), while others are only thought to be crosslinkers but with evidence from only a few reports (eg. NuSAP (Raemaekers *et al*., 2003; Ribbeck *et al*., 2006; Ribbeck *et al*., 2007)).

However, the present study focuses on a non-motor crosslinker, so only this type of inter-MT bridge will be discussed.

PRC1 is arguably the most well characterised bridge of the mitotic spindle. It is an inactive monomer during the early stages of mitosis, and becomes an active dimer at anaphase onset (Jiang *et al*., 1998). The overlapping antiparallel MTs that form the spindle midzone at anaphase (Mastronarde *et al*., 1993) become increasingly dense as they start to form the spindle midbody. To do so, the MTs require the correct localisation and abundance of PRC1 (Mollinari *et al*., 2002) and its binding partner Kif4 (Kurasawa *et al*., 2004), which bundle the MTs into a tightly packed group. The activity of these two proteins is necessary for the correct localisation of a number of other proteins critical to the integrity of the midbody such as Aurora B kinase and CENP-E (Kurasawa *et al*., 2004). The existence of PRC1 bridges was further demonstrated by *in vitro* reconstitution and MT bundling (Mollinari *et al*., 2002; Subramanian *et al*., 2010).

NuMA is another well characterised MT bridge localised around the centrosomes (Lydersen and Pettijohn, 1980). It forms an insoluble matrix around the centrioles which both anchors MT to the centrosomes and focuses their minus ends (Dionne *et al*., 1999)(**Figure 1.7A, B**), with one report indicating that it also possessed MT nucleating abilities (Tousson *et al*., 1991). NuMA is a protein important for both the assembly and the maintenance of the mitotic spindle (Silk *et al*., 2009). Furthermore, its depletion induces loss of centrosome integrity (Gaglio *et al*., 1995; Merdes *et al*., 1996). More recently, NuMA has been found to play a key role in spindle positioning along with LGN and dynein (Kiyomitsu and Cheeseman, 2012).

Another crosslinker in the mitotic spindle is the human kinesin 14 HSET. It possesses minus end-directed motor activity which opposes the activity of Eg5 (Mountain *et al*., 1999), thereby contributing to the regulation of spindle length and morphology (Cai *et al*., 2009b). It is a protein essential for the formation of acentrosomal spindles *in vitro* (Mountain *et al*., 1999), and appears to be involved in centrosome clustering in cell with supernumerary centrosomes (Kwon *et al*., 2008). In *Xenopus*, the HSET-related protein *Xenopus* COOH-terminal kinesin 2 (XCTK2) promotes spindle assembly and bipolarity (Walczak *et al*., 1997), whereas the *Drosophila* homolog Ncd contributes to clustering centrosomes and focusing the

spindle poles (Endow *et al*., 1994; Goshima *et al*., 2005a). HSET is one of the few inter-MT bridges to have been revealed by immunogold labelling and EM, with gold particles mainly found in between MTs of the metaphase spindle (Mountain *et al*., 1999).

The nucleolar and spindle-associated protein (NuSAP) is a further MT crosslinker candidate, due to its ability to bundle MTs when overexpressed in mammalian interphase cells and when added in supraphysiological level in *Xenopus* egg extract (Raemaekers *et al*., 2003; Ribbeck *et al*., 2006). Its presence in *in vitro*-assembled spindles also increased the stability of MTs (Ribbeck *et al*., 2006). In mitotic mammalian cells, NuSAP is found predominantly at the central spindle and in chromatin-proximal MTs, and can bind chromatin when all MTs are depolymerised by the spindle poison nocodazole (Raemaekers *et al*., 2003). It was further demonstrated that NuSAP could promote the polymerisation and stabilisation of MTs from chromatin *in vitro* (Ribbeck *et al*., 2007), suggesting that it may be a key player in spindle self-organisation.

Hepatoma upregulated protein (HURP) is another MAP capable of bundling MTs when present in over-abundance *in vitro* (Sillje *et al*., 2006). Its unusual localisation – on K-fibres near the chromosomes – is due to a RanGTP gradient increasing toward the chromatin and suggests that it plays important roles in K-fibre stability and function (Sillje *et al*., 2006). Indeed, its depletion in cells destabilises K-fibres, reduced inter-kinetochore tension and delays metaphase (Sillje *et al*., 2006; Wong and Fang, 2006). HURP is thought to stabilise MTs by virtue of its ability to promote MT dynamics and polymerisation by regulating its partner protein Kif18A (Wong and Fang, 2006; Ye *et al*., 2011). It further possesses important roles in spindle formation, both by acting as a MTOC in acentrosomal cell division and clustering supernumerary centrosomes (Breuer *et al*., 2010). Furthermore, HURP has been found to interact with XMAP215, TPX2 and Eg5 to promote bipolar spindle assembly *in vitro* (Koffa *et al*., 2006). Intriguingly, it was also shown to wrap an extra sheet of tubulin around MT tips *in vitro* under EM, however it is not known whether this occurs or has any functional significance *in vivo* (Santarella *et al*., 2007). It should be noted that despite the use of immunogold labelling of HURP in this last study, no MT crosslinkers were observable in the micrographs. On top of its role in metaphase K-fibres, HURP is also found on the central spindle interacting

with Eg5, where it stabilises interpolar MTs (Breuer *et al*., 2010) and promotes *de novo* MT polymerisation of interzonal MTs (Uehara and Goshima, 2010).

1.3.5 Forces in the mitotic spindle

The forces exerted in the mitotic spindle are still poorly understood. To date, few studies and reviews have explored and depicted a comprehensive view of the forces exerted within the metaphase spindle. Pioneering work by Bruce Nicklas using spindle micromanipulation determined the pulling force generated by the mitotic spindle of *Melanoplus* (Nicklas, 1983). Since then, technological advances have allowed to perturb the spindle system in more subtle, specific and controlled manners.

Although the mitotic spindle is a highly dynamic system, it maintains a steady shape and size via a precise balance of forces. As mentioned previously, these forces can originate from MT flux, MT sliding by motor proteins, passive MT crosslinking resistance, centromeric stretching and sister chromatid cohesion, and MT depolymerisation-coupled movement. One notable study which investigated the relative contribution of these factors at metaphase was performed in *Drosophila* Schneider 2 (S2) cells using molecular perturbation of specific spindle proteins (Goshima *et al*., 2005). The authors found that whilst spindle length was particularly sensitive to MAPs affecting MT polymerisation dynamics, the spindles were relatively insensitive to the depletion or overexpression of MT motors. This suggests that whilst motors play a role in spindle function and assembly, they do not play an extensive role in the balance of forces within the structure. Interestingly, another study has since shown that HSET overexpression alone caused elongated spindles in HeLa cells, and its depletion caused shorter spindles (Cai *et al*., 2009b). This discrepancy may be explained by the different cell species used in these two studies, in which case we may ask the question: why are these two spindle systems different? And why is the force balance more sensitive to motor protein activity in one cell compared to the other?

Another important study in the field was performed by Dumont and Mitchison (Dumont and Mitchison, 2009a). They applied controlled compression onto mammalian cells at metaphase and imaged the subsequent spindle morphological

changes by microscopy. They found that spindles became both wider and longer when force was applied; whilst these effects were reversible, the lengthening required MT polymerisation (Dumont and Mitchison, 2009a). They also found that K-fibres were under poleward force applied along the fibre, which they believe to be generated by interpolar MT polymerisation. Furthermore, the spindle lengthening took place without affecting the dynamics of kinetochore movement or inter-kinetochore tension, indicating the mechanical switch in response to spindle elongation takes place at the centrosomes. Overall, their study brought significant new insight into the forces generated within the mitotic spindle, and allowed to update the model of spindle forces (Dumont and Mitchison, 2009b).

A final important study on this topic was performed by Shimamoto and colleagues (Shimamoto *et al*., 2011). Using calibrated microneedles, similar to those used by Nicklas, they measured the viscosity, elasticity and resistance of mitotic spindles assembled in *Xenopus* egg extract. A particularly relevant experiment was their assessment of the contribution of MT crosslinkers to the physical properties of the mitotic spindle by adding adenylyl imidodiphosphate (AMP-PNP), a slow-hydrolysing ATP analogue which locks kinesins in a MT-bound state. Although the elasticity and resistance were apparently unaltered, the viscosity of the spindles was almost fully reduced, indicating that dynamic MT crosslinking contributed to this physical parameter. Another important finding was that kMTs and non-kMTs contribute to two temporally distinct parameters of the spindle's elastic response to deformation from the microneedles: whereas the more dynamic non-kMTs are responsible for the fast elastic response, the more stable kMTs are responsible for a slower elastic deformation over longer periods of time to stop the spindle collapsing and maintain its overall organisation. Finally, they found that forces exerted along the spindle width (or short axis) resulted in stronger alteration of spindle width and length that those exerted along its length (or long axis). This suggests that the response to forces applied along the length of the spindle are predominantly viscous, whereas those applied along the width of the spindle are predominantly elastic. This study provided both important insight into the contribution of MT crosslinkers in the mitotic spindle, and also the types of physical perturbations that can alter spindle morphology.

1.4 The TACC3–ch-TOG–clathrin inter-microtubule bridge

1.4.1 TACC3

The transforming acidic coiled-coil (TACC) protein family was first shown to have an important role during mitosis in *Drosophila* (D-TACC (Gergely *et al*., 2000b)). D-TACC was shown to bind MTs, and its inactivation by antibody microinjection caused shorter MTs emanating from the centrosomes and the chromosomes to fail to segregate correctly (Gergely *et al*., 2000a). In mammals, three TACC proteins exist (TACC1, TACC2 and TACC3 (Gergely *et al*., 2000a; Gergely *et al*., 2000b)), and although all three localise to centrosomes in a cell cycle-dependent manner, TACC3 was found to behave most similarly to D-TACC in human cells (Lee *et al*., 2001). Indeed, both D-TACC and TACC3 interact with Msps and ch-TOG (homologues of each other), respectively, at the poles (Lee *et al*., 2001). In *Xenopus*, Maskin is the TACC3 homologue and also interacts with the ch-TOG homologue XMAP215 (O'Brien *et al*., 2005). Homologues of TACC3 and ch-TOG are also found interacting together in other species such as *C. elegans* (TAC-1 and ZYG-9; Srayko *et al*., 2003) and fission yeast (Alp7 and Alp14; Sato *et al*., 2004, Kakui *et al*., 2013). In both cases, the TACC3 and ch-TOG homologues were found to have important roles in microtubule modulation and cell division. Together, these studies suggest that TACC3 is a strongly conserved protein with conserved protein interactions.

The functions of TACC3 are somewhat more contentious. TACC3 requires phosphorylation by Aurora A kinase in order to promote MT nucleation and polymerisation (Kinoshita *et al*., 2005), in particular on serine 558 (Kinoshita *et al*., 2005; Leroy *et al*., 2007).

It is apparent from a number of studies in various species that TACC3, possibly via its interaction with ch-TOG, a known modulator of MT dynamics (Tournebize *et al*., 2000; Popov *et al*., 2001; Popov *et al*., 2002), influences both MT and spindle assembly (Gergely *et al*., 2000a; Gergely *et al*., 2003; Kinoshita *et al*., 2005; O'Brien *et al*., 2005; Peset *et al*., 2005; Lin *et al*., 2010). However, one study suggests that Maskin does not influence MT dynamics and is instead required for MT anchoring at

the centrosome (Albee and Wiese, 2008). It is possible that this difference is due to the ability of Maskin to bind MTs directly, a property not observed in other TACC3 homologues (O'Brien *et al*., 2005; Peset *et al*., 2005). Furthermore, there have been no studies demonstrating that human TACC3 directly influences MT dynamics. In order to function and localise to the mitotic spindle, TACC3 requires phosphorylation by Aurora A kinase (Kinoshita *et al*., 2005), in particular on a conserved residue corresponding to serine 558 in humans (Kinoshita *et al*., 2005; Leroy *et al*., 2007).

In addition to its role in mitotic spindle assembly, TACC3 has also been found to have a role in mRNA translation. Maskin suppresses the translation of cyclin B1 mRNA locally in oocytes by interacting with the RNA-binding protein cytoplasmic polyadenylation element binding protein (CPEB) and the cap binding initiation factor eIF-4E (De Moor and Richter, 1999; Stebbins-Boaz *et al*., 1999; Cao and Richter, 2002). A similar function has been found in the early embryonic development of *Xenopus* (Groisman *et al*., 2000; Groisman *et al*., 2002). However the eIF-4E binding domain is absent from mammalian TACC3, suggesting this function was not evolutionarily conserved (De Moor *et al*., 2005). In mammalian cells during interphase, TACC3 is found diffuse within the cell, with a higher concentration in the nucleus (Gergely *et al*., 2000a; Aitola *et al*., 2003). This localisation was consistent with a second 'moonlighting' function for TACC3 during interphase, when it is responsible for activating the transcription of genes via an interaction with histone acetyltransferases (Sadek *et al*., 2000; Gangisetty *et al*., 2004; Angrisano *et al*., 2006), a role thought to be important during early development (Sadek *et al*., 2000; Sadek *et al*., 2003).

1.4.2 ch-TOG

Homologues of human ch-TOG, such as *Xenopus* XMAP215 and *Drosophila* Msps, have long been known to have essential roles in MT polymerisation (Gard and Kirschner, 1987). Their roles are mediated by the evolutionarily conserved TOG domains (Gard *et al*., 2004), which can bind tubulin dimers and add them to the growing MT tip (Al-Bassam *et al*., 2006; Al-Bassam *et al*., 2007; Slep and Vale, 2007; Brouhard *et al*., 2008; Widlund *et al*., 2011). Studies *in vivo* have shown that their depletion causes short MTs during interphase with reduced polymerisation rates

and increased frequency of catastrophe (Tournebize *et al*., 2000; Brittle and Ohkura, 2005; Kawamura and Wasteneys, 2008), as well as severely disorganised mitotic spindles (Cullen *et al*., 1999; Gergely *et al*., 2003; Cassimeris and Morabito, 2004). There is no strong data to suggest that human ch-TOG also possesses the potent MT polymerase activity of its homologue in *Xenopus*.

ch-TOG also possesses crucial roles in mitotic spindle assembly and organisation, which are linked to its association with TACC3. Its depletion causes highly disorganised spindles with fragmented poles (Gergely *et al*., 2003; Cassimeris and Morabito, 2004). In human cells, ch-TOG localises to the spindle and centrosomes (Gergely *et al*., 2003). There is some evidence to suggest that these are two functionally separate populations of ch-TOG because TACC3 depletion removes ch-TOG from the spindle but not from the centrosomes (Gergely *et al*., 2003; Cassimeris *et al*., 2009; Booth *et al*., 2011; Cheeseman *et al*., 2013). The association of ch-TOG homologues with TACC3 homologues under the influence of Aurora A kinase phosphorylation is highly conserved and occurs with a 1:1 stoichiometry (Barros *et al*., 2005; Kinoshita *et al*., 2005; Peset *et al*., 2005).

It has also been reported that the fission yeast ch-TOG homologue Alp14 along with TACC3 homologue Alp7 are found at the kinetochore and help the capture of kinetochores by MTs of the mitotic spindle (Garcia *et al*., 2001; Hsu and Toda, 2011; Kakui *et al*., 2013), whereas the other fission yeast ch-TOG homologue Dis1 was shown to interact with the Dam1 complex to pull chromosomes poleward (Kakui *et al*., 2013), however there has been no such reports in mammalian cells.

1.4.3 Clathrin

1.4.3.1 Clathrin in membrane trafficking

Clathrin is a protein that has been extensively studied because of its role in endocytosis and membrane trafficking. It has an unusual triskelion shape, formed by 3 light chains and 3 heavy chains (**Figure 1.8A**; (Kirchhausen and Harrison, 1981)). It also possesses a relatively high level of structural flexibility (**Figure 1.8C**), which allows it to assemble into a polyhedral lattice acting as a scaffold around a budding vesicle, called a clathrin-coated vesicle (CCV; **Figure 1.8B, D**). A triskelion of

clathrin is often described as possessing 3 'legs', with the N-terminal domain of clathrin heavy chain (CHC) located at the distal extremity of each leg (Fotin *et al*., 2004). Each leg is around 2 nm wide, and 52 nm in length, as determined by atomic force microscopy (Jin and Nossal, 2000), which corresponds well with the dimensions of an inter-MT bridge.

Clathrin-coated vesicles emerge from clathrin-coated pits (CCPs), which can form on various cellular subcompartments such as the trans-Golgi network (TGN), endosomes and the plasma membrane (Mukherjee *et al*., 1997; Mousavi *et al*., 2004). It can bind membranes via adaptor proteins such as the AP2 and AP1 complexes at the plasma membrane and TGN, respectively (Keen, 1990; Pearse and Robinson, 1990).

The most studied function of clathrin is its role in clathrin-mediated endocytosis at the plasma membrane, a process by which many nutrients and hormones are internalised by the cell (Goldstein *et al*., 1985). The steps of endocytosis are represented in the schematic in **Figure 1.8E**. Adaptor proteins are recruited to the plasma membrane where cargo have bound their membrane receptors, and recruit clathrin triskelia into a polyhedral lattice coat. The coated plasma membrane starts to invaginate, forming a CCP, until a vesicle is pinched off from the membrane by dynamin (Robinson, 1994), forming a CCV. The CCV migrates internally towards endosomes and becomes uncoated; the resulting clathrin and adaptor proteins are then free to be recycled to the plasma membrane and participate in the formation of new CCVs. The uncoated vesicle then fuses with an endosome, and is subsequently processed by the endocytic pathway (**Figure 1.8E**).

Clathrin is similarly involved in trafficking from the TGN to late endosomes and lysosomes (Wu *et al*., 2003). In this case, AP1 is the adaptor protein that recruits the triskelia to mannose-6-phosphate receptors at the membrane, mediated by Golgi-localised, γ-adaptin ear-containing, ARF-binding proteins (GGA) (Dell'angelica *et al*., 2000; Hirst *et al*., 2000).

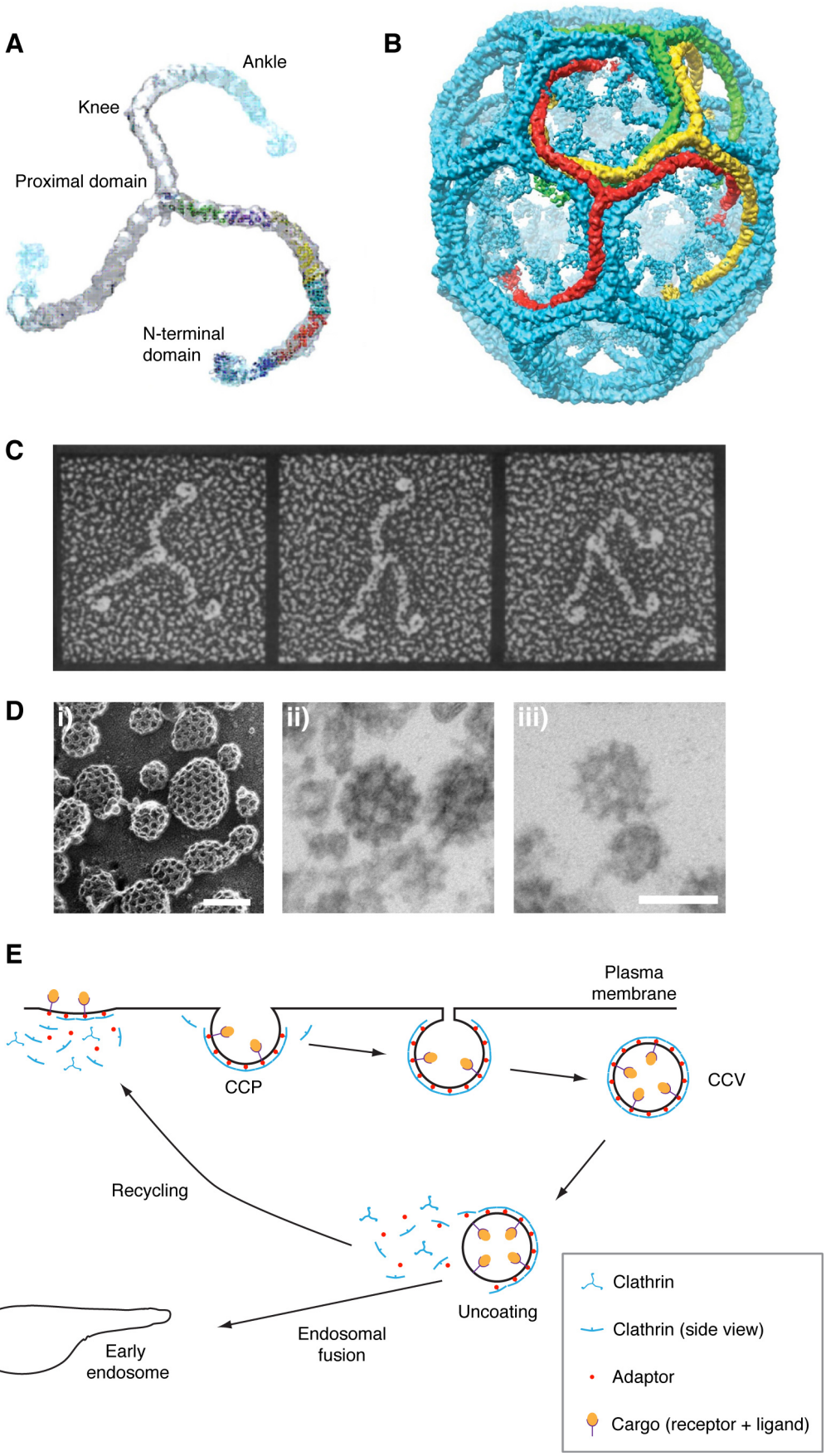
A
Ankle
Knee
Proximal domain
N-terminal domain
B
C
D
i)
ii)
iii)
E
Plasma membrane
CCP
CCV
Recycling
Uncoating
Endosomal fusion
Early endosome
Clathrin
Clathrin (side view)
Adaptor
Cargo (receptor + ligand)

Figure 1.8: The structure of clathrin and its involvement in endocytosis. A. An atomic model of clathrin. A typical clathrin protein is composed of three heavy chains, which can be viewed as the three 'legs' of the triskelion structure, and three light chains that bind the proximal domains. **B.** A representation of a hexagonal barrel-shaped clathrin-coated vesicle (CCV). **A** and **B** are adapted from Fotin *et al*., 2004. **C.** Electron micrographs of clathrin triskelia prepared using freeze-etching and platinum mica sheets. Clathrin exhibits a large degree of flexibility, as illustrated by the various conformations of the protein in the three micrographs. Adapted from Heuser and Kirchhausen, 1985. Box width, 100 nm. **D.** Electron micrographs of CCVs and clathrin-coated pits (CCPs). **i)** Deep-etch electron micrograph of assembled clathrin coats, viewed from the inside of the plasma membrane. Adapted from Heuser and Kirchhausen, 1985. **ii)** Electron micrograph of a fully assembled CCV, purified from HeLa cells. **iii)** Electron micrograph of a CCV coat (without the vesicle), purified from HeLa cells. The hexagonal clathrin coat is discernable in all three micrographs. Scale bars, 100 nm. **E.** Schematic diagram of the role of clathrin in the endocytosis of a cargo protein. The formation of a clathrin-coated pit (CCP), which develops into a budding vesicle and eventually a CCV can be observed, followed by uncoating of the vesicle and recycling of the clathrin and adaptin, whilst the vesicle fuses with an early endosome.

1.4.3.2 Clathrin in mitosis

Clathrin has recently been found to perform a mitotic 'moonlighting' function that is independent of its role in endocytosis and membrane trafficking. During mitosis, endocytosis is shut down (Warren, 1993; Fielding *et al*., 2012), leaving clathrin and the components of the endocytic machinery idle and free to perform other functions. Whilst clathrin had been observed in studies of mitotic spindles (Maro *et al*., 1985; Okamoto *et al*., 2000) and proteomic studies of purified spindle components (Mack and Compton, 2001), no novel mitotic role was described. It was later found that depletion of clathrin causes meiotic and mitotic defects such as chromosome misalignment and missegregation in various species and cell types (Royle *et al*., 2005; Tahara *et al*., 2007; Fu *et al*., 2010; Hoelzenspies *et al*., 2010; Lin *et al*., 2010; Booth *et al*., 2011), and a role for clathrin in the stabilisation of K-fibres was proposed. It is clear that the roles of clathrin in either endocytosis and mitosis are distinct from each other, as it was possible to generate a clathrin mutant which was not functional during endocytosis, but performed its mitotic function with no defects (Royle and Lagnado, 2006) as well as a clathrin mutant which could perform its endocytic role but could not localise to mitotic spindles (Hood and Royle, 2009). Furthermore, clathrin proteins that could dimerise, but not trimerise, were found to be functional during mitosis (Blixt and Royle, 2011).

Several groups independently demonstrated that clathrin is recruited to the mitotic spindle and forms a complex with TACC3 and ch-TOG (Fu *et al*., 2010; Hubner *et al*., 2010; Lin *et al*., 2010; Booth *et al*., 2011). Although the order of protein recruitment within this complex was inconsistent from study to study, it was recently shown that TACC3 phosphorylation on serine 558 modulates an interaction between the TACC domain and the N-terminal domain of clathrin, which together form a MT-binding surface. Therefore, both proteins are required in tandem to bind spindle MTs and subsequently recruit ch-TOG. (Hood *et al*., 2013).

1.4.4 TACC3–ch-TOG–clathrin complexes are thought to stabilise kinetochore fibres

Although the depletion of ch-TOG causes severe mitotic spindle organisation defects (Gergely *et al*., 2003), the depletion of TACC3 or clathrin both cause a similar, less severe phenotype (Royle *et al*., 2005; Fu *et al*., 2010; Lin *et al*., 2010; Booth *et al*., 2011). It is likely that the latter phenotype, but not the former, is caused by the absence of the TACC3–ch-TOG–clathrin complex on the K-fibres because the presence of an independent subpopulation of ch-TOG at the centrosome has been observed (Gergely *et al*., 2003; Cassimeris *et al*., 2009; Booth *et al*., 2011; Cheeseman *et al*., 2013). Whereas depletion of ch-TOG causes severely disorganised and often multipolar spindles (Gergely *et al*., 2003; Cassimeris and Morabito 2004) the depletion of TACC3 or clathrin by RNAi caused misaligned and missegregated chromosomes, destabilised K-fibres and delayed mitosis (Royle *et al*., 2005; Fu *et al*., 2010; Lin *et al*., 2010), and also caused both a loss of MT crosslinkers K-fibres and reduced kMT number and density at metaphase under the electron microscope (Booth *et al*., 2011), Therefore, the TACC3–ch-TOG–clathrin complex was proposed to form an inter-MT bridge which crossbraces and stabilises kMTs of a K-fibre (Booth *et al*., 2011)(**Figure 1.7A, C**, **Figure 1.9**).

However, the studies of the TACC3–ch-TOG–clathrin complex were performed using RNAi-mediated protein depletion, which is slow and can take 24-72 hours for efficient depletion whereas mitosis is a rapid process (~1 hour). This is particularly problematic when studying mitotic phenotypes at metaphase, because TACC3 and ch-TOG have been reported to help spindle assembly. Therefore, it is difficult to assert that TACC3–ch-TOG–clathrin bridges stabilise kMTs (Booth *et al*., 2011) because the missing kMTs may have been caused by reduced MT polymerisation rates. Furthermore, it is possible that some phenotypes may have been obscured by compensatory mechanisms upregulated by the cell during the gradual depletion period.

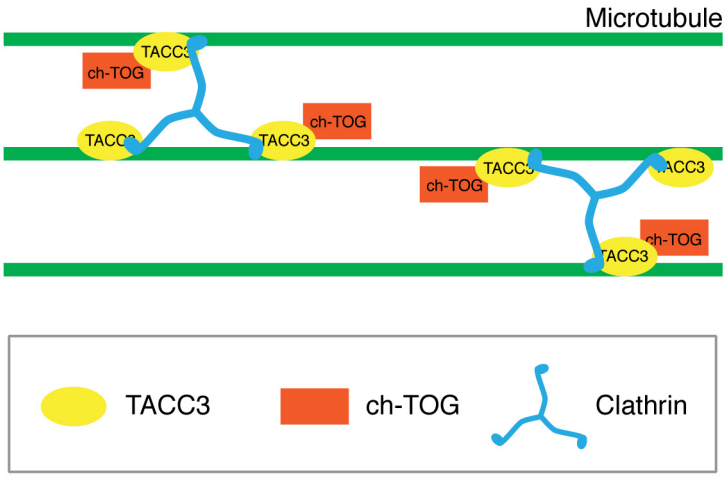

Figure 1.9: The TACC3–ch-TOG–clathrin microtubule crosslinker model. A schematic model of the crosslinker structure. TACC3 (phosphorylated by Aurora A kinase) recruits ch-TOG to the mitotic spindle, but TACC3 and clathrin are both required together to bind microtubules. Clathrin, with its unique triskelion structure, crossbraces adjacent microtubules of the K-fibre, forming a bridge.

In fact, RNAi-mediated depletion is particularly ill suited to study the TACC3–ch-TOG–clathrin complex because both TACC3 and clathrin have moonlighting functions during interphase (TACC3 is involved in mRNA translation (Sadek *et al*., 2000; Gangisetty *et al*., 2004; Angrisano *et al*., 2006); clathrin is involved in endocytosis and trafficking, (Goldstein *et al*., 1985)) and ch-TOG depletion causes mitotic phenotypes so severe it is impossible to study metaphase, so the depletion of any of these proteins would likely cause off-target effects. Furthermore, in addition to their role in K-fibre structure, the TACC3–ch-TOG and TACC3–ch-TOG–clathrin complexes have been reported to contribute to spindle pole clustering and centrosome maturation (Fielding *et al*., 2011; Foraker *et al*., 2012), suggesting that their inactivation prior to mitosis would have further effects on the mitotic spindle and would not be restricted to the K-fibres alone. To study this matter adequately, methods for rapid protein inactivation are required to temporally dissect the roles of the TACC3–ch-TOG–clathrin complex during mitosis.

1.5 The need for rapid protein inactivation methods

RNAi-mediated protein depletion is slow, usually taking 48-72 hours. During this gradual depletion period, the cell can upregulate pathways to compensate for this deficiency. Additionally, in the case of spindle proteins, studying RNAi phenotypes at later stages of mitosis can be confounded by early defects, such as deficient spindle assembly. In other words, is the RNAi phenotype at metaphase due to the absence of the target protein at that stage, or because the absence of the protein caused the assembly of an aberrant spindle? Furthermore, during the RNAi depletion period, the cell will undergo multiple cycles of cell division and may have accumulated defects that could undermine the correct assessment of the RNAi phenotype. To avoid these problems, methods for the rapid inactivation of proteins are required.

1.5.1 Small molecule inhibitors

Small molecule inhibitors are an obvious choice for the rapid inactivation of proteins. These inhibitors can either target the protein of interest directly, for example the inactivation of Eg5 motor activity by monastrol (Mayer *et al*., 1999; Kapoor *et al*., 2000)(**Figure 1.10A**) or can target a different protein that is required for the localisation or activity of the protein of interest, for example the inhibition of Aurora A kinase by MLN8054 (Leroy *et al*., 2007) or MLN8237/Alisertib (Booth *et al*., 2011; Cheeseman *et al*., 2011; Manfredi *et al*., 2011)(**Figure 1.10A**). Because of the effort involved in developing selective and potent inhibitors for protein kinases, a recent strategy was to genetically alter cells to express a mutant kinase of interest. This mutant kinase was sensitive to an inhibitor which did not affect the wild type protein, thus allowing a faster characterisation of kinases (Bishop *et al*., 2000)

However, these approaches have drawbacks. In the case of monastrol, the drug inhibits the motor activity but does not inhibit the crosslinking function of Eg5 (Kapoor *et al*., 2000). This is problematic, because Eg5 RNAi causes monopolar spindles, so the cell cannot reach metaphase for further study of this aspect of the protein. In the case of kinase inhibitors, mitotic kinases have many downstream substrates, meaning that effects on multiple targets will exaggerate or confound the assessment of the phenotype. For instance, Aurora A kinase activity is required to phosphorylate TACC3 in order for TACC3 to localise to MTs, but is also required for the activity of HURP, Eg5 and NuMA (Giet *et al*., 1999; Yu *et al*., 2005; Kettenbach *et al*., 2011). Furthermore, these inhibitors only stop new phosphorylation events, and are dependent on phosphatase activity to remove pre-existing phosphate groups.

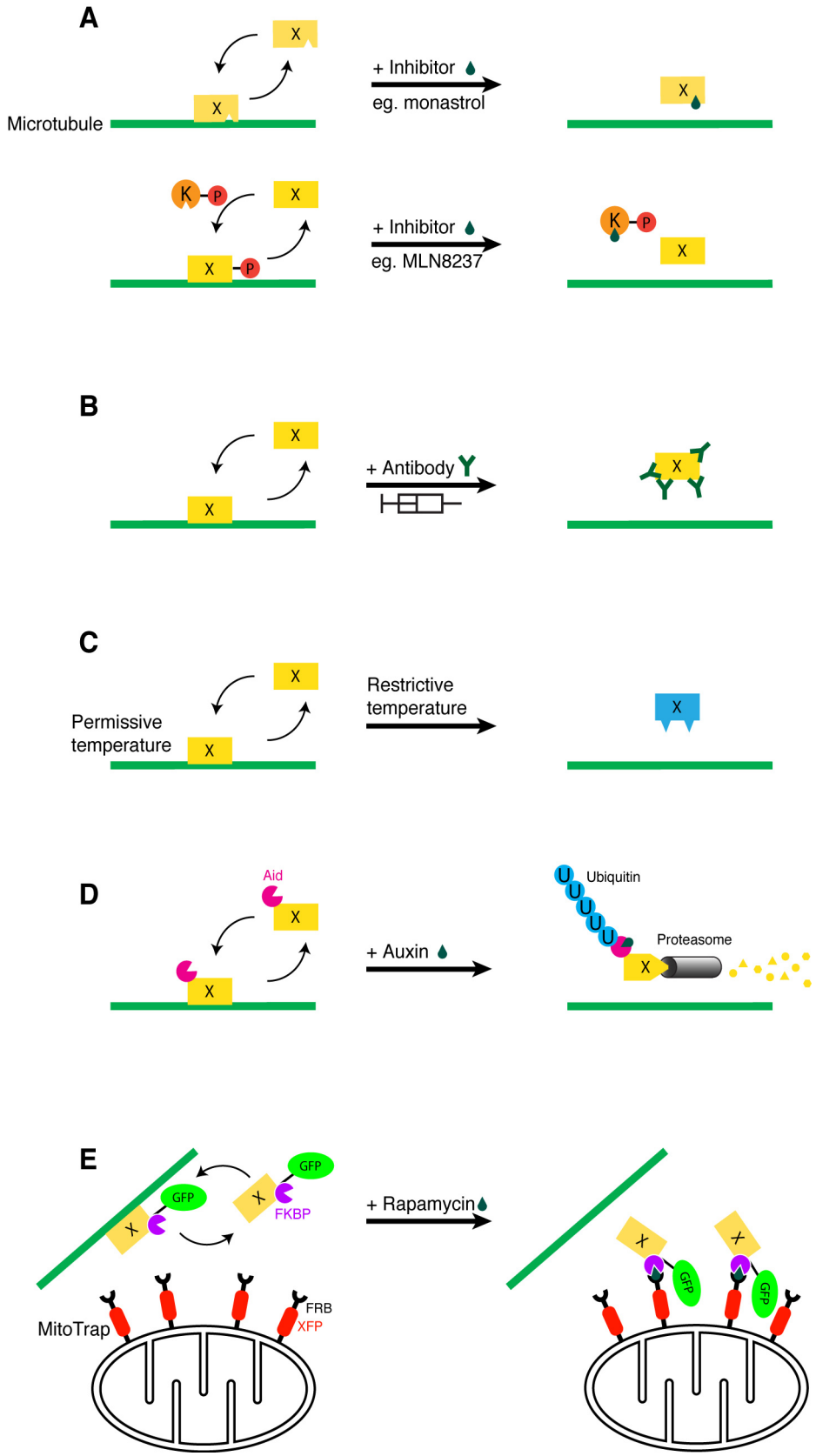
A
X
X
Microtubule
+ Inhibitor
eg. monastrol
X
K
P
X
P
+ Inhibitor
eg. MLN8237
K
P
X
B
X
X
+ Antibody
X
C
X
X
Permissive
temperature
Restrictive
temperature
X
D
Aid
X
X
+ Auxin
Ubiquitin
Proteasome
X
E
GFP
GFP
FKBP
MitoTrap
FRB
XFP
+ Rapamycin
GFP
GFP

Figure 1.10: The different techniques for fast protein inactivation. Diagrams depict the removal of a microtubule associated protein X. **A.** Schematic diagram of protein inactivation by application of a small molecule inhibitor. This inhibitor can bind the target protein directly (such as monastrol inhibition of Eg5) or target a protein responsible for the recruitment of a protein (such as inhibition of Aurora A kinase by MLN8237, which stops recruitment of TACC3 to microtubules). **B.** Protein inactivation by antibody microinjection. This system is very similar to small molecule inhibition, but requires microinjection of an inactivating antibody which targets protein X. **C.** Temperature-sensitive mutants. A recombinant protein X can be activated or inactivated by changes in temperature. The protein is active in permissive temperature, and inactivated in restrictive temperature. **D.** The auxin-degron system. A recombinant target protein is tagged with Aid. Upon treatment with auxin, Aid is ubiquitylated and targeted for degradation. This also induces the degradation of the target protein by the proteasome. **E.** The knocksideways (KS) system. The target protein is tagged with an FKBP domain. In the same cells, the endogenous target protein is depleted by RNAi, and MitoTrap (a mitochondrially-targeted FRB domain) is expressed. Upon application of rapamycin, FKBP heterodimerises with FRB and sequesters protein X on the surface of mitochondria. Note that protein X must dynamically cycle on and off microtubules for KS to be effective.

1.5.2 Inactivating antibody microinjection

The use of microinjection of antibodies that inactivate target proteins precedes the use of RNAi. Antibodies directed against a specific antigen are injected into cells to inactivate it, and the subsequent acute phenotype can then be studied (Lane and Nigg, 1996)(**Figure 1.10B**). However, this method has a number of disadvantages, such as (1) the delicate nature of the manipulation, (2) the low throughput (a single cell can be injected at a time) and high time cost, (3) the requirement for a highly specific antibody, and (4) the limitation of the application of this method to larger cells.

1.5.3 Temperature-sensitive mutants

Temperature-sensitive mutants are an effective method for the rapid inactivation of proteins within a timescale of seconds (Canman *et al*., 2008)(**Figure 1.10C**). In combination with live cell imaging, this proved a highly useful method to study the roles of specific proteins during cytokinesis. However, the technique involves engineering a temperature-sensitive mutant, a task which may be more difficult for some target proteins. Furthermore, this method requires a fast change in temperature from a permissive to a restrictive temperature. Although this required change is generally <10ºC and achieved in under a minute, cellular processes such as mitosis and migration are dependent on the cytoskeleton, a structure which is itself highly sensitive to temperature (Engelborghs *et al*., 1976). Therefore, the alteration of temperature may be inadequate for the study of some phenotypes.

1.5.4 Chromophore-assisted light inactivation

Chromophore-assisted laser inactivation (CALI) is based on the ability of a malachite green chromophore to denature a tagged protein of interest upon excitation by a laser (Jay, 1988). The wavelength used is specific so as to not disturb any other cellular components. Upon excitation, the malachite green chromophore produces highly reactive free radicals which denature the protein tagged to it in a specific and near-instant manner. The short lifespan of the radicals allow the effects to be limited to the close proximity to the chromophore without significantly affecting other proteins (Jacobson *et al*., 2008). In addition to this, the laser beam can be focussed

sufficiently so as to inactivate the target protein only in specific areas of the cell, allowing for spatial analysis of protein loss-of-function. However, use of CALI in dividing cells in the literature is minimal (Tanabe *et al*., 2005; Keppler and Ellenberg, 2009; Ou *et al*., 2010). Although there is no report of incompatibility of this method with dividing cells, it is well known that mitotic cells are highly sensitive to perturbations, therefore the production of free radicals such as reactive oxygen species may be sufficient to perturb division in a non-specific manner, particularly if targeting a MAP.

1.5.5 The auxin-degron system

A recent addition to the cell biologist's toolbox for the rapid inactivation of target proteins is the auxin-degron system (Nishimura *et al*., 2009). It is based on the auxin inducible degron (Aid) tag from *Arabidopsis thaliana* called IAA17 that can be fused to a protein of interest following the RNAi-mediated depletion of the endogenous protein. Upon application of auxin to the cell, the tagged protein is selectively ubiquitylated and targeted for degradation by the proteasome (**Figure 1.10D**). The timescale of degradation using this system is variable depending on the target protein, with CENP-T and Dsn1 taking up to 1 hour for effective depletion (Nishino *et al*., 2013), 30 minutes for GFP fused to a nuclear localisation signal (Nishimura *et al*., 2009), polo-like kinase 4 (Plk4) and telomeric repeat-binding factor 2 (TRF2) (Holland *et al*., 2012), 50 minutes for cyclin B and CENP-A (Holland *et al*., 2012), and 100 minutes for histone 2B (H2B) (Holland *et al*., 2012).

Whereas some of these timescales are compatible with the study of mitotic functions of target proteins, they are not suited for the study of protein roles at a particular mitotic stage, such as metaphase, which lasts under 15 minutes. Nonetheless, this technique is highly robust and is reversible following auxin washout (Holland *et al*., 2012).

1.5.6 The knocksideways system

The knocksideways system is based on the ability of two proteins, FKBP12 and mammalian target of rapamycin (mTOR), to heterodimerise in the presence of rapamycin. The mTOR pathway is a signalling system involved in a number of cellular processes such as migration, growth, proliferation and autophagy (Laplante

and Sabatini, 2012). By fusing the FKBP domain from FKBP12 and the FKBP and rapamycin-binding (FRB) domain from mTOR to target proteins, their heterodimerisation can also be induced by adding rapamycin (Spencer *et al*., 1993). This system, has been used for biological studies for a number of years such as for forcing protein interactions or relocating target proteins to activate them (Spencer *et al*., 1995) or sequestering nuclear proteins in the cytosol (Geda *et al*., 2008) or as a positive control in bimolecular fluorescence complementation assays (Paulmurugan and Gambhir, 2005).

The FKBP and FRB dimerisation system was recently altered to include the prior depletion of the untagged endogenous target protein and was used to sequester the proteins to the outer membrane of mitochondria (Robinson *et al*., 2010)(**Figure 1.10E**). The target protein was tagged with FKBP, and FRB domains were tagged to the import signal of the mitochondrial protein Tom70p, thereby acting as receptors. If the new localisation of the target proteins on the mitochondria is incompatible with their function, then the proteins can be considered inactivated. The study found that inactivation of clathrin adaptor proteins was visible within 3 seconds, and fully inactivated the proteins in less than 10 minutes (Robinson *et al*., 2010). Interestingly, the technique was able to occasionally co-reroute interactors of the target protein (Hirst *et al*., 2012) though this was not systematic (Robinson *et al*., 2010). However, the method requires a target protein that is dynamic. For instance, it is unlikely that knocksideways would be effective to inactivate a membrane-bound protein. Furthermore, the method is not reversible as the interaction between FKBP and FRB in presence of rapamycin is extremely strong.

The FKBP- and FRB-based system has also been used in conjunction with some of the previously mentioned inactivation techniques. One notable example is that of the Shield-1 and ligand-induced degradation technique, where engineered mutants of FKBP acts as destabilisation domains, and the degradation of the tagged target protein can be induced by addition of Shield-1 molecule (Bonger *et al*,. 2011). However, the timescale of the degradation appears to be on the scale of hours rather than minutes for even fluorophores, suggesting this method would be ill suited for dynamic processes such as mitosis (Bonger *et al*., 2010).

Overall, knocksideways is the fastest method available for the inactivation of proteins, with a timescale of complete rerouting that is compatible with the very dynamic stages of mitosis (<15 minutes). Therefore, this method would be well suited to study the TACC3–ch-TOG–clathrin complex at various stages of mitosis to dissect the potential temporally distinct roles of the complex.

2 Chapter 2 – Materials and methods

2.1 Molecular biology

2.1.1 Reagents

All restriction enzymes, their associated buffers, Quick Ligase, CIP and the DNA ladders were purchased from New England Biolabs. Pfu Turbo polymerase was purchased from Agilent Technologies. All chemicals, such as tryptone, boric acid, Ethylenediaminetetraacetic acid (EDTA), Tris-base, agarose, rapamycin, molecular biology grade ethanol and BSA were all purchased from Sigma Aldrich. Oligonucleotide primers were also purchased from Sigma Aldrich. Yeast extract and glycerol were purchased from Fisher Scientific.

2.1.2 Generation of DNA constructs

Some of the DNA plasmids used in this thesis are so-called pBrain constructs. These plasmids express both shRNA targeting a protein of interest, as well as an RNAi-resistant version of the same protein tagged with a fluorescent tag and, in KS experiments, FKBP (**Figure 2.1**). The shRNA is expressed using an H1 promoter and the concomitant protein using a CMV (cytomegalovirus) promoter. The reexpressed protein was made knockdown-proof (KDP) by the insertion of silent mutations in the sequence targeted by the shRNA.

pBrain-GFP-TACC3KDP-shTACC3 was available from previous work (Booth *et al*., 2011). From this construct, pBrain-GFP-FKBP-TACC3KDP-shTACC3, pBrain-mCherry-TACC3KDP-shTACC3 and pBrain-mCherry-FKBP-TACC3KDP-shTACC3 were created as described in Chapters 3 and 4. GFP-LCa was available from previous work (Royle *et al*., 2005), upon which GFP-FKBP-LCa was based (see **Chapter 3**). The MitoTrap proteins were designed based on the pMito-YFP-FRB plasmid used in Robinson *et al*., (2010), as described in Chapter 3. H2B-

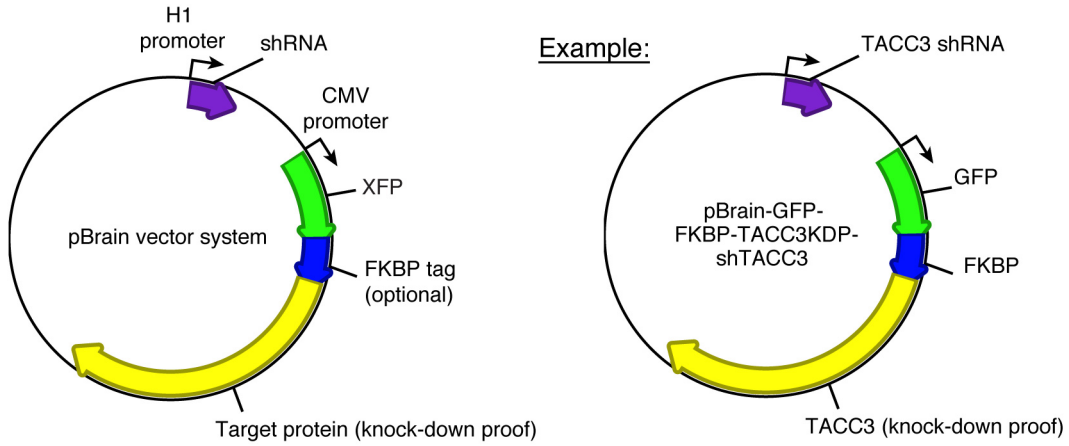

Figure 2.1: The pBrain plasmid system. Schematic diagram of the pBrain plasmid system. Each plasmid contains an H1 promoter for the expression of shRNA targeting a protein of interest, and a CMV promoter for the re-expression of a RNAi-refractory protein, tagged with GFP and in knocksideways experiments, an FKBP domain. Right, example of a pBrain plasmid used for TACC3 knocksideways experiments.

mCherry was created based on H2B-GFP (Royle *et al*., 2005) as described in Chapter 4. pBrain-GFP-HURPKDP-shHURP and pBrain-GFP-FKBP-HURPKDP-shHURP were created as described in Chapter 3.

2.1.3 PCR amplification of DNA

DNA was amplified by polymerase chain reaction (PCR) in a Techne TC-312 thermocycler. A typical reaction tube contained the following: 100 ng of DNA template, 2.5 mM (deoxyribonucleotide triphosphate (dNTP), 2.5 μl DMSO, 5 μl 10X Pfu polymerase buffer, 0 to 2 mM magnesium sulfate, 0.5 μM of each sense and anti-sense oligonucleotides primers, 0.5 μl of Pfu Turbo polymerase. The reaction tube was topped up to a final volume of 50 μl with distilled H_2O. In some instances, Vent polymerase and Thermo polymerase buffer were used instead of Pfu Turbo and Pfu polymerase buffer.

The reaction tube was then subjected to the following:

1. Denaturing at 95ºC for 4 minutes
2. Denaturing at 95ºC for 40 seconds
3. Primer annealing at 60ºC for 1 minute
4. Extension at 72ºC for 1 minute per kilobase (kb) of DNA
5. Extension at 72ºC for 10 minutes

Steps 2 to 4 were cycled 36 times. At the end of the thermocycler protocol, the reaction tubes were cooled and maintained at 4ºC.

2.1.4 Separation of DNA by electrophoresis

Following PCR or endonuclease digest, the resulting DNA was separated on an agarose gel by electrophoresis. Gels were prepared by melting electrophoresis grade agarose (0.8 to 1.2% w/v) in 100 ml of boiling 0.5X TBE buffer (45 mM Tris-base, 45 mM boric acid, 10 mM EDTA, pH 8.3). After the agarose was fully dissolved and the solution had partially cooled, 0.5 μg/ml ethidium bromide was added and mixed. The solution was then poured into a mould, a comb was inserted to create sample wells, and was left to set by cooling at room temperature.

DNA samples were mixed with 6X loading buffer (30% glycerol, 0.25% xylene cyanol FF, 0.25% bromophenol blue, in distilled H_2O) and pipetted into the sample wells. To assess DNA size, 1 kb or 100 bp standard DNA ladders were used alongside the samples. The DNA was then separated by migration through the agarose gel in an electrophoresis tank filled with 0.5X TBE buffer at 90 to 120 V using a BioRad PowerPack. The resulting DNA was images under ultraviolet (UV) light using a transilluminator.

2.1.5 DNA extraction from agarose gel

To extract PCR-amplified or restriction enzyme digested DNA from agarose gel following electrophoresis, the band of interest was identified using the standard DNA ladders on a transilluminator, and excised using a scalpel.

The QIAquick Gel Extraction Kit (Qiagen) was then used to extract the DNA from the gel slice using the manufacturer's instructions. Briefly, the agarose was dissolved in buffer QG at 50ºC, and the DNA precipitated with isopropanol. The sample was collected in a QIAquick spin column by centrifugation, and washed with buffer PE. The spin column membrane was dried by centrifugation and the DNA eluted into a 1.5 ml Eppendorf tube using 30 to 50 μl of buffer EB.

2.1.6 Restriction endonuclease digest of DNA

Restriction enzyme digestion of DNA was used to either create new plasmids or test the correct structure of a new DNA construct. The reactions were performed in 50 and 10 μl, respectively.

A typical reaction tube contained 1 μg DNA, 5 μg bovine serum albumin (BSA), 2 μl restriction enzyme and 5 μl of its corresponding 10X NEB enzyme buffer. The reaction tube was topped up to a final volume of 50 μl with distilled H_2O. These amounts were scaled correspondingly for the 10 μl reactions. The reaction tube was incubated at 37ºC for 1 hour for 10 μl reactions or 3 hours with addition of 1 μl calf intestinal phosphatase (CIP) after 2.5 hours for 50 μl reactions. The CIP treatment was used to facilitate the subsequent ligation of the DNA fragment into a vector backbone by dephosphorylating the vector.

2.1.7 Ligation of target DNA into plasmid vector

To ligate a DNA fragment into a vector backbone, the DNA fragment and CIP-treated vector backbone were mixed in a reaction tube containing 150 ng DNA insert, 50 ng DNA vector, 10 μl Quick Ligase buffer, 1 μl Quick Ligase enzyme. The reaction tube was topped up to a final volume of 20 μl with distilled H_2O and incubated for 5 to 10 minutes at room temperature before being put on ice. A negative control tube containing no DNA insert was used in parallel to assess the amount of circularisation of the vector by itself. The resulting DNA could then be used to transform bacteria.

2.1.8 Bacterial transformation of DNA constructs

The completed ligated construct was then used to transform an ultra-competent XL10-gold strain of *Escherichia coli* by heat shock. 100 μl of XL10-gold bacteria was added to 1 μl of ligated DNA or negative control. The undigested DNA vector was used as a positive control. The tubes were incubated on ice for 30 minutes, and then put in a water bath at 42ºC for 42 seconds before being placed back on ice for 5 minutes. 900 μl of super optimal broth (SOB) medium (0.5% w/v yeast extract, 2% w/v tryptone, 10 mM NaCl, 2.5 mM KCl, 10 mM $MgSO_4$, 10 mM $MgCl_2$ in distilled H_2O, pH 7.0) was added to each reaction, and the tubes were placed in a 37ºC shaker for 1 hour. The bacteria were pelleted by centrifugation for 2 minutes at 5,000 rpm using a bench top centrifuge. 900 μl of the bacterial solution was discarded, and the bacteria resuspended in the remaining 100 μl before being spread on agar LB (lysogeny broth, often but incorrectly called Luria-Bertani; 0.5% w/v yeast extract, 1% w/v tryptone, 171 mM NaCl in distilled H_2O, pH 7.0) plates containing an appropriate antibiotic for the construct being made (kanamycin or ampicillin, both 50 μg/ml). The plates were then incubated at 37ºC overnight.

2.1.9 Recovery of DNA plasmid from bacterial cultures

Single colonies of transformed bacteria were picked using a sterile inoculation loop and grown in LB medium supplemented with antibiotic at 37ºC overnight in an orbital shaker. The resulting bacterial culture was then processed to recover the amplified DNA.

2.1.9.1 Miniprep Kit

Wizard Plus SV Miniprep Kit was used to recover DNA typically used during the creation of a new DNA construct, later used for test digests and ligations.

Transformed bacteria were culture in 5 ml LB medium supplemented with an appropriate antibiotic overnight at 37ºC, and pelleted at 14,000 rpm on a bench top centrifuge. The manufacturer's instructions were then used to recover the plasmid DNA. Briefly, the bacterial pellet was resuspended in 250 μl of cell resuspension solution and lysed in 250 μl of cell lysis solution. 10 μl alkaline phosphatase and 350 μl neutralisation solution were added, and the solution decanted by centrifugation for 10 minutes. The supernatant was collected into a spin column, and the DNA collected on the column membrane by centrifugation and washed twice with 750 μl and 250 μl of column wash solution. The DNA was eluted into a new 1.5 ml Eppendorf tube with 100 μl of nuclease-free water.

2.1.9.2 Midi prep kit

Qiagen HiSpeed Midi Kit was used to recover plasmid DNA once the construct was completed and verified by test digest, to be used in cell transfections.

Transformed bacteria were cultured in 100 ml LB supplemented with an appropriate antibiotic overnight at 37ºC, and pelleted by centrifugation at 6,000 × *g* at 4ºC. The manufacturer's instructions were then used to recover the plasmid DNA. Briefly, the bacterial pellet was resuspended in 4 ml of buffer P1, lysed in 4 ml of buffer P2 and incubated for 5 minutes. 4 ml of chilled buffer P3 were then added and the solution decanted in a QIAfilter Cartridge for 10 minutes, and filtered into an equilibrated HiSpeed Midi Tip. The lysate was allowed to enter the Tip resin by gravity flow, washed with 20 ml buffer QC, and the DNA eluted in 5 ml buffer QF. 3.5 ml isopropanol was added to precipitate the DNA, and the solution applied to a QIAprecipitator using a seringe, washed with 70% ethanol and eluted into a new 1.5 ml Eppendorf tube in 1 ml of buffer TE.

2.2 Cell biology

2.2.1 Reagents

All chemicals such as trypsin, FBS and penicillin/streptomycin were purchased from Sigma Aldrich. siRNA duplexes were also purchased from Sigma Aldrich. Optimem, DMEM and Lipofectamine were purchased from Invitrogen. GeneJuice was purchased from Merck Biosciences. FuGene 6 was purchased from Promega. Tissue culture plasticware such as 75 cm^2 flasks was purchased from Greiner.

2.2.2 Cell lines

HeLa cells derived from epithelial cervical carcinoma were purchased from Health Protection Agency Cultures (Salisbury, UK).

For the kinetochore and spindle pole tracking experiments, HeLa cells stably expressing GFP-CENP-A and centrin-GFP were obtained from Andrew McAinsh (University of Warwick, UK).

2.2.3 Cell culture

Cells were maintained in a humidified cell culture incubator at 37ºC with 5% atmospheric CO_2, and typically grown in Dulbecco's Modified Eagle Medium (DMEM) (Invitrogen) supplemented with 10% foetal bovine serum (FBS) and 100 units/ml penicillin/streptomycin. For the GFP-CENP-A and centrin-GFP HeLa cell line, the cell culture medium was further supplemented with 10 μg/ml puromycin and 25 μg/ml geneticin (G418).

Cells were grown in plastic 75 cm^2 tissue culture flasks and allowed to reach 80 to 100% confluency, upon which the culture medium was removed and the cells resuspended using 3 ml 0.25% trypsin EDTA at 37ºC. 7 ml of supplemented medium was then added and 1 ml of the resulting solution was reseeded into a new tissue culture flask containing 10 to 15 ml of supplement medium.

2.2.4 Transfection of DNA plasmids

HeLa cells were typically transfected using GeneJuice according to the manufacturer's instructions. Briefly, cells were seeded in a 6 well plate at 50 to 80% density one day prior to transfection. On the day of transfection, 3 μl GeneJuice was mixed in 100 μl Optimem and incubated 5 minutes at room temperature, then 1 μg DNA was added to the mix, and incubated 15 minutes at room temperature. The reaction mix was then added to a well containing 3 ml of supplemented medium.

In the case of the GFP-CENP-A and centrin-GFP stable cell line, cells were transfected with FuGene 6 according to the manufacturer's instructions. Briefly, cells were treated as above, however on the day of transfection 4.5 μl FuGene was mixed in 50 μl Optimem, whilst 1 μg DNA was separately mixed in 50 μl Optimem. Both tubes were incubated 5 minutes at room temperature, then mixed together and incubated 20 minutes at room temperature before adding the reaction mix to a well containing 1.5 ml supplemented medium.

Typically, the transfected cells were split and plated into the experimental environment (in an imaging dish or 12 well plate containing glass coverslips) one day after transfection, and the experiment performed 24 to 48 hours later.

2.2.5 Transfection of siRNA

To transfect cells with siRNA oligonucleotides, Oligofectamine (Invitrogen) was used according to the manufacturer's instructions. Briefly, 0.25 ng siRNA was mixed in 125 μl Optimem, whilst 5 μl Lipofectamine was separately mixed with 125 μl Optimem. Both tubes were incubated 5 minutes at room temperature, then mixed together and incubated 20 minutes at room temperature before adding the reaction mix to a well of a 6 well plate containing 2 ml supplemented medium with cells at 50 to 80% density.

Typically, the transfected cells were split and plated into the final dish (in an imaging dish or 12 well plate containing glass coverslips) the day following transfection, and the experiment performed 24 hours later.

2.3 Microscopy

2.3.1 Reagents

Microscope slides and glass coverslips were purchased from Fisher Scientific. BSA, goat serum and all other chemicals were purchased from Sigma Aldrich. CO_2-independent medium was purchased from Invitrogen.

2.3.2 Light microscopy

2.3.2.1 Indirect immunofluorescence

For indirect immunofluorescence, HeLa cells on coverslips were fixed with PTEMF (50 mM PIPES [1,4-Piperazinediethanesulfonic acid], 10 mM EGTA [ethylene glycol tetraacetic acid], 1 mM $MgCl_2$, 0.2% v/v Triton X-100, 4% w/v paraformaldehyde, pH 7.2) at room temperature for 15 minutes, or methanol at -20ºC for 5 minutes for ch-TOG staining. Cells were then permeabilised with PBS with 0.5% v/v Triton X-100 for 10 minutes and blocked using PBS with 5% w/v BSA and 5% v/v goat serum for 1 hour. The coverslips were then treated with primary antibodies diluted in blocking solution for 1 hour at room temperature, rinsed in PBS, and incubated with secondary antibodies diluted in blocking solution for 1 hour at room temperature. Coverslips were rinsed in PBS, then dipped briefly in distilled H_2O and dried in the dark for 30 minutes at room temperature before mounting on microscope slides using Mowiol (Sigma Aldrich) containing 4',6-diamidino-2-phenylindole (DAPI).

2.3.2.2 Fluorescence imaging

Epifluorescence micrographs were acquired using a Nikon Eclipse Ti-U microscope with standard filter sets for visualisation of DAPI, GFP, mCherry/Alexa Fluor 568 and Alexa Fluor 633, a Nikon Digital Sight DS-Qi1Mc camera, a 60× (1.40 NA) oil-immersion objective and NIS acquisition software.

2.3.2.3 Confocal microscopy

Confocal micrographs were acquired using a Leica confocal microscope SP2 with a 63× (1.4 NA) oil-immersion objective. GFP and Alexa568 and Alexa633 were excited using an Argon/Krypton 488 nm and the 543 and 633 nm lines of a Helium/Neon laser, respectively. DAPI was excited using a multiphoton laser. Excitation and collection of emission were performed separately and sequentially. Images were captured at a depth of 8-bit. For quantitation experiments, identical laser power and acquisition settings (pinhole, gain, resolution and zoom) were used.

2.3.2.4 Live cell imaging

Live cell imaging of KS kinetics (**Chapter 3**) was performed on an Olympus IX71 in glass-bottom dishes heated to 37 ℃ (Bioptechs Delta T5 m-environmental culture dish controller) in CO_2-independent medium supplemented with 10% FBS and 100 units/ml penicillin/streptomycin, using Cell-R acquisition software and a Hamamatsu ORCA-ER C4742-80 camera with a 60× oil-immersion objective (1.42 NA).

Live cell imaging of mitotic progression following RNAi or KS (**Chapter 4**) was performed on a Nikon Eclipse Ti with a heated Perspex chamber (OKOlab) using standard filter sets for visualisation of GFP and mCherry, NIS acquisition software, a CoolSNAP HQ2 camera and a 20x air objective (0.45 NA). Cells were kept at 37ºC in supplemented CO_2-independent medium. Light intensity was kept to a minimum to avoid light-induced cell damage. Chromosomes were visualised with mCherry-H2B (imaged once per minute), and GFP monitored every 5 minutes.

2.4 Data collection and analysis

2.4.1 Intensity quantification of fluorescent micrographs

For TACC3 quantitation experiments, identical laser power and acquisition settings of a confocal microscope were used. Fluorescence intensity quantification was performed using ImageJ/Fiji by measuring mean pixel density in a 20×20 pixel ROI placed in the spindle region (determined using the tubulin immunolabel channel in the same cells) and background subtracted.

For live cell imaging of rerouting kinetics, GFP intensity was quantified during KS using ImageJ/Fiji, with an ROI that defined the spindle and one that excluded it, and plotted as $\Delta F/F_0$.

2.4.2 Statistical testing

Statistical testing was performed with InStat or SPSS. In some instances, statistical testing was performed by Stephen Royle. Normally distributed data were compared using one-way ANOVA followed by a Tukey-Kramer *post hoc* test. Student's unpaired t-test was used to compare two data sets. The Kolmogorov-Smirnov test was used to determine if the data followed a Gaussian distribution. Cox regression analysis was used to test for significance of mitotic delays. Tukey box plots show the median, interquartile range and the 10^{th} and 90^{th} percentiles. Error bars show standard deviation or standard error of the mean (s.e.m.) as indicated. Graphs were plotted using IgorPro 6.22A (Wavemetrics) and MATLAB (R2012). Figures were assembled using Adobe Photoshop and Adobe Illustrator.

3 Chapter 3 – Implementing the knocksideways method for spindle proteins

3.1 Introduction

A TACC3–ch-TOG–clathrin microtubule crosslinker has previously been shown to contribute to K-fibre stability (Fu *et al*., 2010; Hubner *et al*., 2010; Lin *et al*., 2010; Booth *et al*., 2011). Indeed, the depletion of clathrin by RNAi was shown to reduce the density and number of MTs in K-fibres at metaphase (Booth *et al*., 2011).

However, studying the roles of mitotic spindle proteins at metaphase by slow depletion methods such as RNAi is problematic because if the depleted proteins are required for spindle assembly, distinguishing the temporal roles of the protein in spindle assembly or maintenance is difficult. A better rationale for studying putative roles of spindle proteins at later stages of mitosis would be to allow a cell to assemble a fully functional mitotic spindle, and then specifically inactivate the target protein at a given stage of mitosis.

Knocksideways is a recently described technique (Robinson *et al*., 2010) which traps proteins of interest on the outer membrane of mitochondria using FKBP and FRB heterodimerisation in presence of rapamycin. If the new localisation of the target protein is incompatible with function, then the protein can be deemed inactivated. For the present study, if the TACC3–ch-TOG–clathrin crosslinker complex is sufficiently dynamic, KS should be a suitable method to deplete the complex rapidly enough to discern its potential temporally distinct roles during mitosis.

3.2 Chapter aims

The aims of this chapter are:

1- To apply the KS method to mitotic spindle proteins, in particular the TACC3–ch-TOG–clathrin complex, and other inter-MT bridge candidates such as HURP.
2- To quantitatively, qualitatively and temporally characterise the removal of spindle proteins by KS compared to RNAi.
3- To use KS to deduce information about the dynamics and binding properties of the TACC3–ch-TOG–clathrin complex.

3.3 Materials and methods

3.3.1 Drug treatments

For KS, rapamycin (Sigma-Aldrich) in ethanol was consistently used at 200 nM in all experiments for 10 or 30 min as indicated. A vehicle control was used (ethanol; 0.1%). MLN8237 (Selleck Chemicals) in DMSO was used at 1 μM for 30 min; vehicle control was DMSO (0.01%). During treatment, cells were incubated at 37ºC, 5% CO_2.

3.3.2 Experimental conditions for KS

In KS or rerouting experiments, 4 conditions were used. To control for effects of the FKBP tag on the activity of the target proteins, control proteins lacking the FKBP domains were used in parallel to FKBP- tagged proteins. Furthermore, to control for effects of rapamycin alone, a vehicle control (ethanol; 0.1%) was used (**Figure 3.1A**).

Because of the multitude of experimental conditions generated for experiments such as those visible in **Figure 3.11** and **Figure 3.12**, a colour-code was designed for each condition, as depicted in **Figure 3.1**. This colour-code remains identical throughout this thesis.

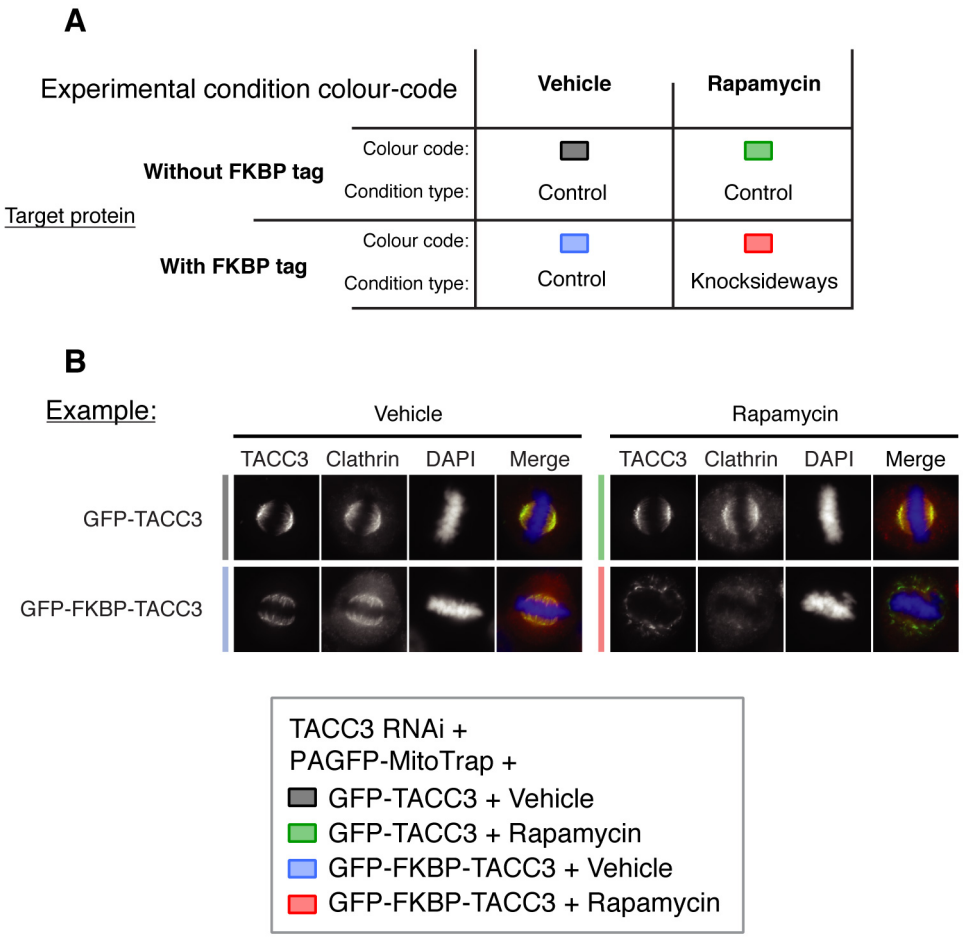

Figure 3.1: The different experimental conditions of knocksideways experiments. **A.** Table of the different experimental conditions colour-coded identically in all experiments throughout this thesis. Experiments are performed in cells expressing the same target protein with and without the FKBP tag, and treated with vehicle or rapamycin. There are 3 control conditions and 1 knocksideways condition in a typical experiment. **B.** Examples fluorescent micrographs of TACC3-depleted HeLa expressing PAGFP-MitoTrap and GFP-TACC3 or GFP-FKBP-TACC3, treated with vehicle or 200 nM rapamycin. The colour-coding of the conditions depicted in the inset legend are indicated to the left of each row of 4 images.

3.3.3 Generating FKBP-tagged constructs

3.3.3.1 TACC3 constructs

pBrain-GFP-TACC3KDP-shTACC3, used in this study to express TACC3 shRNA and RNAi-resistant GFP-TACC3 (without an FKBP tag), was available from previous work (Booth *et al*., 2011).

FKBP was amplified from gamma-FKBP (gift from Margaret S. Robinson, Cambridge Institute for Medical Research, UK; see (Robinson *et al*., 2010)) by PCR and inserted into pBrain-GFP-TACC3KDP-shTACC3 via Acc65I/BsrGI and Acc65I. A schematic diagram of GFP-FKBP-TACC3 is presented in **Figure 3.2B**.

3.3.3.2 pBrain-GFP-FKBP-HURPKDP-shHURP

pBrain-GFP-HURPKDP-shHURP was generated by amplifying HURP (Addgene), which was inserted into an pEGFP-C1 vector via Acc65I and BamHI. In parallel, shRNA oligonucleotides targeting HURP were created according to previously validated sequences (Wong and Fang, 2006).

The oligonucleotides were resuspended in nuclease-free water to 3 μg/μl and annealed into a double stranded DNA cassette. To anneal, 2 μl of oligonucleotides were added to 48 μl annealing buffer (100 mM NaCl, 50 mM HEPES, pH 7.4) and heated to 90°C for 4 min, 70°C for 10 min and slowly cooled to 10°C. To improve ligation efficiency with the vector, the DNA cassette was phosphorylated in a buffer containing 1 μl T4 PNK buffer, 1 μl T4 PNK, 1 μl 10 mM ATP, 1 μl T4 PNK, and 5 μl ddH_2O, incubated for 30 min at 37°C. The oligonucleotides were then ligated into pBrain-SpH (available from previous work (Royle *et al*., 2008) via BglII and HindIII. The shRNA and its associated H1 promoter were then restriction enzyme-digested and inserted into GFP-HURP via ApaLI and NheI.

A GFP-FKBP plasmid was made by inserting an FKBP fragment into pEGFP-C3 via XhoI and HindIII. The GFP-FKBP fragment from this construct was then inserted into GFP-HURP via Acc65I and BamHI to make GFP-FKBP-HURP.

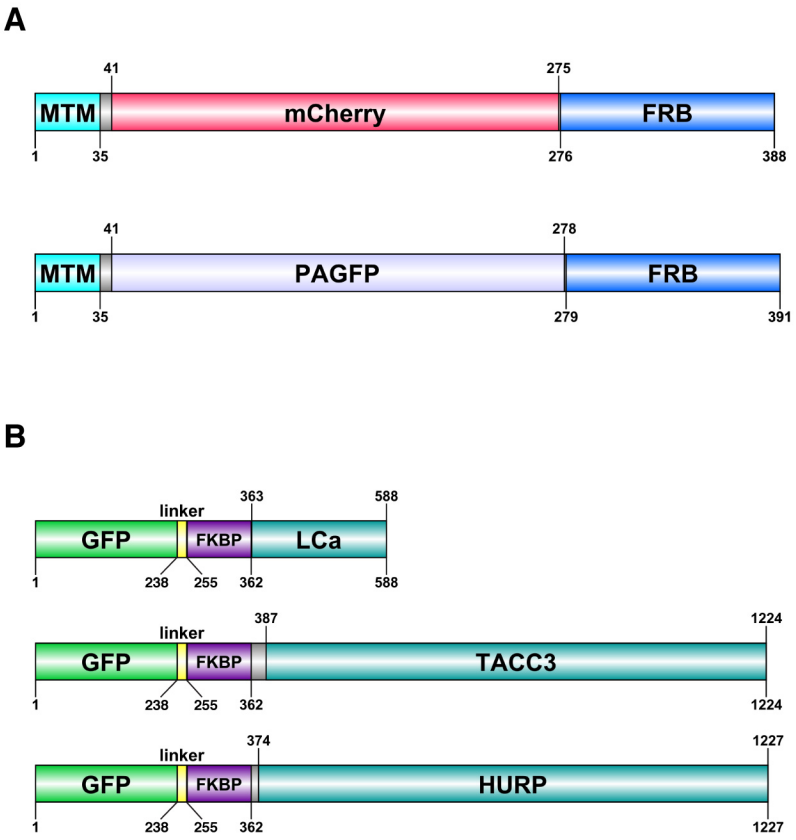

Figure 3.2: The different proteins expressed in the knocksideways experiments of this thesis. A. The MitoTrap proteins. The MitoTrap proteins contain a mitochondrion-targeting motif from Tom70p (MTM) which inserts the protein into the outer membrane of the mitochondria. A fluorescent tag (mCherry, top, or photo-activatable GFP (PAGFP), bottom) is included, followed by an FRB (FKBP and rapamycin-binding) domain. **B.** The FKBP-tagged target proteins. Three target proteins are rerouted to mitochondria in this thesis: clathrin light chain A (LCa), TACC3 and HURP. They are tagged with both a fluorescent label (here, GFP is depicted) and an FKBP domain from FKBP12 which heterodimerises with the FRB domain of MitoTrap in the presence of rapamycin. GFP and FKBP are separated by a 18 amino acid linker domain (yellow). The target proteins (LCa, top; TACC3, middle; HURP, bottom) are tagged with GFP and FKBP at their N-termini.

Silent mutations were then created in the HURP sequence of GFP-HURP and GFP-FKBP-HURP at the target region of the shRNA using site-directed mutagenesis (Wang method, adapted from a combination of Stratagene's QuikChange Site-Directed Mutagenesis Kit and Wang and Malcolm (1999)). Two tubes containing 0.5 μl (25-50 ng) of the target plasmid, 0.4 μl 25 mM dNTP, 2.5 μl DMSO, 5 μl Pfu polymerase buffer, 40 μl ddH_2O, 1 μl PfuTurbo polymerase and 0.4 μl 100 pmol/μl of either the coding or non-coding oligonucleotides primers containing the desired mutation. The tubes were then heated to 95ºC for 1 min, then underwent 10 cycles at 95ºC for 1 min, 55ºC for 1 min 30 sec, then 68ºC for 11 min. 50 μl from each tube were then mixed together, and underwent 18 cycles of the temperature sequence above. The tube was then cooled on ice and DpnI restriction enzyme with its required buffer were added to digest any strands of DNA that were not amplified by PCR.

The GFP-HURPKDP and GFP-FKBP-HURPKDP fragments from the plasmids obtained above were then transferred into pBrain-GFP-shHURP via AgeI and MfeI to create pBrain-GFP-HURPDKP-shHURP and pBrain-GFP-FKBP-HURPKDP-shHURP, respectively. A schematic diagram of the GFP-FKBP-HURP protein is presented in **Figure 3.2B**.

3.3.3.3 GFP-FKBP-LCa

GFP-LCa was available from previous work (Royle *et al*., 2005). FKBP was inserted using Acc65I/BsrGI (compatible ends) and Acc65I to create GFP-FKBP-LCa. A schematic diagram of GFP-FKBP-LCa is presented in **Figure 3.2B**.

3.3.4 Generating MitoTrap constructs

To make mCherry-MitoTrap and PAGFP-MitoTrap, the fluorescent tag in YFP-MitoTrap (gift from Margaret S. Robinson, Cambridge Institute for Medical Research, UK; called pMito-YFP-FRB in Robinson *et al*. (2010) was replaced with either mCherry from pmCherry-C1 or photo-activatable-GFP (PAGFP) from pPAGFP-C1 via AgeI and BsrGI. PAGFP-MitoTrap was used as an 'invisible' MitoTrap to make other channels available for experiments (Willox and Royle, 2012). Schematic diagrams of the MitoTrap proteins are presented in **Figure 3.2A**.

3.3.5 Fluorescence microscopy

3.3.5.1 Live cell imaging

Live cell imaging of rerouting kinetics was performed using an Olympus IX71 in heated glass-bottom dishes at 37ºC (Bioptechs Delta T5 μ-environmental culture dish controller) in CO_2-independent medium (Invitrogen) supplemented with 10% FBS and 100 units/ml penicillin/streptomycin, using Cell-R acquisition software and a Hamamatsu ORCA-ER C4742-80 camera with a 60× oil-immersion objective (1.42 NA). Quantification of GFP intensity during KS was performed using ImageJ/Fiji, with an ROI that defined the spindle and one that excluded it, and plotted as $\Delta F/F_0$.

The GFP-FKBP rerouting movie was acquired by Stephen Royle, who also performed the curve-fitting of the kinetics data for all conditions.

3.3.5.2 Immunofluorescent labeling

HeLa cells on 16 mm diameter glass coverslips were fixed with PTEMF (50 mM PIPES [1,4-Piperazinediethanesulfonic acid], 10 mM EGTA, 1 mM $MgCl_2$, 0.2% Triton X-100, 4% paraformaldehyde, pH 7.2) at room temperature for 15 min, or methanol at -20ºC for ch-TOG staining. Cells were then permeabilised using PBS with 0.5% Triton X-100 for 10 min and blocked for 1 hour using PBS with 5% BSA and 5% goat serum. The following antibodies (diluted in blocking solution) were used: (1) mouse monoclonals: clathrin heavy chain (X22, CRL-2228 ATCC; 1 in 2000), TACC3 (ab56595, Abcam; 1 in 1000), and Eg5 (611186, BD Biosciences; 1 in 500) (2) mouse polyclonal: GTSE1 (H00051512-B01P, Abnova; 1 in 100), (3) rabbit polyclonals: ch-TOG (34032, Autogen Bioclear; 1 in 1000) and β-tubulin (ab6046, Abcam; 1 in 2000), NuMA (3888s, Cell Signaling; 1 in 1000), pericentrin (ab4448, Abcam, 1 in 1000), HURP (kind gift from Erich A. Nigg, University of Basel, Switzerland; 1 in 1000). Fluorescently conjugated secondary antibodies were Alexa488, Alexa568 or Alexa633 (Molecular Probes; all used at 1 in 500). Coverslips were mounted on microscope slides using Mowiol containing 4',6-diamidino-2-phenylindole (DAPI).

3.3.5.3 Epifluorescence microscopy

Epifluorescent micrographs were taken using a Nikon Eclipse Ti-U microscope with standard filter sets for visualisation of DAPI, GFP, mCherry/Alexa Fluor 568 and Alexa Fluor 633, a Nikon Digital Sight DS-Qi1Mc camera, a 60× (1.40 NA) oil-immersion objective and NIS acquisition software.

3.3.5.4 Confocal microscopy

For TACC3 quantitation experiments, identical laser power and acquisition settings were used. Fluorescence intensity quantification was performed using ImageJ/Fiji by measuring mean pixel density in a 20×20 pixel ROI placed in the spindle region (determined using the tubulin immunolabel channel in the same cells) and background subtracted.

3.4 Results

3.4.1 The timescale and kinetics of protein rerouting by KS during mitosis

Live cell imaging of TACC3 KS was performed in HeLa cells at metaphase **(Figure 3.3A).** The removal of TACC3 from the spindle was fast, taking around 5 min (**Figure 3.3A, C**), and this was similar in clathrin rerouting experiments (**Figure 3.3B**). These results indicate that TACC3 is dynamic, cycling on and off MTs with quite a high frequency despite being in a complex with ch-TOG and clathrin.

To analyse the parameters of protein removal using KS, live cell imaging was performed on HeLa cells expressing mCherry-MitoTrap and GFP-FKBP-TACC3 or GFP-FKBP in interphase or mitosis and treated with 200 nM rapamycin. Rerouting of GFP-FKBP was extremely fast in both interphase and mitosis with almost identical kinetics ($t_{1/2}$= 3.1 and 4.2 sec, respectively; **Figure 3.4**). Interestingly, the rerouting of GFP-FKBP-TACC3 was slower than GFP-FKBP, and rerouting of GFP-FKBP-TACC3 was considerably faster during interphase compared to

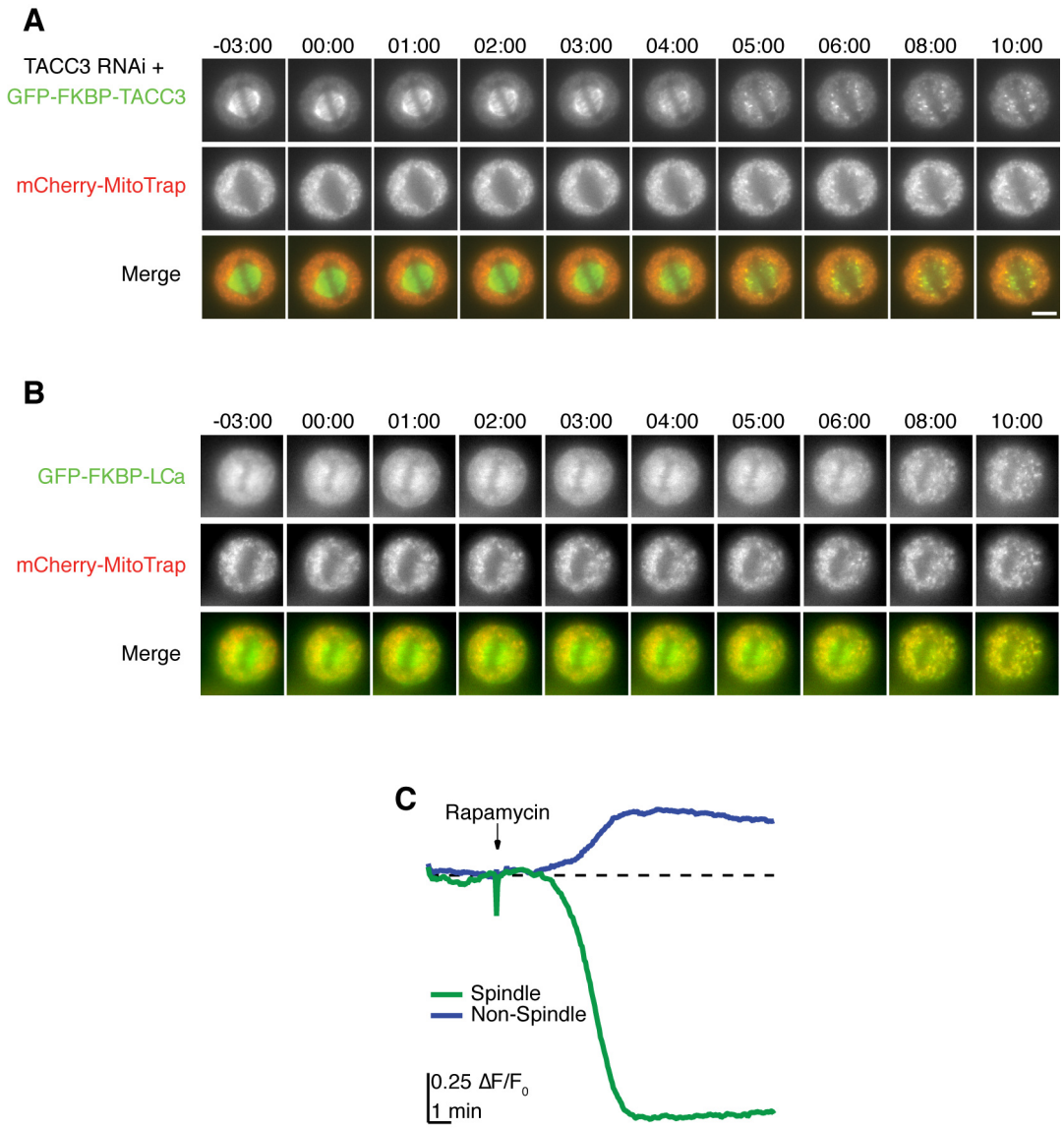

Figure 3.3: Knocksideways and timescale of spindle protein removal during mitosis. **A.** Representative video still images of a TACC3-depleted HeLa cell expressing GFP-FKBP-TACC3 and mCherry-MitoTrap. Rapamycin (200 nM) was added at t_0. GFP-FKBP-TACC3 is depleted from the spindle and co-localises with mCherry-MitoTrap. **B.** Representative video still images of a HeLa cell expressing GFP-FKBP-LCa (green) and mCherry-MitoTrap (red). Rapamycin (200 nM) was added at t_0, and GFP-FKBP-LCa is rerouted to mCherry-MitoTrap. **C.** Quantification of GFP $\Delta F/F_0$ in the indicated areas over time during TACC3 KS in **A**.

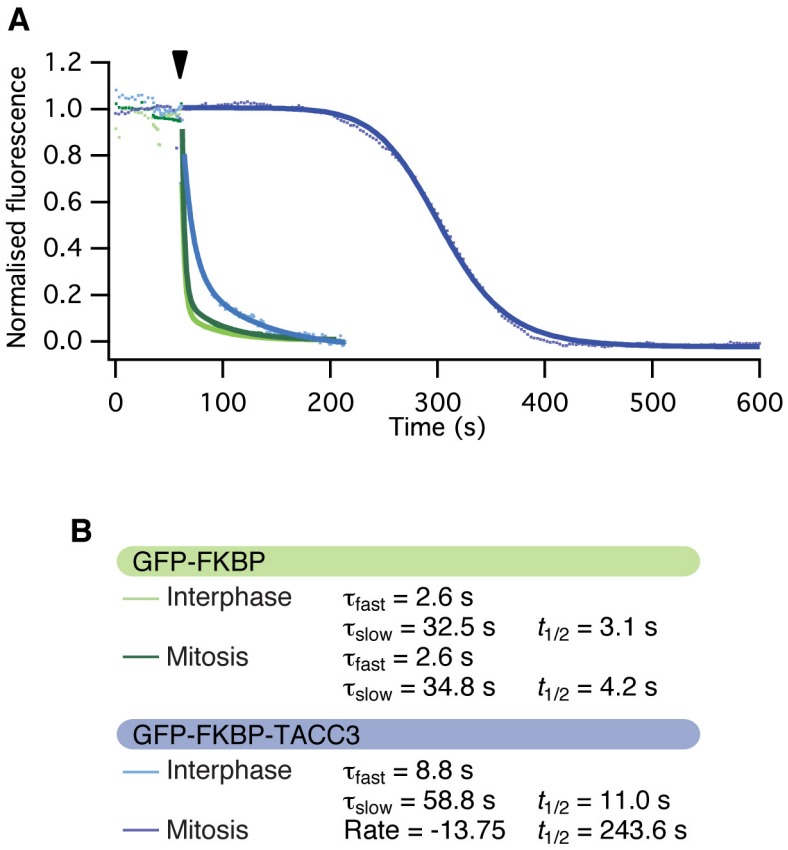

Figure 3.4: Comparing kinetics of protein rerouting by knocksideways. A. Graph of rerouting kinetics for GFP-FKBP-TACC3 (blue) or GFP-FKBP (green) to mitochondria in interphase (lighter colour) or mitosis (darker colour), single cell examples. Rapamycin (200 nM) was applied in each case (indicated by the arrowhead). An overlay of curve fits to describe the rerouting are shown on the same time scale. **B.** Description of kinetics. GFP-FKBP-TACC3 in mitosis was best fit by the Hill logistic function, all other were best fit by a double exponential function.

mitosis ($t_{1/2}$=11.0 and 243.6 sec, respectively; **Figure 3.4**). It is likely that these differences reflect the variable affinity of the target proteins for cellular substrates. Indeed, GFP is situated throughout the cell and is not known to bind any endogenous proteins in either interphase or mitosis, which may explain the very fast and similar rerouting kinetics observed in both interphase and mitosis.

TACC3 is not bound to MTs during interphase, therefore it seems likely that GFP-FKBP-TACC3 would be free in the cytosol during this stage of the cell cycle, explaining its fast rerouting to mitochondria. The considerable slowing of TACC3 rerouting during mitosis ($t_{1/2}$=243.6 sec) compared to interphase ($t_{1/2}$=11 sec) seems therefore likely to be due to MT-binding during mitosis, and dependent on the rate at which TACC3 cycles on and off the spindle.

How can the slower TACC3 rerouting in interphase compared to GFP be explained? Inducing the expression of GFP-TACC3 in interphase causes TACC3 to form aggregates in the cytosol. Although these aggregates disassemble when rapamycin is added (not shown), the slower rerouting kinetics compared to GFP-FKBP may be explained by the presence of the aggregates themselves, which could slow the release of GFP-FKBP-TACC3 located in the centres of the aggregates. Another explanation would be the difference in size between GFP (26.8kDa (Prasher *et al*., 1992)); and GFP-TACC3 (26.8 + 90 kDa; (Still *et al*., 1999)). It has previously been found that protein diffusion in the cytoplasm is a decreasing function of protein size (Arrio-Dupont *et al*., 2000).

3.4.2 Efficient protein inactivation by KS is dependent upon the cellular FKBP/FRB ratio.

It was possible to reroute both TACC3 and clathrin from mitotic spindle in HeLa cells expressing mCherry-MitoTrap and GFP-FKBP-TACC3 or GFP-FKBP-LCa within the time scale of mitosis. However, not all cells displayed full removal of the target protein from the spindle and its co-localisation with MitoTrap. Indeed, full removal was dependent on the FKBP/FRB ratio in each cell (**Figure 3.5**).

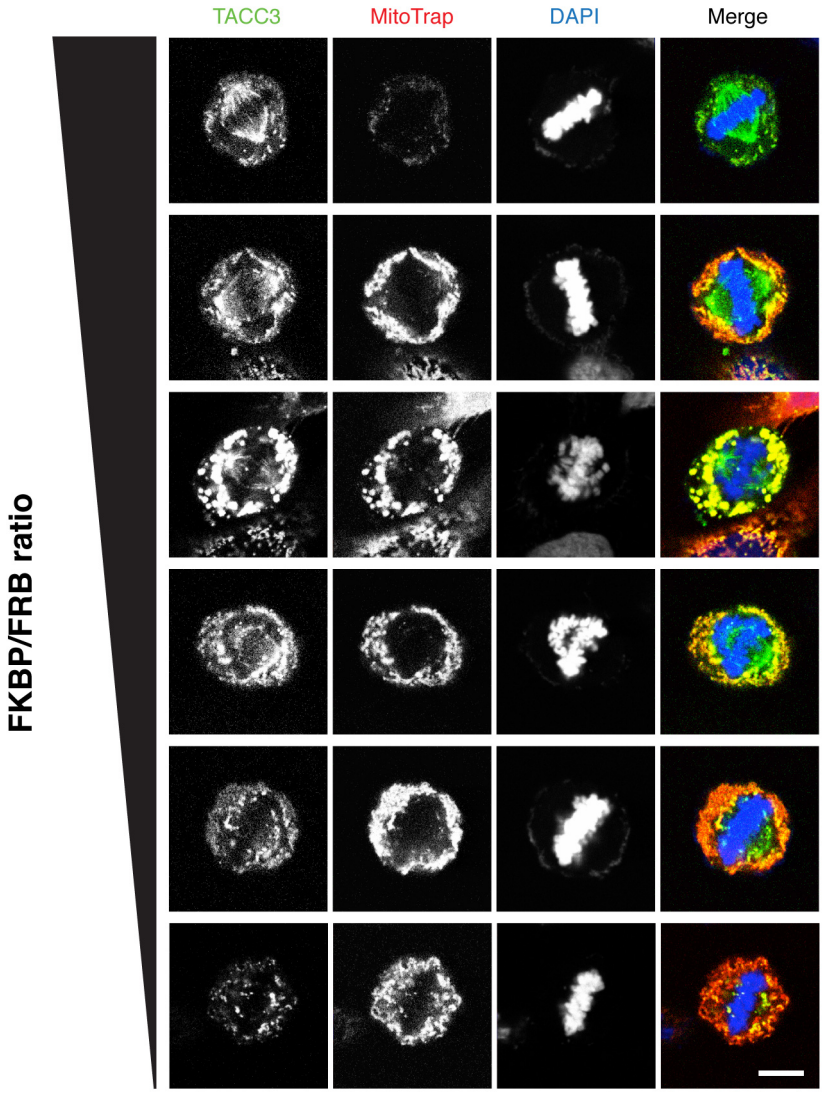

Figure 3.5: Efficient protein inactivation by knocksideways is dependent upon the cellular FKBP/FRB ratio. Confocal fluorescent micrographs of metaphase TACC3-depleted HeLa cells expressing mCherry-MitoTrap (red) and GFP-FKBP-TACC3 (green), fixed and stained with DAPI (blue). When the GFP/mCherry intensity ratio is high (top), removal of TACC3 from the mitotic spindle is incomplete. Progressing downwards through the figure, the GFP/mCherry ratio decreases (determined by eye) and TACC3 (green) is completely removed from the spindle and co-localises with the mitochondria (red). Scale bar, 10 μm.

This result is expected, as the FRB domains on the mitochondria are required to be present in excess compared to the FKBP domains, or they will become saturated before all the 'free' FKBP domains can be bound. Therefore, in all subsequent experiments, only KS cells displaying full rerouting and co-localisation of the target proteins to mitochondria were chosen for further study.

3.4.3 HURP cannot be removed from the spindle using KS within the timescale of mitosis

To investigate a different MT crosslinker candidate present in K-fibres, KS was also tried on HURP. HURP-depleted HeLa cells expressing mCherry-MitoTrap and GFP-HURP or GFP-FKBP-HURP were treated with vehicle or 200 nM rapamycin. Despite increasing the treatment duration up to 45 min, HURP was still present on the mitotic spindle in all conditions (**Figure 3.6**). Partial localisation of HURP to the mitochondria can be seen in the KS condition, but much still remains on the spindle despite strong mCherry-MitoTrap expression, indicating that HURP cannot be efficiently removed from the mitotic spindle using KS within the required timescale.

This is highly surprising, as 45 min is sufficient for the entire length of K-fibres to have depolymerised by flux several times over, signifying that GFP-FKBP-HURP would have necessarily been released from MTs and become free to bind FRB. This result would suggest that not all spindle proteins can be studied using KS. Alternatively, it is possible that the conformation of the FKBP tag may have been affected in the GFP-FKBP-HURP construct, compromising the ability of the domain to heterodimerise with FRB in presence of rapamycin. Whatever the reason, investigating HURP by KS was not pursued in subsequent experiments of this study and the experimental focus was placed on the TACC3–ch-TOG–clathrin inter-MT bridge.

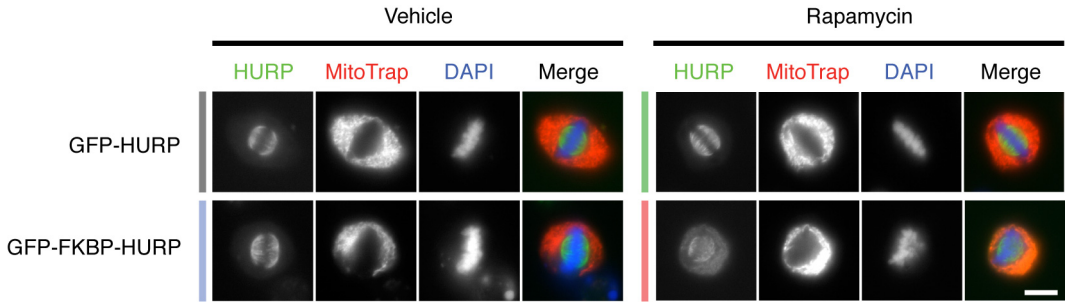

Figure 3.6: HURP cannot be fully removed from the spindle using knocksideways. Representative fluorescent micrographs of HURP-depleted HeLa expressing MitoTrap (red) and either GFP-HURP or GFP-FKBP-HURP (green) treated with vehicle or rapamycin (200 nM) for 45 minutes. Even after prolonged treatment, some HURP is still present on the mitotic spindle in the knocksideways condition (bottom right). Scale bar, 10 μm.

3.4.4 TACC3 KS does not cause disassembly of the mitotic spindle

In the previous experiment using live cell imaging (**3.4.1**), the mitotic spindle was no longer visible following TACC3 KS as no other spindle protein was labelled. It was therefore necessary to determine whether the spindle persisted following TACC3 removal, and whether its morphology was maintained. TACC3-depleted HeLa cells expressing PAGFP-MitoTrap and either GFP-TACC3 or GFP-FKBP-TACC3 were treated for 10 min with vehicle or 200 nM rapamycin, fixed and immunostained for β-tubulin (**Figure 3.7**). The spindle was still present after TACC3 KS and its overall morphology was similar. The spindle appeared smaller than controls, although more measurements were necessary to confirm whether this was the case. In either case, it was evident that TACC3 KS did not drastically affect the gross morphology of the mitotic spindle after 10 min.

3.4.5 TACC3 KS also removes TACC3 without an FKBP tag

There is evidence to suggest that TACC3 forms dimers under normal cellular conditions (unpublished results). Because of this possibility, it was of interest to determine whether GFP-FKBP-TACC3 could dimerise with endogenous TACC3 that may remain after RNAi-mediated TACC3 depletion.

TACC3-depleted HeLa cells expressing PAGFP-MitoTrap, mCherry-TACC3 and either GFP-TACC3 or GFP-FKBP-TACC3 were treated with vehicle or 200 nM rapamycin for 10 min. Both GFP-FKBP-TACC3 and mCherry-TACC3 were completely removed from the mitotic spindle and localised together to puncta in the cytosol consistent with mitochondria (**Figure 3.8**). This result indicates that TACC3 does indeed exist as a polymer, though whether it dimerises remains undetermined.

3.4.6 TACC3 KS removes TACC3 from the mitotic spindle more effectively than RNAi or Aurora A kinase inhibition

Since TACC3 KS also removed TACC3 untagged with FKBP, the efficiency of TACC3 removal by various methods was compared. TACC3 has previously been shown to require Aurora A kinase phosphorylation on serine 558 to localise to MTs

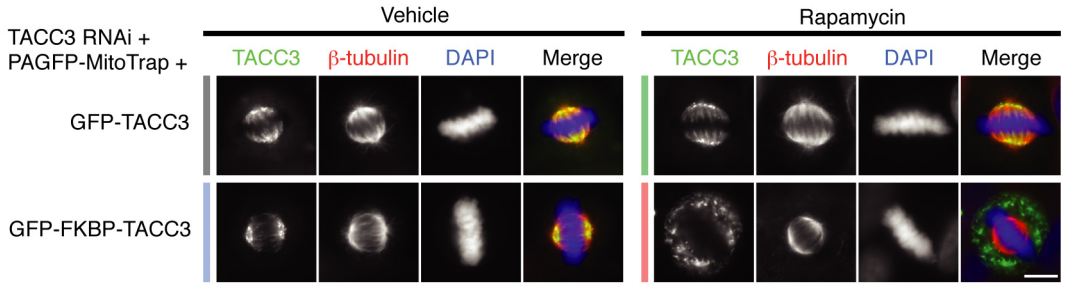

Figure 3.7: TACC3 KS does not cause disassembly of the mitotic spindle. Representative fluorescent micrographs of HeLa depleted of endogenous TACC3 and expressing PAGFP-MitoTrap (not visible) and either GFP-TACC3 or GFP-FKBP-TACC3 (green) treated with vehicle or rapamycin for 10 minutes, fixed and immunolabelled for β-tubulin (red). Scale bar, 10 μm.

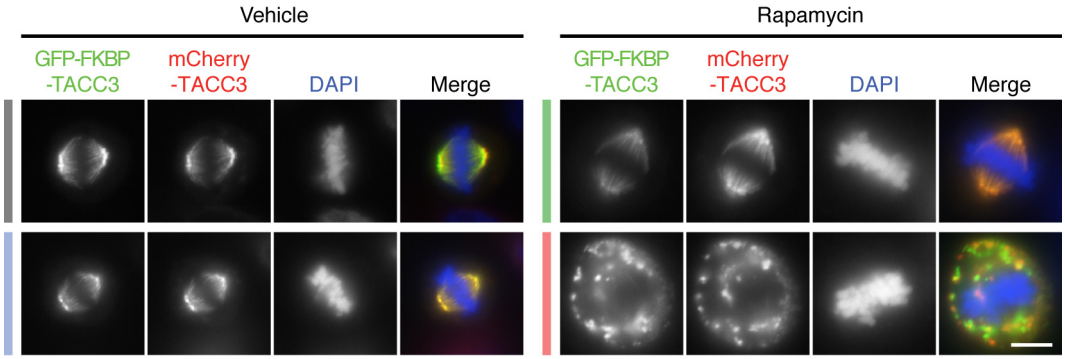

Figure 3.8: TACC3 KS also reroutes TACC3 molecules without an FKBP tag. Representative fluorescent micrographs of TACC3-depleted HeLa expressing PAGFP-MitoTrap (not visible), mCherry-TACC3 (red) and either GFP-TACC3 or GFP-FKBP-TACC3 (green) treated with vehicle or rapamycin (200 nM) for 10 min, fixed and stained with DAPI (blue). mCherry-TACC3 (without an FKBP domain) is also removed in the TACC3 KS condition (bottom right). Scale bar, 10 μm.

(Kinoshita *et al*., 2005; Leroy *et al*., 2007; Fu *et al*., 2010; Lin *et al*., 2010; Booth *et al*., 2011), and inhibition of Aurora A by MLN8237 (also called Alisertib) stopped TACC3 binding to the spindle very effectively within 30 min (Booth *et al*., 2011). Therefore, TACC3 KS and its associated control conditions were compared with cells treated with 1 μM MLN8237 or vehicle for 30 min, and cells expressing GFP and control or TACC3 RNAi, or expressing GFP-TACC3 with no RNAi. The cells were then fixed and immunostained for TACC3 (**Figure 3.9A**). Immunolabel intensity on the spindle or in the cytosolic region of the cells was quantified by confocal microscopy.

MLN8237 treatment significantly disrupted spindle morphology, reduced TACC3 staining on the spindle and increased staining in the cytosol ($p<0.001$; **Figure 3.9A, B**). TACC3 RNAi also significantly reduced TACC3 signal in the spindle region compared to DMSO-treated cells ($p<0.001$) whereas control RNAi did not (**Figure 3.9B**). GFP-TACC3 expression alone significantly increased TACC3 levels both on the mitotic spindle and in the cytosol compared to DMSO control ($p<0.001$, **Figure 3.9B**). In TACC3 KS cells, TACC3 signal in the spindle region was considerably lower than in KS control conditions; in fact, spindle TACC3 intensity was lower than in MLN8237- and TACC3 RNAi-treated cells (**Figure 3.9B**). In contrast, TACC3 levels in the cytosolic region were greatly increased compared to all other conditions, as expected since TACC3 relocates to mitochondria during KS.

Importantly, this experiment also shows that the reexpression of TACC3 in the KS control conditions following selection by the experimenter produced near-endogenous levels of TACC3, and did not overexpress the protein as can be seen in cells expressing GFP-TACC3 without RNAi (**Figure 3.9B**).

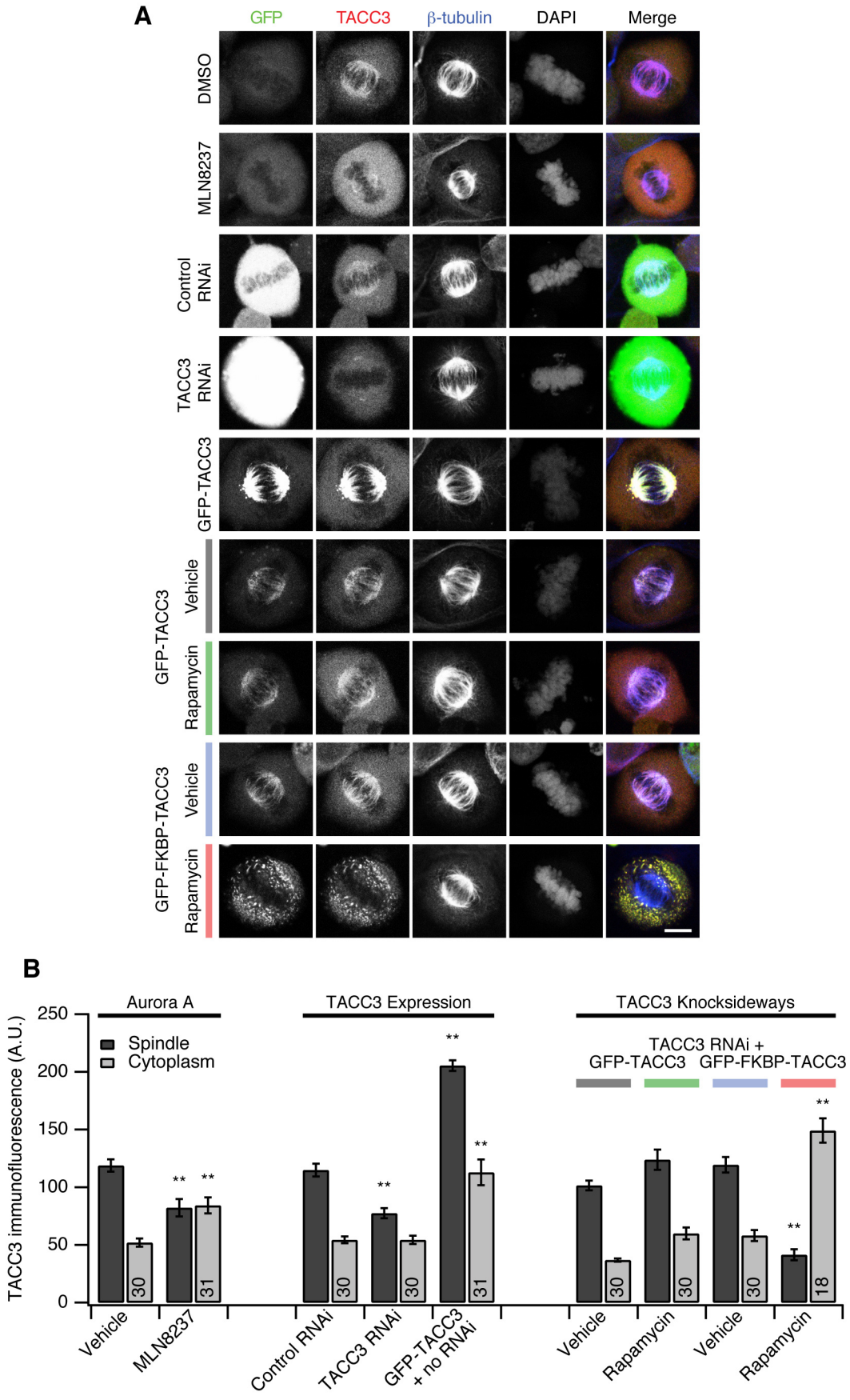
A
GFP
TACC3
β-tubulin
DAPI
Merge
DMSO
MLN8237
Control RNAi
TACC3 RNAi
GFP-TACC3
GFP-TACC3
Vehicle
Rapamycin
GFP-FKBP-TACC3
Vehicle
Rapamycin
B
Aurora A
TACC3 Expression
TACC3 Knocksideways
Spindle
Cytoplasm
TACC3 RNAi +
GFP-TACC3 GFP-FKBP-TACC3
TACC3 immunofluorescence (A.U.)
250
200
150
100
50
0
**
30
31
18
Vehicle
MLN8237
Control RNAi
TACC3 RNAi
GFP-TACC3 + no RNAi
Vehicle
Rapamycin
Vehicle
Rapamycin

Figure 3.9: TACC3 KS removes TACC3 from mitotic spindle more efficiently than Aurora A kinase inhibition or RNAi. A. Representative confocal micrographs of HeLa, fixed and immunolabelled for TACC3 and β-tubulin following the indicated treatments. Aurora-A inhibition: using MLN8237 (1 μM, 30 min) or vehicle (DMSO). TACC3 expression: control RNAi + GFP, TACC3 RNAi + GFP, GFP-TACC3 expression in normal cells (no RNAi). TACC3 KS: TACC3 RNAi + PAGFP-MitoTrap + GFP-TACC3 or GFP-FKBP-TACC3; treated for 30 min with vehicle or rapamycin (200 nM). Scale bar, 10 μm. **B.** Bar chart of the quantification of TACC3 in the various experimental conditions in **A**. Mean ± s.e.m. for spindle regions and cytoplasm. N_{cell} = 18-31 as indicated from two experiments. **, $p < 0.001$ compared to vehicle (far left) values, one-way ANOVA with Tukey-Kramer *post hoc* test.

3.4.7 TACC3 KS removes ch-TOG, clathrin and GTSE1 from the mitotic spindle

After determining that the spindle structure was still present after TACC3 rerouting and that KS is an effective method for depleting TACC3 from the spindle, it was important to find out what effect this removal had on other spindle proteins.

TACC3-depleted HeLa cells expressing PAGFP-MitoTrap and either GFP-TACC3 or GFP-FKBP-TACC3 were treated with vehicle or 200 nM rapamycin for 10 min or 30 min, fixed and immunostained for various spindle components (**Figure 3.10**, **Figure 3.11**).

To determine acute effects of TACC3 rerouting, GFP-FKBP-TACC3 cells treated with vehicle or rapamycin for 10 min were imaged by confocal microscopy (**Figure 3.10**). Both clathrin heavy chain (CHC) and ch-TOG were found to be depleted from the mitotic spindle following TACC3 KS compared to control cells. Importantly, both CHC and ch-TOG co-localised with TACC3 at mitochondria, suggesting that TACC3 KS causes rerouting of the complete TACC3–ch-TOG–clathrin complex. Interestingly, some ch-TOG staining was still present on the centrosomes even when TACC3 KS was complete (**Figure 3.11A, B**), suggesting the existence of a TACC3-independent subpopulation of ch-TOG, which may also be functionally separate. This observation is in agreement with previous reports (Gergely *et al*., 2003; Cassimeris *et al*., 2009; Booth *et al*., 2011).

GTSE1 (G2 and S phase expressed protein 1), a protein reported by one study to be part of the TACC3–ch-TOG–clathrin complex (Hubner *et al*., 2010) was found to also be depleted from the spindle following TACC3 KS compared to control cells, although it was difficult to determine whether it co-rerouted to mitochondria (**Figure 3.10**).

Eg5, NuMA and HURP are MT crosslinkers that localise to different areas of the mitotic spindle (Eg5, all the spindle; NuMA, spindle poles; HURP, K-fibres in proximity to chromosomes) and all require Aurora A kinase phosphorylation for

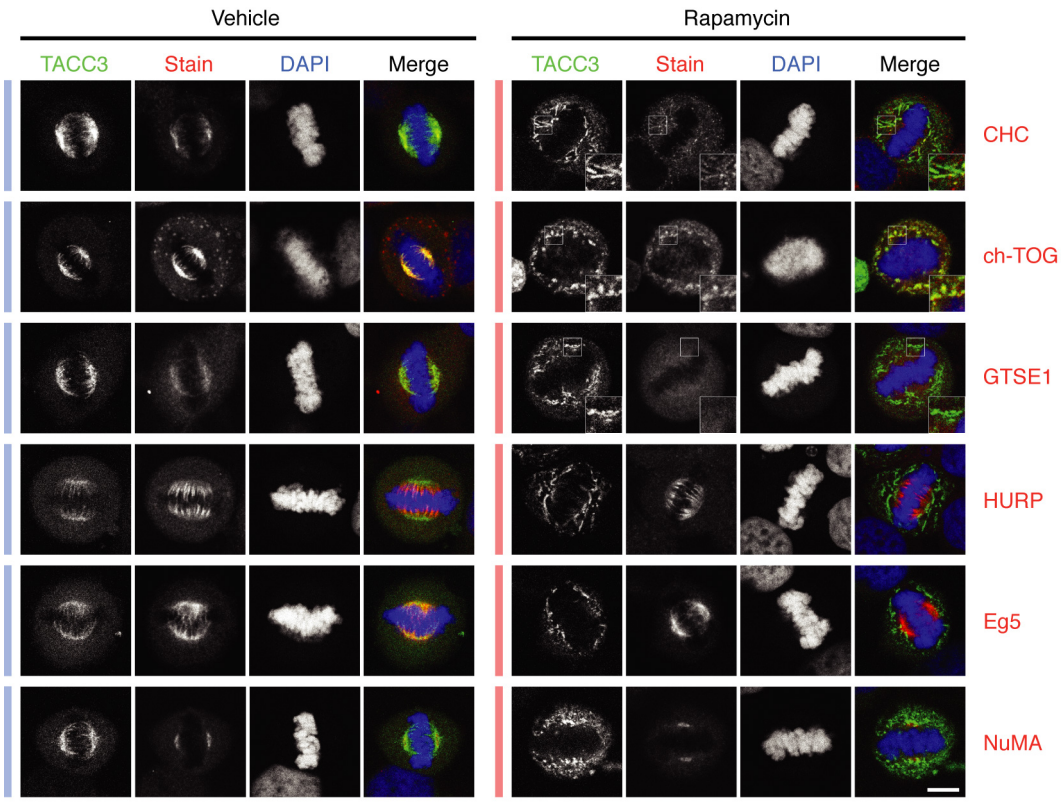

Figure 3.10: TACC3 KS removes ch-TOG, clathrin and GTSE1 from the spindle without affecting other spindle proteins. Representative confocal micrographs of TACC3-depleted HeLa cells at metaphase expressing GFP-FKBP-TACC3 (green) and PAGFP-MitoTrap (not visible) that were treated with vehicle or rapamycin (200 nM) for 10 min, fixed and immunolabelled for the indicated proteins (red). TACC3 KS removed ch-TOG, clathrin heavy chain (CHC) and GTSE1 from the spindle. NuMA, HURP and Eg5 were unaffected by TACC3 KS. Scale bar, 10 μm. Zoomed areas show the co-localisation of proteins at mitochondria following TACC3 KS. See **Fig 3.9** for full results.

their activity similarly to TACC3 (Giet *et al*., 1999; Yu *et al*., 2005; Kettenbach *et al*., 2011). These proteins were unaffected by TACC3 KS, indicating that TACC3rerouting did not affect other spindle proteins, nor did it affect the activity of its interacting kinase Aurora A. To test all experimental conditions of TACC3 KS (with all 3 control types) and also to test whether prolonged TACC3 removal would effectually lead to spindle defects, the same experiment was performed using all KS conditions (GFP-TACC3 or GFP-FKBP-TACC3 treated with vehicle or rapamycin) both 10 and 30 min post-treatment (**Figure 3.11**). No significant differences were seen compared to the previous experiment (**Figure 3.10**), and no alteration of other spindle proteins (tubulin, Eg5, NuMA, HURP) were observed even after 30 min TACC3 KS. Altogether, these results indicate that TACC3 KS is a rapid and specific method to remove the entire TACC3–ch-TOG–clathrin complex.

3.4.8 Clathrin rerouting is equivalent to, but not as efficient as TACC3 KS

In order to perform TACC3 KS, endogenous TACC3 must first be depleted in cells using RNAi. In the case of CHC, shown to be a key part of the TACC3–ch-TOG–clathrin complex, this depletion is difficult in HeLa cells because the high abundance of the protein requires around 5 days of RNAi to achieve a sufficient knockdown. However, this depletion could be rendered unnecessary by expression of an FKBP-tagged clathrin light chain A (LCa). Similarly to the GFP tag in GFP-LCa, the FKBP tag would be incorporated into newly synthesised clathrin triskelia in GFP-FKBP-LCa. In theory, a single FKBP-tagged LCa protein should be sufficient to trap a whole triskelion on MitoTrap, avoiding the need for RNAi. This clathrin rerouting method was therefore tested for comparison with TACC3 KS.

HeLa cells expressing PAGFP-MitoTrap and GFP-LCa or GFP-FKBP-LCa were treated with vehicle or 200 nM rapamycin for 10 or 30 min, fixed and immunostained for various spindle proteins (**Figure 3.12**). LCa rerouting was found to also reroute CHC, indicating that GFP-

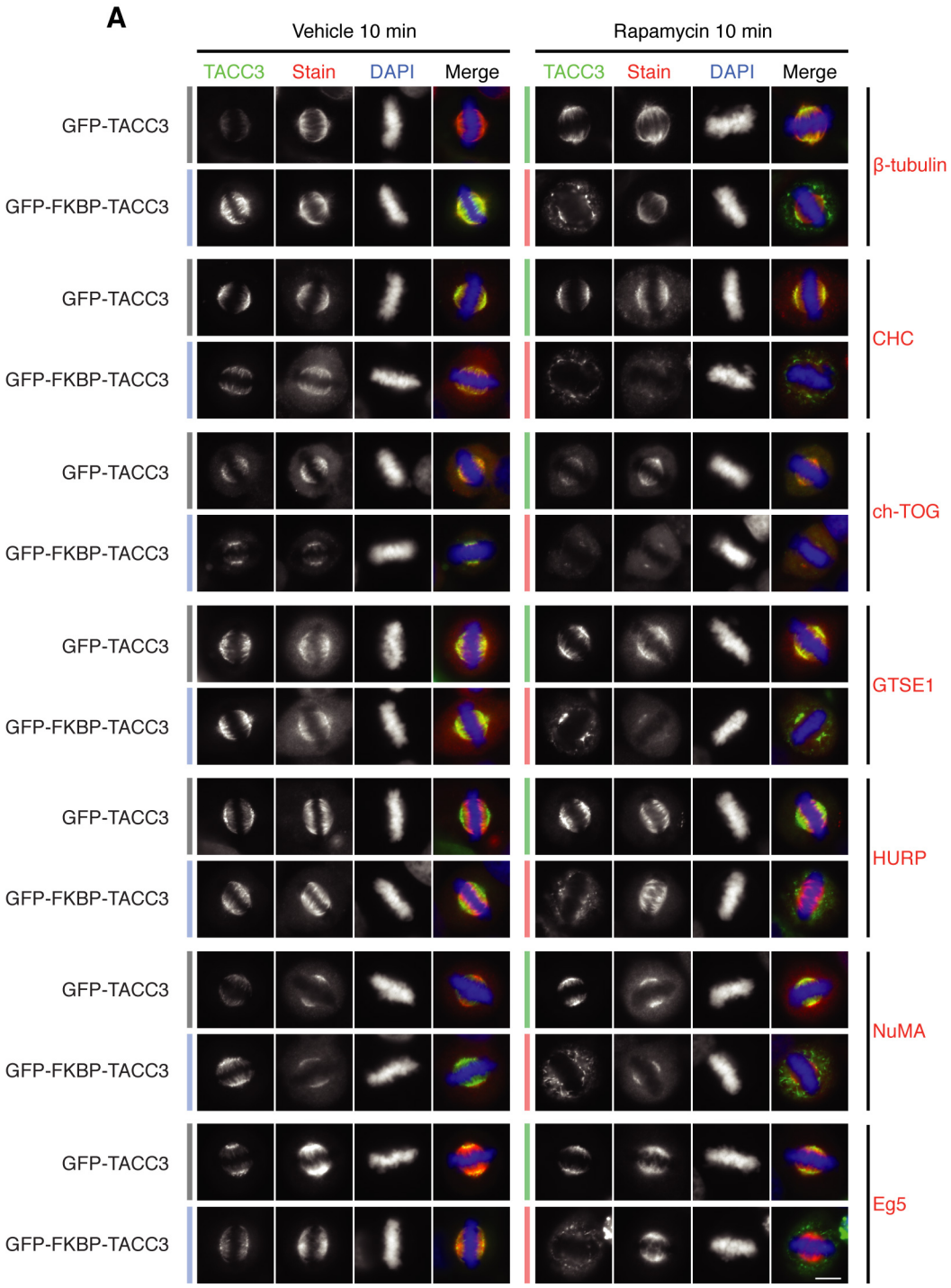
A
Vehicle 10 min
Rapamycin 10 min
TACC3
Stain
DAPI
Merge
GFP-TACC3
GFP-FKBP-TACC3
β-tubulin
CHC
ch-TOG
GTSE1
HURP
NuMA
Eg5

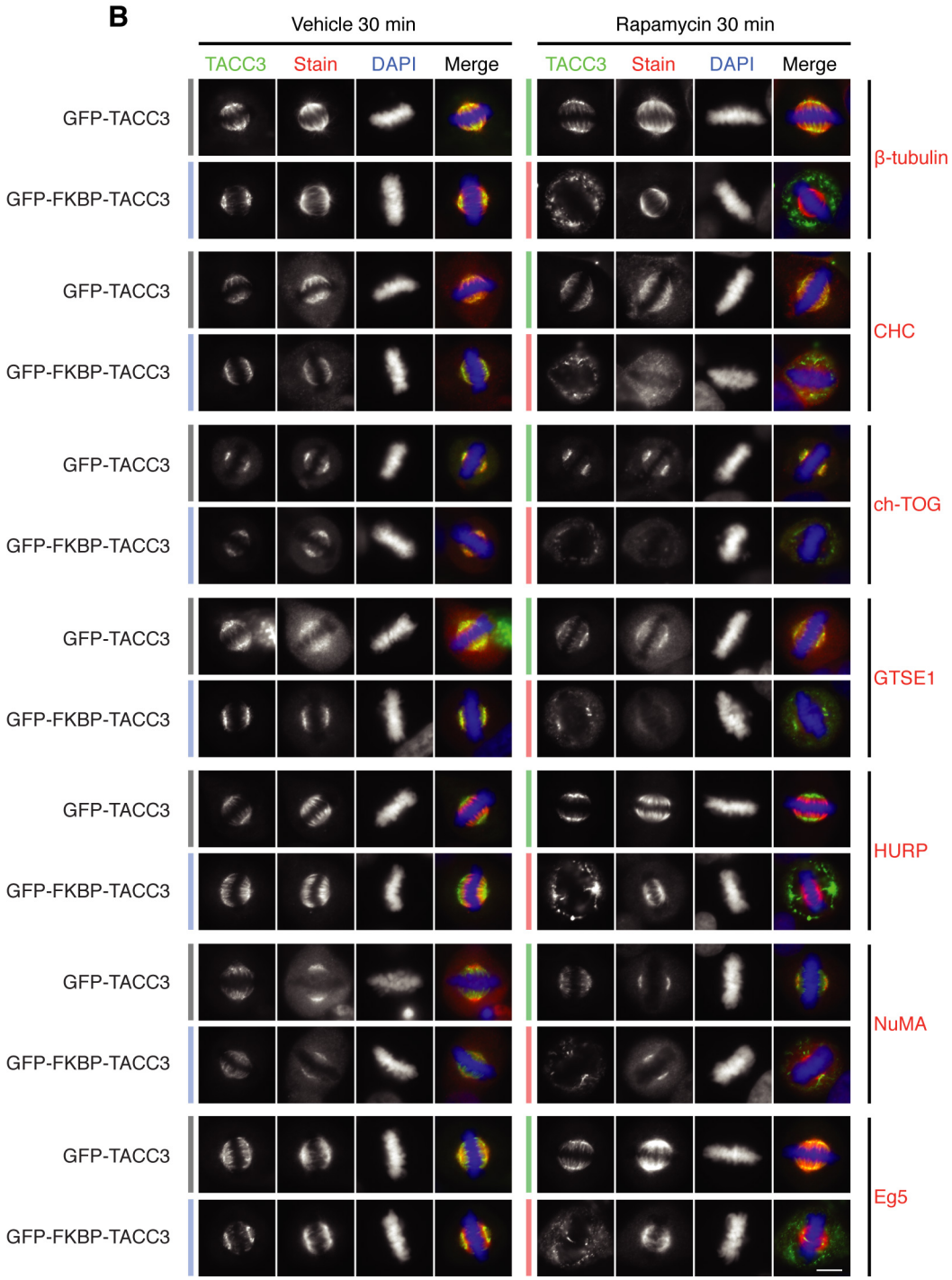
B
Vehicle 30 min
Rapamycin 30 min
TACC3
Stain
DAPI
Merge
TACC3
Stain
DAPI
Merge
GFP-TACC3
GFP-FKBP-TACC3
β-tubulin
GFP-TACC3
GFP-FKBP-TACC3
CHC
GFP-TACC3
GFP-FKBP-TACC3
ch-TOG
GFP-TACC3
GFP-FKBP-TACC3
GTSE1
GFP-TACC3
GFP-FKBP-TACC3
HURP
GFP-TACC3
GFP-FKBP-TACC3
NuMA
GFP-TACC3
GFP-FKBP-TACC3
Eg5

Figure 3.11: TACC3 KS removes ch-TOG, clathrin and GTSE1 from the spindle without affecting other spindle proteins, even after prolonged removal. **A-B.** Representative fluorescent micrographs of TACC3-depleted HeLa cells at metaphase expressing PAGFP-MitoTrap (not visible) and GFP-TACC3 or GFP-FKBP-TACC3 (green) that were treated with vehicle or rapamycin (200 nM) for 10 min (**A**) or 30 min (**B**), fixed and immunolabelled for the indicated proteins (red). TACC3 KS removed ch-TOG, clathrin heavy chain (CHC) and GTSE1 from the spindle. NuMA, HURP and Eg5 were unaffected by TACC3 KS. Scale bar, 10 μm.

FKPB-LCa was indeed incorporated into newly synthesised triskelia. Similarly to TACC3 KS, GFP-FKBP-LCa co-rerouted its interacting partners TACC3 and ch-TOG in presence of rapamycin and also frequently left a pool of ch-TOG on the centrosomes (**Figure 3.12A, B**).

GTSE1 was also found to be depleted from mitotic spindles, and could be observed on the mitochondria more clearly than in TACC3 KS experiments (**Figure 3.12A**). It is difficult to tell whether this is a genuine effect of rerouting clathrin rather than TACC3, as the GTSE1 antibody used in this study did not produce consistent results. Similarly to TACC3 KS, Eg5, HURP and NuMA were unaffected by clathrin rerouting. Furthermore, drug treatment for 30 min did not produce any further effects compared to the 10 min timepoint (**Figure 3.12B**)

However, one noticeable difference in clathrin rerouting experiments compared to TACC3 KS is that in some cells, the efficient co-rerouting of TACC3, ch-TOG and CHC was not always complete. Indeed, spindle staining could be seen in some cases (see, for example, TACC3 staining in **Figure 3.12A**) indicating that co-rerouting was not efficient. The likely cause of this discrepancy is the high relative abundance of clathrin compared to TACC3 as previously mentioned, thus producing higher FKBP/FRB cellular ratios (see **3.4.2**) and saturated MitoTrap proteins, hindering the binding of the entire cellular pool of clathrin. Therefore, TACC3 KS was favoured compared to clathrin rerouting in subsequent experiments.

3.4.9 No evidence for clathrin-dependent TACC3 on spindle MTs or centrosomes

Protein co-rerouting is potentially a useful tool to study protein interactions. Since TACC3 and ch-TOG were found in complex with clathrin on the mitotic spindle (Fu *et al*., 2010; Hubner *et al*., 2010; Lin *et al*., 2010; Booth *et al*., 2011), one particular question that has been asked is whether TACC3 and ch-TOG exist separately from clathrin during mitosis as they are thought to be involved in MT nucleation and spindle assembly (Gergely *et al*., 2003). Results in **3.4.7** and **3.4.8** have shown the existence of a TACC3- and clathrin-independent pool of ch-TOG, which has been

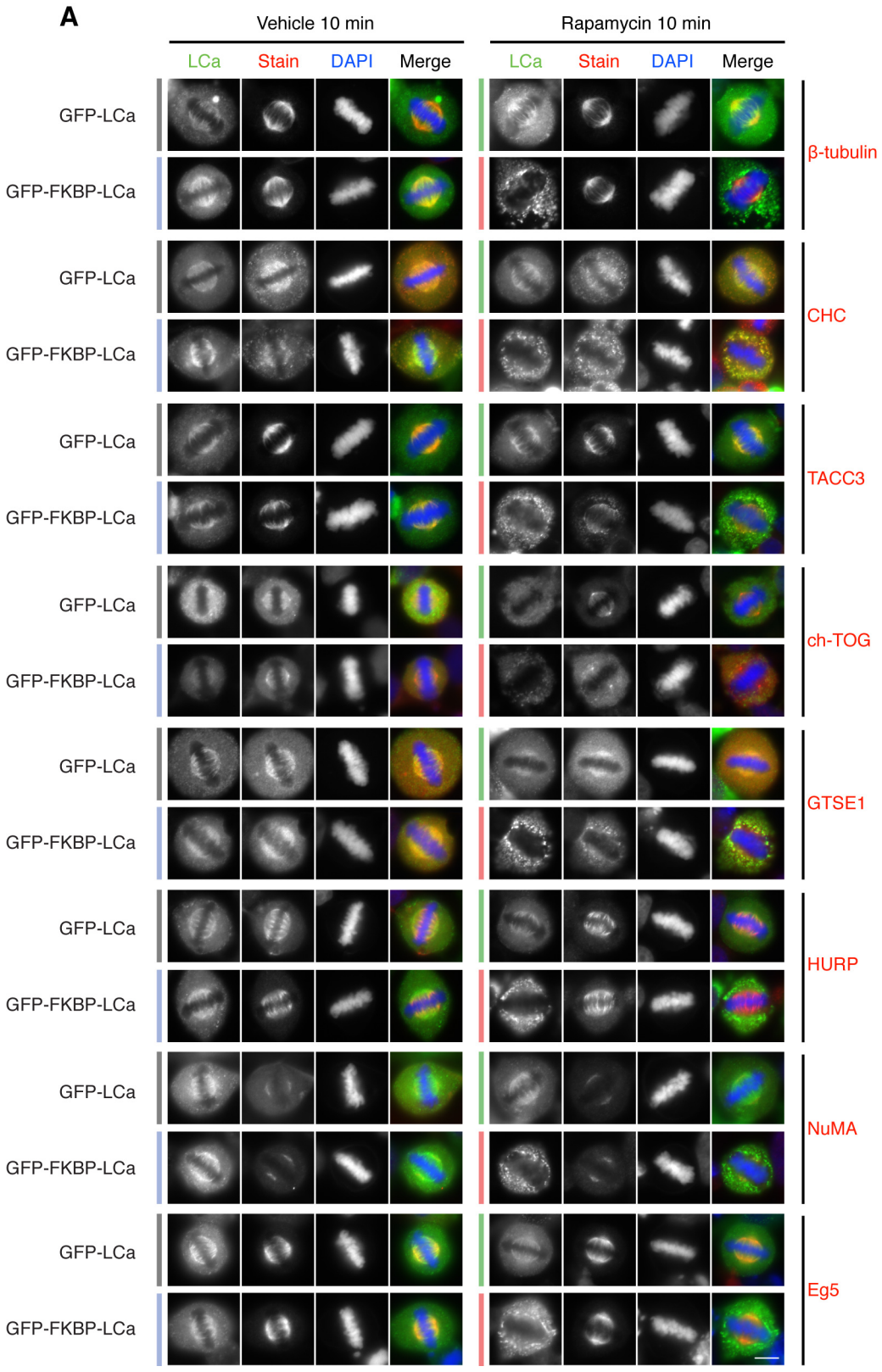
A
Vehicle 10 min
Rapamycin 10 min
LCa
Stain
DAPI
Merge
GFP-LCa
GFP-FKBP-LCa
β-tubulin
CHC
TACC3
ch-TOG
GTSE1
HURP
NuMA
Eg5

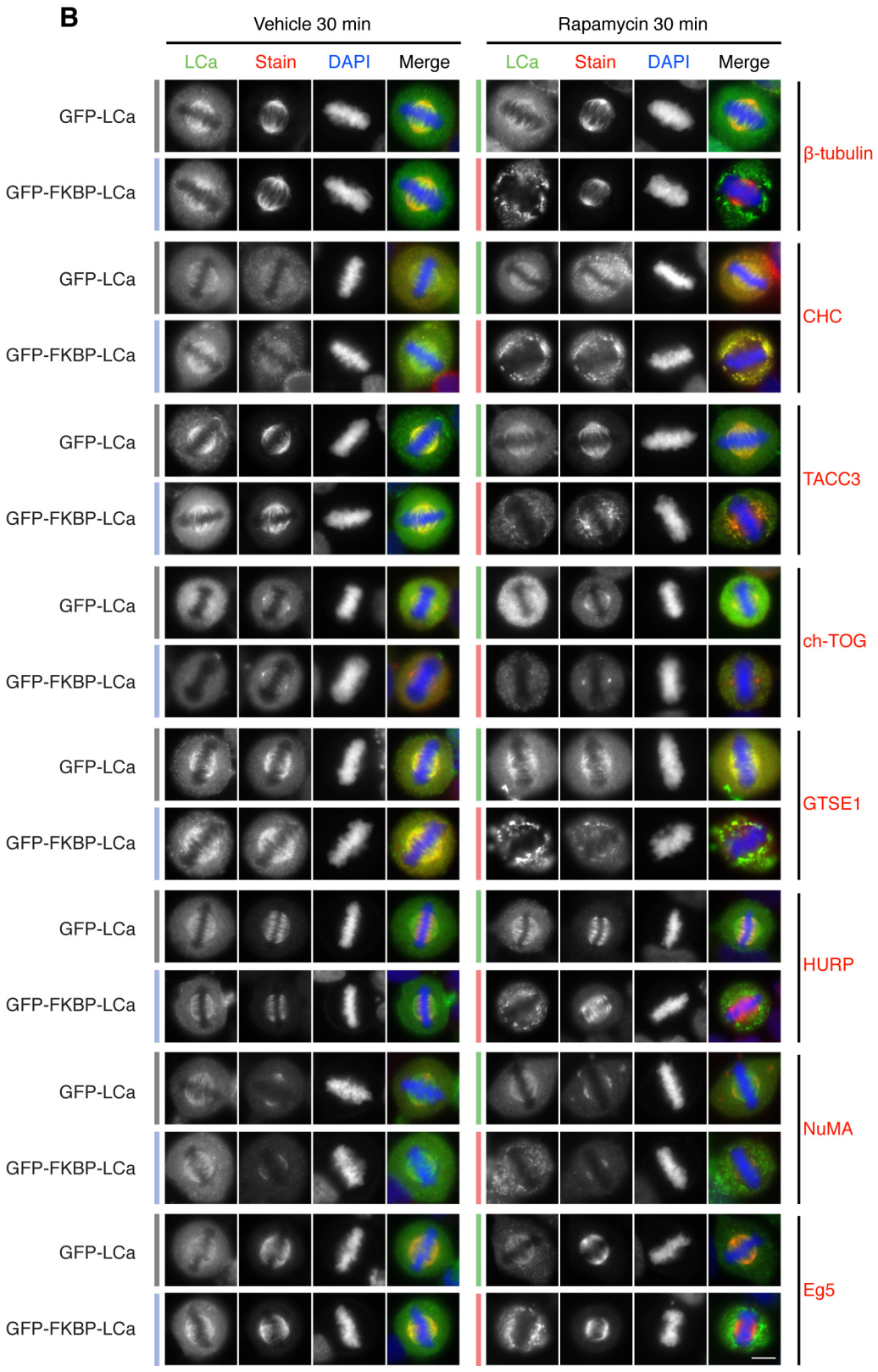
B
Vehicle 30 min
Rapamycin 30 min
LCa
Stain
DAPI
Merge
GFP-LCa
GFP-FKBP-LCa
β-tubulin
CHC
TACC3
ch-TOG
GTSE1
HURP
NuMA
Eg5

Figure 3.12: Effect of clathrin rerouting at metaphase on other spindle proteins. Representative fluorescent micrographs of HeLa cells at metaphase expressing PAGFP-MitoTrap (not visible) and either GFP-LCa or GFP-FKBP-LCa and treated with vehicle or rapamycin (200 nM) for 10 min (**A**) or 30 min (**B**), fixed and immunostained for other spindle proteins (red). LCa rerouting also removed clathrin heavy chain (CHC), ch-TOG, TACC3 and GTSE1 from the spindle. Tubulin, HURP, NuMA and Eg5 were unaltered after 10 and 30 min rapamycin application, indicating that removal of TACC3-ch-TOG-clathrin complexes by LCa rerouting did not alter the localisation or function of other spindle proteins. Scale bar, 10 μm.

previously reported (Gergely *et al*., 2003; Cassimeris *et al*., 2009; Booth *et al*., 2011). Using cells in which clathrin rerouting was complete, we could investigate whether total co-rerouting of TACC3 was observed. HeLa cells expressing PAGFP-MitoTrap and GFP-FKBP-LCa were treated with vehicle or 200 nM rapamycin for 10 min, fixed and immunostained for TACC3 and pericentrin. Cells at metaphase or in early prometaphase were imaged by confocal microscopy (**Figure 3.13**). In cells where clathrin rerouting was complete, TACC3 was not observed in the spindle region, and was absent from centrosomes in both prometaphase and metaphase. Although TACC3 staining could be seen in puncta in close proximity to centrosomes (**Figure 3.13**, 3rd row from top), these did not co-localise with pericentrin. Rather, these structures are likely to be mitochondria frequently seen around spindle poles in other experiments (for example, see **Figure 3.5**). These results indicate that although ch-TOG forms a clathrin- and TACC3-independent subpopulation at the spindle poles, there is no clathrin-independent TACC3 on the mitotic spindle or centrosomes, even at early mitosis.

3.5 Discussion

Knocksideways has been shown here to be a valid tool for the study of acute and specific protein removal from mitotic spindles within the timescale of mitosis, while bypassing disadvantages of other protein depletion methods.

RNAi is the most commonly used protein depletion method, however it is slow, typically requiring 48-72 hours for efficient depletion. When used to study mitotic proteins, this can be problematic as the cell can accumulate defects in the cell cycles undergone during the gradual depletion period. In addition, the cell may be able to compensate for the depleted protein, which may lead to the underestimation of the depletion phenotype; this may explain the striking discrepancies between RNAi-mediated depletion of AP-1 versus KS of AP-1 in another study (Hirst *et al*., 2012). Finally, if the depleted protein is involved in spindle assembly, studying the protein's role at later stages (such as metaphase or anaphase) can be difficult because defects in spindle assembly can confound the phenotype seen at later stages. In other words,

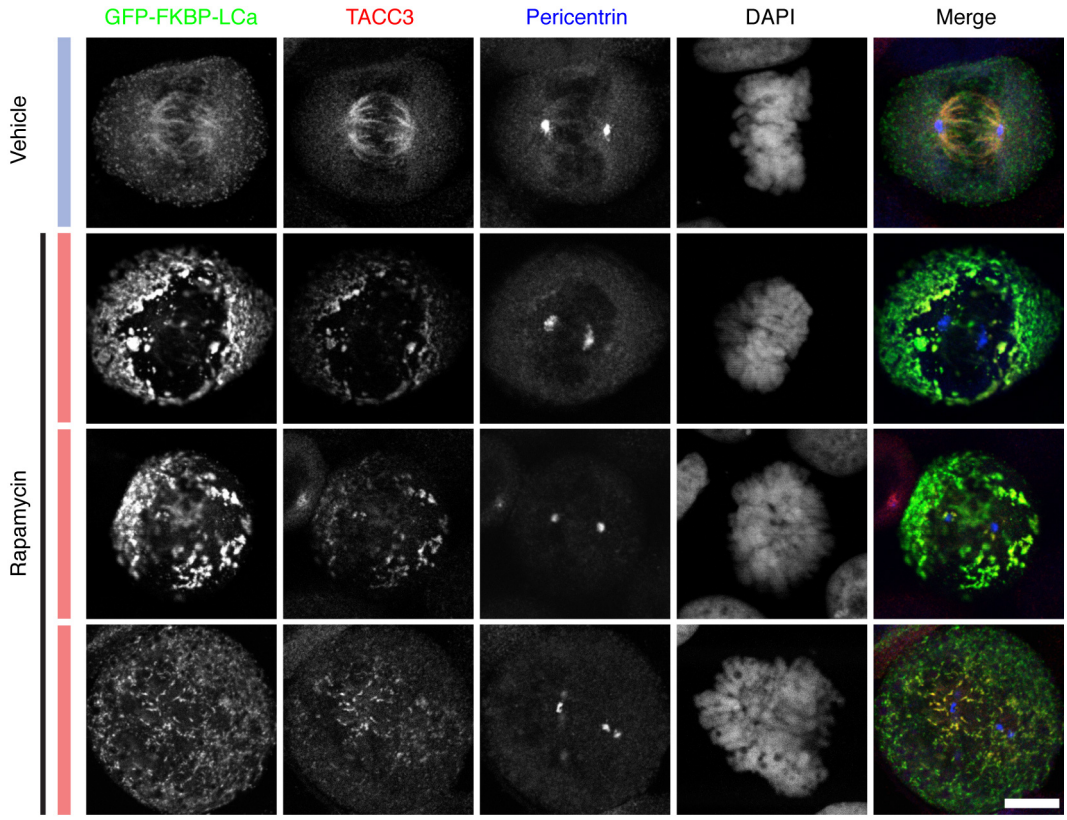

Figure 3.13: No evidence for clathrin-independent TACC3 on spindle microtubules or centrosomes. Representative confocal micrographs of HeLa expressing GFP-FKBP-LCa (green) and PAGFP-MitoTrap (not visible) and treated with vehicle or rapamycin (200 nM) for 10 minutes. Treated cells were fixed and immunostained for TACC3 (red) and pericentrin (blue). Note the complete co-localisation of clathrin and TACC3 and the lack of TACC3 on spindle microtubules and centrosomes. Scale bar, 10 μm.

is the phenotype observed due to the absence of the protein at that stage, or is it a by-product of defective spindle assembly? Fast depletion methods can resolve some of these issues. As shown in **3.4.6**, Aurora A kinase inhibition by MLN8237 is a fast method to deplete spindle proteins and has the additional advantage of being reversible in many cases by washing the cells. However, as can be seen in **Figure 3.9**, the morphology of mitotic spindle is drastically affected by the treatment. This is most likely because inhibition of Aurora A will affect many substrates and not only TACC3. As mentioned in **3.4.7**, Eg5, NuMA and HURP are examples of other spindle proteins that rely on Aurora A phosphorylation for their activity (Giet *et al*., 1999; Yu *et al*., 2005; Kettenbach *et al*., 2011). This result is in agreement with results from a previous study (Cheeseman *et al*., 2011). Therefore, such inhibitor drugs are too broad acting to perform targeted protein studies. Other, more specific drugs such as monastrol to inhibit Eg5 are more targeted, however their effects are not always suited to the experiment. For instance, monastrol inhibits Eg5 activity, but does not affect protein binding (Kapoor *et al*., 2000). It is therefore unsuitable to study the effects of the crosslinking function of Eg5.

Perhaps the most precise method is the auxin-degron system, which allows the inducible degradation of a protein of interest (Nishimura *et al*., 2009). Similarly to KS, it requires the depletion of the endogenous protein of interest and the reexpression of the protein tagged with an Aid degron (IAA17 from *Arabidopsis thaliana*), which is targeted for degradation in the presence of auxin (Nishimura *et al*., 2009). The degradation of the protein is a more definitive manner of inactivating a protein than the subcellular sequestering used in KS experiments, and may be better suited for signalling proteins on the spindle such as proteins of the spindle checkpoint. Although the auxin-degron method has been used for mitotic proteins (Holland *et al*., 2012; Nishino *et al*., 2013), the timescale of protein inactivation is slower than KS, usually taking at least 30 minutes and up to 100 minutes for some target proteins (Holland *et al*., 2012). This timescale would be ill suited for studying proteins during very short mitotic stage, for instance metaphase or anaphase, which last under 15 min.

Therefore, it appears that KS is the best-suited method for studying the effects of rapid depletion of structural proteins from the mitotic spindle within the timescale of short mitotic stages. However, KS did not allow for the removal of HURP (**3.4.3**).

Although it cannot be ruled out that the functionality of the FKBP tag was affected by the tertiary structure of the protein, it is more likely that it is due to the strong affinity of HURP for MTs as shown in some experiments (Song and Rape, 2010).

In addition to its potential use in studying protein function by fast inactivation, KS was shown here to have further possible applications in characterising other aspects of target proteins. Firstly, studying the kinetics of TACC3 and GFP rerouting by KS during mitosis versus during interphase provided insight into the dynamics of the proteins (**3.4.1**), similarly to a previous study (Silvius *et al*., 2006). Whereas GFP rerouting dynamics were similar in interphase and mitosis, TACC3 displayed slower kinetics at both stages of the cell cycle, particularly during mitosis. The underlying parameters of these differences are likely to be the affinity of the proteins for cellular structures such as the spindle. Therefore, KS could provide information on protein dynamics similar to fluorescence recovery after photobleaching (FRAP; (Jacobson *et al*., 1976). Secondly, both TACC3 and clathrin co-rerouted their partner proteins in the TACC3–ch-TOG–clathrin complex (**3.4.7**, **3.4.8**). This is interesting, as KS of γ-adaptin did not co-reroute interacting proteins such as clathrin in a previous study (Robinson *et al*., 2010), however KS of the clathrin adaptor AP-1 did co-reroute interacting proteins such as aftiphilin and γ-synergin but not others such as epinR and clathrin (Hirst *et al*., 2012). These discrepancies between co-rerouted interactors are likely caused by the variability of protein-protein affinity, and the duration of the interaction. Thus, it is likely that γ-adaptin interacts relatively weakly with clathrin compared to the TACC3-clathrin interaction during mitosis.

4 Chapter 4 – TACC3–ch-TOG–clathrin removal at metaphase deregulates kinetochore fibre tension

4.1 Introduction

A TACC3–ch-TOG–clathrin complex was found to crosslink K-fibre MTs during mitosis and contribute to their stability, thus helping to align chromosomes at metaphase and segregate them at anaphase (Fu *et al*., 2010; Hubner *et al*., 2010; Lin *et al*., 2010; Booth *et al*., 2011). The depletion of TACC3 or clathrin by RNAi causes misaligned chromosomes and K-fibres with lower MT density at metaphase (Fu *et al*., 2010; Lin *et al*., 2010; Booth *et al*., 2011).

However, the use of RNAi to deplete TACC3 or clathrin has drawbacks because TACC3 and ch-TOG have been reported to be required for spindle assembly (Gergely *et al*., 2003), so distinguishing the roles of TACC3 and clathrin in spindle assembly versus at metaphase is difficult. The MT loss observed in K-fibres at metaphase in clathrin-depleted cells may be due to the assembly of a defective spindle rather than a role for TACC3–ch-TOG–clathrin in MT stability.

In Chapter 3, knocksideways was shown to be a valid and useful method for the rapid and inducible depletion of the entire TACC3–ch-TOG–clathrin complex from mitotic spindles within the timeframe of mitosis, and this depletion was more efficient than RNAi. In fact, TACC3 KS was fast enough to deplete the complex within the timeframe of metaphase itself (~10 min). With a method to inducibly and specifically remove TACC3–ch-TOG–clathrin from mitotic spindles, the role of the complex in K-fibres at different stages of mitosis could be investigated.

4.2 Chapter aims

The aims of this chapter are:

1- To compare the effects of the depletion of TACC3–ch-TOG–clathrin from mitotic spindles by KS versus RNAi
2- To study the effects of TACC3 KS at different stages of mitosis on mitotic progression
3- To investigate the effects of TACC3 KS on K-fibre ultrastructure and function

4.3 Materials and methods

4.3.1 Light microscopy

4.3.1.1 Live cell imaging

GFP was exchanged with mCherry to make H2B-mCherry from H2B-GFP using AgeI/NotI. H2B-GFP was available from previous work (Royle *et al*., 2005).

Live cell imaging of mitotic progression following RNAi or KS was performed on a Nikon Eclipse Ti with a heated Perspex chamber (OKOlab) using standard filter sets for visualisation of GFP and mCherry, NIS acquisition software, a CoolSNAP HQ2 camera and a 20× air objective (0.45 NA). Cells were kept at 37ºC in supplemented CO_2-independent medium. Light intensity was kept to a minimum to avoid light-induced cell damage. Chromosomes were visualised with H2B-mCherry (imaged once per minute) and GFP was monitored every 5 min. Rapamycin was applied at a final concentration of 200 nM by adding 500 μl of 600 nM rapamycin in medium to 1 ml medium in the dish. Note that, for rerouting at metaphase, KS was induced at a variable time after the last chromosome aligned. It is likely therefore that the metaphase delay has been underestimated.

4.3.1.2 Immunofluorescence labelling

HeLa cells on 16 mm diameter glass coverslips were fixed with PTEMF (50 mM PIPES [1,4-Piperazinediethanesulfonic acid], 10 mM EGTA, 1 mM $MgCl_2$, 0.2% Triton X-100, 4% paraformaldehyde, pH 7.2) at room temperature for 15 min. Cells were then permeabilised using PBS with 0.5% Triton X-100 for 10 min and blocked for 1 hour using PBS with 5% BSA and 5% goat serum. The following antibodies (diluted in blocking solution) were used: (1) rabbit polyclonals: β-tubulin (ab6046, Abcam; 0.5 μg/ml; 1 in 2000), Mad2 (Covance; 1 in 200), (2) human polyclonal: CREST (CS1058, Europa Bioproducts; 1 in 5000). Fluorescently conjugated secondary antibodies were Alexa488, Alexa568 or Alexa633 (Molecular Probes; all used at 4 μg/ml; 1 in 500). Coverslips were mounted on microscope slides using Mowiol containing 4',6-diamidino-2-phenylindole (DAPI).

4.3.1.3 Fluorescence microscopy

Epifluorescence micrographs were acquired using a Nikon Eclipse Ti-U microscope with standard filter sets for visualisation of DAPI, GFP, Alexa Fluor 568 and Alexa Fluor 633, a Nikon Digital Sight DS-Qi1Mc camera, a 60× (1.40 NA) oil-immersion objective and NIS acquisition software.

To quantify Mad2 recruitment to the kinetochore, cells immunostained for Mad2 and CREST were imaged throughout the full Z dimension of the metaphase plate, and Mad2 puncta that co-localised with CREST were counted.

4.3.1.4 Cold-stable assay

Cold-stable MT assay and analysis was performed as described previously (Toso *et al*., 2009). Briefly, cells treated with RNAi (48 hours) or KS (30 minutes), were placed in ice-cold medium and incubated on ice for 10 minutes. The cells were then fixed with PTEMF and stained for tubulin and CREST. Confocal Z-stacks were taken of metaphase cells and analysed using Imaris software as described in **4.3.1.5**.

4.3.1.5 Three dimensional intensity quantification of confocal Z-stacks

For cold-stable spindle experiments, tubulin intensity was quantified in 3D in proximity to individual kinetochores as described in Toso *et al*. (2009). Confocal Z-stacks of cold-treated and fixed metaphase spindles were assembled in Imaris software (Bitplane), and the CREST-stained kinetochores detected using the particle detection module. The particles were verified and altered manually where erroneous particles were detected. Each particle was then expanded into a sphere 0.58 μm in diameter, and the signal from the tubulin channel within this diameter was measured (**Figure 4.1**).

To background-subtract these measurements, 20 identical spheres 0.58 μm in diameter were placed at random in the cytosol of the same cell, and tubulin intensity measured as described above. The average intensity within these spheres was then subtracted from the individual measurements in proximity to each kinetochore.

4.3.1.6 3D live cell imaging

Three-dimensional live cell imaging and kinetochore and spindle pole tracking was performed as described previously (Jaqaman *et al*., 2010). HeLa cells stably expressing GFP-CENP-A and centrin-GFP were seeded in 35-mm Fluorodishes (WPI) in DMEM with 10% FBS and imaged on a widefield imaging system (Personal DeltaVision, Applied Precision) fitted with an environmental chamber maintained at 37ºC and 10% CO_2 atmospheric concentration. Images were acquired with a 100× 1.35 NA objective (Olympus) and a CCD camera (CoolSnap HQ2, Photometrics). Image acquisition was controlled by the softWoRx software suite (Applied Precision). 15 image stacks spaced 0.5 μm apart were collected every 7.5 seconds for 5 minutes (41 time-points). Pixels were set to 1x1 binning (65 nm effective pixel size).

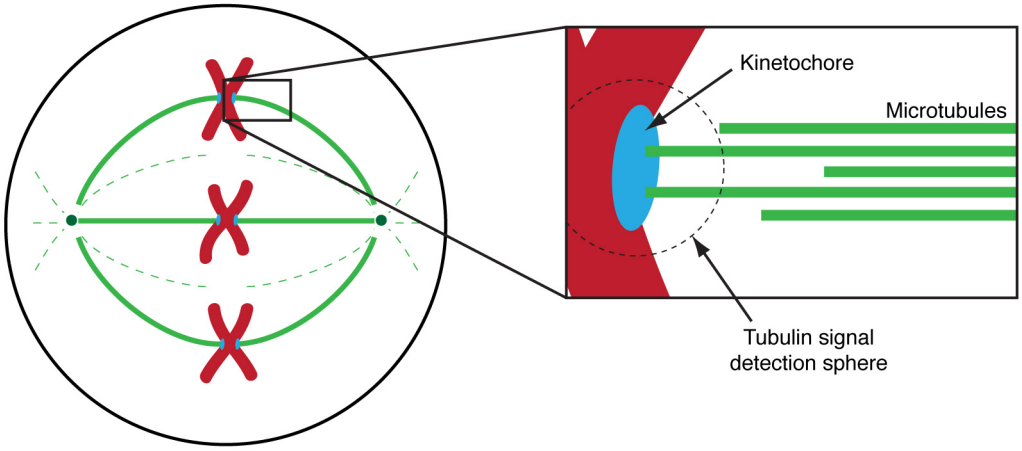

Figure 4.1: Three-dimensional analysis of K-fibre tubulin intensity in proximity to kinetochores following cold treatment. Schematic diagram of a cold-treated metaphase cell. Astral and interpolar microtubules are represented by dashed lines as they are destabilised by cold treatment. Inset, each kinetochore is detected in confocal Z-stacks, and 0.65 μm diameter spheres (dashed line) centred on each kinetochore in Imaris software. Tubulin intensity was measured in each sphere and background subtracted, thus indicating the amount of microtubules stably attached to the kinetochore remaining in the K-fibre.

4.3.1.7 Four dimensional analysis of kinetochore and spindle pole movements

Analysis and particle tracking of the 4D movies was performed by Edward Harry and Andrew McAinsh.

Movies were deconvolved in softWoRx before tracking analysis. Automatic kinetochore tracking was performed as described (Jaqaman *et al*., 2010). All analysis was performed in MATLAB R2012a (MathWorks) with core algorithms written in C (compiled with the MATLAB MEX compiler). Only inlier kinetochores were used for analysis (spots that were <2.5σ from metaphase plate). Analysis steps are shown in **Figure 4.2**.

Spindle poles were tracked using additional algorithms written in MATLAB by Andrew McAinsh and Edward Harry. Spindle pole tracks were identified by assigning a cost to each pair of tracks. The cost was defined as $c = |d\text{-}s| \times a$ where d was the average distance between the tracks, s was the expected average spindle length, set to 11 μm and a was the average angle between the tracks and the metaphase plate. Tracks were only considered if d >5 μm and a <30°, and if both tracks were unaligned throughout both their lifetimes. The pair of tracks with the lowest cost was chosen. Since both centrioles in each pole were tagged, the second centriole track for each pole was found by assigning a cost: $c = g^{-1}$ where g was the cross-correlation between the pole track and the candidate track. Tracks were only considered if g >0.9 and if the average distance between the tracks was less than 1 μm. The track with the lowest cost was chosen for each pole as its respective second centriole.

For pole tracks where two centrioles were found, the position of the spindle pole was defined as the center point between the two, otherwise the position of a single centriole was used. Spindle length was taken as the 3D distance between the two poles.

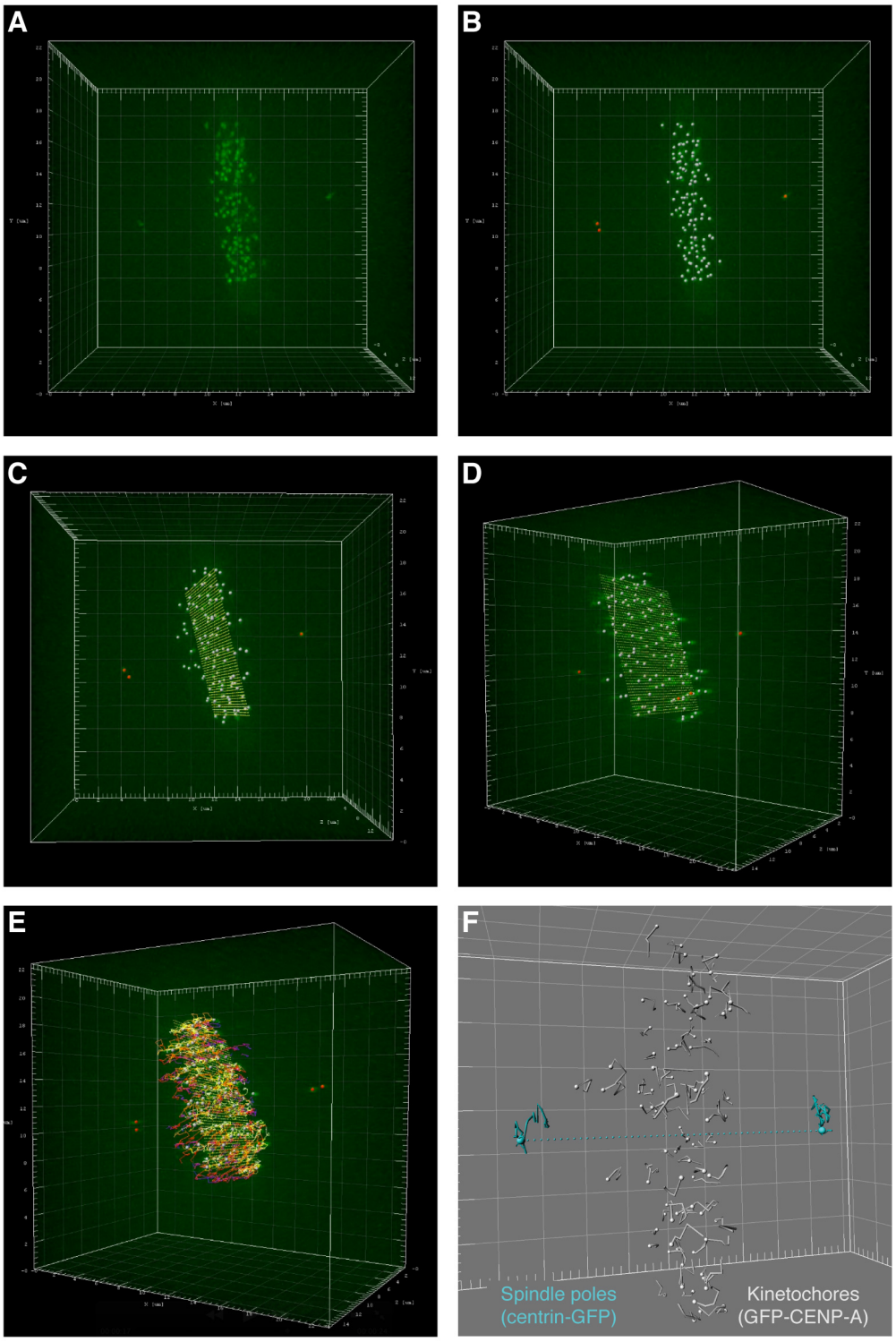
A
B
C
D
E
F
Spindle poles
(centrin-GFP)
Kinetochores
(GFP-CENP-A)

Figure 4.2: Four-dimensional imaging and software tracking of kinetochores and spindle poles. **A-F**, 3D video still images of kinetochores and spindle poles tracked in mitotic HeLa cells stably expressing GFP-CENP-A and centrin-GFP. **A.** 3D fluorescent still image of kinetochores (GFP-CENP-A) and spindle poles (centrin-GFP) in a metaphase HeLa cell. **B.** Software tracking of kinetochores and spindle poles. Aligned kinetochores are annotated with white spheres, and unaligned kinetochores in red. Note that spindle poles are not distinguished in **A-E**, and are annotated as unaligned kinetochores. **C, D.** A virtual plate is fitted to the metaphase plate using 3D alignment of sister centres, allowing to assess overall chromosome alignment. Note that a pair of unaligned sister kinetochores are visible in **D**, annotated by red spheres. **E.** Tracks of kinetochore movements in 4D are annotated by lines colour-coded for spatio-temporal position of kinetochores during movie acquisition. **F.** Spindle poles (turquoise) are detected separately from kinetochores (white) by software and can be tracked in 4D. Euclidian pole-to-pole distance can also be measured (dashed line).

4.3.2 Electron microscopy

4.3.2.1 Reagents

All reagents, such as copper grids, formvar and resin were purchased from Agar Scientific.

4.3.2.2 Preparation of formvar-coated sample grids

Copper 200 hexagonal mesh sample grids were used to pick up section samples following a coating with a fine film of formvar plastic. To do so, the grids were briefly rinsed in 70% ethanol, then in 100% acetone and dried. Glass microscope slides were polished with a chamois leather cloth, coated with 0.2% formvar in 100% chloroform using a dip miser set (Electron Microscopy Sciences) and dried at room temperature for 10 minutes. Both sides of the coated slides were scored along the edges using a razor blade, and submerged vertically into water to detach the fine coats of formvar, which float on the water surface.

The cleaned grids were then deposited onto the plastic film, and collected on a new microscope slide covered with paper labels. The grids were left to dry overnight before use.

4.3.2.3 Sample processing and embedding in resin

Transfected HeLa cells were seeded at 40,000 cells per 35 mm CLEM dish (MatTek) in preparation for imaging and resin-embedding the sample the following day. On the day of the experiment, cells were imaged in CLEM dishes, which contain a glass coverslip photo-etched with coordinates. Transfected cells were identified by fluorescence microscopy in CO_2-independent medium, then incubated for 10 or 30 minutes with 200 nM rapamycin or vehicle, reimaged under the microscope and fixed at room temperature for 1 hour. The fixative solution consisted of EM grade fixatives: 3% w/v glutaraldehyde (Agar Scientific), 0.5% w/v paraformaldehyde (Agar Scientific) in 0.05 M phosphate buffer (PB; obtained by mixing 0.2 M Na_2HPO_4 with 0.2 M NaH_2PO_4 and diluted to 0.05 M, pH 7.4).

After fixation, the fixative solution was replaced with 1-2 ml wash solution (buffer PB, 1 M sucrose) with 0.1% Hoechst-33342 or DAPI, incubated for 5 minutes,

rinsed three times with 1-2 ml of wash solution (leaving 1 ml of the final wash) and the dish was returned to the microscope to image the chromosomes.

Next, the wash solution was replaced with a few drops of 1% osmium tetroxide in water for 1 hour. The osmium was removed, and the cells gently rinsed twice for 30 minutes with 1-2 ml of double-distilled H_2O. The water was then replaced with 1-2 ml of 30% ethanol for 30 minutes, and replaced with a few drops of 0.5% uranyl acetate in 30% ethanol for 1 hour. Next, the cells were dehydrated using a gradient of sequential 1-2 ml solutions containing increasing amounts of ethanol (50%, 60%, 70%, 80% and 90% ethanol) then twice with 100% ethanol, incubating at each step for 5 minutes.

The cells were then infiltrated with resin using 1-2 ml of 1:2 ratio of resin:ethanol solution for 20 minutes, then with 1-2 ml of a 1:1 ratio of resin:ethanol solution for 20 minutes. The infiltration solution was then replaced with a 2-3 mm thick layer of 100% resin covering the bottom of the dish. For orthogonally sectioned samples, the dish was placed in a 60ºC oven for 48-72 hours. For longitudinal samples, half of an embedding capsule (size 0, Agar Scientific) was filled with 100% resin, and gently placed open-side down onto the cell of interest. The dish was then placed in the oven.

4.3.2.4 Correlative light-electron microscopy

Two planes of sectioning were used in this thesis – orthogonal and longitudinal relative to the spindle axis. A schematic of both of these sectioning angles is presented in **Figure 4.3A**.

In both cases, the resin was detached from the CLEM dish, and the cell of interest located in the resin by using the imprint of the photo-etched coordinates. The sample was roughly trimmed using a junior hacksaw and then a 100 μm by 100 μm block face around the cell of interest was created by using an ultramicrotome (UC6, Leica) and glass knives.

Longitudinal sectioning is the conventional EM method for viewing cells. Sections parallel to the plane of the coverslip are taken from the base of the cell moving progressively upwards (**Figure 4.3A**). This plane of sectioning allows extended lengths of microtubules to be observed, and is therefore particularly useful for

analysing microtubule attachment to the kinetochore, or quantifying microtubule crosslinkers (**Figure 4.3B**). To section longitudinally, the resin capsule was inserted into a microtome chuck, allowing for a sectioning plane parallel to that of the dish going from the bottom of the cell upwards.

Orthogonal sectioning involves taking sections that are perpendicular to the spindle axis. In mitotic cells, this is useful to view and quantify most K-fibre microtubules within a single section (**Figure 4.3C**). Quantifying K-fibre microtubules is possible using longitudinal serial sections (McEwen *et al*., 1997), however this method was be avoided because: (1) serial sections are particularly difficult to acquire, and (2) spatial distribution analysis cannot be performed, as the compression forces exerted on each section of a serial reconstruction by the knife will likely deform the sample more than a single orthogonal cross-section through a K-fibre. To section orthogonally, a long strip of resin going along the spindle axis was cut and trimmed end-on until the cell of interest was reached. The cell was then sectioned from one spindle pole to the other using a diamond knife.

Sections collected on sample grids were then post stained for 7 minutes in each 5% uranyl acetate in 50% ethanol and Reynolds' lead citrate solution (Reynolds, 1963), with 1 minute of rinsing in distilled H_2O after each incubation. The samples were then imaged using an FEI Tecnai G2 Spirit BioTWIN microscope at 100 kV, typically at 60,000×.

4.3.2.5 Electron tomography

Electron tomography is a powerful method that provides a high-resolution 3D view of a resin section. To image orthogonal sections under the microscope, full analysis of the K-fibre requires sample tilting. This is because microtubules are most easily recognisable when they are perpendicular to the imaging plane, as they appear as characteristic electron dense rings. Not all microtubules will be at the correct angle,

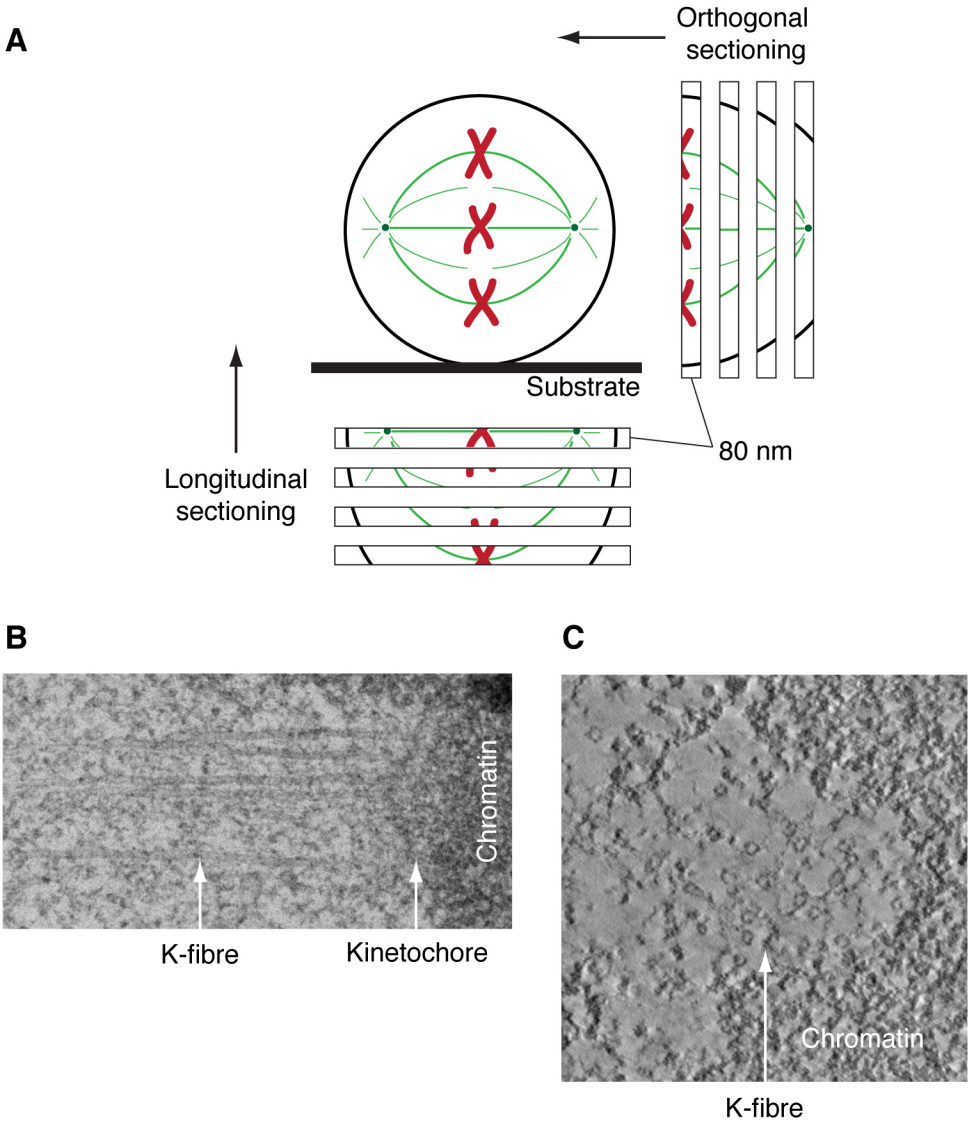
A
Orthogonal sectioning
Substrate
80 nm
Longitudinal sectioning
B
Chromatin
K-fibre
Kinetochore
C
Chromatin
K-fibre

Figure 4.3: Two sectioning planes of the mitotic spindle for analysis by electron microscopy. **A.** Schematic diagram of the two sectioning planes of a mitotic cell (green, microtubules; red, chromosomes). Sections longitudinal to the spindle axis are parallel to the cell substrate and progress upwards through the cell. Sections orthogonal to the spindle axis are parallel to the metaphase plate and progress from one spindle pole to the other. **B.** Typical electron micrograph of a longitudinal section of a kinetochore fibre and its kinetochore. Microtubules of the K-fibre can be seen connecting with the kinetochore. The two plates of the kinetochore are also visible. This sectioning plane is well suited for studying K-fibre morphology and quantification of inter-microtubule bridges. **C.** Typical electron tomogram image of an orthogonal section of a K-fibre within 1 μm of the kinetochore. Microtubules of the K-fibre can be observed as electron-dense rings. This sectioning plane is well suited for quantification of K-fibre microtubules and their spatial analysis.

which increases the risk of quantification error. This error can be minimised by imaging the sample at various tilt angles. Previous work has shown that a single axis tilt of ± 45º (90º in total) is sufficient to reveal 80% of microtubules in a K-fibre (Booth *et al*., 2011). A dual tilt along perpendicular axes is necessary to obtain 100% coverage. Here, single-tilt image acquisition was performed at 60,000× to 90,000× magnification, typically from -50º to +50º with 1º increments using FEI software, and the tilt series assembled into tomograms using IMOD's Etomo software package (Boulder Laboratory for 3-Dimensional Electron Microscopy).

4.3.2.6 Longitudinal analysis of inter-microtubule bridges

Sections longitudinal to the spindle axis were imaged under a transmission electron microscope and 4x4 multiple image alignments (MIAs) were taken at 60,000× at random in proximity to the metaphase plate. If K-fibres were present in the MIAs, total length of MT and total number of inter-MT bridges were measured using AnalySIS software (Soft Imaging System) by an experimenter blind to the conditions of the experiment (**Figure 4.5B**). The criteria used to define an inter-MT bridge were the same as described initially by (Hepler *et al*., 1970) and listed in Chapter 1. These criteria were (1) electron-dense under the EM, (2) linking neighbouring MTs, (3) 2-5 nm in width, (4) 20-40 nm in length. However in the present study, crosslinkers that were 5 to 80 nm in length were observed, so these were also included in the bridge counts. The bridge number for each MIA was normalised to the total length of MT in the MIA.

4.3.2.7 Orthogonal analysis of K-fibres

For sections orthogonal to the spindle axis, K-fibres within 1 μm of the metaphase plate were identified, and single-tilt series acquired at 60,000× magnification were taken. Tomograms were generated using eTOMO software (Boulder Laboratory for 3D Electron Microscopy), and MT positions and cross-sectional area were plotted and calculated. For measurement of K-fibre cross-sectional area, a 40 nm perimeter was computed around clusters of annotated MTs and measured using ImageJ/FIJI. MTs within this boundary were counted as part of the K-fibre, as described previously (Booth *et al*., 2011)(**Figure 4.4A**).

4.3.2.8 Nearest neighbour analysis

To measure inter-MT distances, a map of MTs was created using IMOD Software (Boulder Laboratory for 3D Electron Microscopy) and the coordinates exported using the model2point package. The distance between each point was calculated in Microsoft Excel using Pythagoras' theorem (**Figure 4.4B**), from here the distance between each MT and its nearest neighboring MT was selected. To give the edge-to-edge distance, 20 nm (the approximate diameter of a MT) was subtracted from these measurements.

4.3.2.9 Neighbour density analysis

Neighbour density analysis was performed using the nda package in IMOD as described in McDonald *et al*. (1992). MTs were annotated as circles of 25 nm in diameter throughout the Z slices, and flattened to a single Z plane. MTs within 80 nm of each other were padded by 50 nm using a convex polygon boundary.

Neighbour density analysis software measures MT density within annuli of variable diameter, taking into account the irregular outline of the K-fibre (McDonald *et al*., 1992). Thus, the area of an annulus falling outside the K-fibre perimeter is discarded (**Figure 4.4C**). This has the effect of increasing the weighting of MTs located on the periphery of the fibre.

4.4 Results

4.4.1 TACC3 KS at metaphase decreases inter-MT bridge frequency in K-fibres

To demonstrate KS as a tool to deplete TACC3–ch-TOG–clathrin and demonstrate the loss of inter-MT bridges following KS similarly to that observed by RNAi-mediated depletion (Booth *et al*., 2011), CLEM was performed on TACC3 KS cells.

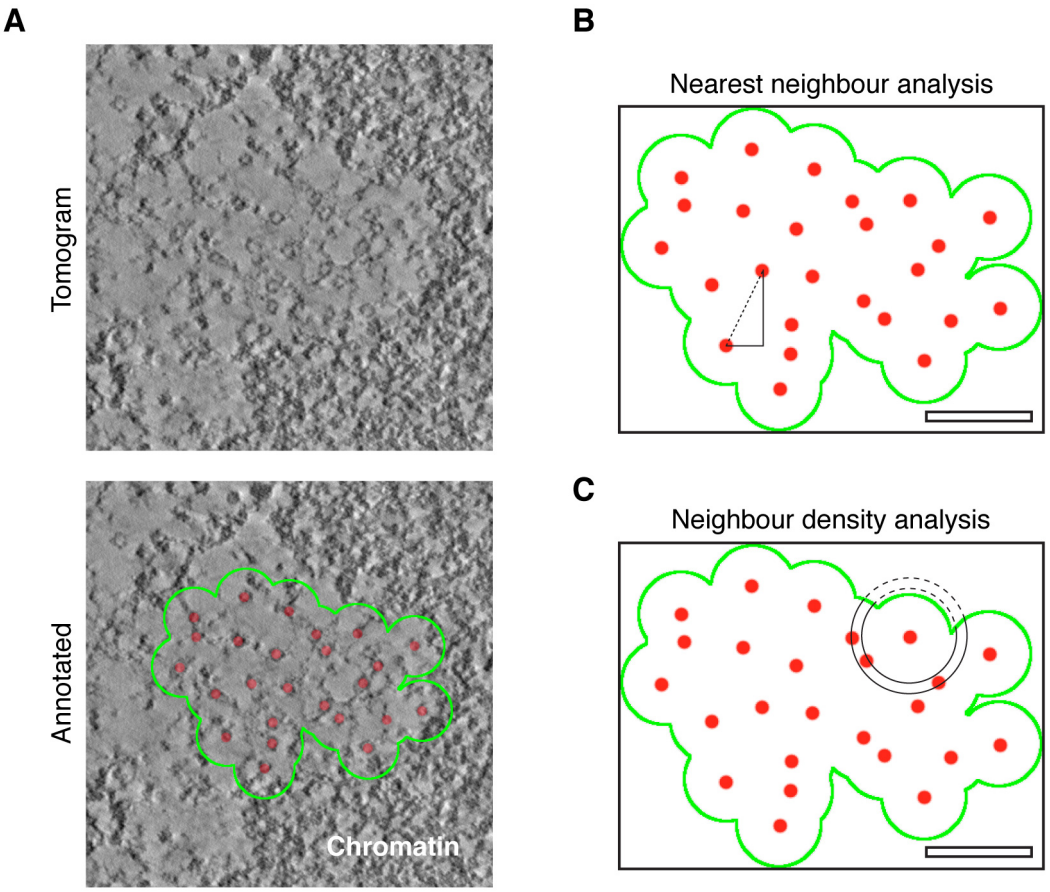

Figure 4.4: Spatial analysis of K-fibre microtubules. **A.** Representative electron tomogram of a cross-section of a K-fibre within 1 μm of the kinetochore. Below, the tomogram is annotated with microtubules (red) and an arbitrary boundary 40 nm from each microtubule (green). **B-C.** Representations of the annotated K-fibre shown in **A**, with annotations depicting the spatial analysis (**B**, nearest neighbour analysis; **C**, neighbour density analysis). **B.** Nearest neighbour analysis was performed using Pythagoras' theorem between each pair of microtubules in a K-fibre (dashed line). **C.** Neighbour density analysis was performed in IMOD software using the NDA package (as described in McDonald *et al*., 1992). An annulus of determined diameter and width is place around each microtubule, and the annulus area outside the K-fibre perimeter is subtracted (dashed lines). The number of microtubules within the remaining annulus area are counted, and a density (MT/μm^2) is calculated. Scale bar, 100 nm.

HeLa cells at metaphase expressing mCherry-MitoTrap and either GFP-TACC3 or GFP-FKBP-TACC3 were treated with vehicle or 200 nM rapamycin for 10 min. The cells were then fixed and processed for CLEM. Sections longitudinal to the spindle axis (80 nm thick) were taken and inter-MT bridge frequency was quantified by an experimenter who was unaware of the conditions of the experiment (**Figure 4.5A, B**).

A small but significant reduction in median MT crosslinker frequency was observed in TACC3 KS (**Figure 4.5C**), supporting the role of the TACC3–ch-TOG–clathrin complex in MT crosslinking (Booth *et al*., 2011).

4.4.2 TACC3 depletion by RNAi delays mitosis, and is rescued by reexpression of TACC3 KS constructs

To quantify the effect of TACC3 depletion on mitosis and demonstrate that GFP-TACC3 and GFP-FKBP-TACC3 were functional and could rescue the depletion of endogenous TACC3, live cell imaging was performed on HeLa cells with altered TACC3 levels. All cells were TACC3-depleted, expressed H2B-mCherry and PAGFP-MitoTrap, and expressed GFP or GFP-TACC3 or GFP-FKBP-TACC3. Cells were monitored as they progressed through mitosis by imaging H2B-mCherry (**Figure 4.6A**), and nuclear envelope breakdown (NEBD)-to-metaphase and metaphase-to-anaphase timings were measured (**Figure 4.6B**).

TACC3-depleted cells expressing GFP displayed both delayed metaphase and delayed anaphase onset, with some cells failing to achieve anaphase before the end of the image acquisition (circles; **Figure 4.6C**). These observations are in agreement with previous studies (Fu *et al*., 2010; Lin *et al*., 2010).

When TACC3-depleted cells reexpressed GFP-TACC3 or GFP-FKBP-TACC3, normal NEBD-metaphase and metaphase-anaphase timings were restored, and the mitotic defects from TACC3 depletion were rescued (**Figure 4.6D**). This indicates both that the TACC3 constructs are functional, and that the levels of reexpressed TACC3 are suitable for normal mitotic timings, in agreement with results **3.4.6**.

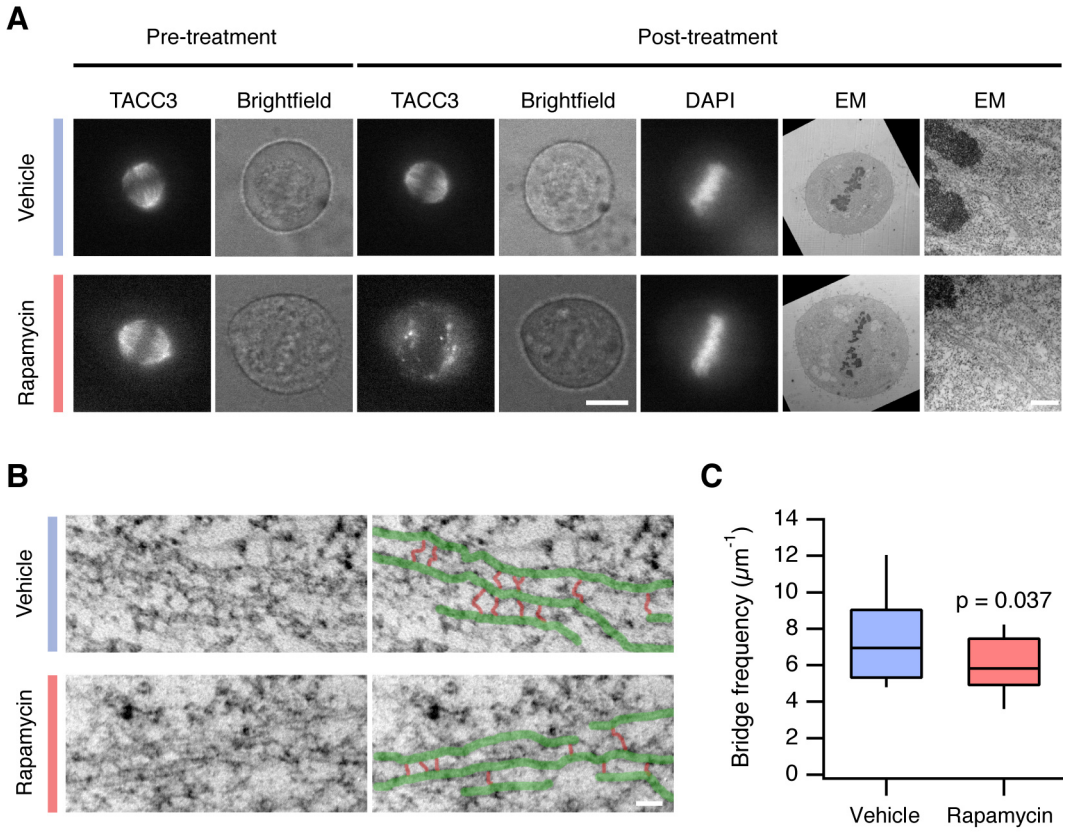

Figure 4.5: TACC3 KS at metaphase decreases inter-microtubule bridge frequency in K-fibres. **A.** TACC3-depleted HeLa cells at metaphase expressing GFP-FKBP-TACC3 and mCherry-MitoTrap were treated with vehicle or rapamycin (200 nM) for 10 min, fixed and processed for CLEM. The cell was located and 80 nm longitudinal sections were taken (EM), and bridge frequency in K-fibres was quantified. Scale bar, 10 μm (left) and 500 nm (right). **B.** Example micrographs to show visualisation of inter-microtubule bridges for quantification. Annotated micrograph (right) shows microtubules (green) and crosslinkers (red). Scale bar, 50 nm. **C.** Tukey box plot of inter-microtubule bridge frequency in K-fibres, expressed per micron of total microtubule length. In TACC3 KS cells, a significant loss of microtubule crosslinkers was observed (control n=4 cells [20 sections], TACC3 KS n=5 cells [25 sections]; Student's t-test, p=0.037). Tukey box plots show the median, interquartile range and the 10th and 90th percentile.

4.4.3 Mitosis is unaffected by protein accumulation at the mitochondrial membrane

The use of KS to deplete proteins from the spindle during mitosis could produce mitotic defects or delays as a by-product of protein loading on the mitochondrial outer membrane. This loading could affect mitochondrial function and cause a secondary mitotic defect.

To investigate this possibility, live cell imaging was performed on HeLa cells expressing PAGFP-MitoTrap and GFP-FKBP, treated with 200 nM rapamycin at the onset of NEBD, and imaged through mitosis (**Figure 4.7A**). NEBD-to-metaphase and metaphase-to-anaphase timings were measured. GFP rerouting to the mitochondria did not affect mitosis duration (**Figure 4.7C**), indicating that mitochondrial loading with proteins does not affect the progression of mitosis.

4.4.4 TACC3 KS at NEBD severely delays mitosis

To investigate the role of the TACC3–ch-TOG–clathrin complex in early mitosis, live cell imaging was performed on HeLa cells expressing H2B-mCherry, PAGFP-MitoTrap and either GFP-TACC3 or GFP-FKBP-TACC3, and treated with vehicle or 200 nM rapamycin at NEBD onset (**Figure 4.8A, B**). NEBD-metaphase and metaphase-anaphase timings were measured.

Whereas control cells displayed mitotic timings similar to control cells (**Figure 4.6C, D**), TACC3 KS cells were severely delayed (**Figure 4.8C**). Indeed, all but one of these cells failed to achieve chromosomal alignment before the end of the image acquisition, which lasted up to 10 hours (**Figure 4.8C**). This similar to results in previous studies (Gergely *et al*., 2003; Schneider *et al*., 2007; Fu *et al*., 2010; Lin *et al*., 2010) and also to results observed in TACC3 RNAi cells (**4.4.2**, **Figure 4.6C**), suggesting that TACC3–ch-TOG–clathrin are involved in chromosome congression to the metaphase plate, possibly by promoting spindle assembly. However, the extent of the delay observed following TACC3 KS is dramatically more severe than observed in those previous studies and in the TACC3 RNAi-treated cells. There are several possible explanations for this effect (discussed below in **4.5**).

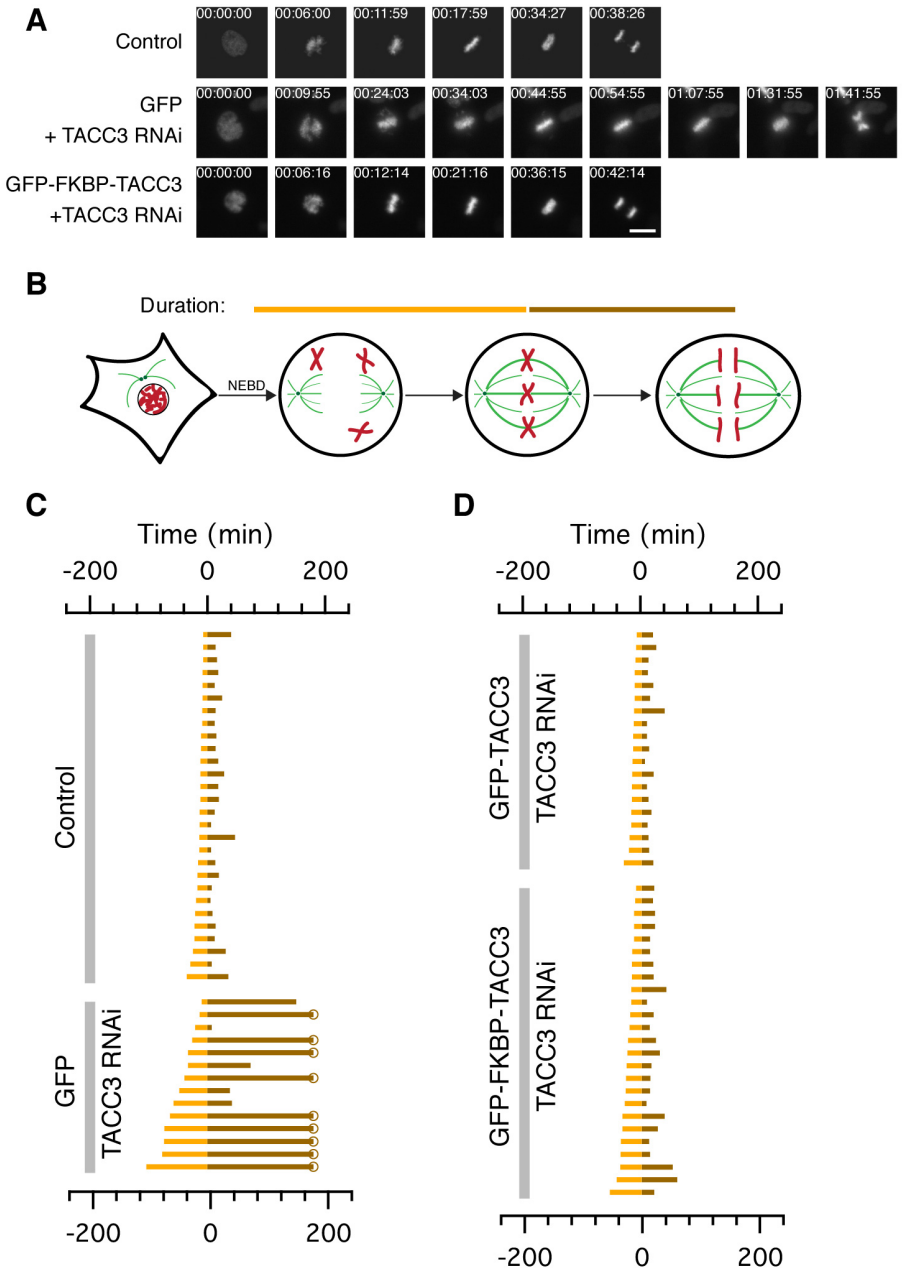
A
Control
00:00:00
00:06:00
00:11:59
00:17:59
00:34:27
00:38:26
GFP
+ TACC3 RNAi
00:00:00
00:09:55
00:24:03
00:34:03
00:44:55
00:54:55
01:07:55
01:31:55
01:41:55
GFP-FKBP-TACC3
+TACC3 RNAi
00:00:00
00:06:16
00:12:14
00:21:16
00:36:15
00:42:14
B
Duration:
NEBD
C
Time (min)
-200
0
200
Control
GFP
TACC3 RNAi
-200
0
200
D
Time (min)
-200
0
200
GFP-TACC3
TACC3 RNAi
GFP-FKBP-TACC3
TACC3 RNAi
-200
0
200

Figure 4.6: The effects of TACC3 depletion and reexpression on mitosis. A. Video still images of HeLa expressing H2B-mCherry in control cells, or TACC3-depleted cells expressing GFP or GFP-FKBP-TACC3. Time is in hh:mm:ss. Scale bar, 20 μm. **B.** Schematic diagram of the experiment. NEBD-metaphase timings are in gold, and metaphase-anaphase timings are in brown. **C.** Mitotic timings of control or TACC3-depleted cells expressing GFP. Circles indicate cells that did not complete mitosis within the timeframe of the movie. **D.** Mitotic timings of TACC3-depleted cells expressing GFP-TACC3 or GFP-FKBP-TACC3. All cells in the experiment also expressed PAGFP-MitoTrap.

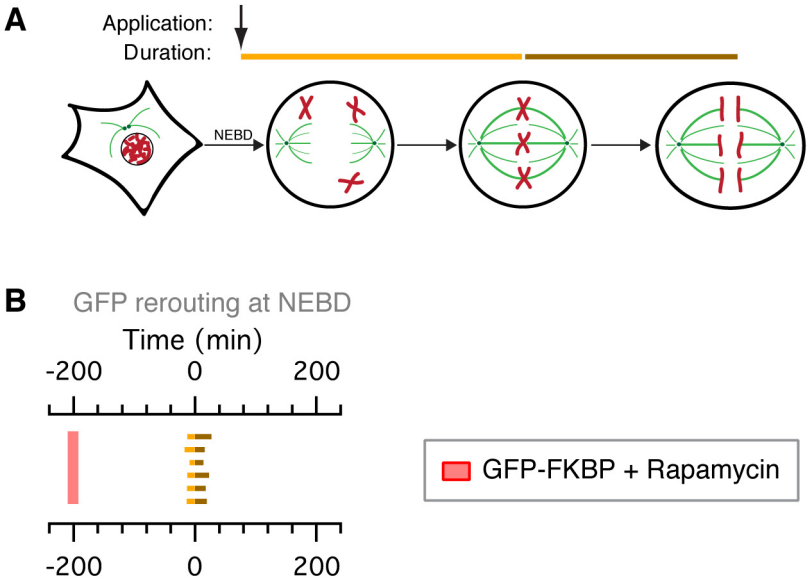

Figure 4.7: Mitosis is unaffected by protein accumulation at the mitochondrial membrane. A. Schematic diagram of the experiment. NEBD-metaphase timings are in gold, and metaphase-anaphase timings are in brown. Rapamycin (200 nM) was applied at NEBD. **B.** Mitotic timings of HeLa cells expressing H2B-mCherry, PAGFP-MitoTrap and GFP-FKBP with rapamycin (200 nM) added at NEBD.

4.4.5 TACC3 KS at metaphase delays anaphase onset

The rapidity of TACC3–ch-TOG–clathrin depletion from assembled mitotic spindles could allow the dissection of the potential temporally distinct roles of the complex at different stages of mitosis. One particular aim of this thesis was to study the role of this crosslinking complex at metaphase, after the mitotic spindle has assembled normally. Therefore, TACC3 KS was performed at metaphase, once all chromosomes had aligned along the equator of the cell and following a normal prometaphase (**Figure 4.9B**), and the temporal downstream effects on mitotic progression were analysed.

Live cell imaging was performed on TACC3-depleted HeLa cells expressing H2B-mCherry, PAGFP-MitoTrap and either GFP-TACC3 or GFP-FKBP-TACC3, treated with vehicle or 200 nM rapamycin at metaphase (**Figure 4.9A**), and the metaphase-to-anaphase timings were measured (**Figure 4.9B, C**).

Whilst the vast majority of control cells progressed to anaphase, TACC3 KS cells displayed more frequent metaphase arrest, with some cells failing to undergo anaphase onset before the end of the movie (circles, **Figure 4.9C**). This effect is likely to have been under-estimated, because KS was performed at a variable time following alignment of the last chromosome. This effect was statistically significant ($p<0.001$, Cox regression analysis; **Figure 4.9D**). This is surprising, because these cells had undergone a normal prometaphase, formed a mitotic spindle and had aligned their chromosomes at the time of TACC3 KS, yet a mitotic delay was still observed. This suggests that the TACC3–ch-TOG–clathrin MT crosslinking complex still performs a vital function in the mitotic spindle at later stages of mitosis.

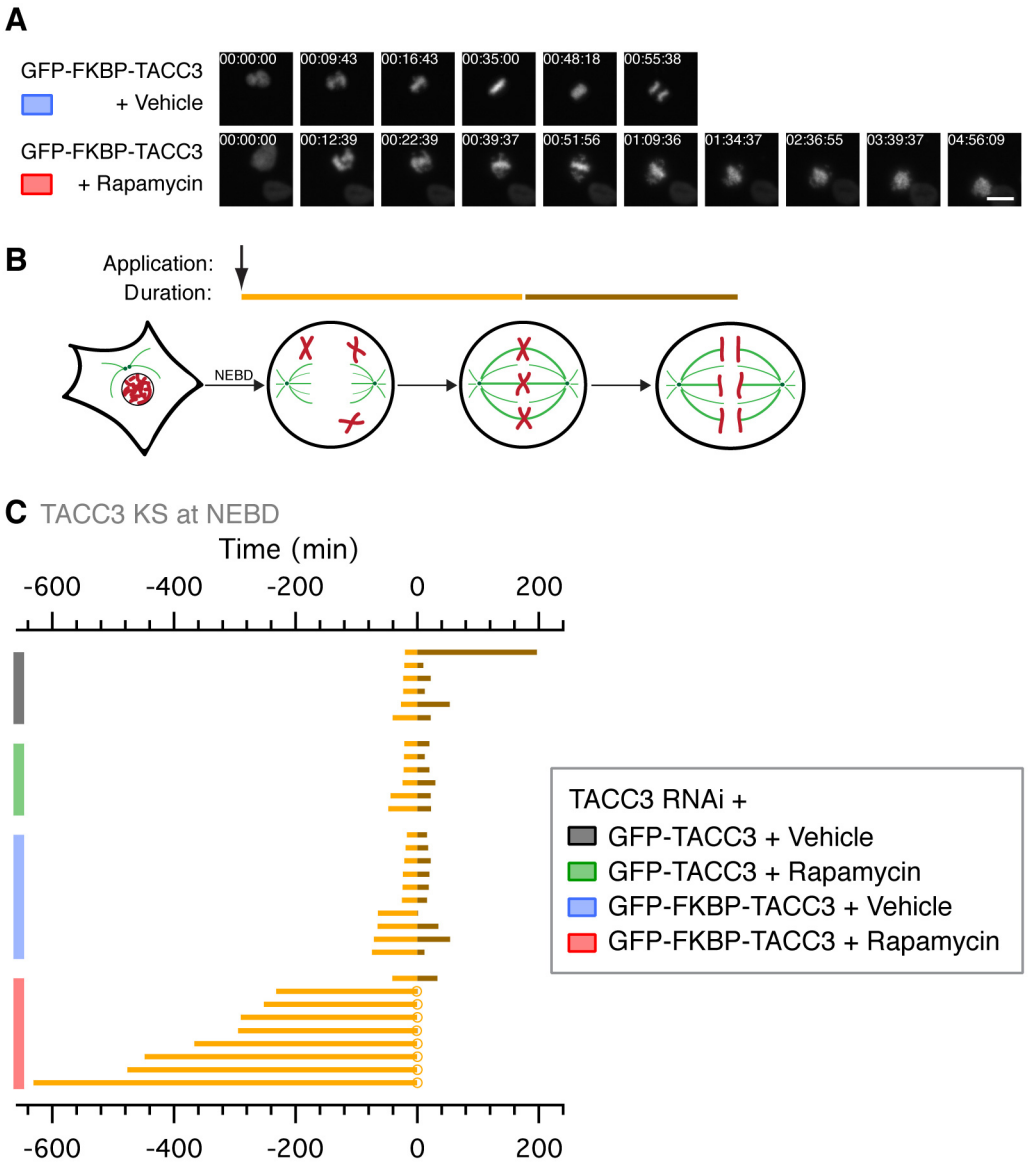

Figure 4.8: TACC3 KS at NEBD severely delays mitosis. A. Video still images of TACC3-depleted HeLa expressing PAGFP-MitoTrap, H2B-mCherry and GFP-FKBP-TACC3, treated with vehicle or rapamycin (200 nM) at NEBD. Time is in hh:mm:ss. Scale bar, 20 μm. **B.** Schematic diagram of the experiment, with vehicle or rapamycin (200 nM) applied at NEBD onset. NEBD-metaphase timings are in gold, and metaphase-anaphase timings are in brown. **C.** Mitotic timings of cells in experimental conditions colour-coded as indicated in the key, treated with vehicle or rapamycin (200 nM) at NEBD. Circles indicate cells that did not complete mitosis within the timeframe of the movie.

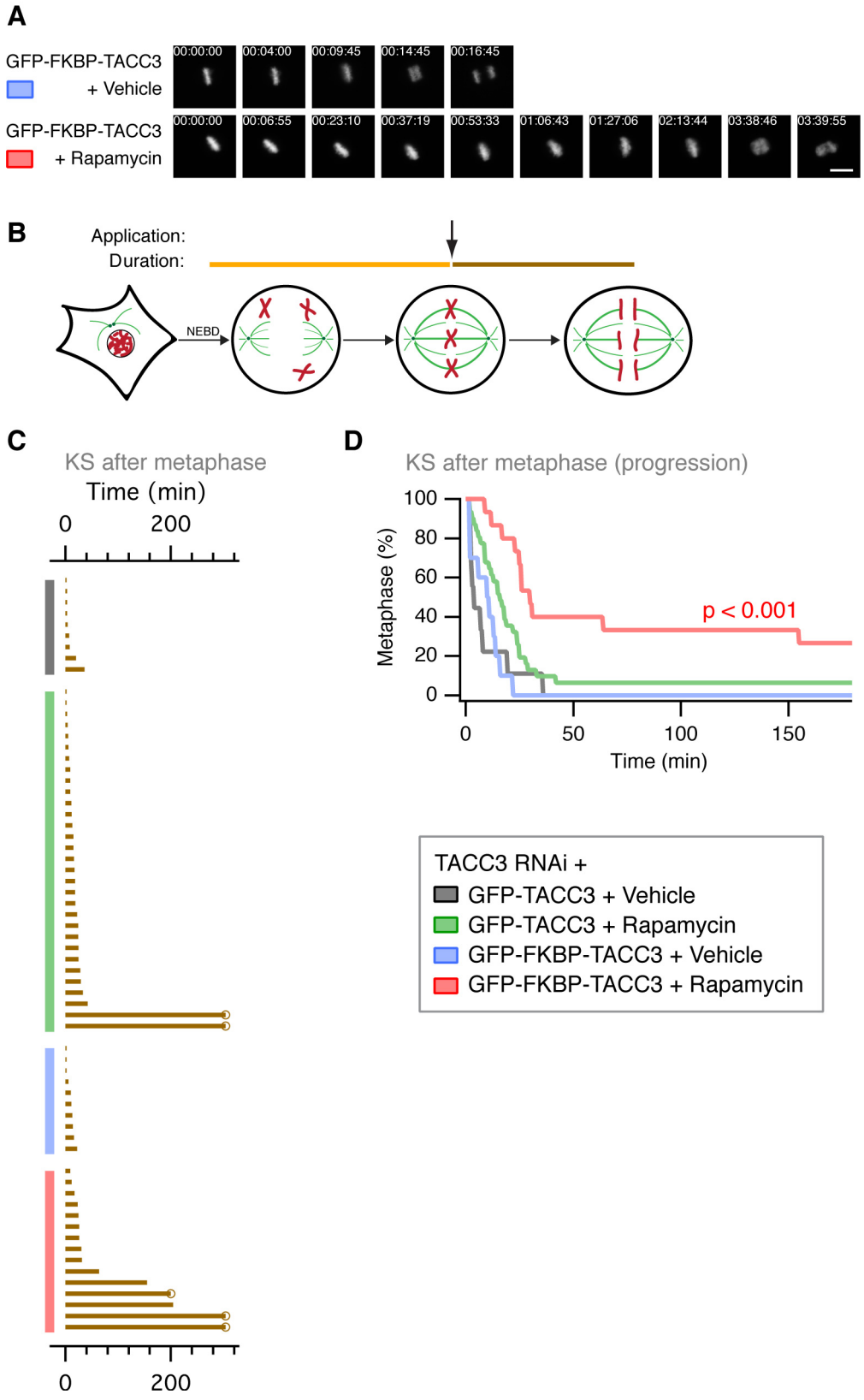
A
GFP-FKBP-TACC3
+ Vehicle
00:00:00
00:04:00
00:09:45
00:14:45
00:16:45
GFP-FKBP-TACC3
+ Rapamycin
00:00:00
00:06:55
00:23:10
00:37:19
00:53:33
01:06:43
01:27:06
02:13:44
03:38:46
03:39:55
B
Application:
Duration:
NEBD
C
KS after metaphase
Time (min)
0
200
0
200
D
KS after metaphase (progression)
Metaphase (%)
100
80
60
40
20
0
p < 0.001
0
50
100
150
Time (min)
TACC3 RNAi +
GFP-TACC3 + Vehicle
GFP-TACC3 + Rapamycin
GFP-FKBP-TACC3 + Vehicle
GFP-FKBP-TACC3 + Rapamycin

Figure 4.9: TACC3 KS after metaphase delays anaphase onset. **A.** Video still images of TACC3-depleted HeLa cells expressing PAGFP-MitoTrap, H2B-mCherry and GFP-FKBP-TACC3, treated with vehicle or rapamycin (200 nM) at metaphase. Time is in hh:mm:ss. Scale bar, 20 μm. **B.** Schematic diagram of the experiment, with vehicle or rapamycin (200 nM) applied after alignment of all the chromosomes. Metaphase-anaphase timings are in brown. **C.** Mitotic timings of cells in conditions colour-coded as indicated in the key, treated with vehicle or rapamycin (200 nM) at metaphase. Circles indicate cells that did not complete mitosis within the timeframe of the movie. **D.** 'Survival curves' of the data shown in **C**, analysed using Cox regression analysis.

4.4.6 TACC3 KS at metaphase activates the spindle checkpoint

To investigate the underlying causes of the mitotic delay observed after TACC3 KS at metaphase, the status of the spindle checkpoint was assessed in these cells.

TACC3-depleted metaphase HeLa cells expressing PAGFP-MitoTrap and GFP-TACC3 or GFP-FKBP-TACC3 were treated for 30 min with vehicle or 200 nM rapamycin, fixed and immunostained for CREST and Mad2 (**Figure 4.10A**). The CREST antibody labels the centromere and kinetochore regions of chromosomes. Mad2 is a spindle checkpoint protein that localises to incorrectly attached kinetochores when the spindle checkpoint is active (Li and Murray, 1991; Chen *et al*., 1996; Waters *et al*., 1998). The number of Mad2 puncta that co-localised with CREST in metaphase cells was counted (**Figure 4.10B**).

TACC3 KS at metaphase increased the number of Mad2-positive kinetochores per cell (**Figure 4.10A, B**). In addition, the number of cells with a satisfied spindle checkpoint (that is to say, with no Mad2 staining on their kinetochores) was reduced by ~40% compared to controls (**Figure 4.10B**). These results suggest that TACC3 KS at metaphase reactivated the spindle checkpoint, explaining the metaphase arrest observed in **4.4.5** since control cells had progressed normally to anaphase **(Figure 4.9).**

4.4.7 TACC3 KS at metaphase reduces K-fibre tension

To investigate the cause of Mad2 recruitment to kinetochore following TACC3 KS at metaphase, K-fibre function was assessed in these cells by measuring the distance between sister kinetochores, which increases under tension as the centromeric DNA between them stretches.

TACC3-depleted metaphase HeLa cells expressing PAGFP-MitoTrap and GFP-TACC3 or GFP-FKBP-TACC3 were treated for 30 min with vehicle or 200 nM rapamycin, fixed and immunostained for CREST. Confocal microscopy was used to measure inter-kinetochore distances between unambiguous pairs of sister kinetochores (**Figure 4.11**).

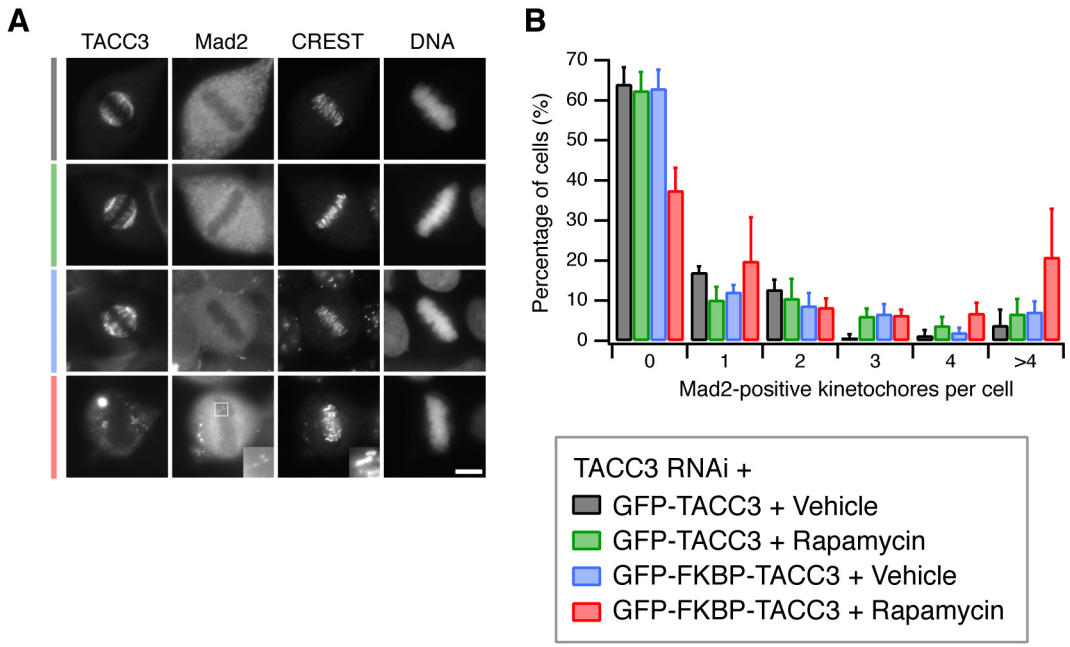

Figure 4.10: TACC3 KS at metaphase activates the spindle checkpoint. A. Representative fluorescence micrographs showing the recruitment of Mad2 to kinetochores following TACC3 KS at metaphase. TACC3-depleted HeLa cells expressing PAGFP-MitoTrap and GFP-TACC3 or GFP-FKBP-TACC3 were treated with vehicle or rapamycin (200 nM) for 30 min, fixed and immunostained for CREST and Mad2. Inset shows three Mad2-positive kinetochores (2.5× zoom). Scale bar, 10 μm. **B.** Bar chart to show the proportion of cells with a satisfied or active spindle checkpoint, as revealed by Mad2 presence at kinetochores. Bars show mean ± s.e.m. of three experiments are shown (n=90-93 cells).

Inter-kinetochore distances in TACC3 KS cells at metaphase were shorter than control cells (**Figure 4.11**). The average inter-kinetochore distance was significantly shifted from 1.68 ± 0.06 μm (mean ± s.e.m.) in vehicle-treated cells to 1.38 ± 0.04 μm in KS cells. However, this was not a complete loss of tension as the average unattached (prometaphase) inter-kinetochore distance was 0.83 ± 0.06 μm. Additionally, there is no subpopulation of kinetochore distances appearing between 0.8 and 1 μm (the unattached distance) following TACC3 KS, suggesting that there is no loss of kinetochore attachment or complete loss of tension in a subset of kinetochores. Rather, TACC3 KS causes an overall shift to smaller inter-kinetochore distances.

4.4.8 TACC3 KS at metaphase does not significantly alter K-fibre stability or MT occupancy at the kinetochore

Although there was no emerging 'unattached' population of kinetochores following TACC3 KS, the inter-kinetochore distances were only measured in unambiguous pairs of sister kinetochores so a bias could have potentially occurred. Loss of K-fibre attachment at the kinetochore could explain both the spindle checkpoint activation and the loss of K-fibre tension following TACC3 KS. Treatment of mitotic spindles with ice-cold temperature causes the depolymerisation of all unstable MTs. Therefore, the stability of K-fibre attachment at the kinetochore following cold-treatment was assessed in a more systematic and sensitive manner to detect more subtle variations and verify the results in **4.4.7**.

TACC3-depleted metaphase HeLa cells expressing PAGFP-MitoTrap and GFP-TACC3 or GFP-FKBP-TACC3 were treated for 30 min with vehicle or 200 nM rapamycin, cold-treated for 10 min, then fixed and immunostained for tubulin and CREST (**Figure 4.12A**). Nuf2 depletion by RNAi (48 hours) was used as a positive control. Nuf2 is a protein essential for stable kinetochore–microtubule attachment and its depletion causes highly unstable K-fibres (**Figure 4.12A**; (DeLuca *et al*., 2002)). Confocal Z-stacks were taken of metaphase cells and the background subtracted tubulin intensity was measured surrounding each kinetochore in 3D using Imaris software as described in **Figure 4.1** (Toso *et al*., 2009).

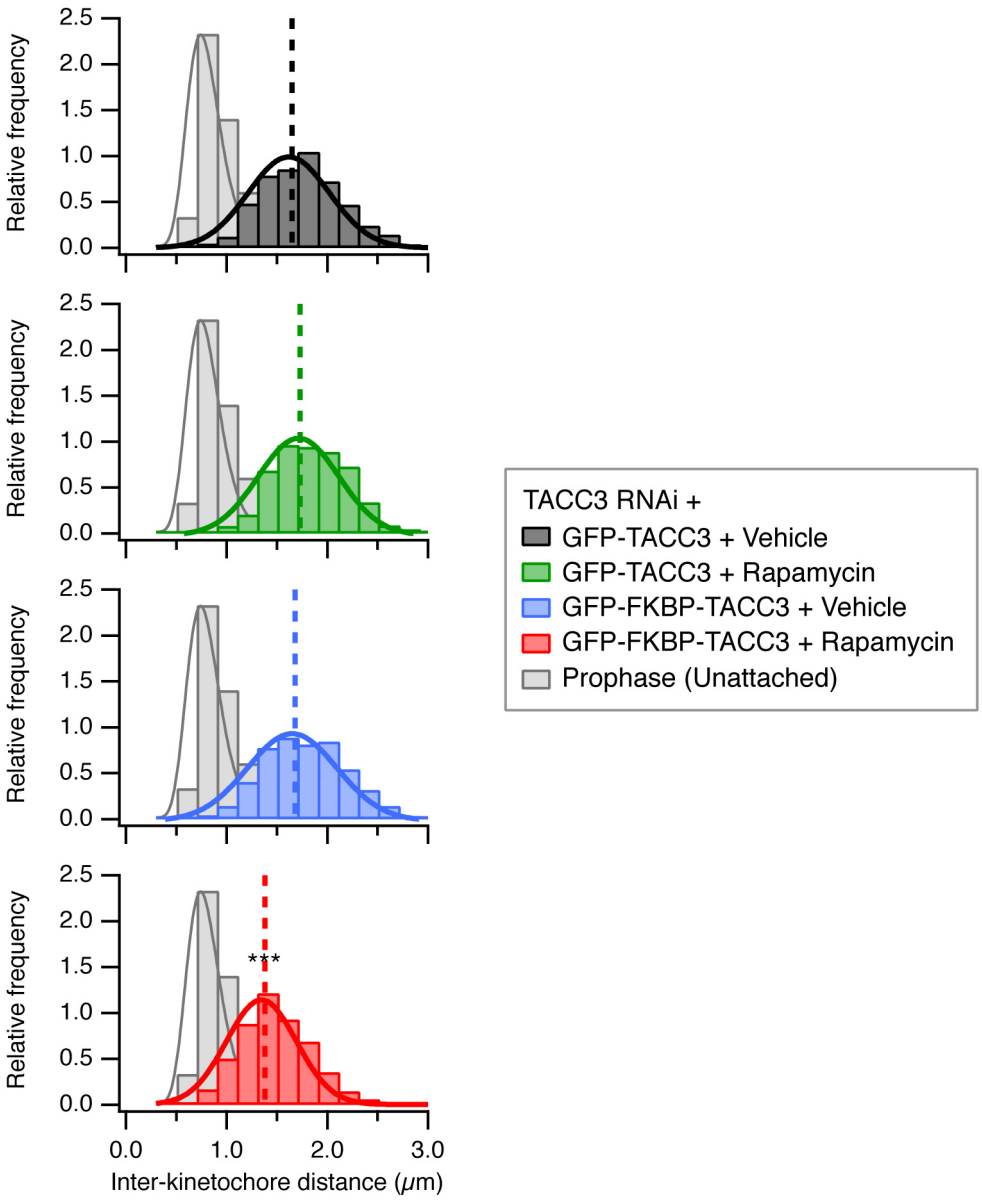
Relative frequency
2.5
2.0
1.5
1.0
0.5
0.0
***
0.0
1.0
2.0
3.0
Inter-kinetochore distance (μm)
TACC3 RNAi +
GFP-TACC3 + Vehicle
GFP-TACC3 + Rapamycin
GFP-FKBP-TACC3 + Vehicle
GFP-FKBP-TACC3 + Rapamycin
Prophase (Unattached)

Figure 4.11: TACC3 KS at metaphase reduces K-fibre tension. Histograms of inter-kinetochore distances. Metaphase TACC3-depleted HeLa cells expressing PAGFP-MitoTrap and GFP-TACC3 or GFP-FKBP-TACC3 were treated with vehicle or rapamycin (200 nM) for 30 min, fixed and immunostained for CREST. A histogram for each condition is overlaid on a histogram of unattached inter-kinetochore distances from prophase/early prometaphase cells (light grey). The mean inter-kinetochore distance is shown by a dashed line. The unattached data were fitted with a log-normal function, whilst all other data were fitted with a single Gaussian function. TACC3 KS cells (red, n=645 from 20 cells) displayed significantly reduced inter-kinetochore distance compared to controls ($p<0.001$, ***; grey, n=654 from 22 cells; green, n=656 from 23 cells; blue, n=578 from 23 cells), but was not significantly different from unattached kinetochores (n=238 from 8 cells).

As expected, Nuf2-depleted cells had highly unstable K-fibre attachments, as reflected by the weak tubulin signal surrounding the majority of kinetochores in these cells (**Figure 4.12B**). However, the tubulin signal surrounding kinetochores in TACC3 KS was no different to that of the KS control cells or of control RNAi-treated cells (**Figure 4.12B**). This indicates that there is no loss of MT-kinetochore attachment stability and MT occupancy at the kinetochore following TACC3 KS at metaphase.

4.4.9 TACC3 KS at metaphase does not significantly alter K-fibre MT number

TACC3 KS at metaphase was found to leave K-fibre attachment stability unaltered. Another possibility underlying the reactivation of the spindle checkpoint and loss of K-fibre tension in these cells is the alteration of K-fibre ultrastructure, either by reducing kMT number or modifying their spatial organisation. To investigate this possibility, CLEM was performed to study K-fibre ultrastructure.

TACC3-depleted metaphase HeLa cells expressing mCherry-MitoTrap and GFP-TACC3 or GFP-FKBP-TACC3 were treated for 10 or 30 min with vehicle or 200 nM rapamycin, then fixed and processed for CLEM. 80 nm orthogonal sections were taken, and tomograms of K-fibre cross-sections within 1 μm of the kinetochore were generated (**Figure 4.13A**). A 40 nm boundary was placed around each kMT to measure K-fibre cross-sectional area (**Figure 4.13A**).

After 10 min, TACC3 KS cells had significantly fewer kMTs per fibre compared to vehicle-treated control cells (ANOVA with Tukey-Kramer *post-hoc* test; **Figure 4.13B**, top) but not compared to GFP-TACC3-expressing cells treated with rapamycin (**Figure 4.13B**, top). All conditions, including TACC3 KS cells, had median and mean kMT numbers within 20-40 MTs/fibre, which is the normal range for mammalian K-fibres (Bajer, 1973; McIntosh *et al*., 1975; Rieder, 1982; McDonald *et al*., 1992). The reason for the difference between controls is unknown. It is possible that rapamycin alone accentuated kMT loss, however this seems unlikely given that no effect of rapamycin alone was

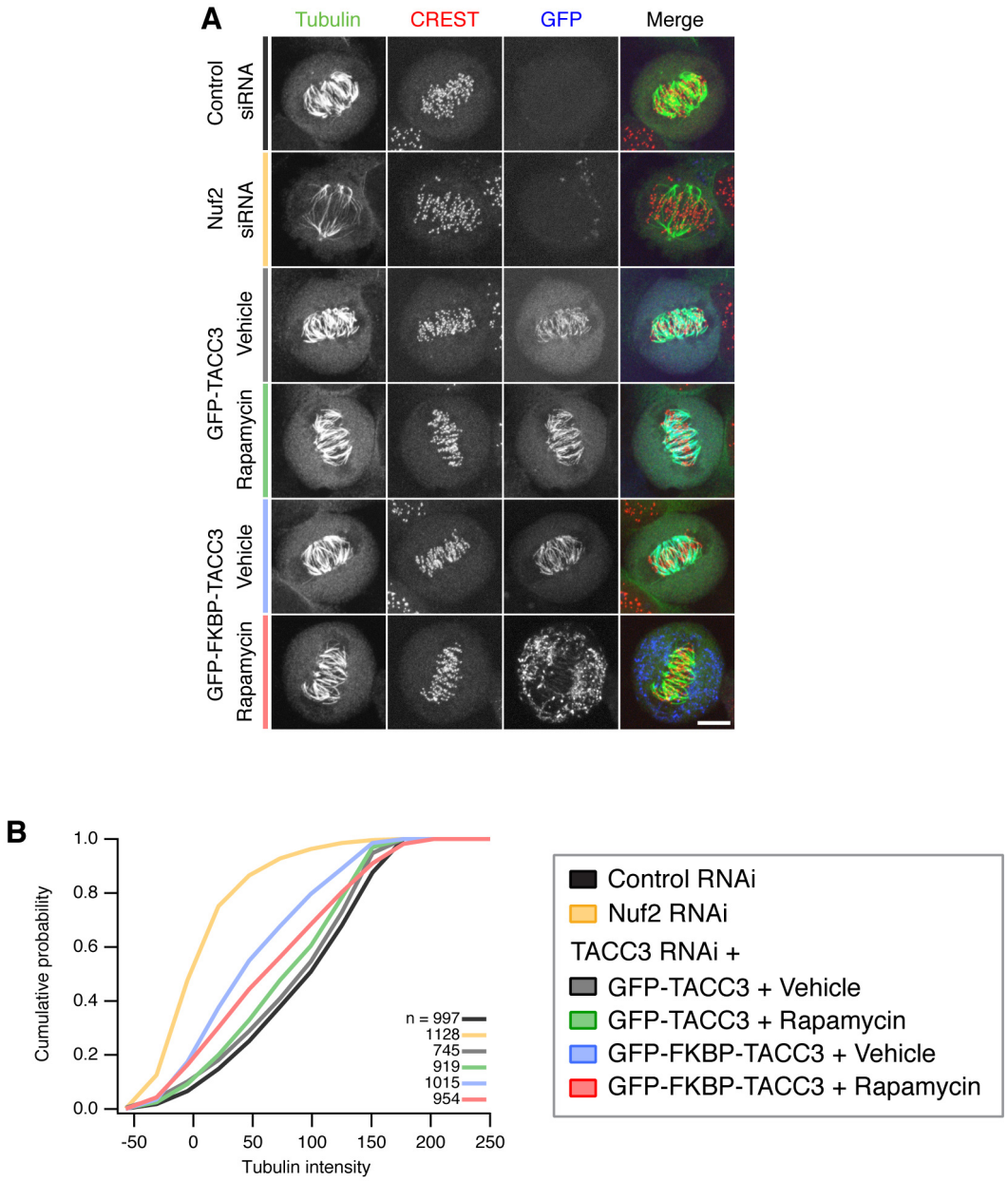
A
Tubulin
CREST
GFP
Merge
Control siRNA
Nuf2 siRNA
GFP-TACC3 Vehicle
GFP-TACC3 Rapamycin
GFP-FKBP-TACC3 Vehicle
GFP-FKBP-TACC3 Rapamycin
B
Cumulative probability
1.0
0.8
0.6
0.4
0.2
0.0
-50
0
50
100
150
200
250
Tubulin intensity
n = 997
1128
745
919
1015
954
Control RNAi
Nuf2 RNAi
TACC3 RNAi +
GFP-TACC3 + Vehicle
GFP-TACC3 + Rapamycin
GFP-FKBP-TACC3 + Vehicle
GFP-FKBP-TACC3 + Rapamycin

Figure 4.12: TACC3 KS at metaphase does not significantly alter kinetochore microtubule occupancy. **A.** Representative images of each condition analysed are shown as maximum intensity projections of confocal Z-series micrographs. Metaphase TACC3-depleted HeLa cells expressing PAGFP-MitoTrap and GFP-TACC3 or GFP-FKBP-TACC3 were treated with vehicle or rapamycin (200 nM) for 30 min, then cold-treated, fixed and immunostained for tubulin (green) and CREST (red), the GFP channel is in blue. Scale bar, 10 μm. **B.** Analysis of confocal Z-series micrographs to detect cold-stable kinetochore-microtubule attachments. Cumulative graph to show the average tubulin signal adjacent to kinetochores in 3 dimensions. N_{cell}=9-12 from two experiments. $N_{kinetochore}$ is indicated bottom right.

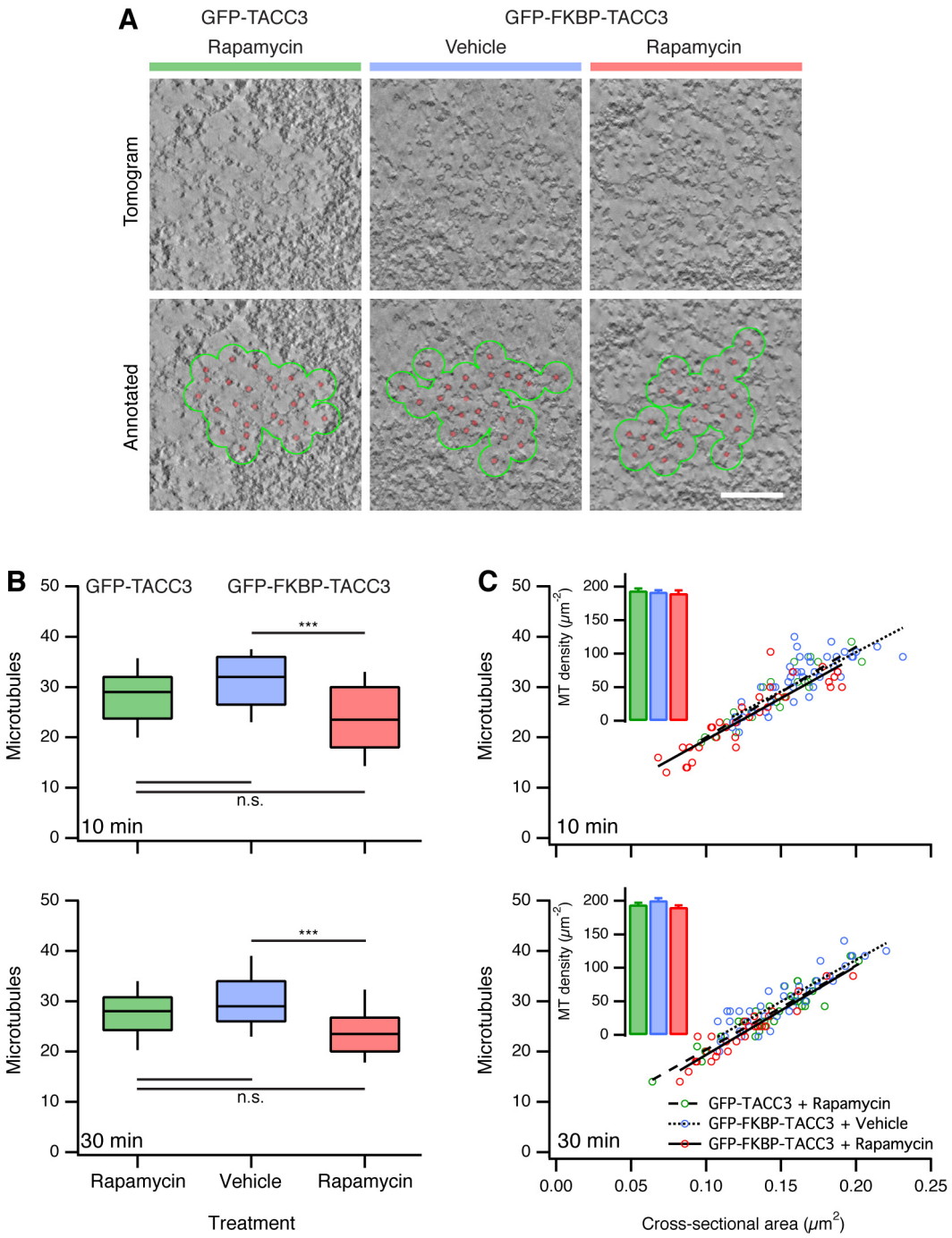
A
GFP-TACC3
GFP-FKBP-TACC3
Rapamycin
Vehicle
Rapamycin
Tomogram
Annotated
B
GFP-TACC3
GFP-FKBP-TACC3
Microtubules
***
n.s.
10 min
30 min
Rapamycin
Vehicle
Rapamycin
Treatment
C
Microtubules
MT density (μm-2)
10 min
30 min
GFP-TACC3 + Rapamycin
GFP-FKBP-TACC3 + Vehicle
GFP-FKBP-TACC3 + Rapamycin
Cross-sectional area (μm2)
TACC3 RNAi +
GFP-TACC3 + Rapamycin
GFP-FKBP-TACC3 + Vehicle
GFP-FKBP-TACC3 + Rapamycin

Figure 4.13: TACC3 KS at metaphase does not significantly alter K-fibre microtubule number. A. Representative views of electron tomograms of orthogonal sections of K-fibres in metaphase HeLa cells expressing mCherry-MitoTrap and GFP-TACC3 or GFP-FKBP-TACC3, and treated as indicated. Overlaid are microtubules (red) and the calculated K-fibre perimeter (green). Scale bar, 100 nm. **B.** Tukey box plots of K-fibre microtubule number in TACC3-depleted HeLa cells expressing mCherry-MitoTrap and GFP-TACC3 or GFP-FKBP-TACC3, treated with vehicle or rapamycin (200 nM) for 10 min (top) or 30 min (bottom). TACC3 KS (red) causes a slight reduction in microtubules of K-fibres after both 10 min and 30 min of rapamycin application. The reduction was significantly lower than for vehicle-treated cells (ANOVA with Tukey-Kramer *post-hoc* test $p<0.01$, ***), but not when compared with rapamycin-treated GFP-TACC3-expressing cells ($p>0.05$, n.s.). Tukey box plots show the median, interquartile range and the 10^{th} and 90^{th} percentile. **C.** Plots of microtubule number versus K-fibre cross-sectional area after 10 min and 30 min treatment. Lines of best fit show the similar microtubule density in all conditions. Insets, bar chart to show mean ± s.e.m. K-fibre microtubule density in control (green, blue) or TACC3 KS cells (red) (10 min data: green, n=22 K-fibres; blue, n=54; red, n=32. 30 min data: green, n=32; blue, n=38; red, n=28).

observed in any of the other experiments, including the cold-stable assay in **4.4.8**. Since no detectable loss of kMTs was observable 10 min after KS, perhaps allowing for a longer delay after rapamycin application would reveal a progressive loss of MTs. Therefore, the same analysis was performed in cells 30 min after treatment with vehicle or rapamycin (**Figure 4.13B**, bottom). No significant difference was observed between the data at 10 min and 30 min for each condition (**Figure 4.13B**, bottom), and median kMT number in all conditions remained >20. Therefore, there was no progressive loss of kMTs following TACC3 KS at metaphase.

Furthermore, the density of the K-fibres was analysed at each timepoint (**Figure 4.13C**). The MT density of K-fibres in all conditions and at both timepoints was unaltered (**Figure 4.13C**, lines of best fit and insets). The scatter plots in **Figure 4.13C** demonstrate further that most K-fibres in TACC3 KS cells have normal MT numbers (between 20 and 40), albeit at the lower end. These results are in agreement with the results of the cold-stable assay in **4.4.8** indicating that TACC3 KS at metaphase does not affect kMT number or their attachment to kinetochores.

4.4.10 TACC3 KS at metaphase does not alter the spatial organisation of K-fibres

Although there was no detectable loss of MTs in K-fibres following 10 min or 30 min TACC3 KS, it was nonetheless possible that an alteration in K-fibre organisation could cause the phenotypes seen in **4.4.5** and **4.4.6**. Therefore, spatial analysis of the MTs in K-fibres of control or TACC3 KS cells was performed using neighbour density analysis at 10 and 30 min (**Figure 4.14A**) and nearest neighbour analysis at 30 min (**Figure 4.14B**). With neither analysis was a difference observed between control conditions and TACC3 KS.

4.4.11 TACC3 KS at metaphase alters kinetochore dynamics

The previous results, such as the reactivation of the spindle checkpoint and loss of K-fibre tension but without loss of kMTs, suggest that the phenotypes observed after TACC3 KS at metaphase are due to a reason unrelated to K-fibre organisation, MT

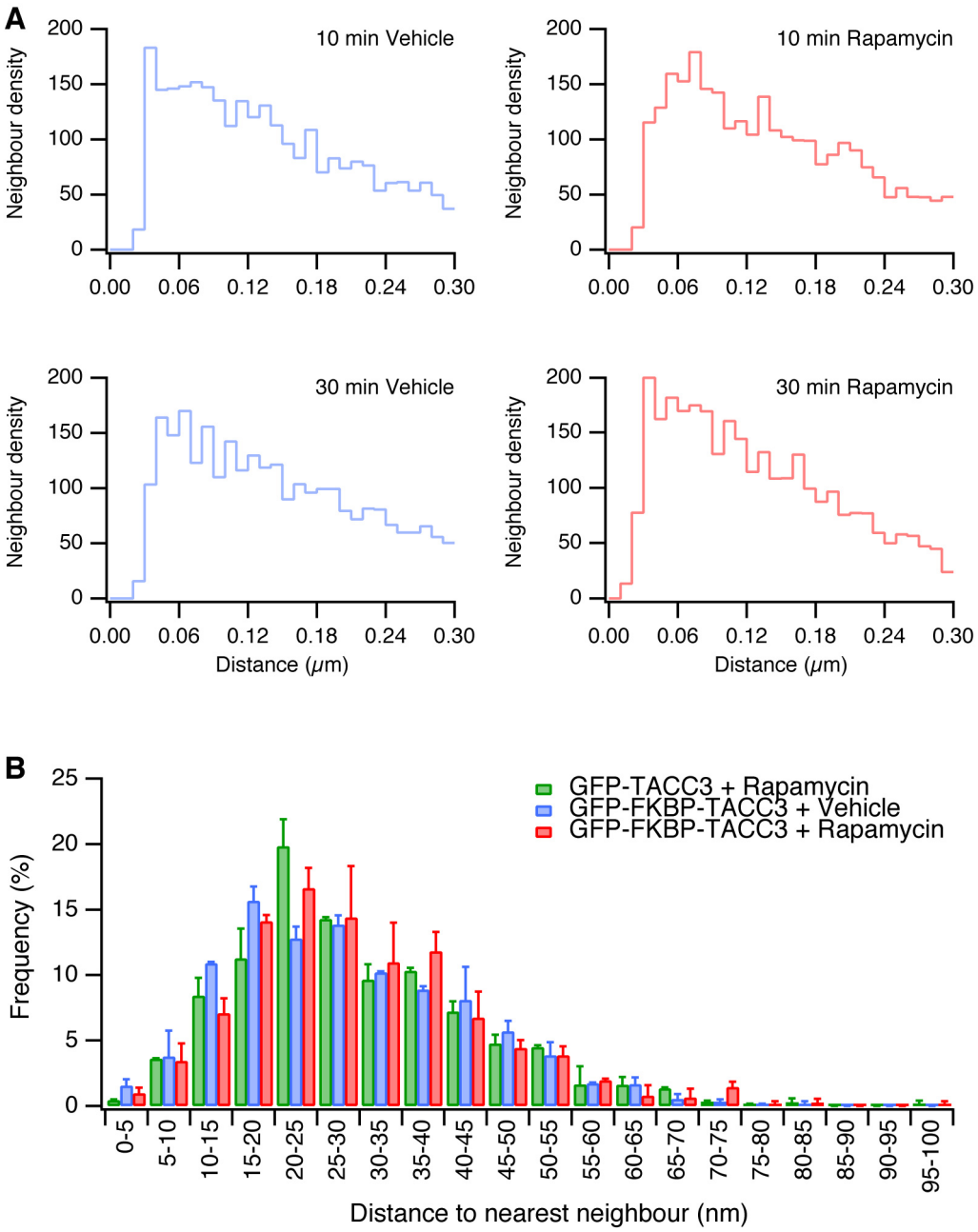

Figure 4.14: TACC3 KS at metaphase does not alter the spatial organisation of K-fibres. A. Typical neighbour density analysis (nda) plots (McDonald *et al*., 1992) are shown for K-fibres of cells expressing GFP-FKBP-TACC3 treated with vehicle or rapamycin (200 nM) for 10 or 30 min. These plots show the preferred spacing within a K-fibre and no obvious qualitative difference was seen following TACC3 KS. **B.** Bar chart to show the mean ± s.e.m. of the distance of each microtubule to its to nearest neighbouring microtubule.

number or attachment. Therefore, studying kinetochore dynamics could reveal further information about the underlying cause of the mitotic delay. TACC3-depleted metaphase HeLa cells stably expressing GFP-CENP-A and centrin-GFP transfected with PAGFP-MitoTrap and mCherry-TACC3 or mCherry-FKBP-TACC3 were treated with vehicle or 200 nM rapamycin, and imaged in 4 dimensions. The motions of the kinetochores were tracked and analysed as described in (Jaqaman *et al*., 2010), and the spindle poles as described in **4.3.1.7** and **Figure 4.2**.

The kinetochores oscillations were visibly dampened following TACC3 KS compared to control conditions (**Figure 4.15A, B, C**). In agreement with this, both the period and half-period of kinetochore oscillations in TACC3 KS cells were reduced compared to control cells as indicated by analysis of sister centre displacement (Δx; **Figure 4.15F**). However, sister displacement cross-correlation analysis showed no alteration of kinetochore 'breathing' by TACC3 KS (not shown), indicating that MT plus tip dynamics remained unchanged. A plane was fitted to the metaphase plate to assess kinetochore alignment (see **Figure 4.2C, D**) and the sister centre alignment was quantified (**Figure 4.15D**) to measure metaphase plate thickness. The distance of sister centre alignment from the plate was more variable in TACC3 KS than in control cells (σ_X values; **Figure 4.15E**), indicating that the metaphase plate was thicker (Barlett's statistic, 87.799, $p<0.001$; **Figure 4.15E**). This variability is likely much larger because kinetochores >2.5σ from the plate were rejected from the analysis. Furthermore, a reduction in inter-kinetochore distance was observed, indicating that the results in **Figure 4.11** were reproducible in live cells (μ_d values). In addition, mean squared displacement analysis for kinetochore pairs showed that the movements of kinetochores following TACC3 KS were less constrained compared to controls (**Figure 4.15G**). In other words, for a given duration, kinetochores have moved further following TACC3 KS than in cells with normal levels of TACC3 on the spindle.

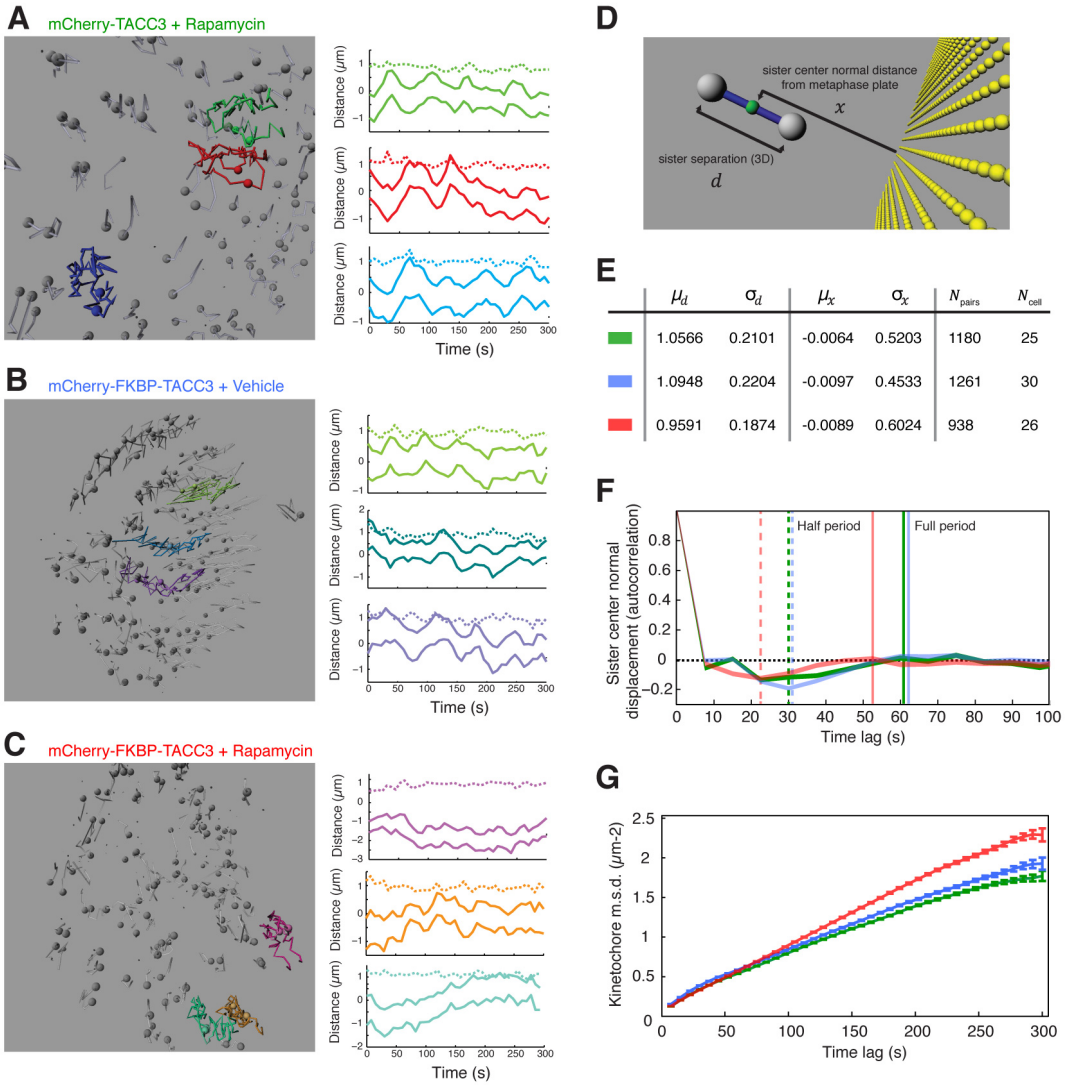

	μ_d	σ_d	μ_x	σ_x	N_{pairs}	N_{cell}
	1.0566	0.2101	-0.0064	0.5203	1180	25
	1.0948	0.2204	-0.0097	0.4533	1261	30
	0.9591	0.1874	-0.0089	0.6024	938	26

Figure 4.15: TACC3 KS at metaphase alters kinetochore dynamics. Analysis of kinetochore motions in live HeLa cells stably expressing GFP-CENP-A and centrin-GFP. Cells were depleted of endogenous TACC3 and expressed PAGFP-MitoTrap and either mCherry-TACC3 or mCherry-FKBP-TACC3 and were treated with vehicle or rapamycin (200 nM). **A-C.** Three example kinetochore trajectories from typical cells are shown. Left, image of automated kinetochore tracking. Right, plots of kinetochore distances relative to the metaphase plate as a function of time for the coloured kinetochores in the example images. Tracks of two sisters are shown for each pair, difference plot is shown (dotted line). **D.** Schematic diagram to show the measurement of d and x. **E.** Table to show population data for sister separation (d, inter-kinetochore distance) and sister center normal position (x). **F.** Sister center normal displacement (Δx auto-correlation). Line thickness represents 95% confidence interval. Peaks of negative and positive lobes (half- and full-period) are shown by dashed and full vertical lines, respectively. **G.** Mean squared displacement analysis for kinetochore pairs. Error bars show s.e.m. Analysis in all figure panels is from 4 independent experiments.

All of these observations suggest a loss of tension within the spindle. This would explain the alteration of kinetochore oscillations following TACC3 KS without affecting breathing dynamics, which are dependent on MT plus end dynamics (Jaqaman *et al*., 2010), as well as the increased metaphase plate thickness, and the increased mean squared displacement.

4.4.12 TACC3 KS at metaphase reduces spindle length

4D tracking of kinetochore motions in live cells following TACC3 KS consistently supported a loss of K-fibre tension (**Figure 4.15**), as did the measurements of inter-kinetochore distance in fixed cells (**Figure 4.11**). However, it would be of interest to know whether this loss of tension is restricted to the K-fibres, or whether a similar phenotype can be observed elsewhere in the mitotic spindle. Therefore, spindle poles were imaged and tracked in 4D using centrin-GFP in the movies acquired in **4.4.11**, and their motions analysed using novel algorithms (Cheeseman *et al*., 2013; see **4.3.1.7**, **Figure 4.16A**).

In TACC3 KS cells, mean pole-to-pole distance over the duration of the movies (41 timepoints) was reduced by 12% compared to controls (**Figure 4.16B**). To test whether this spindle shortening was merely an overall reduction in spindle size, the average interpolar distance was plotted against the average inter-kinetochore distance for each cell (**Figure 4.16C**). There was no correlation between the lower inter-kinetochore distance and the reduced interpolar distance, indicating that this was a genuine loss of tension, and not an overall shrinkage of the mitotic spindle.

4.5 Discussion

This chapter has demonstrated the utility of KS in temporally dissecting the functions of proteins of the mitotic spindle. However, in contrast to previous work on the TACC3–ch-TOG–clathrin complex using RNAi, the results observed here were sometimes drastically different, which allowed the clarification of our view of the functions of this complex.

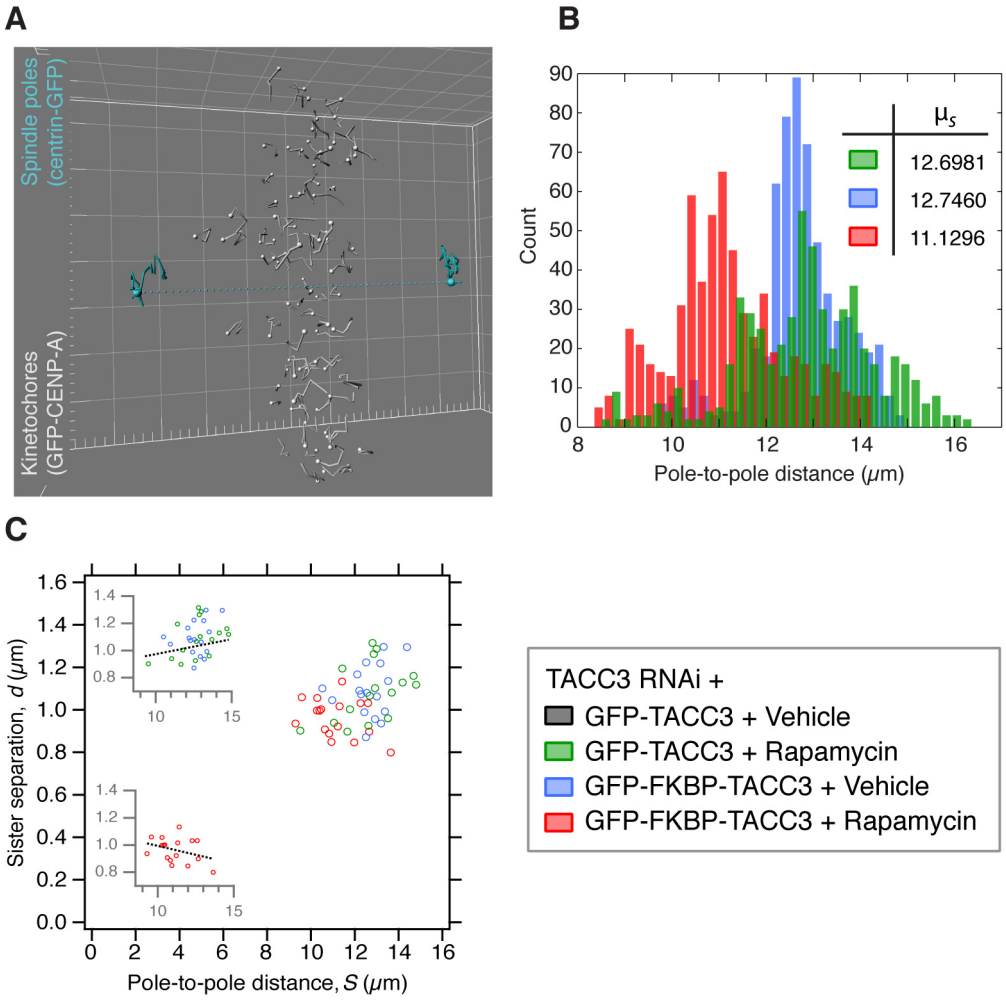

Figure 4.16: TACC3 KS at metaphase reduces spindle length. Analysis of spindle pole motions in live HeLa cells stably expressing GFP-CENP-A and centrin-GFP. Cells were depleted of endogenous TACC3 and expressed PAGFP-MitoTrap and either mCherry-TACC3 or mCherry-FKBP-TACC3 and were treated with vehicle or rapamycin (200 nM). **A.** Image to show the automated 4D tracking of spindle poles (centrin-GFP) in addition to kinetochores. **B.** Histogram to show the Euclidian interpolar distances (*S*) for each condition. Inset, mean interpolar distance (μm) for each condition. **C.** Scatter plots to show that the average inter-kinetochore distance (d) does not vary as a function of spindle length (*S*). Inset, plots show control data (above) and TACC3 KS data (below), for reference a line of best fit is shown (r^2 = 0.08 and 0.11, respectively). Analysis in all figure panels is from 4 independent experiments.

Firstly, CLEM performed on TACC3 KS cells revealed a loss of inter-MT bridges in K-fibres, consistent with previous work (Booth *et al*., 2011). In addition, the TACC3 homologue in fission yeast has also been reported to have a crosslinking activity, indicating that the role of TACC3–ch-TOG–clathrin as a crosslinker is a conserved function (Thadani *et al*., 2009). However, the reduction in this frequency was far smaller than that observed using RNAi to deplete clathrin or TACC3 (Booth *et al*., 2011) or following Aurora A inhibition (Cheeseman *et al*., 2011). Can this smaller reduction reflect an incomplete depletion of TACC3? This is unlikely, as the post-depletion levels of TACC3 on the spindle were lower following KS than in cells treated with TACC3 RNAi or MLN8237 (**3.4.6**, **Figure 3.9**). One possibility is that the alteration of K-fibre structure, such as the loss of kMTs and density seen by Booth and colleagues following RNAi-mediated depletion, skewed the quantification of crosslinker frequency. For example, it could be considered that some types of crosslinkers may initially bundle MTs into K-fibres, whereas others may simply maintain the bundling. Should the former be depleted, it may hinder the binding of the latter type. The loss of kMTs observed using RNAi might also have hindered the binding of inter-MT bridges (Booth *et al*., 2011). Furthermore, MLN8237 affects all Aurora A substrates, not just TACC3, and it is possible that TACC3 RNAi had off-target effects, which exaggerated the phenotypes in these cells (Booth *et al*., 2011; Cheeseman *et al*., 2011). A final possibility is that a pool of the TACC3–ch-TOG–clathrin remains tightly bound to the spindle following TACC3 KS. This seems unlikely, and the remaining protein levels would need to be sufficiently low to show full depletion of GFP-FKBP-TACC3 on the spindle by light microscopy, but leave behind a enough of the protein to show incomplete depletion by electron microscopy. Whatever the answer, it is possible that previous inter-MT bridge quantification phenotypes have been exaggerated.

Another surprising result was the increased magnitude of the mitotic delay seen using TACC3 KS at NEBD compared to RNAi, even though these manipulations were predicted to have similar effects. One likely explanation is the higher efficiency of depletion of TACC3 from the mitotic spindle using KS compared to RNAi (**Figure 3.9**), probably due to dimerisation of GFP-FKBP-TACC3 with residual endogenous TACC3 (**Figure 3.8**). Another possibility is that TACC3 KS co-reroutes ch-TOG and clathrin, stopping them from performing potential functions that are

independent of the complex. Furthermore, it is also possible that TACC3, along with ch-TOG and clathrin, may possess additional functions other than merely physical cross-bracing. Enzymatic activity of the complex, such as the potential modulation of MT growth similarly to the homologues of TACC3 and ch-TOG in other species, has yet to be determined. A final possibility is that during the 48-hour depletion time using TACC3 RNAi, the cell is able to partially compensate for the missing proteins by upregulating separate pathways. In any case, it is possible that the depletion phenotype of other proteins have been similarly underestimated.

Using KS, it was possible to show that the TACC3–ch-TOG–clathrin complex still performs a crucial function at metaphase, and that the metaphase arrest seen in TACC3 RNAi-treated cells was not solely due to the assembly of a defective spindle. It was then possible to use KS to study this later-stage function.

TACC3 KS at metaphase was shown to reactivate the spindle checkpoint and reduce K-fibre tension. This loss of tension was not due to a loss of MT-kinetochore attachment stability and occurred without detectable loss of kMTs. It therefore suggests that the spindle checkpoint is able to monitor a reduction of K-fibre tension independently of K-fibre attachment, which is a topic of debate in the literature (Nezi and Musacchio, 2009). There is strong evidence to show that tension is not sensed by the spindle checkpoint such as the application of taxol, a MT stabiliser, which reduces K-fibre tension without causing the recruitment of Mad2 to kinetochores (Waters *et al*., 1998), although it should be noted that the authors reported the presence of Mad2 on a subset of kinetochores following loss of tension, similarly to the present study. On the other hand, other studies have shown that treatment with low-dose vinblastine, a MT-depolymerising drug, which does not significantly alter the spindle, arrests cells at metaphase and reduces K-fibre tension without recruiting Mad2 (Skoufias *et al*., 2001). But there have also been reports indicating that tension is an important factor in activating or silencing the SAC (Stern and Murray, 2001; Uchida *et al*., 2009), and that this is mediated by specific proteins (Indjeian *et al*., 2005). CLEM performed on TACC3 KS cells showed no detectable loss of kMTs, even after prolonged removal, arguing for the separate detection of tension and attachment. However, not all K-fibres could be studied in these cells, and a single unattached kinetochore is sufficient to arrest cells at metaphase (Rieder *et al*., 1994), a possibility that cannot be ruled out here. Furthermore, kMT numbers in TACC3 KS

cells were within normal range, albeit towards the lower end. It cannot be ruled out that a small reduction in kMT number is sufficient to activate the spindle checkpoint. A final possibility is that the loss of inter-kinetochore tension caused the spindle checkpoint protein Aurora B kinase to destabilise a small subset of MT attachments at kinetochores (Cheeseman *et al*., 2002), which subsequently recruited Mad2. Interestingly, it has been reported in fission yeast that depletion of the TACC3 homologue Alp7 also causes Mad2-dependent metaphase arrest (Sato *et al*., 2003), potentially by helping to ensure stable MT-kinetochore attachment (Tang *et al*., 2013) and bipolar spindle formation (Sato *et al*., 2004).

In relation to K-fibre tension, the experiments found different control inter-kinetochore distances in fixed (**Figure 4.11**) versus live (**Figure 4.15**) cells. Although both cell lines were HeLa, several explanations for this discrepancy are possible. Firstly, the sample processing for IF, such as fixing and drying, may alter the size of the sample. Secondly, the live cells were stably expressing two fluorescently tagged proteins, and the methods used to obtain stable cell lines may have selected for cells with a smaller inter-kinetochore distance. Thirdly, the fixed cell inter-kinetochore distances were measured by hand whereas the live cell inter-kinetochore distance was measured in an automated manner. Although both methods used centroid-to-centroid measurements, there may have been differences between the automated and manual measurements. Finally, different kinetochore markers will produce variable inter-kinetochore measurements, and strong differences between live/fixed cells and use of CENP-A or CREST have previously been observed (Wong and Fang, 2006).

A further interesting discrepancy in this study compared to previous RNAi-based studies is that TACC3 KS at metaphase did not cause a detectable loss of kMTs. Schneider *et al*., (2007) had reported impaired MT-kinetochore attachment following TACC3 RNAi, while Booth *et al*., (2011) had observed a dramatic loss of MTs from K-fibres using clathrin RNAi, and a concomitant loss of kMT density. This effect was not seen in this study, with only a small loss of kMTs and no alteration of fibre density suggesting that the MT loss was limited to the periphery of the K-fibre. This difference is likely due to the time at which the proteins were depleted. Rather than suggesting that the TACC3–ch-TOG–clathrin complex stabilises kMTs at metaphase, it now appears more likely that the complex helps spindle assembly and

K-fibre maturation during prometaphase, perhaps by helping to recruit MTs into K-fibres (thus explaining that clathrin RNAi apparently reduced kMT numbers). However, once MTs have attached at the kinetochore they may become stabilised by the structure itself and depletion of the TACC3–ch-TOG–clathrin no longer causes loss of kMTs. Testing this hypothesis would require a CLEM study of cells in which TACC3 KS was performed at NEBD.

The key finding of this study was the role of TACC3–ch-TOG–clathrin in maintaining K-fibre tension at metaphase. This is a clear phenotype, as many of the results from different experiments point to this. These results include reduced inter-kinetochore distance (**Figure 4.11**) without loss of kMTs (**Figure 4.13**) or attachment (**Figure 4.12**), reduced pole-to-pole distance (**Figure 4.16**) and dampened kinetochore oscillations without alteration of kinetochore breathing (**Figure 4.15**).

How can the loss of TACC3–ch-TOG–clathrin inter-MT bridges at metaphase cause this loss of tension? One possibility is that the inter-MT bridges help keep individual kMTs straight throughout the K-fibre and their removal might therefore increase individual kMT bending, reducing the rigidity of the K-fibres and thus decreasing K-fibre tension. In this scenario, one would expect K-fibre density to be reduced and kMT spacing to increase, a feature that has already been reported (McDonald *et al*., 1992). This was not the case (**Figure 4.14**), although the biggest alteration in fibre organisation would be expected at the midpoint between the pole and the kinetochore, whereas the spatial kMT analysis in this study was performed within 1 μm of the kinetochore.

A second possibility is that the MT crosslinkers help distribute tensile forces throughout the K-fibre by the physical cross-bracing of MTs, thereby increasing the tensile strength of the fibre. An analogy of this would be the weaving of a rope, which increases its tensile strength compared to an unconnected bundle of its constitutive filaments. This possibility is supported by the results of an *in vitro* study, which demonstrated that bundles of MTs crosslinked by Eg5 had more resistance when tension was applied to them compared to MTs without Eg5 (Charlebois *et al*., 2011).

A third possibility is that TACC3 KS does not alter K-fibres directly, but affects non-kMTs. This is supported by the absence of correlation between reduced inter-kinetochore distance and interpolar distance (**Figure 4.16**), in agreement with a previous study (Dumont and Mitchison, 2009a), suggesting they are two independent observations. Reduced pole-to-pole distance therefore needs to be considered as a phenotype in itself. If considered in the context of the model of spindle forces suggested by Dumont and Mitchison (Dumont and Mitchison, 2009b), pole-to-pole distance is not governed by K-fibres, rather the poles are pushed apart by interpolar MTs. How can a loss of TACC3–ch-TOG–clathrin from mitotic spindles contribute to this? Whilst MT motor proteins such as the kinesin 14 and kinesin 5 protein families have been shown to slide anti-parallel interpolar MTs (kinesin 14: (Sharp *et al*., 1999); kinesin 5: (Mountain *et al*., 1999; Kapitein *et al*., 2005)), there is evidence to suggest that passive MT crosslinking can affect MT-MT sliding by acting as a brake to counter-balance sliding forces (Braun *et al*., 2011). There have been no reports of endogenous TACC3, ch-TOG, or clathrin observed on interpolar MTs, however we cannot exclude this possibility. This warrants further investigation and poses a number of supplemental questions, such as (1) Can TACC3–ch-TOG–clathrin crosslink anti-parallel MTs as well at the parallel kMTs? (2) If so, does this require a change in complex conformation? (3) If the complex is only found on K-fibres, how would TACC3–ch-TOG–clathrin inter-MT bridges specifically oppose forces pushing the poles together, and not those pushing the poles apart?

A final possibility is that the phenotypes observed in this study are due to alterations in MT dynamics rather than spindle mechanics following removal of TACC3–ch-TOG–clathrin at metaphase. This possibility is supported by previous reports indicating that TACC3 and/or ch-TOG promote MT nucleation and polymerisation (Popov *et al*., 2001; Popov *et al*., 2002; Kinoshita *et al*., 2005; Peset *et al*., 2005; Barr and Gergely, 2008; Peset and Vernos, 2008; Cassimeris *et al*., 2009) and stabilise MT minus ends (Tournebize *et al*., 2000; Kinoshita *et al*., 2001). Although there has been no study of MT dynamics following TACC3 KS in the present study, it could explain the mitotic delay seen during chromosome alignment following TACC3 KS at NEBD (**Figure 4.8**), and using TACC3 RNAi (**Figure 4.6C**) as reported previously (Gergely *et al*., 2003; Schneider *et al*., 2007; Lin *et al*., 2010). The role of TACC3/ch-TOG in MT minus end stability may also explain the reduced

pole-to-pole distance (**Figure 4.16**) and altered kinetochore microdynamics (**Figure 4.15**). Although this aspect of spindle function following TACC3 KS has been overlooked here, it would be of considerable interest to investigate MT dynamics in these conditions in future.

Interestingly, many of the phenotypes observed here are similar or linked to those seen in yeast by depletion of the TACC3 and ch-TOG homologues Alp7 and Alp14. Indeed, both yeast homologues have been found to be involved in microtubule crosslinking (Thadani *et al.,* 2009), bipolar spindle formation (Sato *et al.,* 2004), kinetochore-microtubule attachment (Tang *et al.,* 2013), chromosome alignment (Kakui *et al.*, 2013) and spindle checkpoint satisfaction (Sato *et al.*, 2003). These studies support the results in this thesis, and are indicative of a strong conservation of the TACC3 and ch-TOG functions through evolution. In mammals, clathrin has joined the TACC–TOG complex, but it seems the functions have remained unchanged. The extent of this functional conservation suggests that this complex has retained important roles during mitosis, as the present study has shown, and merits to be studied further to uncover how the TACC3–ch-TOG–clathrin complex contributes to K-fibre formation.

Overall, these results have brought us detailed new insight into the temporally distinct roles of the TACC3–ch-TOG–clathrin complex which would not have been possible by using RNAi alone. Although it is clear that this type of inter-MT bridge is critical at early mitosis to align chromosomes, a new role at metaphase has been identified in the maintenance of mitotic spindle integrity by ensuring that tension is applied to kinetochores and that the spindle checkpoint is satisfied.

5 Chapter 5 – Discussion

This thesis has demonstrated the use of the knocksideways technique to dissect the temporally distinct roles of proteins during mitosis, and provided new insight into the roles of TACC3–ch-TOG–clathrin in K-fibres.

This is the first use of the knocksideways system during mitosis. Whereas other techniques such as the auxin-degron system have been successfully used for the depletion of mitotic proteins (Holland *et al*., 2012; Nishino *et al*., 2013), KS remains amongst the fastest inactivation methods (Cheeseman *et al*., 2013). It was also revealed that KS was equally as effective – if not more – at depleting TACC3 from mitotic spindles as RNAi.

This new addition to the cell biologist's toolbox will be very useful in the study of dynamic processes such as mitosis and endocytosis. As demonstrated in this thesis, KS was able to reveal information about the roles of proteins during mitosis that was unavailable using RNAi-mediated depletion. KS was furthermore able to help investigate protein-protein interactions by (1) demonstrating that the interactions between TACC3, ch-TOG and clathrin are strong, as shown by the co-rerouting of proteins, and (2) that there is no clathrin-independent TACC3 even at the centrosome. Additionally, I've shown that KS can reveal information about the dynamics of proteins within the cell, as demonstrated by the variable rerouting time of different proteins and at different stages of the cell cycle, similarly to a previous study (Silvius *et al*., 2006).

Concerning the TACC3–ch-TOG–clathrin microtubule crosslinker complex, this study has shown similarly to previous studies that TACC3, ch-TOG and clathrin are important during early mitosis for chromosome congression and alignment (Gergely *et al*., 2003; Royle *et al*., 2005; Schneider *et al*., 2007; Fu *et al*., 2010; Lin *et al*., 2010), but also in later mitosis by helping to maintain K-fibre tension and spindle checkpoint satisfaction at metaphase after a normal prometaphase.

These results contribute to a better understanding of the molecular basis of the involvement of TACC3, ch-TOG and clathrin in cancer. All three proteins have

previously been associated with the disease. ch-TOG is overexpressed in some colon and liver tumours (Charrasse *et al*., 1995) and its role in spindle organisation poses a clear link to tumour aneuploidy and genetic instability (Conte *et al*., 2003; Gergely *et al*., 2003; Cassimeris and Morabito, 2004). Clathrin gene fusions have also been linked to cancer. Clathrin heavy chain (CHC) fused to anaplastic lymphoma kinase (ALK) has been found in large B-cell lymphoma (Cools *et al*., 2002; Chikatsu *et al*., 2003; De Paepe *et al*., 2003; Gascoyne *et al*., 2003) and inflammatory myofibroplastic tumour (Bridge *et al*., 2001; Cools *et al*., 2002), whilst CHC fusion to transcription factor binding to IGHM enhancer 3 (TFE3) has been found in pediatric renal adenocarcinoma (Argani *et al*., 2003). However, these mutations are not thought to be linked to the mitotic functions of clathrin (Blixt and Royle, 2011). TACC3, along with TACC1 and 2, have been linked to some forms of cancer. In particular, TACC3 gene fusions with the fibroblast growth factor receptor 3 (FGFR3) have been associated with multiple myeloma (Still *et al*., 1999), glioblastoma (Singh *et al*., 2012; Parker *et al*., 2013) and bladder cancer (Williams *et al*., 2013), and displayed oncogenic activity in cells and mice (Singh *et al*., 2012). TACC3 overexpression has been linked to oncogenic behaviour (Fielding *et al*., 2011; Ha *et al*., 2013), non small-cell lung cancer (Jung *et al*., 2006) and breast cancer (Schmidt *et al*., 2010), whereas TACC3 aberrations and downregulation have been linked to ovarian cancer (Lauffart *et al*., 2005).

These associations with various forms of cancer, in particular by ch-TOG and TACC3, indicate that these proteins could serve as important diagnostic biomarkers or therapeutic targets in cancer treatment. An important study found that TACC3 disruption caused the regression of lymphoma tumours in mice *in vivo* as well as several lymphoma cell lines by inducing the formation of multipolar spindles followed by apoptosis (Yao *et al*., 2012). Previous studies also indicated that TACC3 depletion could increase the sensitivity of tumour cells to paclitaxel (Taxol) (Schneider *et al*., 2008; Schmidt *et al*., 2010).

The present study contributes to our knowledge of these proteins and their involvement in the development and progression of cancer. Although sudden onset inactivation of TACC3–ch-TOG–clathrin in whole mammals *in vivo* is unlikely due to the slow speed at which drugs can enter the bloodstream and penetrate the plasma membrane, it is important to understand the full molecular effects that these drugs

might have. The results presented here show that there are several important temporally distinct effects of the inactivation of the TACC3–ch-TOG–clathrin complex during mitosis. It appears that the most important role played by the MT crosslinker is its contribution to chromosomal congression and alignment, as demonstrated by the almost complete failure of cells to form a metaphase plate following TACC3 KS. The effect of TACC3 KS at metaphase was less severe, with most cells able to reach anaphase following a period of delay. This new information may help target cancer therapies in more subtle ways, such as by potentiating anti-TACC3 drugs by combining them with drugs targeting effectors of spindle assembly.

To conclude, this study has brought new insight into the roles of inter-microtubule bridges in K-fibres during mitosis. Previous work had suggested that these bridges could stabilise MTs by protecting them against depolymerisation (Booth *et al*., 2011). Here, I've shown that this is not the case after maturation of the K-fibre, since the inactivation of the TACC3–ch-TOG–clathrin complex at metaphase did not cause the disassembly of K-fibres. Nonetheless, it is clear that this protein complex has a critical role for chromosomal alignment, potentially by contributing to mitotic spindle assembly, and a further role in maintaining spindle function and kinetochore microdynamics and satisfying the spindle checkpoint. Using KS, it will be important to investigate the function of this complex in spindle assembly in future, and also to similarly revisit the roles of other spindle proteins to get a clearer view of their functions.

6 Appendices

6.1 Aurora A kinase activity is required for the localization of TACC3/ch-TOG/clathrin inter-microtubule bridges

ARTICLE ADDENDUM

Communicative & Integrative Biology 4:4, 409-412; July/August 2011; ©2011 Landes Bioscience

Aurora A kinase activity is required for localization of TACC3/ch-TOG/clathrin inter-microtubule bridges

Liam P. Cheeseman, Daniel G. Booth, Fiona E. Hood, Ian A. Prior and Stephen J. Royle*

The Physiological Laboratory; University of Liverpool; Liverpool, UK

Accurate chromosome segregation during mitosis is achieved by the kinetochore fibers (K-fibers) of the spindle apparatus. These fibers are bundles of microtubules (MTs) connected by non-motor bridges. We recently identified a TACC3/ch-TOG/clathrin complex that constitutes the shortest class of inter-MT bridge in K-fibers. TACC3 anchors the complex to MTs and this is dependent on phosphorylation by Aurora A kinase. Here we show that inhibition of Aurora A kinase using MLN8237 results in (1) loss of clathrin and TACC3 from spindles, (2) destabilization of K-fibers and (3) loss of inter-MT bridges. These results are similar to those in cells depleted of clathrin or TACC3; suggesting that TACC3/ch-TOG/clathrin bridges are the major class of bridge that is regulated by this kinase.

Key words: aurora A kinase, cancer, ch-TOG, clathrin, inter-microtubule bridge, microtubule, mitotic spindle, MLN8237, MLN8054, TACC3

Submitted: 02/19/11

Accepted: 02/19/11

DOI: 10.4161/cib.4.2.15250

*Correspondence to: Stephen J. Royle; Email: s.j.royle@liverpool.ac.uk

Addendum to: Booth DG, Hood FE, Prior IA, Royle SJ. A TACC3/ch-TOG/clathrin complex stabilizes kinetochore fibres by inter-microtubule bridging. EMBO J 2011; 30:906–19; PMID: 21297582; DOI:10.1038/emboj.2011.15.

The mitotic spindle is responsible for the accurate segregation of chromosomes that occurs during mitosis.[1] The spindle apparatus is a dynamic assembly of microtubules (MTs), motors and non-motor proteins.[2,3] Chromosome movements are performed by the kinetochore fibers (K-fibers) of the spindle. K-fibers are bundles of 20–40 MTs that run from the kinetochore on the chromosome to the spindle pole.[4] The stability of these fibers is important for chromosome movement and successful mitosis.

In electron micrographs, the MTs in K-fibers are connected by electron-dense inter-MT bridges.[5,6] These bridges are hypothesized to allow for the uniform transduction of forces throughout the MT bundle and to contribute to fiber stability. The inter-MT bridges in K-fibers vary in length from ~16 to ~60 nm[5,7] and are thought to be comprised of non-motor proteins.[2,3] In a recent paper, we described that the shortest type of bridges in K-fibers are comprised of a complex of transforming acidic coiled-coil protein 3 (TACC3), colonic, hepatic tumor overexpressed gene (ch-TOG) and clathrin.[7] Depletion of clathrin heavy chain (CHC) by RNAi resulted in K-fibers that lacked the shortest type of inter-MT bridges. Similar results were found in TACC3-depleted cells. Longer bridges were still present, indicating that different proteins may constitute these other bridge classes. Finally, we showed labeling of inter-MT bridges with clathrin immunogold. Our results suggested that clathrin is the actual cross-bracing molecule with TACC3/ch-TOG acting as anchor points on adjacent microtubules. This interpretation accounts for our results[7-10] and those of others.[11-13]

The activity of the mitotic kinase Aurora A was found to be crucial for the localization of the TACC3/ch-TOG/clathrin complex components on the spindle. We found that phosphorylation of TACC3, presumably at serine 558, by Aurora A kinase is required for TACC3 to bind to MTs and to subsequently recruit clathrin to the spindle.[7] Acute inhibition of Aurora A kinase with the specific inhibitor MLN8237 (0.3 μM) resulted in a loss of TACC3 and clathrin from the spindle within 35 min. In addition, mutation of serine 558 to alanine completely blocked recruitment of TACC3 and clathrin to the spindle.[7]

A drawback of RNAi is that protein depletion is relatively prolonged compared to the length of the cell cycle. The mitotic

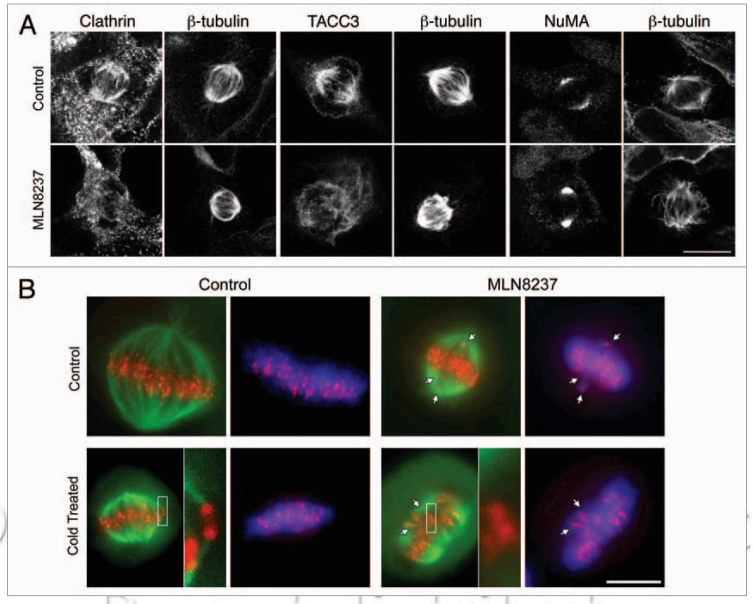

Figure 1. Effect of inhibition of Aurora A kinase on TACC3/clathrin localization and K-fiber stability. (A) Inhibition of Aurora A kinase resulted in loss of clathrin and TACC3 from mitotic spindles. HEK293 cells near metaphase were treated with MLN8237 (0.5 μM, 40 min) prior to fixation and staining with the indicated antibodies. All experimental details are as described previously in reference 7, anti-NuMA (#3888, Cell Signaling). Bar, 10 μm. (B) Inhibition of Aurora A kinase resulted in destabilization of kinetochore fibers. HeLa cells near metaphase were treated with no drug (Control) or MLN8237 (0.3 μM, 40 min) and then incubated for 6 min in warm (control) or cold (cold treated) media to depolymerize any non-stable MTs. Cells were fixed and stained for β-tubulin (green), CENP-B (red) and DNA (DAPI, blue). Bar, 10 μm. Note the misaligned chromosomes (arrows) and the "orphan" centromeres in the inset. Similar observations were reported in clathrin-depleted cells.[9,10]

spindle is constructed in the absence of the protein of interest and so compensatory mechanisms may complicate the interpretation of the experiment. The acute removal of clathrin and TACC3 from spindles by chemical inhibition of Aurora A kinase presents an opportunity to confirm that removal of these proteins results in loss of inter-MT bridges from spindles that have assembled normally.

As reported previously in reference 7, treatment of cells near metaphase with MLN8237 (0.5 μM, 40 min) resulted in a loss of clathrin and TACC3 from mitotic spindles (**Fig. 1A**). Inhibition of Aurora A kinase did not result in a non-specific loss of all spindle proteins because NuMA, a protein that crosslinks MTs at the spindle pole,[14] was still present. This indicated that the effect on TACC3 and clathrin was likely due to blocking phosphorylation of TACC3, a known Aurora A kinase substrate.[15,16]

We next examined kinetochore fiber stability using a qualitative immunofluorescence assay. Previously, depletion of CHC was shown to result in misaligned chromosomes in metaphase-like cells.[9] These cells had K-fibers that were not stably attached and could be depolymerized by cold treatment. We tested whether or not cells treated with MLN8237 (0.3 μM) for 40 min had a similar mitotic defect. **Figure 1B** shows that control HeLa cells at metaphase had good alignment of the metaphase plate and most kinetochores had cold-stable K-fiber attachments. In cells where Aurora A kinase had been inhibited, misaligned chromosomes were evident and several "orphan" kinetochores could be found. Orphan kinetochores could be found at the metaphase plate suggesting that they had congressed normally but had lost their stable attachment to the spindle (**Fig. 1B**). The effect of inhibiting Aurora A kinase during metaphase is therefore similar to depletion of CHC by RNAi.[9]

In a previous study, we found that depletion of either CHC or TACC3 resulted in a loss of inter-MT bridges from K-fibers. The missing bridges were the shortest form of inter-MT bridge and the longer types of bridges were found to be slightly upregulated.[7] We analyzed by electron microscopy the inter-MT bridges in K-fibers of cells close to metaphase where Aurora A kinase was inhibited using MLN8237 (**Fig. 2A**). The frequency of bridges per unit length of total MT or of parallel MT was reduced by ~37% (**Fig.**

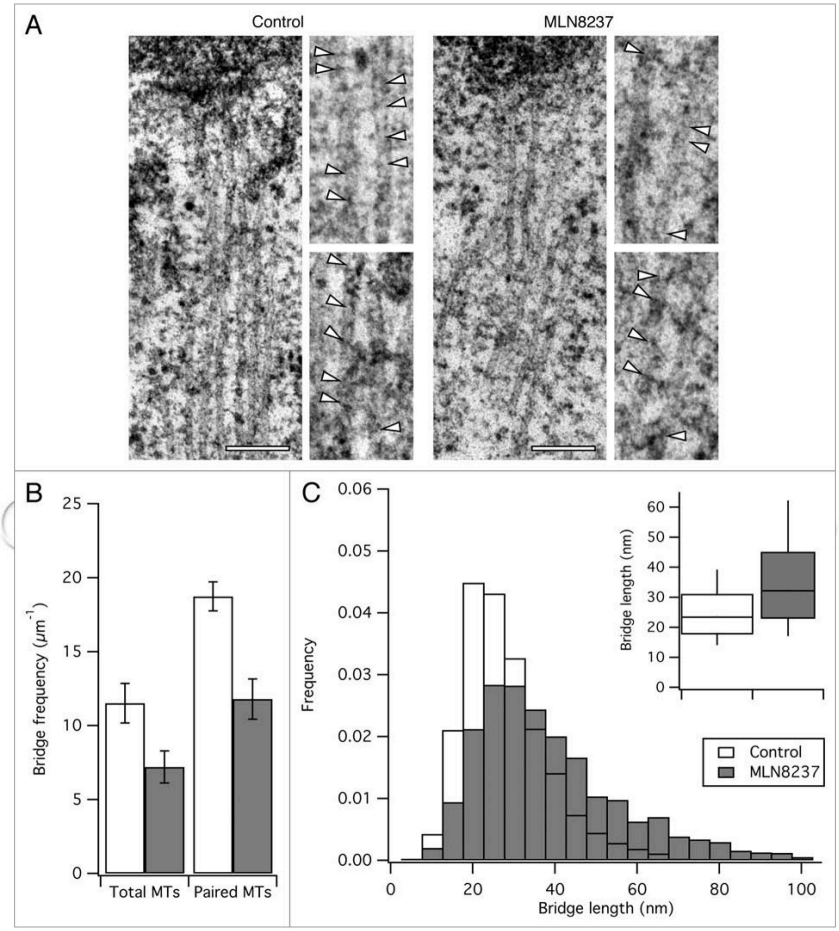

Figure 2. Effect of inhibition of Aurora A kinase on inter-MT bridges. Inhibition of Aurora A kinase resulted in loss of inter-MT bridges. MLN8237-treated HeLa cells near metaphase were processed for EM. (A) Representative sections to show the morphology of K-fibers. Zoomed regions show bridges indicated by arrowheads. Scale bar, 200 nm. (B and C) Quantification of inter-MT bridges in K-fibers from control or MLN-treated cells. (B) Bar chart to show the average frequency of bridges per unit length of total or paired MTs. Student's t-test, $p = 0.066$ and $p = 0.014$; $N_{cell} = 3$; Bars, mean ± SEM. (C) Frequency histogram to show the length distribution of inter-MT bridges. Inset: Tukey plots of the length distribution data.

2B). The frequency distribution of bridge lengths was also altered with median bridge lengths of 23.4 and 32.2 nm in controls versus MLN8237-treated cells (**Fig. 2C**). Again, these results are broadly similar to the data from clathrin-depleted and TACC3-depleted cells.[7] This suggests that these defects arise from the removal of clathrin/TACC3 from K-fibers.

MLN8237 is a specific inhibitor of Aurora A kinase and so off-target effects are minimized.[17] However, there are many other Aurora A substrates[18] whose localization or function at the spindle is likely to depend on the activity of the kinase. The observed changes in inter-MT bridges following brief incubation with low concentrations of MLN8237 represent a very specific

change in spindle structure. This suggests that TACC3/ch-TOG/clathrin bridges are the main class of bridge whose localization is dependent of Aurora A kinase. However, the antiproliferative property of this class of inhibitors[19] is more likely to result from the global inhibition of Aurora A phosphorylations rather than solely on the specific effect of inter-MT bridge removal.

Rapid and specific removal of spindle proteins is likely to be a major advance over long-term depletion studies. For example, in clathrin-depleted cells, loss of short inter-MT bridges appeared to precede loss of MTs in K-fibers.[7] It may be possible to separate temporally bridge loss and MT loss using chemical inhibition. Future studies will therefore concentrate on methods to rapidly remove spindle proteins specifically.

Acknowledgements

We thank Bill Earnshaw for the gift of anti-CENP-B. This work was supported by a Career Establishment Award from Cancer Research UK (C25425/A8722). L.P.C. and D.G.B. are recipients of Wellcome Trust Prize Studentships and I.A.P. is a Royal Society University Research Fellow.

References

1. Scholey JM, Brust-Mascher I, Mogilner A. Cell division. Nature 2003; 422:746-52.
2. Peterman EJ, Scholey JM. Mitotic microtubule crosslinkers: insights from mechanistic studies. Curr Biol 2009; 19:1089-94.
3. Manning AL, Compton DA. Structural and regulatory roles of nonmotor spindle proteins. Curr Opin Cell Biol 2008; 20:101-6.
4. Rieder CL. Kinetochore fiber formation in animal somatic cells: dueling mechanisms come to a draw. Chromosoma 2005; 114:310-8.
5. Hepler PK, McIntosh JR, Cleland S. Intermicrotubule bridges in mitotic spindle apparatus. J Cell Biol 1970; 45:438-44.
6. Witt PL, Ris H, Borisy GG. Structure of kinetochore fibers: microtubule continuity and inter-microtubule bridges. Chromosoma 1981; 83:523-40.
7. Booth DG, Hood FE, Prior IA, Royle SJ. A TACC3/ch-TOG/clathrin complex stabilizes kinetochore fibres by inter-microtubule bridging. EMBO J 2011; 30:906-19.
8. Hood FE, Royle SJ. Functional equivalence of the clathrin heavy chains CHC17 and CHC22 in endocytosis and mitosis. J Cell Sci 2009; 122:2185-90.
9. Royle SJ, Bright NA, Lagnado L. Clathrin is required for the function of the mitotic spindle. Nature 2005; 434:1152-7.
10. Royle SJ, Lagnado L. Trimerisation is important for the function of clathrin at the mitotic spindle. J Cell Sci 2006; 119:4071-8.
11. Fu W, Tao W, Zheng P, Fu J, Bian M, Jiang Q, et al. Clathrin recruits phosphorylated TACC3 to spindle poles for bipolar spindle assembly and chromosome alignment. J Cell Sci 2010; 123:3645-51.
12. Hubner NC, Bird AW, Cox J, Splettstoesser B, Bandilla P, Poser I, et al. Quantitative proteomics combined with BAC TransgeneOmics reveals in vivo protein interactions. J Cell Biol 2010; 189:739-54.
13. Lin CH, Hu CK, Shih HM. Clathrin heavy chain mediates TACC3 targeting to mitotic spindles to ensure spindle stability. J Cell Biol 2010; 189:1097-105.
14. Gaglio T, Saredi A, Compton DA. NuMA is required for the organization of microtubules into aster-like mitotic arrays. J Cell Biol 1995; 131:693-708.
15. Kinoshita K, Noetzel TL, Pelletier L, Mechtler K, Drechsel DN, Schwager A, et al. Aurora A phosphorylation of TACC3/maskin is required for centrosome-dependent microtubule assembly in mitosis. J Cell Biol 2005; 170:1047-55.
16. LeRoy PJ, Hunter JJ, Hoar KM, Burke KE, Shinde V, Ruan J, et al. Localization of human TACC3 to mitotic spindles is mediated by phosphorylation on Ser558 by Aurora A: a novel pharmacodynamic method for measuring Aurora A activity. Cancer Res 2007; 67:5362-70.
17. Sloane DA, Trikic MZ, Chu ML, Lamers MB, Mason CS, Mueller I, et al. Drug-resistant aurora A mutants for cellular target validation of the small molecule kinase inhibitors MLN8054 and MLN8237. ACS Chem Biol 2010; 5:563-76.
18. Sardon T, Pache RA, Stein A, Molina H, Vernos I, Aloy P. Uncovering new substrates for Aurora A kinase. EMBO Rep 2010; 11:977-84.
19. Manfredi MG, Ecsedy JA, Meetze KA, Balani SK, Burenkova O, Chen W, et al. Antitumor activity of MLN8054, an orally active small-molecule inhibitor of Aurora A kinase. Proc Natl Acad Sci USA 2007; 104:4106-11.

6.2 Studying kinetochore-fiber ultrastructure using correlative light-electron microscopy

CHAPTER

Studying Kinetochore-Fiber Ultrastructure Using Correlative Light-Electron Microscopy

20

Daniel G. Booth[*,†,1], **Liam P. Cheeseman**[*,1], **Ian A. Prior**[*] **and Stephen J. Royle**[*,‡]

[*]*Department of Cellular & Molecular Physiology, Institute of Translational Medicine, University of Liverpool, Liverpool, United Kingdom*

[†]*Wellcome Trust Centre for Cell Biology, University of Edinburgh, Edinburgh, United Kingdom*

[‡]*Centre for Mechanochemical Cell Biology, Division of Biomedical Cell Biology, Warwick Medical School, University of Warwick, Coventry, United Kingdom*

CHAPTER OUTLINE

[1]These authors contributed equally to this work.

Methods in Cell Biology, Volume 115 **ISSN 0091-679X**

http://dx.doi.org/10.1016/B978-0-12-407757-7.00020-7

Abstract

Electron microscopy (EM) has dominated high-resolution cellular imaging for over 50 years, thanks to its ability to resolve on nanometer-scale intracellular structures such as the microtubules of the mitotic spindle. It is advantageous to view the cell of interest prior to processing the sample for EM. Correlative light-electron microscopy (CLEM) is a technique that allows one to visualize cells of interest by light microscopy (LM) before being transferred to EM for ultrastructural examination. Here, we describe how CLEM can be applied as an effective tool to study the spindle apparatus of mitotic cells. This approach allows transfected cells of interest, in desirable stages of mitosis, to be followed from LM to EM. CLEM has often been considered as a technically challenging and laborious technique. In this chapter, we provide step-by-step pictorial guides that allow successful CLEM to be achieved. In addition, we explain how it is possible to vary the sectioning plane, allowing spindles and microtubules to be analyzed from different angles, and the outputs that can be obtained from these methods when applied to the study of kinetochore fiber ultrastructure.

INTRODUCTION

The mitotic spindle is a complex machine consisting of microtubules, motor proteins, and nonmotor proteins which, together, generate the forces needed to separate the sister chromatids between the two daughter cells (Scholey, Brust-Mascher, & Mogilner, 2003). A better visualization of its ultrastructure is necessary to understand the mechanisms underlying its functions.

Light microscopy (LM) and the discovery of the green fluorescent protein (GFP) led to many important discoveries due to the possibility of tracking protein dynamics in live cells. However, LM has a relatively low resolution, which does not allow one to visualize structures smaller than ~200 nm. This diffraction limit has been a major imaging weakness, and electron microscopy (EM) has been one of the few techniques to overcome it. Another disadvantage of LM is the restricted number of separate wavelength channels which can be used on a single sample without overlap, while the rest of the cell remains unobservable.

EM also possesses its share of drawbacks, other than the tricky and time-consuming nature of sample preparation. Only static samples can be observed, making the analysis of dynamic changes impossible. Also, routine EM does not allow one to easily locate cells of interest, such as cells expressing a fluorescent protein or in a particular stage of the cell cycle. It is possible to overcome these limitations by combining the ease and dynamic nature of LM with the subnanometer resolving power of EM in the form of correlative light-electron microscopy (CLEM).

CLEM techniques are useful for studying the mitotic spindle. The complexity of spindle microtubules means that they cannot be viewed individually by LM. Also, mitosis is a very dynamic process; each of its stages lasts less than

30 min, so pinpointing the exact stage of the cell cycle for a particular cell is critical before engaging in time-costly EM sample preparation. This is why the ability to observe and select cells of interest using LM prior to EM sample processing is a great advantage; allowing both the stages of mitosis to be chosen carefully, and to ensure that the cell is adequately expressing a fluorescent protein of interest.

Studies using EM to research mitotic spindles have yielded outstanding data, such as the quantification of microtubule polarity by Euteneuer and McIntosh (1981), the study of microtubule spacing, position, displacement, and length (McDonald, O'Toole, Mastronarde, & McIntosh, 1992), or the more recent whole-cell reconstruction by electron tomography to study cytoskeletal elements (Hoog et al., 2007).

Here, we describe our own application of CLEM to study the ultrastructure of the mitotic spindle, particularly kinetochore fibers (K-fibers) (Booth, Hood, Prior, & Royle, 2011; Cheeseman, Booth, Hood, Prior, & Royle, 2011). We describe both longitudinal and orthogonal sectioning relative to the spindle axis (Fig. 20.1), which reveal different information about spindle architecture (Fig. 20.1D), and how we can quantify such results. Longitudinal sectioning has allowed us to quantify microtubule cross-linkers between K-fiber microtubules, whereas sample-tilting of orthogonally sectioned K-fibers allowed the quantification of the number of microtubules forming the fiber. Subsequent analysis of the spacing of these microtubules allows us to measure their density and distribution.

20.1 MATERIALS

1. 35-mm glass-bottomed dishes with etched coordinates (MatTek Corporation, P35G-2-14-C-GRD)—referred to here as CLEM dishes
2. 0.1 M phosphate buffer (PB): mix 0.2 M Na_2HPO_4 with 0.2 M NaH_2PO_4 and dilute to 0.1 M. Solution should be at pH 7.4
3. Fix solution (EM grade fixatives: 3%, w/v, glutaraldehyde (Agar Scientific R1020), 0.5%, w/v, paraformaldehyde (Agar Scientific R1026) in 0.05 M PB)
4. Wash solution (0.05 M PB, 0.1 M sucrose)
5. DNA stain solution (0.1%, w/v, Hoechst-33342 in wash solution, or other similar DNA dye)
6. 1% osmium tetroxide (Agar Scientific R1015) in water
7. 0.5% (w/v) uranyl acetate (Agar Scientific R1260A) in 30% ethanol
8. Molecular grade 100% ethanol (Sigma-Aldrich 270741-1L)
9. EPON resin (Agar Scientific R1031, made up using the supplier's specifications for a "medium" block. Make sure resin mix is fully homogenized, and containing as few bubbles as possible. 200 ml of resin can be made up at a time, aliquoted into small glass vials, and kept frozen at −20 °C)

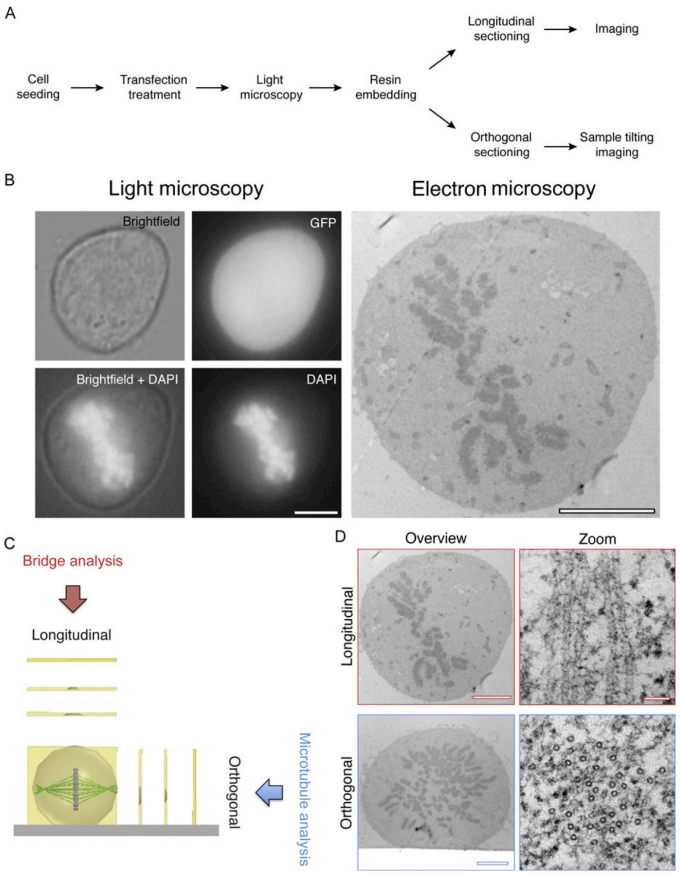

FIGURE 20.1

CLEM performed on mitotic cells. (A) A workflow to achieve CLEM using longitudinal or orthogonal sectioning. (B) A transfected mitotic HeLa observed by LM (Brightfield, GFP, and DAPI) and by electron microscopy. Scale bar 5 μm. (C) Schematic of longitudinal and orthogonal EM sectioning, and examples of output analysis. (D) Representative electron micrographs of cells sectioned longitudinally (above) and orthogonally (below) with high magnification of microtubules (right). Scale bar 4 μm (overview) and 50 nm (zoom).

10. Gelatin capsules (Size 0, Agar Scientific AGG29210)
11. Copper mesh sample grids, coated with formvar (Agar Scientific R1202). We routinely use 200 hexagonal mesh grids (TAAB GG017/C), but 100 mesh or slot grids can also be used. Beware, as the larger the gaps between the copper bars, the more easily the sample will distort and can tear
12. High precision tweezers. We prefer self-closing tweezers as they facilitate the handling of sample grids
13. 5% (w/v) uranyl acetate (Agar Scientific R1260A) in 50% ethanol
14. Reynold's lead citrate solution (see Reynolds 1963)

20.2 METHODS

20.2.1 Cell transfection and observation

Cells are seeded into CLEM dishes that contain a coordinate-engraved glass coverslip, providing a pattern to be left in the base of the resin, once embedded. The coordinates are essential for the LM to EM transfer as they allow cells of interest to be tracked throughout the entire CLEM process.

Seeding the appropriate amount of cells into the dishes is important: too many will make locating the cell of interest among many other unwanted cells difficult once the sample is embedded in resin; it will also make reading the coordinates under the light microscope difficult. However, seeding too few cells reduces the chances of finding a suitable cell of interest. We, therefore, seed cells at 5% density, or 40,000 HeLa cells per 35-mm dish in preparation for imaging and resin-embedding the sample the following day. If the cells require transfection for over 24 h, we usually transfect in separate plates (such as 6-well plates) and reseed them into the CLEM dishes at the appropriate time to attain the required density. Aim for a cell density of 10–15% on the day of processing for CLEM.

20.2.2 Fixation and sample preparation

20.2.2.1 Fixative solution osmolarity

The physiological osmolality of mammalian tissue is ~290 mOsm, depending on species, tissue type, and hydration status (Loqman, Bush, Farquharson, & Hall, 2010; Mathieu, Claassen, & Weibel, 1978). Fixative solutions should mimic physiological osmolality, providing an iso-osmotic equilibrium between intracellular and extracellular fluids. Figure 20.2 shows the examples of orthogonally sectioned cells fixed with solutions of varying osmotic strengths. At 440 and 1100 mOsm, a large amount of cell shrinkage can be observed, with poor spindle apparatus preservation and unusually dense cytosol. Therefore, we routinely use a fixing solution of ~280 mOsm, consisting of 3% glutaraldehyde, 0.5% paraformaldehyde in 0.05 M PB.

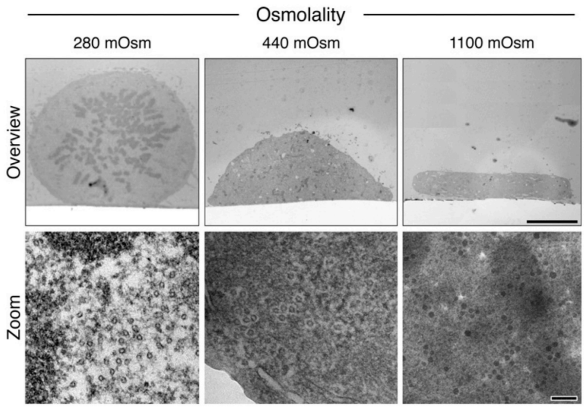

FIGURE 20.2

Optimization of mitotic spindle and cell structure preservation. Orthogonal sections of cells fixed with 280, 440, or 1100 mOsm solutions. Representative high-magnification electron micrographs of the cytosol in each condition are shown below. Scale bars 5 μm (overview) and 100 nm (bottom).

20.2.2.2 Light microscopy

On the day of sample processing, cells of interest can be identified under the light microscope with a 20× air objective. The low magnification allows images to be acquired containing a large field of view, useful for cell relocation during later processing. Some cells expressing fluorescent proteins require prefixation imaging as their fluorescence is obscured by the autofluorescence created by glutaraldehyde. Once the cell of interest has been located and imaged, add fixative solution for 1 h. It should be noted that microtubules are sensitive to temperature changes (Engelborghs, Heremans, Demaeyer, & Hoebeke, 1976); we, therefore, recommend that imaging of unfixed cells is carried out using an appropriate live imaging chamber at 37 °C.

After fixation, replace the fixative solution with 1–2 ml wash solution with 0.1% Hoechst-33342 (or similar DNA dye), incubate for ~20 min, rinse three times with wash solution (leaving on 1 ml of the final wash), and return the dish to the microscope. This second round of imaging is an opportunity to acquire high-magnification images of cells of interest, using 60× or 100× oil-immersion objectives (Fig. 20.1B, left). Take fluorescent and white light images of the cell, and also images of the same field of view focused on the coordinates. These will serve as references later to pinpoint the cell in the resin block and determine the orientation of the spindle axis. It helps at this stage to carefully wipe off any immersion oil with ethanol,

and mark the approximate location of the cell with a fine marker pen on the underside of the dish.

20.2.2.3 Resin embedding

Cells become round during mitosis and are, therefore, less adherent to their substrate. This means that during all steps up to resin embedding, dishes must be handled with extreme care so as to not detach or change the orientation of the cell.

Next, replace the wash solution with a few drops of 1% osmium tetroxide on the coverslip for 1 h. Remove the osmium and gently rinse the cells twice for 30 min with double-distilled water. Remove the water and replace with 30% ethanol for 30 min, then replace with a small amount of 0.5% uranyl acetate in 30% ethanol for 1 h. Next, the cells need to be dehydrated using a gradient of sequential solutions containing increasing amounts of ethanol. Replace stepwise with each of the following solutions: 30%, 50%, 60%, 70%, 80%, and 90% ethanol, then twice with 100% ethanol, incubating at each step for 10 min.

The cells can now be infiltrated with resin. Mix a 1:2 ratio of resin:ethanol solution, making sure that it is fully homogenized using a 3-ml plastic Pasteur pipette. Remove the ethanol from the dish and lightly cover the bottom of the dish with the resin infiltration mix for 20 min. Remove and replace with a 1:1 ratio of resin:ethanol solution for 20 min. Remove the mix and replace with a ~2-mm layer of 100% resin covering the bottom of the dish. If the sample is to be sectioned orthogonally, the dish can be placed in a 60 °C oven for 48–72 h. For longitudinal sectioning, fill either half of an embedding capsule with 100% resin and gently place it open-side down onto the cell (Fig. 20.3A), which you should be able to locate using the pen mark placed earlier. The dish can then be placed in the oven.

We recommend the use of EPON resin as other resin types (e.g., Agar Scientific Low Viscosity Resin) that we have tested react and bind the CLEM dish, making the separation steps (below) much more difficult.

20.2.3 Longitudinal sectioning

Longitudinal sectioning is the conventional EM method for viewing cells. Sections parallel to the plane of the coverslip are taken from the base of the cell moving progressively upward (see Fig. 20.1C). This plane of sectioning allows extended lengths of microtubules to be observed and is, therefore, particularly useful for analyzing microtubule attachment to the kinetochore, or quantifying microtubule cross-linkers (Fig. 20.1D).

Once the resin has fully polymerized, the dishes can be removed from the oven. Figure 20.3 contains a pictorial guide of the steps required to separate the resin and dish up to the sectioning. Using pliers, start by cutting-off the edges of the dish entirely (Fig. 20.3A–C) so that the seam between resin and plastic is accessible all the way around the dish. Very carefully insert a razor blade between the plastic and resin (Fig. 20.3D), slowly forcing the razor toward the center of the dish all the way around

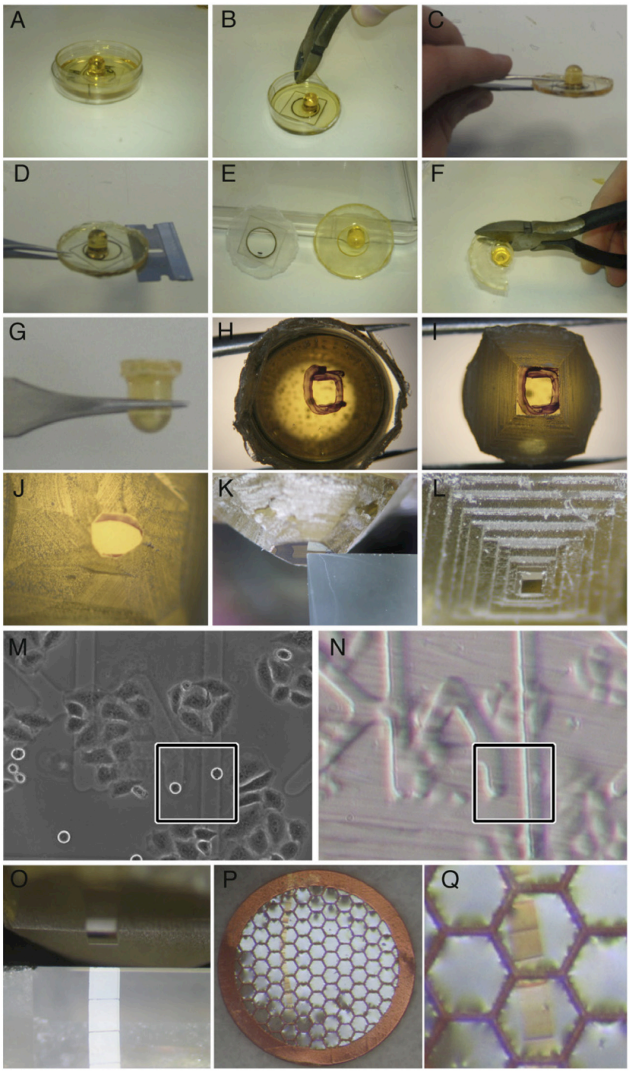

FIGURE 20.3

Pictorial guide to CLEM processing for sectioning longitudinally to the spindle axis. Following polymerization, resin was separated from the CLEM dish. Unwanted plastic was removed from the edges of the dish using pliers (A–C) allowing a razor to be inserted between the resin

the resin, to separate them (Fig. 20.3E). This must be performed with extreme care, as too much leverage by the razor will shatter the glass. This shattering usually renders the sample unusable, as removing all the glass fragments from the resin is very difficult without damaging the sample, and any microscopic shards of glass remaining will damage the diamond knife during sectioning. Dipping the resin and dish into liquid nitrogen for 1–2 s can help separate them, as the difference in thermal expansion between resin and plastic will eventually detach them. Other protocols use 40% hydrofluoric acid to dissolve the glass, bypassing this tricky step (Polishchuk, Polishchuk, & Luini, 2012).

Once detached, excess resin can be trimmed away until only the capsule remains (Fig. 20.3F and G). The coordinates imprinted on the underside of the capsule can be observed using a tissue dissection microscope; draw around the coordinate containing your cell of interest using a thin marker pen, the LM images serving as reference (Fig. 20.3H). Using a microtome chuck and bench-top vice to firmly hold the resin block in place, remove excess resin around the coordinate using a junior hacksaw (Fig. 20.3I), making sure that it never scratches the coordinate surface. This risk can be minimized by trimming away the resin using razor blades (Fig. 20.3J).

The remainder of the resin trimming and sectioning is performed using an ultramicrotome with glass knives (Fig. 20.3K) and a diamond knife (Fig. 20.3O), respectively. It is possible to make out the cell of interest and the etched coordinate using microtome binoculars (Fig. 20.3M and N). We routinely trim a square block face, up to ∼50 μm from the cell edge (Fig. 20.3L), but a wider space can be left according to one's experience. The larger the block face created during sectioning, the more difficult it will be to locate the cell in the sections under the EM. A square block face is optimal, as this helps acquire serial sections during sectioning. Sections 80 nm in thickness are taken using the diamond knife and collected using the copper grids coated with formvar (Fig. 20.3P and Q). To handle the grids, high-precision tweezers should be used at all times, carefully gripping the grid by its outer edge only, so as to not tear or damage the formvar or sample sections.

To attain optimal contrast under the microscope, we post-stain the sections by placing each grid section-side-down onto a drop of 5% uranyl acetate in 50% ethanol for 7–8 min, gently rinse in distilled water for 1 min, and place face-down on a drip of Reynold's lead citrate solution for 7–8 min. The grid is then rinsed in water again for 1 min. Both solutions should be centrifuged in 1.5-ml Eppendorf tubes at

and the dish base (D). Following the separation of resin and dish (E), excess resin was removed using pliers (F) until just the capsule remained (G). The cell of interest was marked (H) with the aid of LM images (M) and resin coordinates (N). Unwanted resin was removed using a junior hacksaw (I) and a razor (J). Resin was trimmed using a microtome and a glass knife (K) until a neat block was generated at the top of a pyramid (L). Blocks were sectioned using a diamond knife (O) and ribbons collected using 100 mesh copper grids (P and Q), coated with formvar.

8000 × *g* for 5 min before use to remove unwanted precipitate. Grids should be dried face-up for at least 2 h on clean filter paper before imaging, and kept in a clean, dust-free environment (such as a Petri dish or grid storage box).

20.2.4 Orthogonal sectioning

Orthogonal sectioning involves taking sections that are perpendicular to the spindle axis. In mitotic cells, this is useful to view and quantify most K-fiber microtubules within a single section. Quantifying K-fiber microtubules is possible using longitudinal serial sections (McEwen, Heagle, Cassels, Buttle, & Rieder, 1997); however, we avoided this method because (1) serial sections are particularly difficult to acquire and (2) spatial distribution analysis cannot be performed, as the compression forces exerted on each section of a serial reconstruction by the knife will likely deform the sample more than a single orthogonal cross-section through a K-fiber.

Figure 20.4 contains a pictorial guide of the steps required to prepare the sample for orthogonal sectioning. The samples to be sectioned orthogonally should consist of a flat layer of resin (without the resin capsule; Fig. 20.4A). Once removed from the oven, separate the dish from the resin using the same method as for the longitudinal samples (see above) and with the same amount of care (Fig. 20.4B–D). Using a tissue dissection microscope, find the coordinate containing your cell of interest and circle it using a marker pen (Fig. 20.4H). Using the coordinate grid and the LM images taken previously as references (Fig. 20.4E–G), determine the position and direction of the spindle axis and draw an elongated rectangle around the cell of interest (Fig. 20.4H–J). Cut out the rectangle using the hacksaw (Fig. 20.4K and L), paying attention not to touch or damage the surface of the marked coordinate. You should end up with a strip of resin (Fig. 20.4M). Carefully remove excess off one end, so the cell is near the tip, and insert it into a microtome chuck (Fig. 20.4N and O).

Using an ultramicrotome, you should be able to see the coordinates and can trim excess resin from the tip using glass knives until you approach the cell of interest (Fig. 20.4P–R). Trim away resin from either side of the cell to a depth of ∼100 μm, leaving a 50- to 100-μm buffer zone around the cell. Finally, trim away excess resin from the "upper" side of the strip, which is the block face positioned reverse-parallel to the one imprinted with coordinates. The thickness should be similar to the width on either side of the cell edge so that the block face is square shaped. The cell can now be sectioned using a diamond knife; we routinely take 80–100 nm slices. Sections should be collected and treated as described for longitudinal sectioning (see above), along with the same poststaining method.

20.2.5 Imaging and sample tilting

In longitudinal sections, K-fibers can be identified as bundles of microtubules in parallel conformation terminating at the kinetochore. During image capture, we typically take 4 μm by 3 μm images at 60,000× magnification. This allows us to distinguish adjacent microtubules and the material that cross-links them with enough

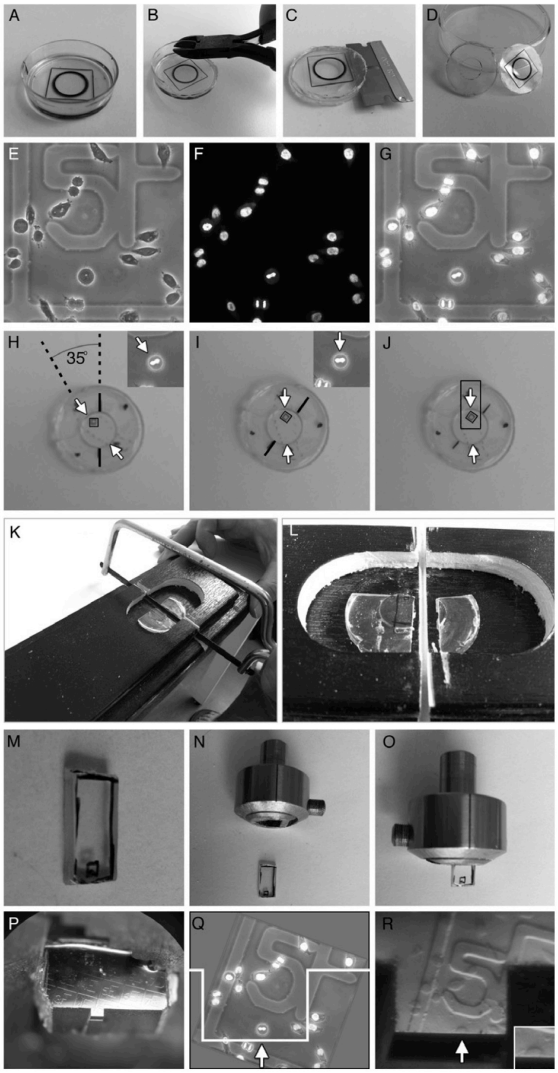

FIGURE 20.4

A pictorial guide to orthogonal CLEM processing. Following polymerization, resin was separated from the CLEM dish (A–D). Unwanted plastic was removed from the edges of the CLEM dish using pliers (B) allowing a razor to be inserted between the resin and the dish

Continued

resolution to measure the length of each element. One particular type of analysis that we have performed on such images is the quantification of microtubule cross-linker frequency (Booth et al., 2011; Cheeseman et al., 2011), but the qualitative assessment of microtubule attachment to kinetochores and of the overall organization of the fiber is also possible.

To image orthogonal sections under the microscope, full analysis of the K-fiber requires sample tilting. This is because microtubules are most easily recognizable when they are perpendicular to the imaging plane, as they appear as characteristic electron-dense rings. Not all microtubules will be at the correct angle, which increases the risk of quantification error. We can minimize this error by imaging the sample at various tilt angles (Fig. 20.5A). Our optimization shows that a single axis tilt of $\pm 45^\circ$ (90° in total) is sufficient to reveal 80% of microtubules in a K-fiber (Fig. 20.5B and C). A dual tilt along perpendicular axes is necessary to obtain 100% coverage. We perform image acquisition for a typical mammalian K-fiber at 60,000–90,000 × magnification.

Additionally, once the image tilt series (.raw file) is acquired, it can be assembled into a tomogram using IMOD software's Etomo package (Boulder Laboratory for Three-Dimensional Electron Microscopy). The final tomogram is a stack of images detailing the sample section in three dimensions and also removes some background compared to an unaltered electron micrograph.

We use ImageJ/Fiji software and IMOD's Neighbor Density Analysis (NDA) package to analyze the spatial distribution of microtubules within a fiber (McDonald et al., 1992). The output is a probability distribution graph, indicating the distance from any given microtubule at which one is most likely to find another microtubule. Other examples of types of spatial analyses which can be performed are (1) nearest neighbor analysis, which calculates the average distance between a microtubule and its nearest neighbor in the fiber and (2) the angular distribution of neighboring microtubules surrounding any given microtubule (also performed using the IMOD NDA package) (Ding, McDonald, & McIntosh, 1993).

20.3 DISCUSSION

CLEM remains among the most powerful imaging techniques available. The ability to view a live cell, in any state, or undergoing any particular or rare event, and to take an EM snapshot to be viewed at ~100,000 × magnification remains an outstanding

FIGURE 20.4—Cont'd base (C). Following separation (D), the position of the spindle was estimated using the reference LM images (E–G). These images allowed the reorientation of the resin (H and I) so that an appropriate block could be marked (J) before excision using a junior hacksaw and a miter block (K and L). The excised block (M) was inserted into a microtome chuck (N and O) and fine trimmed using a glass knife (P) before serial sections were taken of the cell, in the desired orientation (Q and R).

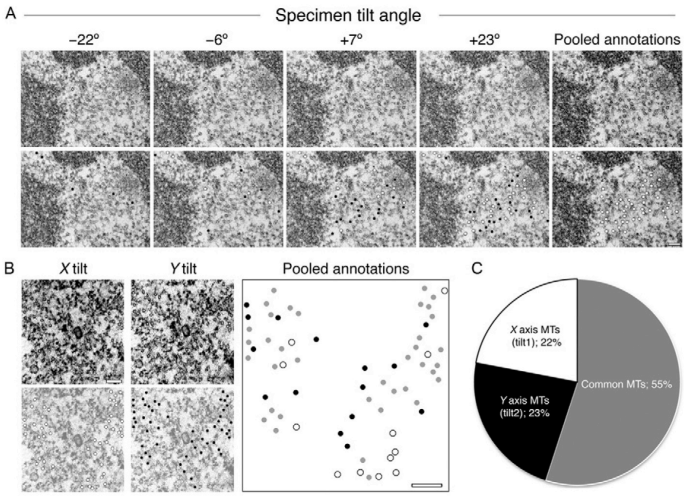

FIGURE 20.5

Sample tilting is necessary to achieve full coverage of microtubules in orthogonal sections. (A) Example electron micrographs taken from a −45° to +45° tilt series of a K-fiber. Observable microtubules are marked with dots (bottom row). Black dots represent microtubules that are unique to that tilt frame. White dots represent the accumulating microtubules identified in previous tilt frames. The total number of microtubule annotations were pooled together onto one frame (far right) giving a fair overview of the whole K-fiber. Scale bar 100 nm. (B and C) A dual tilt series of one K-fiber was carried out. (B) Representative electron micrographs taken from the central region of both *X* and *Y* tilts (A-top). All microtubules observed in each tilt series were annotated (bottom; *X* axis in white, *Y* axis in black). The sum of microtubules from both tilts were pooled together on to a single blank image, any microtubules that were common to both tilts were marked gray. Scale bar 100 nm. (C) A pie chart showing the percentage of total microtubules that were unique to each tilt and also the common ones.

tool to study cellular processes. However, this technique is often overlooked as it is considered too time-consuming and technically challenging.

Our CLEM protocol has been optimized for the study of mitotic spindles, where a great amount of attention has been placed on the preservation of the ultrastructure of microtubules and other spindle components. Our osmolality tests have shown that fixative solution osmolality must be as close to physiological conditions as possible. But further improvements could potentially be achieved during sample dehydration steps, at which point cell shrinkage can occur, as well as partial cytosolic washout.

Our protocol uses chemical fixation which is suboptimal for microtubule preservation. High-pressure freezing is an alternative fixation method, which uses the combination of ultra-low temperature to snap freeze the cell while applying pressure to inhibit the formation of ice crystals which would rupture and damage cellular structures. This fixation has been shown to substantially improve preservation of cellular architecture and organelle appearance (Wolf, Stockem, Wohlfarthbottermann, & Moor, 1981). Some studies have used CLEM with high-pressure freezing to study mitotic or meiotic events with remarkable success (Pelletier, O'Toole, Schwager, Hyman, & Mueller-Reichert, 2006). However, the implementation of this method with CLEM considerably increases the difficulty of the overall protocol, particularly when studying mitotic spindles. The size of the sample that can be frozen is very small, and as microtubules are particularly sensitive to temperature variation, a fast transfer from the light microscope/incubator to the high-pressure freezer is needed.

A useful addition to our CLEM protocol would be the ability to readily view proteins of interest under both light and electron microscopes. There has been recent focus on developing hybrid genetic tags that are both fluorescent and can be converted into an electron-dense signal to serve this purpose such as MiniSOG (Shu et al., 2011) and GFP-APEX (Martell et al., 2012). However, these tags have yet to be used to study the mitotic spindle.

Although our experimental purposes have only required standard epifluorescence micrographs before switching to EM, confocal microscopy could easily be implemented instead. This would allow the above protocol to be expanded, by combining confocal Z stacks and serial EM section imaging to create correlated 3D reconstructions in both light (confocal) and electron micrographs or electron tomograms. However, obtaining serial sections remains a challenge even for experienced electron microscopists. Nonetheless, there are currently several labs attempting the EM reconstruction of entire mitotic spindles, and whole-cell tomographic reconstruction has been achieved to study cytoskeletal structures (Hoog & Antony, 2007; Hoog et al., 2007), indicating the feasibility of this approach. Moreover, the recent effort by EM equipment suppliers to develop dual-beam EM microscopes which are able to both section and image the sample in an automated fashion could revolutionize this field. These machines, which are able to repeatedly remove 5 nm layers of sample and image the back-scattering of electrons using high-resolution scanning EM, bypass all the major difficulties involved with EM. So far, the resolution of this equipment is sufficient to comfortably reconstruct synaptic vesicles and other organelles (Knott, Rosset, & Cantoni, 2011), but it is not yet enough to view cytoskeletal elements such as microtubules in high detail.

Overall, CLEM is a powerful imaging method able to give unrivaled cellular structural detail, which we have applied to the study of K-fiber ultrastructure. We believe that the further integration of such tools as hybrid tags and dual-beam microscopes with CLEM will unlock a vast potential for the field of EM, which will maintain a firm place in research, regardless of the development of other super-resolution imaging systems.

Acknowledgments

We would like to thank Alison Beckett for technical help and discussions. D. G. B. and L. P. C. were supported by Prize Studentships from The Wellcome Trust. I. A. P. is a Royal Society University Research Fellow. S. J. R. is a Senior Cancer Research Fellow for Cancer Research UK.

References

Booth, D. G., Hood, F. E., Prior, I. A., & Royle, S. J. (2011). A TACC3/ch-TOG/clathrin complex stabilises kinetochore fibres by inter-microtubule bridging. *EMBO Journal*, *30*, 906–919. http://dx.doi.org/10.1038/emboj.2011.15.

Cheeseman, L. P., Booth, D. G., Hood, F. E., Prior, I. A., & Royle, S. J. (2011). Aurora A kinase activity is required for localization of TACC3/ch-TOG/clathrin inter-microtubule bridges. *Communicative & Integrative Biology*, *4*, 409–412.

Ding, R., McDonald, K. L., & McIntosh, J. R. (1993). Three-dimensional reconstruction and analysis of mitotic spindles from the yeast, Schizosaccharomyces pombe. *The Journal of Cell Biology*, *120*, 141–151.

Engelborghs, Y., Heremans, K. A. H., Demaeyer, L. C. M., & Hoebeke, J. (1976). Effect of temperature and pressure on polymerization equilibrium of neuronal microtubules. *Nature*, *259*, 686–689. http://dx.doi.org/10.1038/259686a0.

Euteneuer, U., & McIntosh, J. R. (1981). Structural polarity of kinetochore microtubules in Ptk1-cells. *The Journal of Cell Biology*, *89*, 338–345. http://dx.doi.org/10.1083/jcb.89.2.338.

Hoog, J. L., & Antony, C. (2007). Whole-cell investigation of microtubule cytoskeleton architecture by electron tomography. *Methods Cell Biol*, *79*, 145–167.

Hoog, J. L., Schwartz, C., Noon, A. T., O'Toole, E. T., Mastronarde, D. N., McIntosh, J. R., et al. (2007). Organization of interphase microtubules in fission yeast analyzed by electron tomography. *Developmental Cell*, *12*, 349–361. http://dx.doi.org/10.1016/j.devcel.2007.01.020.

Knott, G., Rosset, S., & Cantoni, M. (2011). Focussed ion beam milling and scanning electron microscopy of brain tissue. *Journal of Visualized Experiments*, *53*, e2588. http://dx.doi.org/10.3791/2588.

Loqman, M. Y., Bush, P. G., Farquharson, C., & Hall, A. C. (2010). A cell shrinkage artefact in growth plate chondrocytes with common fixative solutions: Importance of fixative osmolarity for maintaining morphology. *European Cells & Materials*, *19*, 214–227.

Martell, J. D., Deerinck, T. J., Sancak, Y., Poulos, T. L., Mootha, V. K., Sosinsky, G. E., et al. (2012). Engineered ascorbate peroxidase as a genetically encoded reporter for electron microscopy. *Nature Biotechnology*, *30*, 1143–1148. http://dx.doi.org/10.1038/nbt.2375 nbt.2375 [pii].

Mathieu, O., Claassen, H., & Weibel, E. R. (1978). Differential effect of glutaraldehyde and buffer osmolarity on cell dimensions—Study on lung-tissue. *Journal of Ultrastructure Research*, *63*, 20–34. http://dx.doi.org/10.1016/s0022-5320(78)80041-0.

McDonald, K. L., O'Toole, E. T., Mastronarde, D. N., & McIntosh, J. R. (1992). Kinetochore microtubules in Ptk cells. *The Journal of Cell Biology*, *118*, 369–383. http://dx.doi.org/10.1083/jcb.118.2.369.

Appendices

McEwen, B. F., Heagle, A. B., Cassels, G. O., Buttle, K. F., & Rieder, C. L. (1997). Kinetochore fiber maturation in PtK1 cells and its implications for the mechanisms of chromosome congression and anaphase onset. *The Journal of Cell Biology*, *137*, 1567–1580. http://dx.doi.org/10.1083/jcb.137.7.1567.

Pelletier, L., O'Toole, E., Schwager, A., Hyman, A. A., & Mueller-Reichert, T. (2006). Centriole assembly in Caenorhabditis elegans. *Nature*, *444*, 619–623. http://dx.doi.org/10.1038/nature05318.

Polishchuk, R. S., Polishchuk, E. V., & Luini, A. (2012). Visualizing live dynamics and ultrastructure of intracellular organelles with preembedding correlative light-electron microscopy. *Methods in Cell Biology*, *111*, 21–35.

Reynolds, E. S. (1963). The use of lead citrate at high pH as an electron- opaque stain in electron microscopy. *The Journal of Cell Biology*, *17*, 208–212.

Scholey, J. M., Brust-Mascher, I., & Mogilner, A. (2003). Cell division. *Nature*, *422*, 746–752.

Shu, X., Lev-Ram, V., Deerinck, T. J., Qi, Y., Ramko, E. B., Davidson, M. W., et al. (2011). A genetically encoded tag for correlated light and electron microscopy of intact cells, tissues, and organisms. *PLoS Biology*, *9*, e1001041. http://dx.doi.org/10.1371/journal.pbio.1001041.

Wolf, K. V., Stockem, W., Wohlfarthbottermann, K. E., & Moor, H. (1981). Cytoplasmic actomyosin fibrils after preservation with high-pressure freezing. *Cell and Tissue Research*, *217*, 479–495.

6.3 Specific removal of TACC3–ch-TOG–clathrin at metaphase deregulated kinetochore fiber tension

2102 Research Article

Specific removal of TACC3–ch-TOG–clathrin at metaphase deregulates kinetochore fiber tension

Liam P. Cheeseman[1], Edward F. Harry[2,3], Andrew D. McAinsh[2], Ian A. Prior[1] and Stephen J. Royle[1,2,*]

[1]Department of Cellular and Molecular Physiology, Institute of Translational Medicine, University of Liverpool, Crown Street, Liverpool L69 3BX, UK
[2]Centre for Mechanochemical Cell Biology, Division of Biomedical Cell Biology, Warwick Medical School, University of Warwick, Gibbet Hill Road, Coventry CV4 7AL, UK
[3]Molecular Organization and Assembly in Cells Doctoral Training Centre, University of Warwick, Coventry CV4 7AL, UK
*Author for correspondence (s.j.royle@warwick.ac.uk)

Accepted 1 February 2013
Journal of Cell Science 126, 2102–2113

doi: 10.1242/jcs.124834

Summary

Microtubule-associated proteins of the mitotic spindle are thought to be important for the initial assembly and the maintenance of spindle structure and function. However, distinguishing assembly and maintenance roles for a given protein is difficult. Most experimental methods for protein inactivation are slow and therefore affect both assembly and maintenance. Here, we have used 'knocksideways' to rapidly (~5 minutes) and specifically remove TACC3–ch-TOG–clathrin non-motor complexes from kinetochore fibers (K-fibers). This method allows the complex to be inactivated at defined stages of mitosis. Removal of TACC3–ch-TOG–clathrin after nuclear envelope breakdown caused severe delays in chromosome alignment. Inactivation at metaphase, following a normal prometaphase, significantly delayed progression to anaphase. In these cells, K-fiber tension was reduced and the spindle checkpoint was not satisfied. Surprisingly, there was no significant loss of K-fiber microtubules, even after prolonged removal. TACC3–ch-TOG–clathrin removal during metaphase also resulted in a decrease in spindle length and significant alteration in kinetochore dynamics. Our results indicate that TACC3–ch-TOG–clathrin complexes are important for the maintenance of spindle structure and function as well as for initial spindle assembly.

Key words: Checkpoint, Knocksideways, Microtubule, Mitotic spindle, Rapid inactivation

Journal of Cell Science

Introduction

Accurate chromosome segregation by the mitotic spindle is essential for life. It must proceed error-free in order to prevent cell death, cancer or birth defects (Murray, 2011). The spindle apparatus is an ensemble of microtubules (MTs), motors and non-motor proteins (Peterman and Scholey, 2009). Non-motor spindle proteins are involved in the initial assembly of the spindle and the maintenance of spindle structure and function. However, distinguishing the role in assembly and maintenance for a given spindle protein is problematic.

Over the last decade, RNA interference (RNAi) has dominated cell biology and it is the method of choice for understanding the function of spindle proteins. However, interpreting depletion phenotypes at later stages of mitosis is problematic because any defects observed could be due to errors that occurred at earlier stages, e.g. assembly of a defective spindle. In this study, we have used the 'knocksideways' method to rapidly and inducibly reroute spindle proteins to nearby mitochondria (Robinson et al., 2010). This allowed us to examine the role of inter-MT bridges at specific stages of mitosis, and particularly, in mature K-fibers following normal assembly of the mitotic spindle. Briefly, the knocksideways (KS) method exploits the binding of mammalian target of rapamycin (mTOR) to a complex of rapamycin bound to FKBP12. Rapamycin binds via the FKBP domain of FKBP12 and this binds the FRB (FKBP and rapamycin-binding) domain of mTOR kinase. KS involves the depletion of the target protein by RNAi and the re-expression of a version of the target protein that is refractory to RNAi and is tagged with the FKBP domain from FKBP12. In the same cells, MitoTrap, a mitochondrially targeted FRB domain is also expressed. Addition of rapamycin induces the heterodimerization of FKBP and FRB domains. This results in the protein of interest being rerouted from one subcellular location to mitochondria on a timescale of seconds (Robinson et al., 2010). If this new localization is incompatible with function, then the protein is inactivated.

TACC3 is an essential non-motor protein that binds the MT polymerase ch-TOG and localizes it to spindle fibers (Gergely et al., 2003; Gergely et al., 2000a; Gergely et al., 2000b; Lee et al., 2001; Piekorz et al., 2002). It was originally proposed that TACC3–ch-TOG are important for promoting spindle assembly by stabilizing MT minus ends at the centrosome or by antagonizing the depolymerizing activity of MCAK (Barr and Gergely, 2008; Kinoshita et al., 2005; Peset and Vernos, 2008). Later, it was found that TACC3–ch-TOG are bound to clathrin (Booth et al., 2011; Fu et al., 2010; Hubner et al., 2010; Lin et al., 2010), and possibly GTSE1 (Borner et al., 2012; Hubner et al., 2010) on kinetochore fibers (K-fibers) of the spindle. Here, TACC3–ch-TOG–clathrin complexes are thought to crosslink MTs by forming inter-MT bridges, suggesting a possible role for this non-motor complex in maintenance of spindle structure (Booth et al., 2011; Cheeseman et al., 2011; Royle, 2012; Royle et al., 2005). A rapid method of inactivation is therefore required to distinguish the role of the TACC3–ch-TOG–clathrin complex in assembly and maintenance of spindle structure. Furthermore, clathrin has distinct functions in

membrane trafficking and centrosome maturation in interphase (Brodsky, 2012) and TACC3 has a role in mRNA translation (Peset and Vernos, 2008). Slow inactivation methods alter these processes, which may cause indirect effects on mitosis and further confuse the interpretation of mitotic phenotypes.

In this study we use KS to remove TACC3–ch-TOG–clathrin complexes from mitotic spindles following normal spindle assembly and chromosome alignment. We find that TACC3–ch-TOG–clathrin complexes are required for the maintenance of K-fiber tension. Our findings demonstrate the utility of KS versus RNAi alone and describe the importance of non-motor proteins in the maintenance of spindle structure and micromechanics beyond initial assembly.

Results

Knocksideways is effective in mitosis for rapid, inducible removal of TACC3 from the mitotic spindle

We began by determining if rapid removal of spindle proteins is feasible during mitosis using knocksideways (KS), and on what timescale it could occur. To do this, we co-transfected HeLa cells with a plasmid to express mCherry-MitoTrap and a pBrain vector that simultaneously depleted endogenous TACC3 via shRNA and re-expressed a shRNA-refractory version of TACC3 that was tagged with GFP and FKBP (Fig. 1A). Live cells at metaphase were identified and imaged, with addition of rapamycin (200 nM) after 3 minutes (supplementary material Movie 1; Fig. 1B). We observed the removal of GFP-FKBP-TACC3 from the metaphase spindle within ~5 minutes of rapamycin application, and its colocalization to the mitochondria surrounding the spindle (Fig. 1B,C). Rerouting of GFP-FKBP-TACC3 to mitochondria was slower than in interphase, where rerouting followed a double exponential decay (Fig. 1D). We suspect that this difference is due to absence of a spindle in interphase to which TACC3 binds. By comparison, GFP-FKBP was rerouted extremely rapidly to mitochondria in interphase and at metaphase (Fig. 1D).

In a typical KS experiment we used four conditions, three controls and one test condition (Fig. 2A). In vehicle-treated cells, GFP-FKBP-TACC3 remained unaltered; and in cells expressing GFP-TACC3 without the FKBP domain, localization was unaffected by vehicle or rapamycin addition (Fig. 2A; supplementary material Fig. S1).

We found that effective rerouting of TACC3 KS depended on co-transfection of both plasmids and good expression of MitoTrap, which must be present in excess. For the method to be useful, the levels of TACC3 prior to KS must be within the normal range and after KS, the levels must be comparable to RNAi or Aurora A inhibition with MLN8237 (Booth et al., 2011). We assessed the levels of TACC3 on the spindle and in the cytoplasm for all conditions (Fig. 2B). This analysis showed that our re-expression of shRNA-refractory TACC3 in cells depleted of endogenous TACC3 was equivalent to endogenous levels and was not overexpressed (Fig. 2B). In addition, TACC3 KS resulted in a lower level of TACC3 at the spindle compared to RNAi or Aurora A inhibition.

TACC3 KS specifically removes the entire TACC3–ch-TOG–clathrin complex from the mitotic spindle

We next asked whether the rapid removal of TACC3 from the spindle affected other spindle proteins. To answer this question, we tested for rerouting of a number of other spindle proteins

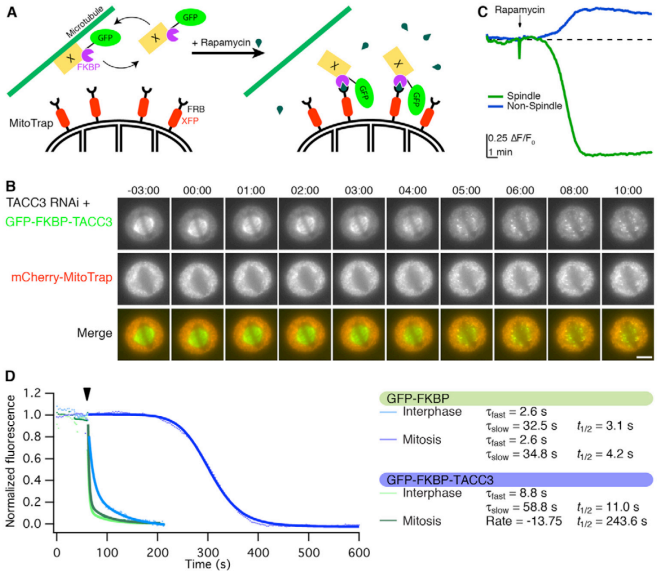

Fig. 1. Rapid, induced removal of TACC3 by knocksideways. (**A**) Diagram of knocksideways of a microtubule-associated protein. Protein X is depleted by RNAi and a shRNA-refractory version is re-expressed. Left: In the absence of rapamycin, the recombinant GFP- and FKBP-tagged protein X cycles on and off the microtubule. Right: Upon addition of rapamycin, the FKBP domain heterodimerizes with the FRB of XFP-MitoTrap (red) located on the mitochondria. (**B**) Video stills of TACC3 KS in a metaphase HeLa cell. Rapamycin (200 nM) was added at time zero (time is shown in minutes:seconds). GFP-FKBP-TACC3 is completely removed in ~5 minutes. Scale bar: 10 µm. (**C**) Quantification of GFP $\Delta F/F_0$ in the indicated areas over time during TACC3 KS. See supplementary material Movie 1. (**D**) Comparison of rerouting kinetics for GFP-FKBP-TACC3 or GFP-FKBP to mitochondria in interphase or mitosis, single cell examples. An overlay of curve fits to describe the rerouting are shown on the same time scale. Rapamycin application is denoted by the arrowhead. GFP-FKBP-TACC3 in mitosis was best fit by the Hill logistic function, all other data were best fit by a double exponential function.

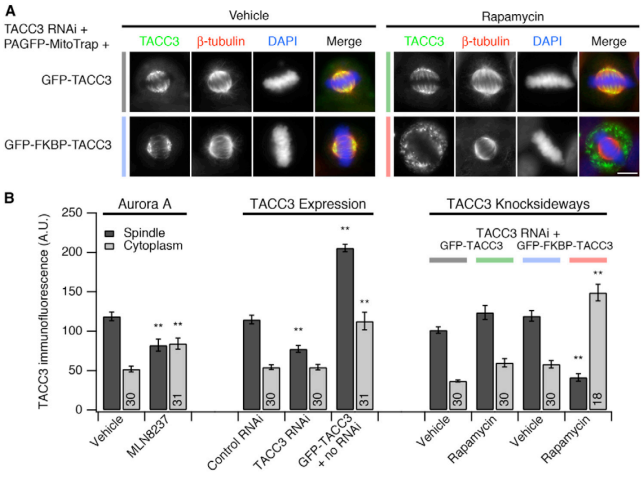

Fig. 2. Removal of TACC3 from mitotic spindles by knocksideways. (**A**) Representative micrographs of TACC3 KS. TACC3-depleted cells expressing PAGFP-MitoTrap (not visible) and the indicated TACC3 construct were treated for 30 minutes with 200 nM rapamycin or vehicle, fixed and stained for tubulin. Color coding for KS conditions is used throughout the paper. Full results are shown in supplementary material Fig. S1. Scale bar: 10 µm. (**B**) Bar chart to show quantification of TACC3 immunofluorescence in various experimental conditions. Total TACC3 was detected using anti-TACC3/A568 and analyzed by confocal microscopy. Aurora-A inhibition: using MLN8237 (1 µM) compared to vehicle. TACC3 expression: control RNAi + GFP, TACC3 RNAi + GFP and GFP-TACC3 expression (with no RNAi). TACC3 KS: TACC3 RNAi + PAGFP-MitoTrap + GFP-TACC3 or GFP-FKBP-TACC3; treated with vehicle or rapamycin (200 nM). Mean ± s.e.m. for spindle regions and cytoplasm. Number of cells was 18–31 as indicated, from two experiments. $^{**}P<0.001$ compared with vehicle (far left) values, one-way ANOVA with Tukey–Kramer post-hoc test.

following 10 minutes of rapamycin application (Fig. 3). Indirect immunofluorescence showed that TACC3 KS caused the removal of clathrin and ch-TOG from the spindle. In both cases, clathrin and ch-TOG were found colocalized with TACC3 at the mitochondria. Interestingly, GTSE1, a protein reported to be part of the TACC3–ch-TOG–clathrin complex (Hubner et al., 2010; Royle, 2012), was also lost from the spindle following TACC3 KS, although it was difficult to detect co-rerouting of GTSE1 at mitochondria (Fig. 3). Normal localizations of ch-TOG, clathrin and GTSE1 were observed in control cells, where GFP-FKBP-TACC3 was expressed and vehicle-treated (Fig. 3) or where GFP-TACC3 (without an FKBP domain) was expressed and cells treated with either rapamycin or vehicle (supplementary material Fig. S1). We also examined NuMA, Eg5 and HURP, as

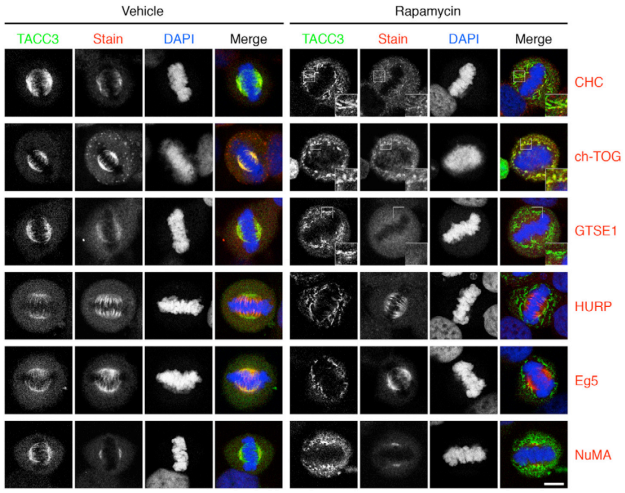

Fig. 3. TACC3 KS removes ch-TOG, clathrin and GTSE1 from the spindle without affecting other spindle proteins. Representative confocal micrographs of TACC3-depleted HeLa cells in metaphase expressing GFP-FKBP-TACC3 (green) and PAGFP-MitoTrap (not visible) that were treated with vehicle or rapamycin (200 nM) for 10 minutes, fixed and stained for the indicated proteins (red). TACC3 KS removed ch-TOG, clathrin heavy chain (CHC) and GTSE1 from the spindle. NuMA, HURP and Eg5 were unaffected by TACC3 KS. Zoomed areas show the colocalization of proteins at mitochondria following TACC3 KS. The results are typical of this experiment, repeated four times. See supplementary material Fig. S1 for full results. Scale bar: 10 µm.

these proteins localize to different areas of the spindle yet require phosphorylation by Aurora-A kinase for their activity, similarly to TACC3 (Giet et al., 1999; Kettenbach et al., 2011; Yu et al., 2005). The localization of all three proteins was unaltered by TACC3 KS (Fig. 3). We also tested whether TACC3 removal from the spindle would eventually cause deficiencies after prolonged drug application. The results of these experiments, with 30 minutes of drug application, were very similar to those with 10 minutes application (supplementary material Fig. S1). TACC3 KS is therefore a useful method to remove TACC3–ch-TOG–clathrin complexes specifically from spindles on a rapid timescale and that this will allow the molecular dissection of TACC3–ch-TOG–clathrin function at different stages of mitosis.

Rerouting clathrin to mitochondria is equivalent to TACC3 KS

We also used a similar system to reroute clathrin from the spindle to mitochondria during mitosis (supplementary material Fig. S2). Removal occurred with similar kinetics to TACC3 KS (supplementary material Movie 2). Analysis of spindle protein localization showed that rerouting of clathrin also removed members of the TACC3–ch-TOG–clathrin complex including GTSE1, whereas Eg5, NuMA and HURP were unaffected (supplementary material Fig. S2). In cells with good rerouting of clathrin to mitochondria, TACC3 was completely colocalized with clathrin on the mitochondria (supplementary material Fig. S3). TACC3 was lost from spindle microtubules and centrosomes, even in early mitosis, arguing against the existence of a clathrin-independent pool of TACC3. However, due to the abundance of clathrin in the cell, we could not rule out the possibility that clathrin removal in some cells may be incomplete (supplementary material Fig. S2). Therefore TACC3 KS was used to remove TACC3–ch-TOG–clathrin in all subsequent experiments.

TACC3 KS causes loss of a subpopulation of inter-MT bridges in K-fibers

K-fibers are bundles of parallel MTs that are crosslinked by inter-MT bridges (Hepler et al., 1970; McDonald et al., 1992; Nicklas et al., 1982). Previously, we showed that TACC3–ch-TOG–clathrin complexes form a subset of inter-MT bridges in K-fibers (Booth et al., 2011; Cheeseman et al., 2011; Royle, 2012; Royle et al., 2005). We next used correlative light-electron microscopy (CLEM) to verify if removal of TACC3–ch-TOG–clathrin complexes by KS resulted in a concomitant loss of inter-MT bridges. To do this, metaphase cells expressing GFP-FKBP-TACC3 and mCherry-MitoTrap were identified by fluorescence microscopy, and rapamycin (200 nM) or vehicle was applied for 10 minutes. TACC3 KS was visualized and the cells were then fixed and processed (Fig. 4A). The target cell was relocated in the resin and sectioned longitudinally relative to the spindle axis, and imaged by EM (Fig. 4A). Inter-MT bridges were quantified as previously described (Booth et al., 2011) (Fig. 4B). We found that there was a significant loss of inter-MT bridges in K-fibers after 10 minutes of TACC3 KS (Fig. 4C). This indicates that the removal of TACC3–ch-TOG–clathrin complexes from spindles by TACC3 KS results in removal of some inter-MT bridges. Many bridges clearly remain and these bridges must be composed of other proteins. With a method to inducibly and specifically remove TACC3–ch-TOG–clathrin bridges in hand we could investigate the role of these structures in K-fibers at different stages of mitosis.

Removal of TACC3–ch-TOG–clathrin complexes at NEBD or after metaphase reveals two different aspects of crosslinking function

Our next aim was to use live-cell imaging and TACC3 KS to assess the role of TACC3–ch-TOG–clathrin inter-MT bridges at different stages in mitosis. For reference, TACC3 KS was compared with depletion of TACC3 by RNAi. Progression through mitosis of live HeLa cells expressing mCherry-H2B was visualized and the time from NEBD-to-metaphase and from metaphase-to-anaphase was measured (Fig. 5A). In agreement with previous studies, depletion of TACC3 by RNAi prolonged the time from NEBD to metaphase and the time from metaphase to anaphase, relative to untransfected cells (Gergely et al., 2003; Lin et al., 2010; Schneider et al., 2007) (Fig. 5B). These defects

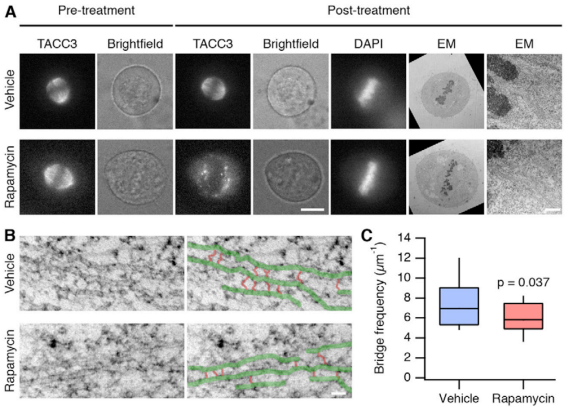

Fig. 4. Loss of inter-microtubule bridges from K-fibers following TACC3 KS. (**A**) TACC3-depleted HeLa cells at metaphase expressing GFP-FKBP-TACC3 and mCherry-MitoTrap were treated with rapamycin (200 nM) or vehicle for 10 minutes, fixed and processed for CLEM. The cell was located, 80-nm longitudinal sections taken (EM) and the bridge frequency in K-fibers quantified. Scale bars: 10 µm (left) and 500 nm (right). (**B**) Example micrographs to show visualization of inter-MT bridges for quantification. Annotated micrograph (right) shows MTs (green) and bridges (red). Scale bar: 50 nm. (**C**) Tukey box plot of inter-MT bridge frequency in K-fibers, expressed per micron of total MT length. In TACC3 KS cells, a significant loss of MT crosslinkers was observed: control $n=4$ cells (20 sections), TACC3 KS $n=5$ cells (25 sections); Student's *t*-test, $P=0.037$.

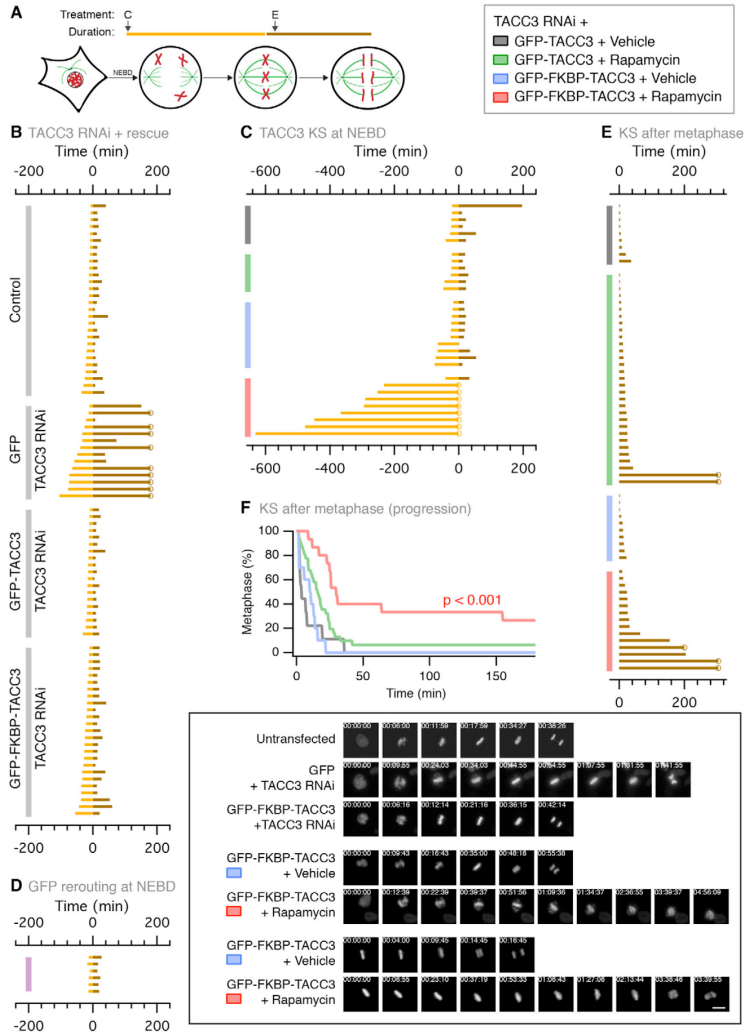

Fig. 5. TACC3 KS at NEBD or after metaphase reveals two different aspects of crosslinking function. (**A**) Diagram to show the timing of mitosis and experimental conditions. (**B**) Mitotic progression of control cells (no RNAi) and TACC3-depleted cells expressing GFP, GFP-TACC3 or GFP-FKBP-TACC3. TACC3 RNAi caused delay in chromosomal alignment in HeLa cells (NEBD-to-metaphase timing, gold) and also a delay in anaphase onset (metaphase-to-anaphase timing, brown). Cells that did not reach anaphase within the movie are marked with a circle. (**C**) Mitotic progression of TACC3-depleted HeLa cells expressing GFP-TACC3 or GFP-FKBP-TACC3; either vehicle or rapamycin (200 nM) was added at NEBD. (**D**) Normal mitotic progression of cells where GFP-FKBP was rerouted to mitochondria at NEBD. (**E**) Similar graph as in C except that TACC3 KS was performed after metaphase. All cells in the figure coexpressed H2B-mCherry for chromosome visualization and PAGFP-MitoTrap. (**F**) 'Survival curves' of the data shown in E. Example video stills from the indicated conditions are shown in the boxed area. Timings are indicated in hh:mm:ss. Scale bar: 20 µm.

Journal of Cell Science

were rescued by re-expression of shRNA-refractory GFP-TACC3 or GFP-FKBP-TACC3 (Fig. 5B), which indicates that the RNAi phenotype is specific to depletion of TACC3 and that our constructs are functional when expressed in cells depleted of TACC3. Delayed progression to anaphase in TACC3-depleted cells could be due to a role for MT crosslinking in K-fiber function at metaphase or simply a defect that is secondary to the prolonged prometaphase. These possibilities could now be distinguished using KS.

We next tested the effect of TACC3 KS at NEBD. To do this, live HeLa cells expressing PAGFP-MitoTrap, mCherry-H2B and TACC3 shRNA together with either GFP-TACC3 or GFP-FKBP-TACC3, were imaged with either vehicle or rapamycin added at NEBD. TACC3 KS at NEBD resulted in a severely prolonged prometaphase (Fig. 5C). The defects in chromosome alignment were so extreme that most TACC3 KS cells did not attain metaphase within several hours of imaging (Fig. 5C). The three control groups had normal prometaphase and subsequent metaphase-to-anaphase timings indicating that the effect of TACC3 KS was indeed due to removal of TACC3-containing complexes and not to application of rapamycin itself. This suggests that TACC3–ch-TOG–clathrin complexes are essential for an efficient and successful prometaphase, a time when the K-fiber matures.

TACC3 KS at NEBD produced a much stronger phenotype than TACC3 RNAi. To rule out the possibility that loading protein onto mitochondria delays mitosis non-specifically ('neomorphic' phenotype), we tested the effect of rerouting GFP-FKBP to mitochondria at NEBD. In six out of six cells, no delay was seen in NEBD–metaphase or in metaphase–anaphase timing (Fig. 5D). Furthermore, in TACC3 KS experiments, mitotic entry did not appear blocked in neighboring G2 cells. These observations indicate that the stronger phenotype upon rapid removal of TACC3 (compared to TACC3 RNAi), reflects a genuine difference between the methodologies.

To test the effect of TACC3–ch-TOG–clathrin complexes in mature spindles, we performed the same experiments but applied rapamycin after all chromosomes had aligned. These cells had therefore undergone a normal prometaphase and attained metaphase. Any changes caused by TACC3 KS would only be the result of TACC3–ch-TOG–clathrin loss from mature spindles and not from problems earlier in mitosis. TACC3 KS after metaphase caused a delay in anaphase onset (Fig. 5E), when compared with the three control groups (Fig. 5F). This indicates that removal of this complex from mature spindles at metaphase results in perturbed K-fiber function. Thus, TACC3–ch-TOG–clathrin inter-MT bridges are important for the function of mature K-fibers as well as having essential roles earlier in mitosis, e.g. in spindle assembly.

TACC3 KS during metaphase reduces K-fiber tension and this is sensed by the spindle checkpoint

We next investigated the cause of the metaphase-to-anaphase delay that resulted from TACC3 KS at metaphase. First, we assessed the spindle checkpoint by quantifying Mad2-positive kinetochores in metaphase cells following rapamycin treatment (30 minutes). The number of Mad2 immunoreactive puncta per cell that colocalized with the anti-centromere antibody CREST was quantified (Fig. 6A,B). The proportion of cells containing no Mad2-positive kinetochores was decreased by 40% following

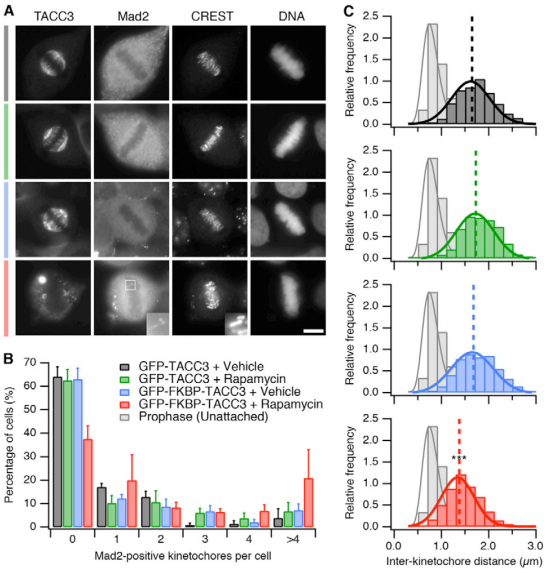

Fig. 6. TACC3 KS at metaphase reduces K-fiber tension and cells are arrested by the spindle checkpoint. (**A**) Representative confocal micrographs to show the recruitment of Mad2 to kinetochores following TACC3 KS. TACC3-depleted HeLa cells expressing GFP-TACC3 or GFP-FKBP-TACC3 were treated as indicated in the key in B. Inset shows three Mad2-positive kinetochores (2.5× zoom). Scale bar: 10 μm. (**B**) Proportion of cells with a satisfied or active spindle checkpoint, as revealed by Mad2 presence at kinetochores. Bars show mean ± s.e.m. of three experiments (n=90–93 cells). (**C**) Histograms of inter-kinetochore distances. Histograms (colored according to the key in B) are shown for GFP-TACC3 or GFP-FKBP-TACC3 treated with vehicle or rapamycin (200 nM) for 30 minutes, overlaid on a histogram of unattached inter-kinetochore distances from prophase/early prometaphase cells (light grey). The mean inter-kinetochore distance is shown by a dashed line. The unattached data were fitted with a log-normal function and all other data were fitted with a single Gaussian function. TACC3 KS cells (red, n=645 from 20 cells) displayed significantly reduced inter-kinetochore distance compared with controls (grey, n=654 from 22 cells; green, n=656 from 23 cells; blue, n=578 from 23 cells), but was not significantly different from unattached kinetochores (n=238 from 8 cells); ***P<0.001.

TACC3 KS compared to controls (Fig. 6B). In addition, the proportion displaying >4 Mad2-positive kinetochores was increased 3-fold following the removal of TACC3–ch-TOG–clathrin inter-MT bridges from K-fibers (Fig. 6B). Second, we assessed the effect of TACC3 KS on K-fiber tension by measuring inter-kinetochore distances. After rapamycin application (30 minutes), we observed a decrease in the mean ± s.d. inter-kinetochore distance from 1.68±0.06 µm (vehicle) to 1.38±0.04 µm (rapamycin). This suggested that the kinetochores were still attached but were under less tension because in prometaphase cells, unattached kinetochores had a mean inter-kinetochore distance of 0.83±0.06 µm (Fig. 6C). The distribution of inter-kinetochore distances showed an overall shift to lower values following TACC3 KS with no emergence of a second population around 0.6–1 µm suggesting no loss of attachment following TACC3 KS (Fig. 6C). Together, these results indicate that the slowed progression to anaphase following TACC3 KS was due to spindle checkpoint signaling. As the control cells had silenced the checkpoint satisfactorily and maintained tension, we interpret this to mean that the spindle checkpoint had been 're-activated' and that this re-activation was due to a loss of K-fiber tension.

TACC3 KS from mature K-fibers causes minimal MT loss

In order to determine whether kinetochores had lost attachment to the spindle following TACC3 KS, we tested the number of kinetochores with cold-stable microtubule attachments in metaphase cells (Fig. 7A,B). In control or TACC3 KS cells, all kinetochores had cold-stable attachment to the spindle. Depletion of Nuf2 served as a positive control to show that we could detect kinetochores that lacked cold-stable attachments (Fig. 7B). TACC3 KS did not significantly alter the remaining tubulin signal in cold-treated cells relative to control cells, which suggested that MT occupancy is normal.

To investigate this further we used CLEM to analyze MT number in K-fibers sectioned orthogonally relative to the spindle axis (Fig. 7C). We found only a small decrease in MT number compared to controls after 10 minutes TACC3 KS, and this remained stable at 30 minutes (Fig. 7D), i.e. there was no progressive loss of MTs ($P>0.05$). Neither of these decreases was statistically significant compared to rapamycin-treated control K-fibers ($P>0.05$), although there was significant decrease when compared to vehicle-treated K-fibers ($P<0.001$). The cross-sectional area of K-fibers was estimated and the relation between K-fiber area and MT number plotted (Fig. 7E). These plots illustrate that after TACC3 KS, MT number per K-fiber is within the normal range, albeit at the lower end. The MT density within K-fibers was equivalent suggesting that any MT loss that occurred following TACC3 KS was limited to the periphery of the fiber. Nearest neighbor analysis and neighbor density analysis both failed to show any effect of TACC3 KS on MT spacing or distribution within K-fibers compared to control cells following 10 or 30 minutes rapamycin application (supplementary material Fig. S3). These results are in contrast to our previous analysis of K-fibers in clathrin RNAi cells, where MT loss occurred throughout the K-fiber (Booth et al., 2011). The difference is likely due to the fact that TACC3 KS was performed at metaphase after the K-fiber had accumulated the correct number of MTs and stabilized them; whereas clathrin-depleted cells may have been unable to accumulate MTs during prometaphase. Together, these results show that the number of attachments and the MT occupancy at kinetochores is normal following TACC3 KS. The mitotic delay and re-activated spindle checkpoint signaling following TACC3 KS indicates that the spindle checkpoint can sense reduced K-fiber tension that occurs without detectable loss of MT attachment.

TACC3 KS from mature K-fibers causes changes in spindle shape and dynamicity

How does removal of TACC3–ch-TOG–clathrin inter-MT bridges result in reduced K-fiber tension? To address this question we examined mitotic spindle dynamics following removal of TACC3–ch-TOG–clathrin complexes, using 4D kinetochore and spindle pole tracking in live HeLa cells stably expressing GFP-CENP-A and centrin-GFP (Fig. 8). TACC3 KS was performed using mCherry-tagged TACC3 constructs at late prometaphase/metaphase. Cells were imaged and time-lapse datasets were analyzed as previously described (Jaqaman et al., 2010) and also with a new algorithm (see Materials and Methods), allowing kinetochore and spindle pole motions to be tracked in an automated manner (Fig. 8).

Removal of TACC3–ch-TOG–clathrin complexes by TACC3 KS resulted in a number of changes in kinetochore dynamics. First, kinetochore oscillations in typical trajectories from TACC3 KS cells were visibly dampened compared to controls (Fig. 8A–C). Second, inter-kinetochore distance was reduced by ~10% (Fig. 8D,E) confirming in live cells our earlier observations in fixed cells that K-fiber tension was decreased despite normal MT occupancy. Third, the metaphase plate was thicker following TACC3 KS, as the distance of sister kinetochore centers was more variable than in cells without TACC3 removal (Fig. 8E; Bartlett's statistic, 87.799, $P<0.001$). Note, that this variability is likely much larger as the analysis rejects kinetochores where $x>2.5\sigma$. Fourth, auto-correlation analysis of sister center displacement (Δx) showed that kinetochore oscillations had a reduced periodicity following TACC3 KS (Fig. 8F), whereas sister displacement cross-correlation analysis showed no alteration of kinetochore 'breathing' by TACC3 KS. Fifth, mean squared displacement analysis for kinetochore pairs showed that movement of kinetochores following TACC3 KS was less constrained compared to controls (Fig. 8G). In other words, for a given duration, kinetochores have moved further following TACC3 KS than in cells with normal levels of TACC3 on the spindle. This observation is in agreement with the increased variability in x (Fig. 8E). All of these changes in kinetochore dynamics following TACC3 KS during metaphase are consistent with a decrease in K-fiber tension.

We also analyzed the motions of spindle poles in the same cells using automated tracking (Fig. 8H). This analysis revealed that the pole-to-pole distance of spindles was reduced by ~12% following TACC3 KS (Fig. 8I). This decrease in spindle length (S), which was noted previously (Fig. 2A), was the only detectable change in spindle pole dynamics. The movement of spindle poles is random, i.e. they do not undergo oscillations over time; and there was no alteration in the mean squared displacement (m.s.d.) of spindle poles following TACC3 KS. The average inter-kinetochore distance (d) was plotted as a function of the average pole-to-pole distance (S) for each cell analyzed across four experiments (Fig. 8J). This showed that the d and S did not scale with one another and argues that the decrease in d is not caused by the reduction in S. These results indicate that removal of TACC3–ch-TOG–clathrin complexes

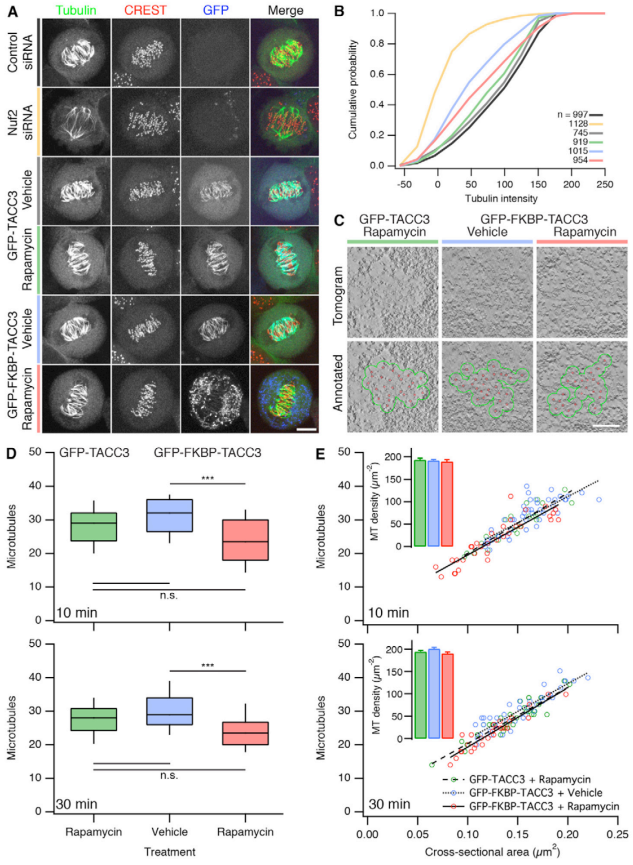

Fig. 7. TACC3 KS at metaphase does not significantly alter kinetochore–microtubule attachments. (**A**,**B**) Cold-stable kinetochore–microtubule attachments. (A) Representative pictures of each condition analyzed are shown as maximum intensity projections of confocal Z-series micrographs. Metaphase cells were cold-treated, fixed and stained with anti-tubulin (green) and CREST (red); GFP channel (blue) shows TACC3 KS. Scale bar: 10 µm. (B) Analysis of confocal *z*-series micrographs to detect cold-stable kinetochore–microtubule attachments. Cumulative frequency plot to show the average tubulin signal adjacent to kinetochores. N_{cell}=9–12 from two experiments. $N_{kinetochore}$ is shown in the legend. (**C**) Representative views of electron tomograms of orthogonal sections of K-fibers in metaphase HeLa cells expressing mCherry-MitoTrap and GFP-TACC3 or GFP-FKBP-TACC3 treated as indicated. Overlaid are microtubules (red) and the calculated K-fiber perimeter (green). Scale bar: 100 nm. (**D**) Tukey box plots of K-fiber MT number in TACC3-depleted HeLa cells expressing mCherry-MitoTrap and GFP-TACC3 or GFP-FKBP-TACC3, treated with vehicle or rapamycin (200 nM) for 10 minutes (top) or 30 minutes (bottom). TACC3 KS (red) causes a slight reduction in MTs of K-fibers after both 10 minutes and 30 minutes of rapamycin application. The reduction was significantly lower than for vehicle-treated cells (ANOVA with Tukey–Kramer post-hoc test, ***P<0.01), but not when compared with rapamycin-treated GFP-TACC3-expressing cells (n.s. indicates P>0.05). (**E**) Plots of MT number versus K-fiber cross-sectional area after 10 minutes and 30 minutes of treatment. Lines of best fit show the similar MT density in all conditions. Insets show mean ± s.e.m. K-fiber MT density in control (green, blue) or TACC3 KS cells (red) (10-minute data: green, n=22 K-fibers; blue, n=54; red, n=32. 30-minutes data: green, n=32; blue, n=38; red, n=28). See supplementary material Fig. S4 for spatial analysis of K-fibers.

from mitotic spindles that had completed a normal prometaphase caused the following changes: reduced spindle length, reduced K-fiber tension and decreased micromechanics of the spindle.

Discussion

We investigated the requirement for one class of non-motor MT crosslinker (TACC3–ch-TOG–clathrin) for the function of mature K-fibers. Such an investigation was made possible by the knocksideways technique which allowed the inducible, rapid removal of certain inter-MT bridges from K-fibers at different stages of mitosis. Our findings demonstrated the utility of KS versus RNAi and a role for TACC3–ch-TOG–clathrin complexes in the shape and micromechanics of mature spindles.

The advantages of KS over RNAi are clear, given that protein depletion via RNAi is slow (24–72 hours) compared to the timescale of mitosis (1–2 hours). Using RNAi, attempts to determine the function of a spindle protein are complicated because the cell may have undergone several cell cycles with gradually declining levels of the protein. In this time, the cell may upregulate alternative pathways to compensate for the reduced protein, potentially masking the true phenotype. For spindle proteins with distinct interphase functions the picture is further complicated (Royle, 2011). In addition, trying to understand RNAi phenotypes at later stages of mitosis are potentially confounded by earlier defects. In other words, is the phenotype caused by a true requirement for the depleted protein at that later stage or is it because the earlier absence of the protein produced a defective spindle? It is now possible to dissect these differences using KS. Rapid inactivation methods are particularly crucial for mitosis, which is a succession of steps, each lasting less than 30 minutes.

The effectiveness of KS on a timescale of ~5 minutes makes it better suited than methods for inducible protein degradation, which work on the timescale of 30 minutes (Nishimura et al., 2009). Besides the use of KS as a tool for protein inactivation (Hirst et al., 2012; Robinson et al., 2010), we showed indirectly two additional uses for the method. First, the lifetime of proteins on the spindle could be inferred by comparing the kinetics of rerouting in mitotic and interphase cells. Second, testing which proteins are co-rerouted to mitochondria upon KS is a useful way to determine which proteins bind one another in cells.

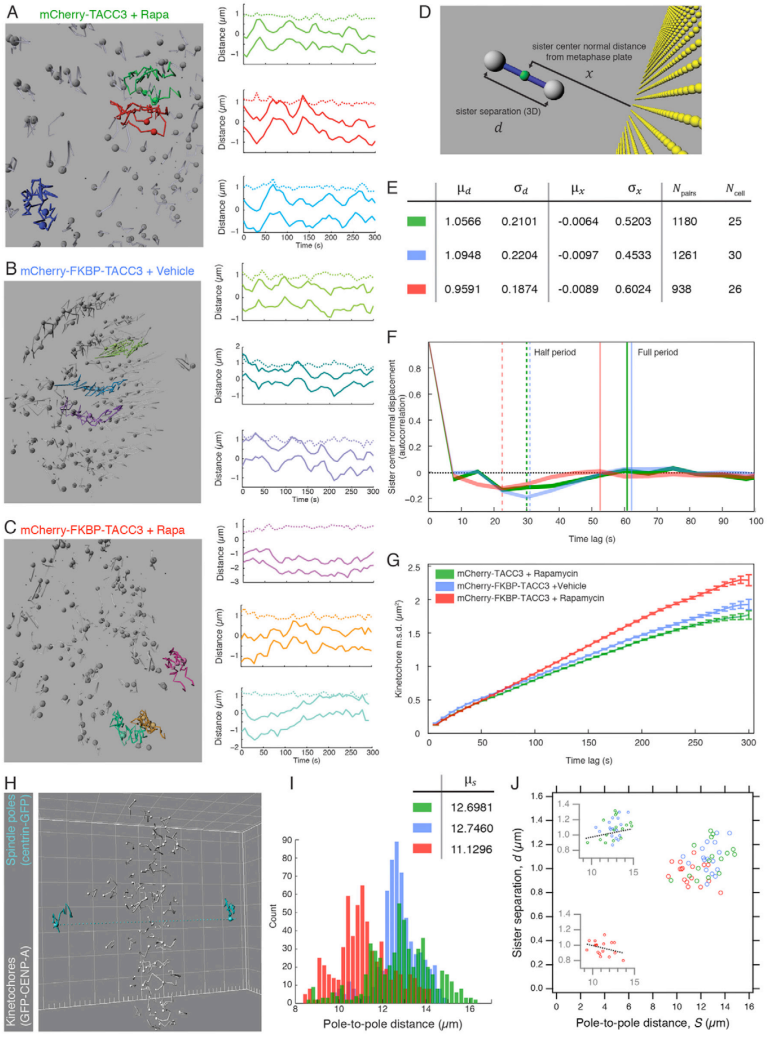

Fig. 8. See next page for legend.

Appendices

Journal of Cell Science

TACC3 KS caused the specific rerouting of ch-TOG and clathrin from the spindle to mitochondria. Importantly, these partners were co-rerouted with TACC3 to the mitochondria, rather than being simply lost from the spindle, unable to bind in the absence of TACC3. This observation indicates that TACC3 KS reroutes the intact TACC3–ch-TOG–clathrin complex. Moreover, the co-rerouting suggests that interactions within the complex, for example between clathrin and TACC3, are of higher affinity than clathrin–adaptor interactions, as it was shown previously that AP-2 KS did not co-reroute clathrin to mitochondria (Robinson et al., 2010). We note that a pool of ch-TOG was retained at the spindle pole after TACC3 KS (supplementary material Fig. S1), which presumably corresponds to a functionally separate ch-TOG population, as previously described (Booth et al., 2011; Cassimeris et al., 2009; Gergely et al., 2003). Since the discovery of clathrin as a binding partner of TACC3–ch-TOG, it has been debated whether TACC3–ch-TOG can operate independently of this complex (Booth et al., 2011; Fu et al., 2011; Fu et al., 2010; Hubner et al., 2010; Lin et al., 2010; Royle, 2012). Co-rerouting of TACC3 and clathrin was complete, indicating that these proteins do not exist as functionally separate entities at the spindle and are probably interdependent for their recruitment to the spindle (Royle, 2012).

TACC3 KS caused the loss of some inter-MT bridges. However, we found that the extent of loss following TACC3 KS was less than that observed after RNAi of TACC3 or clathrin (Booth et al., 2011) or after inhibition of Aurora-A kinase using MLN8237–Alisertib (Cheeseman et al., 2011). As KS is a more rapid and specific method for protein inactivation, we interpret this to mean that our previous analyses overestimated the size of this population of inter-MT bridge. If correct, this points to secondary effects of RNAi or Alisertib beyond the simple removal of TACC3–ch-TOG–clathrin complexes. For example, clathrin-depleted K-fibers had fewer MTs than control RNAi and this could have confounded the quantification of bridge frequency (Booth et al., 2011). As noted previously, many crosslinkers remain in the K-fiber following TACC3 KS and this underscores that other inter-MT bridges exist in K-fibers that are not composed of TACC3–ch-TOG–clathrin.

Using TACC3 KS to remove TACC3–ch-TOG–clathrin inter-MT bridges at metaphase, following a normal prometaphase, we observed delays in the progression to anaphase. We found a net decrease in K-fiber tension despite normal MT attachment and that this state was detected by the spindle checkpoint. These observations could be taken as evidence that the spindle checkpoint can sense K-fiber tension, distinctly from MT attachment (Khodjakov and Pines, 2010). However, the number of Mad2-positive kinetochores was only a small fraction of the total kinetochores despite an overall shift to lower tension at all kinetochores. This result is similar to delayed progression to anaphase in taxol-treated PtK1 cells, where tension is reduced, MT attachment is normal, but Mad2 is only recruited to a subset of kinetochores (McEwen et al., 1997; Waters et al., 1998). The range of MTs/fiber had a tendency to be lower after TACC3 KS and so it is difficult to exclude the possibility that Mad2 is recruited to those kinetochores with fewest MTs.

The decrease in inter-kinetochore distance following TACC3 KS was 10%, while the decrease in pole–pole distance was ~12%. Although these changes are equivalent, several observations suggest that the decreases in inter-kinetochore distance are due to loss of K-fiber tension rather than being simply scaled with spindle size. First, experimental manipulation of pole–pole distance and the resultant change of spindle size have little effect on kinetochore separation (Dumont and Mitchison, 2009). Second, MT crosslinkers increase the tensile strength of MT bundles *in vitro* (Charlebois et al., 2011) and so the removal of a crosslinker is consistent with decreased K-fiber tension. Third, we saw changes in the dynamicity of the spindle and behavior of kinetochores, which argues that TACC3 KS affects the micromechanical properties of the K-fibers in addition to spindle size. Finally, plots of the average inter-kinetochore distance versus pole-to-pole distance showed that these two measures were independent.

One further surprising finding was the magnitude of mitotic delay induced by TACC3 KS at NEBD. This manipulation was predicted to be equivalent to TACC3 RNAi, but was far more severe. Using RNAi, TACC3-depleted cells had a delayed prometaphase but did eventually align their chromosomes. By contrast, cells with TACC3 KS at NEBD were unable to align the chromosomes at all. Four possibilities to explain this difference are: (i) TACC3-depleted cells may have time to compensate for the loss of TACC3 during the depletion period; (ii) removal of TACC3 from spindles by KS may be more extensive than RNAi, due to dimerization of GFP-FKBP-TACC3 with residual TACC3; (iii) rerouting of the whole TACC3–ch-TOG–clathrin complex may result in a significant fraction of ch-TOG and clathrin being trapped on mitochondria and thus unavailable for potential functions that are independent of the complex; (iv) a 'neomorphic' phenotype, where loading mitochondria with heterologous proteins delays mitosis non-specifically. This latter possibility was ruled out by the normal NEBD–anaphase times for cells with rerouting of GFP-FKBP and the observation that TACC3 KS does not impede mitotic entry. Quantification of TACC3 levels on spindle MTs following KS versus TACC3 RNAi suggest that the levels are indeed lower, arguing for the second possibility. Whatever the reason, we think that it is possible that RNAi phenotypes of other spindle proteins may

Fig. 8. TACC3 KS at metaphase alters kinetochore dynamics and decreases spindle length. Analysis of kinetochore motions in live HeLa cells stably expressing CENP-A-GFP and Centrin-GFP. Cells were depleted of endogenous TACC3 and were coexpressing PAGFP-MitoTrap and either mCherry-TACC3 or mCherry-FKBP-TACC3 and were treated with DMSO (vehicle) or rapamycin (200 nM). (**A–C**) Three example kinetochore trajectories from typical cells are shown. Left: Images of automated kinetochore tracking. Right: Plots of kinetochore distances relative to the metaphase plate as a function of time. Tracks of two sisters are shown for each pair; difference plot is shown (dotted line). (**D**) Diagram to show the measurement of d and x. (**E**) Population data for sister separation (d, inter-kinetochore distance) and sister center normal position (x). (**F**) Sister center normal displacement (Δx auto-correlation). Line thickness represents 95% confidence interval. Peaks of negative and positive lobes (half- and full-period) are shown by dashed and full vertical lines, respectively. (**G**) Mean squared displacement analysis for kinetochore pairs. Error bars show s.e.m. (**H**) Image to show the automated 4D tracking of spindle poles (centrin-GFP) in addition to kinetochores (see Materials and Methods). See supplementary material Movie 3. (**I**) Euclidian interpolar distances (S) for each condition. Color coding is the same as in previous figures. (**J**) Scatter plots to show that the average inter-kinetochore distance (d) does not vary as a function of spindle length (S). Insets show control data (above) and TACC3 KS data (below) for reference; a line of best fit is shown (r^2=0.08 and 0.11, respectively). Analysis in all figure panels is from four independent experiments.

have been similarly underestimated. Revisiting some of these proteins using KS in the future may give a more accurate picture of their mitotic function(s).

Materials and Methods

Molecular biology

To make pBrain-GFP-FKBP-TACC3KDP-shTACC3, an FKBP fragment was amplified from gamma-FKBP by PCR and inserted into pBrain-GFP-TACC3KDP-shTACC3 via Acc65I/BsrGI and Acc65I. To make mCherry- or PAGFP-MitoTrap, YFP in YFP-MitoTrap (pMito-YFP-FRB) was replaced with either mCherry or photo-activatable-GFP (PAGFP) via AgeI and BsrGI. PAGFP-MitoTrap was used as an 'invisible' MitoTrap to make other channels available for experiments (Willox and Royle, 2012). Gamma-FKBP and YFP-MitoTrap were kind gifts from Prof. M. S. Robinson (Cambridge Institute for Medical Research, UK).

For clathrin rerouting experiments, GFP-FKBP-LCa was used with no RNAi. GFP-FKBP-LCa was made by inserting a PCR-amplified FKBP fragment between GFP and LCa via BsrGI/Acc65I. GFP was exchanged with mCherry to make mCherry-H2B using AgeI/NotI from GFP-H2B. GFP-H2B, GFP-LCa and pBrain-GFP-TACC3KDP-shTACC3 were available from previous work (Booth et al., 2011; Royle et al., 2005).

Cell culture, reagents and antibodies

HeLa cells were cultured in Dulbecco's Modified Eagle Medium (Invitrogen) supplemented with 10% fetal bovine serum (FBS) and 100 U/ml penicillin/streptomycin at 37℃ and 5% CO_2. Cells were transfected using GeneJuice (Novagen). Rapamycin (SigmaAldrich) was used at 200 nM, vehicle was ethanol (0.1%). MLN8237 (Selleck) was used at 1 µM, vehicle was DMSO (0.01%).

For indirect immunofluorescence, HeLa on coverslips were fixed with PTEMF (50 mM PIPES [1,4-Piperazinediethanesulfonic acid], pH 7.2, 10 mM EGTA, 1 mM $MgCl_2$, 0.2% Triton X-100, 4% paraformaldehyde) at room temperature, or methanol at −20℃ for ch-TOG staining. Cells were then permeabilized (PBS with 0.5% Triton X-100) and blocked (PBS with 5% BSA and 5% goat serum). The following antibodies were used: (1) mouse monoclonals: clathrin heavy chain (X22, CRL-2228 ATCC), TACC3 (ab56595, Abcam), and Eg5 (611186, BD Biosciences) (2) mouse polyclonal: GTSE1 (H00051512-B01P, Abnova), (3) rabbit polyclonals: ch-TOG (34032, Autogen Bioclear) and β-tubulin (ab6046, Abcam), NuMA (3888s, Cell Signaling), HURP (kind gift from Prof. E. A. Nigg, University of Basel, Switzerland), Mad2 (Covance), (4) human polyclonal: Crest (CS1058, Europa Bioproducts). Fluorescently-conjugated secondary antibodies were Alexa488, Alexa568 or Alexa633 (Molecular Probes). Coverslips were mounted using Mowiol containing 4′,6-diamidino-2-phenylindole (DAPI).

Light microscopy

Live-cell imaging of KS kinetics was performed on an Olympus IX71 in glass-bottom dishes heated to 37℃ (Bioptechs Delta T5 µ-environmental culture dish controller) in CO_2-independent medium (Invitrogen) supplemented with 10% FBS and 100 U/ml penicillin/streptomycin, using Cell-R acquisition software and a Hamamatsu ORCA-ER C4742-80 camera with a 60× oil-immersion objective (1.42 NA). Quantification of GFP intensity during KS was performed using ImageJ, with an ROI that defined the spindle and one that excluded it, and plotted as $\Delta F/F_0$.

Live-cell imaging of mitotic progression following RNAi or KS was performed on a Nikon Eclipse Ti with a heated Perspex chamber (OKOlab) using standard filter sets for visualization of GFP and mCherry, NIS acquisition software, a CoolSNAP HQ2 camera and a 20× air objective (0.45 NA). Cells were kept at 37℃, in supplemented CO_2-independent medium. Light intensity was kept to a minimum to avoid light-induced cell damage. Chromosomes were visualized with mCherry-H2B (imaged once per minute), and GFP monitored every 5 minutes. Rapamycin was added to 200 nM by adding a concentrated media solution at 37℃ to the cell culture medium. Note that, for rerouting at metaphase, KS was induced at a variable time after the last chromosome aligned. It is likely therefore that we have underestimated the metaphase delay.

Confocal imaging was performed using a Leica confocal microscope SP2 with a 63× (1.4 NA) oil-immersion objective as described previously (Booth et al., 2011). For inter-kinetochore distance measurements, Z-stacks of CREST-immunostained cells were taken, assembled in ImageJ and distances between unambiguous CREST-positive kinetochore pairs in the stack were measured. For measurement of TACC3 levels, fixed, stained cells were imaged using identical acquisition parameters for all conditions. Mean pixel intensity for TACC3 was measured in a 20×20 pixel ROI using ImageJ software and the background subtracted.

Epifluorescence images of fixed cells were taken using a Nikon Eclipse Ti-U microscope with standard filter sets for visualization of DAPI, GFP, Alexa Fluor 568 and Alexa Fluor 633, a Nikon Digital Sight DS-Qi1Mc camera, a 60× (1.40 NA) oil-immersion objective and NIS acquisition software. To quantify Mad2 recruitment to the kinetochore, cells immunostained for Mad2 and CREST were imaged throughout the full Z dimension of the metaphase plate, and Mad2 puncta which colocalized with CREST were counted.

Cold-stable MT assay and analysis was performed as described previously (Toso et al., 2009). Briefly, cells treated with RNAi (48 hours) or KS (30 minutes), were placed in ice-cold medium, and incubated on ice for 10 minutes. The cells were then fixed with PTEMF and stained for tubulin and CREST. Confocal Z stacks were taken of metaphase cells and analyzed using Imaris as described.

4D kinetochore and spindle pole tracking

Cells were seeded in 35-mm Fluorodishes (WPI) in DMEM with 10% FBS and imaged on a widefield imaging system (Personal DeltaVision; Applied Precision) fitted with an environmental chamber maintained at 37℃ and 10% CO_2 atmospheric concentration. Images were acquired with a 100× 1.35 NA objective (Olympus) and a CDC (CoolSnap HQ2; Photometrics). Image acquisition was controlled by the softWoRx software suite (Applied Precision), 15 image stacks spaced 0.5 µm apart were collected every 7.5 seconds for 5 minutes (41 time-points). Pixels were set to 1×1 binning (65 nm effective pixel size).

Movies were deconvolved in softWoRx before tracking analysis. Automatic kinetochore tracking was performed as described (Jaqaman et al., 2010). All analysis was performed in MATLAB R2012a (MathWorks) with core algorithms written in C (compiled with the MATLAB MEX compiler). Only inlier kinetochores were used for analysis (spots that were $<2.5\sigma$ from metaphase plate).

Spindle pole tracks were identified by assigning a cost to each pair of tracks. The cost was defined as $c=|d-s| * a$ where d was the average distance between the tracks, s was the expected average spindle length, set to 11 µm and a was the average angle between the tracks and the metaphase plate. Tracks were only considered if $d>5$ µm and $a<30°$, and if both tracks were unaligned throughout both their lifetimes. The pair of tracks with the lowest cost was chosen. Since both centrioles in each pole were tagged, the second centriole track for each pole was found by assigning a cost: $c=g^{-1}$ where g was the cross-correlation between the pole track and the candidate track. Tracks were only considered if $g>0.9$ and if the average distance between the tracks was less than 1 µm. The track with the lowest cost was chosen for each pole as its respective second centriole.

For pole tracks where two centrioles were found, the pole position was defined as the center point between the two, otherwise the position of a single centriole was used. Spindle length was taken as the 3D distance between the two poles.

Correlative light-electron microscopy

Correlative light-electron microscopy was performed as previously (Booth et al., 2011). HeLa cells were transfected with mCherry-MitoTrap and either pBrain-GFP-FKBP-TACC3KDP-shTACC3 or pBrain-GFP-TACC3KDP-shTACC3. Tomograms were assembled from tilt image series using eTOMO software (Boulder Laboratory for 3D Electron Microscopy). Quantification of EM images was carried out by an experimenter blind to the conditions of the experiment. All methods were as described previously (Booth et al., 2011), with the following exceptions. MT positions and cross-sectional area were plotted and calculated in tomograms. For measurement of K-fiber cross-sectional area, a 40 nm perimeter was computed around clusters of annotated MTs and measured using ImageJ. MTs within this boundary were counted as part of the K-fiber. To measure inter-MT distances, a map of MTs was created using IMOD Software (Boulder Laboratory for 3D Electron Microscopy), the coordinates were exported using model2point. The distance between each point was calculated in Microsoft Excel, from here the distance for each MT and its nearest neighboring MT was selected. To give the edge-to-edge distance, 20 nm was subtracted from these measurements. Neighbor density analysis was performed using nda in IMOD. MTs were annotated as circles of ~25 nm diameter throughout the Z slices, and flattened to a single Z plane. MTs within 80 nm of each other were padded by 50 nm using a convex polygon boundary.

Data analysis

Statistical testing was performed with InStat or SPSS. Normally distributed data were compared using one-way ANOVA followed by a Tukey–Kramer *post hoc* test. Student's unpaired *t*-test was used to compare two data sets. Non-parametric data were compared using Kruskal–Wallis' ANOVA test. The Kolmogorov–Smirnov test was used to determine if the data followed a Gaussian distribution. Cox regression analysis was used to test for significance of mitotic delays. Tukey box plots show the median, interquartile range and the 10th and 90th percentile. Figures were assembled using IgorPro 6.22A (Wavemetrics), Matlab (R2012), Adobe Photoshop and Adobe Illustrator.

Acknowledgements

We thank members of the Royle laboratory for useful comments and Sylvie Urbé for generous access to her live-cell imaging system. We are grateful to Scottie Robinson and Erich Nigg for essential reagents and David Mastronarde for advice and help with nda/IMOD. The authors declare that they have no conflict of interest.

Appendices

Journal of Cell Science

Author contributions

L.P.C. designed, carried out and analyzed the experiments, E.F.H. and A.D.M. helped with tracking experiments and analysis, I.A.P. helped with the design and implementation of electron microscopy, S.J.R. designed the experiments, analyzed data, coordinated the work and wrote the manuscript with input from all authors.

Funding

L.P.C. is the recipient of a Wellcome Trust Prize Studentship. This work was supported by a Career Establishment Award from Cancer Research UK [grant number C25425/A8722 to S.J.R.]. S.J.R. is a Senior Cancer Research Fellow for Cancer Research UK. A.D.M. was supported by a Biotechnology and Biological Sciences Research Council (BBSRC) project grant [grant number BB/I021353/1]. E.F.H. was supported by the Engineering and Physical Sciences Research Council (EPSRC) [grant number EP/F500378/1] via the MOAC doctoral training centre. Deposited in PMC for release after 6 months.

Supplementary material available online at
http://jcs.biologists.org/lookup/suppl/doi:10.1242/jcs.124834/-/DC1

References

Barr, A. R. and Gergely, F. (2008). MCAK-independent functions of ch-Tog/XMAP215 in microtubule plus-end dynamics. *Mol. Cell. Biol.* **28**, 7199-7211.
Booth, D. G., Hood, F. E., Prior, I. A. and Royle, S. J. (2011). A TACC3/ch-TOG/clathrin complex stabilises kinetochore fibres by inter-microtubule bridging. *EMBO J.* **30**, 906-919.
Borner, G. H., Antrobus, R., Hirst, J., Bhumbra, G. S., Kozik, P., Jackson, L. P., Sahlender, D. A. and Robinson, M. S. (2012). Multivariate proteomic profiling identifies novel accessory proteins of coated vesicles. *J. Cell Biol.* **197**, 141-160.
Brodsky, F. M. (2012). Diversity of clathrin function: new tricks for an old protein. *Annu. Rev. Cell Dev. Biol.* **28**, 309-336.
Cassimeris, L., Becker, B. and Carney, B. (2009). TOGp regulates microtubule assembly and density during mitosis and contributes to chromosome directional instability. *Cell Motil. Cytoskeleton* **66**, 535-545.
Charlebois, B. D., Kollu, S., Schek, H. T., Compton, D. A. and Hunt, A. J. (2011). Spindle pole mechanics studied in mitotic asters: dynamic distribution of spindle forces through compliant linkages. *Biophys. J.* **100**, 1756-1764.
Cheeseman, L. P., Booth, D. G., Hood, F. E., Prior, I. A. and Royle, S. J. (2011). Aurora A kinase activity is required for localization of TACC3/ch-TOG/clathrin inter-microtubule bridges. *Commun. Integr. Biol.* **4**, 409-412.
Dumont, S. and Mitchison, T. J. (2009). Compression regulates mitotic spindle length by a mechanochemical switch at the poles. *Curr. Biol.* **19**, 1086-1095.
Fu, W., Tao, W., Zheng, P., Fu, J., Bian, M., Jiang, Q., Clarke, P. R. and Zhang, C. (2010). Clathrin recruits phosphorylated TACC3 to spindle poles for bipolar spindle assembly and chromosome alignment. *J. Cell Sci.* **123**, 3645-3651.
Fu, W., Jiang, Q. and Zhang, C. (2011). Novel functions of endocytic player clathrin in mitosis. *Cell Res.* **21**, 1655-1661.
Gergely, F., Karlsson, C., Still, I., Cowell, J., Kilmartin, J. and Raff, J. W. (2000a). The TACC domain identifies a family of centrosomal proteins that can interact with microtubules. *Proc. Natl. Acad. Sci. USA* **97**, 14352-14357.
Gergely, F., Kidd, D., Jeffers, K., Wakefield, J. G. and Raff, J. W. (2000b). D-TACC: a novel centrosomal protein required for normal spindle function in the early Drosophila embryo. *EMBO J.* **19**, 241-252.
Gergely, F., Draviam, V. M. and Raff, J. W. (2003). The ch-TOG/XMAP215 protein is essential for spindle pole organization in human somatic cells. *Genes Dev.* **17**, 336-341.
Giet, R., Uzbekov, R., Cubizolles, F., Le Guellec, K. and Prigent, C. (1999). The Xenopus laevis aurora-related protein kinase pEg2 associates with and phosphorylates the kinesin-related protein XlEg5. *J. Biol. Chem.* **274**, 15005-15013.
Hepler, P. K., McIntosh, J. R. and Cleland, S. (1970). Intermicrotubule bridges in mitotic spindle apparatus. *J. Cell Biol.* **45**, 438-444.
Hirst, J., Borner, G. H., Antrobus, R., Peden, A. A., Hodson, N. A., Sahlender, D. A. and Robinson, M. S. (2012). Distinct and overlapping roles for AP-1 and GGAs revealed by the 'knocksideways' system. *Curr. Biol.* **22**, 1711-1716.
Hubner, N. C., Bird, A. W., Cox, J., Splettstoesser, B., Bandilla, P., Poser, I., Hyman, A. and Mann, M. (2010). Quantitative proteomics combined with BAC TransgeneOmics reveals in vivo protein interactions. *J. Cell Biol.* **189**, 739-754.
Jaqaman, K., King, E. M., Amaro, A. C., Winter, J. R., Dorn, J. F., Elliott, H. L., McHedlishvili, N., McClelland, S. E., Porter, I. M., Posch, M. et al. (2010). Kinetochore alignment within the metaphase plate is regulated by centromere stiffness and microtubule depolymerases. *J. Cell Biol.* **188**, 665-679.
Kettenbach, A. N., Schweppe, D. K., Faherty, B. K., Pechenick, D., Pletnev, A. A. and Gerber, S. A. (2011). Quantitative phosphoproteomics identifies substrates and functional modules of Aurora and Polo-like kinase activities in mitotic cells. *Sci. Signal.* **4**, rs5.
Khodjakov, A. and Pines, J. (2010). Centromere tension: a divisive issue. *Nat. Cell Biol.* **12**, 919-923.
Kinoshita, K., Noetzel, T. L., Pelletier, L., Mechtler, K., Drechsel, D. N., Schwager, A., Lee, M., Raff, J. W. and Hyman, A. A. (2005). Aurora A phosphorylation of TACC3/maskin is required for centrosome-dependent microtubule assembly in mitosis. *J. Cell Biol.* **170**, 1047-1055.
Lee, M. J., Gergely, F., Jeffers, K., Peak-Chew, S. Y. and Raff, J. W. (2001). Msps/XMAP215 interacts with the centrosomal protein D-TACC to regulate microtubule behaviour. *Nat. Cell Biol.* **3**, 643-649.
Lin, C. H., Hu, C. K. and Shih, H. M. (2010). Clathrin heavy chain mediates TACC3 targeting to mitotic spindles to ensure spindle stability. *J. Cell Biol.* **189**, 1097-1105.
McDonald, K. L., O'Toole, E. T., Mastronarde, D. N. and McIntosh, J. R. (1992). Kinetochore microtubules in PTK cells. *J. Cell Biol.* **118**, 369-383.
McEwen, B. F., Heagle, A. B., Cassels, G. O., Buttle, K. F. and Rieder, C. L. (1997). Kinetochore fiber maturation in PtK1 cells and its implications for the mechanisms of chromosome congression and anaphase onset. *J. Cell Biol.* **137**, 1567-1580.
Murray, A. W. (2011). A brief history of error. *Nat. Cell Biol.* **13**, 1178-1182.
Nicklas, R. B., Kubai, D. F. and Hays, T. S. (1982). Spindle microtubules and their mechanical associations after micromanipulation in anaphase. *J. Cell Biol.* **95**, 91-104.
Nishimura, K., Fukagawa, T., Takisawa, H., Kakimoto, T. and Kanemaki, M. (2009). An auxin-based degron system for the rapid depletion of proteins in nonplant cells. *Nat. Methods* **6**, 917-922.
Peset, I. and Vernos, I. (2008). The TACC proteins: TACC-ling microtubule dynamics and centrosome function. *Trends Cell Biol.* **18**, 379-388.
Peterman, E. J. and Scholey, J. M. (2009). Mitotic microtubule crosslinkers: insights from mechanistic studies. *Curr. Biol.* **19**, R1089-R1094.
Piekorz, R. P., Hoffmeyer, A., Duntsch, C. D., McKay, C., Nakajima, H., Sexl, V., Snyder, L., Rehg, J. and Ihle, J. N. (2002). The centrosomal protein TACC3 is essential for hematopoietic stem cell function and genetically interfaces with p53-regulated apoptosis. *EMBO J.* **21**, 653-664.
Robinson, M. S., Sahlender, D. A. and Foster, S. D. (2010). Rapid inactivation of proteins by rapamycin-induced rerouting to mitochondria. *Dev. Cell* **18**, 324-331.
Royle, S. J. (2011). Mitotic moonlighting functions for membrane trafficking proteins. *Traffic* **12**, 791-798.
Royle, S. J. (2012). The role of clathrin in mitotic spindle organisation. *J. Cell Sci.* **125**, 19-28.
Royle, S. J., Bright, N. A. and Lagnado, L. (2005). Clathrin is required for the function of the mitotic spindle. *Nature* **434**, 1152-1157.
Schneider, L., Essmann, F., Kletke, A., Rio, P., Hanenberg, H., Wetzel, W., Schulze-Osthoff, K., Nürnberg, B. and Piekorz, R. P. (2007). The transforming acidic coiled coil 3 protein is essential for spindle-dependent chromosome alignment and mitotic survival. *J. Biol. Chem.* **282**, 29273-29283.
Toso, A., Winter, J. R., Garrod, A. J., Amaro, A. C., Meraldi, P. and McAinsh, A. D. (2009). Kinetochore-generated pushing forces separate centrosomes during bipolar spindle assembly. *J. Cell Biol.* **184**, 365-372.
Waters, J. C., Chen, R. H., Murray, A. W. and Salmon, E. D. (1998). Localization of Mad2 to kinetochores depends on microtubule attachment, not tension. *J. Cell Biol.* **141**, 1181-1191.
Willox, A. K. and Royle, S. J. (2012). Stonin 2 is a major adaptor protein for clathrin-mediated synaptic vesicle retrieval. *Curr. Biol.* **22**, 1435-1439.
Yu, C. T., Hsu, J. M., Lee, Y. C., Tsou, A. P., Chou, C. K. and Huang, C. Y. (2005). Phosphorylation and stabilization of HURP by Aurora-A: implication of HURP as a transforming target of Aurora-A. *Mol. Cell. Biol.* **25**, 5789-5800.

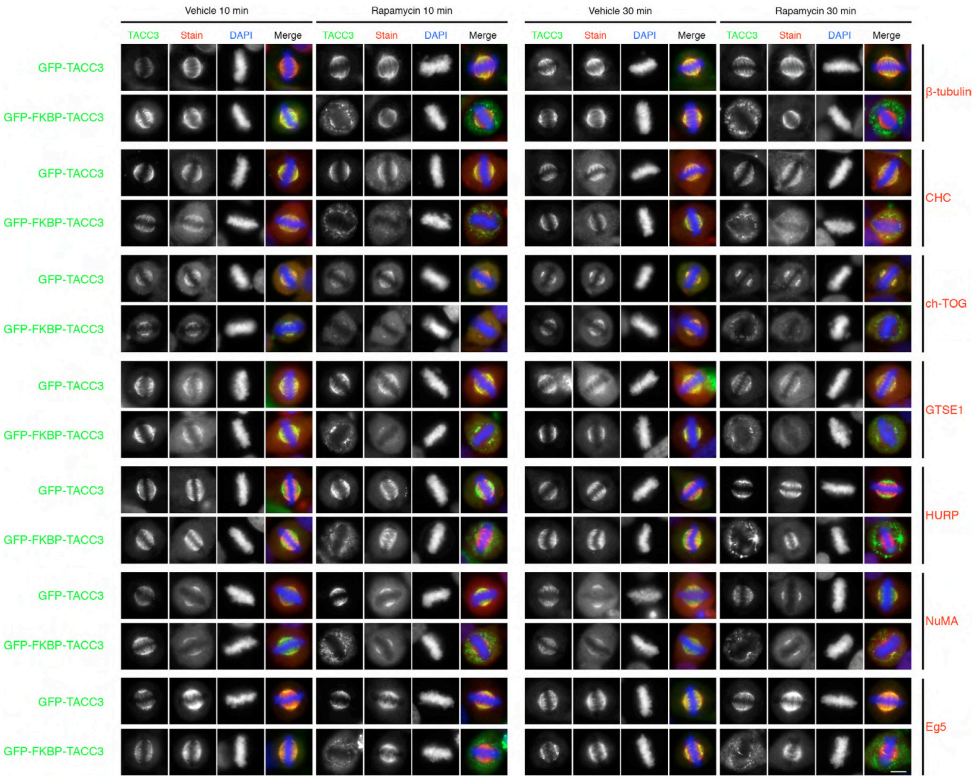

Fig. S1. Effect of TACC3 KS on other spindle proteins. Representative micrographs of TACC3-depleted HeLa cells expressing PAGFP-MitoTrap and either GFP-TACC3 or GFP-FKBP-TACC3 and treated with vehicle or rapamycin (200 nM) for 10 min or 30 min. Cells were fixed and stained for other spindle proteins (red). TACC3 KS caused removal of its partners (ch-TOG, clathrin and GTSE1). The gross morphology of the spindle was not affected (tubulin). Other spindle proteins (HURP, NuMA, Eg5) were unaltered. There were no differences between the two timepoints, indicating that removal of TACC3/ch-TOG/clathrin by TACC3 KS did not alter the localization of other spindle proteins over time. An abbreviated version of this figure showing only 1 control and the 10 min timepoint is shown as Fig. 2. Scale bar: 10 μm.

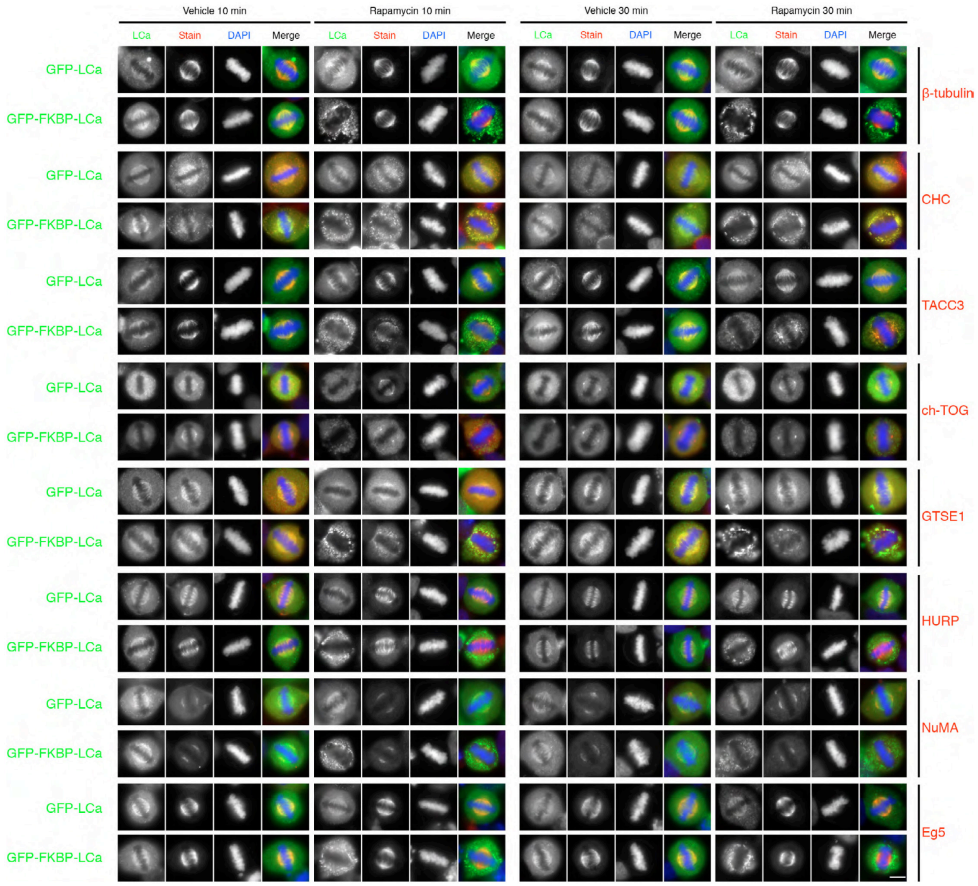

Fig. S2. Effect of clathrin rerouting on other spindle proteins. Representative micrographs of HeLa cells expressing PAGFP-MitoTrap and either GFP-LCa or GFP-FKBP-LCa and treated with vehicle or rapamycin (200 nM) for 10 min or 30 min. Cells were fixed and stained for other spindle proteins (red). LCa rerouting also removed clathrin heavy chain, ch-TOG, TACC3 and GTSE1 from the spindle. Again, tubulin, HURP, NuMA and Eg5 were unaltered after 10 and 30 min rapamycin application, indicating that removal of TACC3/ch-TOG/clathrin complexes by LCa rerouting did not alter the localization or function of other spindle proteins. Scale bar: 10 μm.

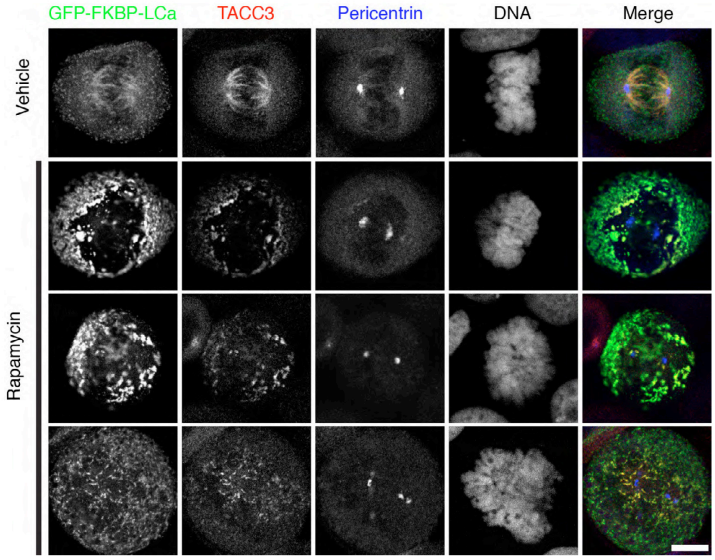

Fig. S3. No evidence for clathrin-independent TACC3 on spindle MTs or centrosomes. Representative confocal micrographs of a clathrin rerouting experiment (as shown in supplementary material Fig. S2). Treated cells were fixed and stained for TACC3 (red) and pericentrin (blue). Note the complete co-localization of clathrin and TACC3 and the lack of TACC3 on spindle MTs and centrosomes. Scale bar: 10 μm.

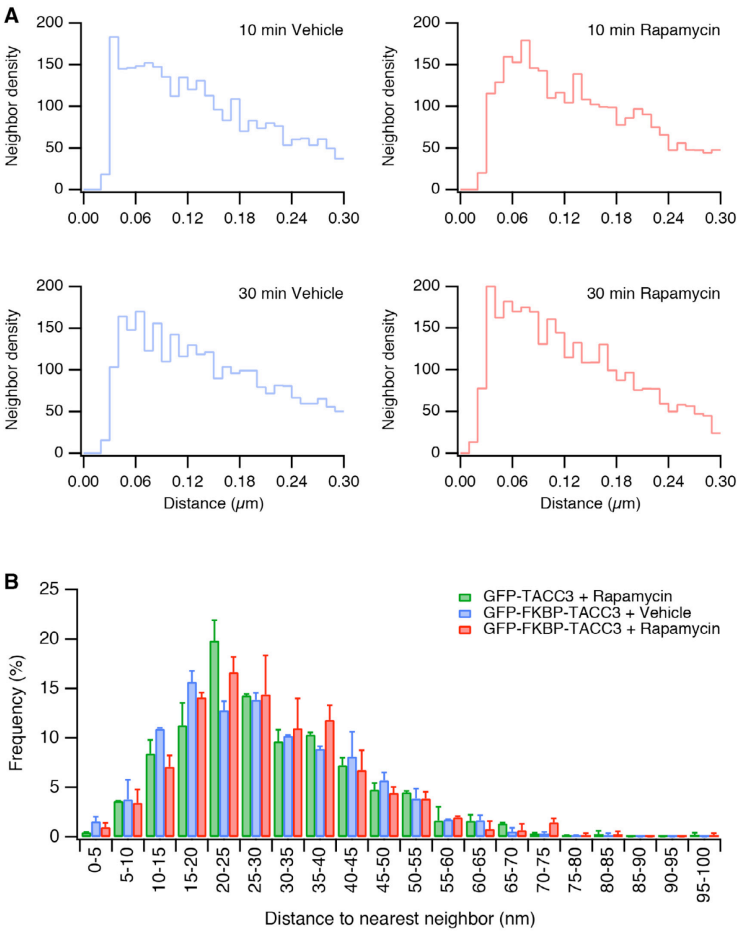

Fig. S4. TACC3 KS causes no change in the spatial organization of K-fibers. (**A**) Typical neighbor density analysis (nda) plots (McDonald et al., 1992) are shown for GFP-FKBP-TACC3 expressing K-fibers treated with vehicle or rapamycin for 10 or 30 min. These plots show the preferred spacing within a K-fiber and no obvious qualitative difference was seen following TACC3 KS. (**B**) Bar chart to show the mean±s.e.m. of the distance of each MT to its nearest neighboring microtubule.

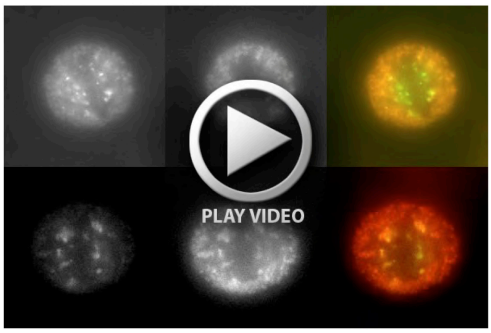

Movie 1. Live-cell imaging of rapamycin-induced rerouting of TACC3 to mitochondria. Two mitotic TACC3-depleted HeLa cells expressing GFP-FKBP-TACC3 (left, green) and mCherry-MitoTrap (middle, red). Rapamycin (200 nM) is added part way through the movie. Movie plays at 30× real time. See Fig. 1B for still images of upper cell.

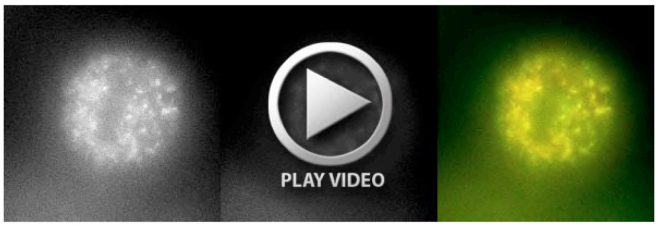

Movie 2. Live-cell imaging of rapamycin-induced rerouting of clathrin to mitochondria. Mitotic HeLa cell expressing GFP-FKBP-clathrin light chain a (LCa) and mCherry-MitoTrap. Rapamycin (200 nM) is added part way through the movie. Movie plays at 30× real time. Relates to supplementary material Fig. S2.

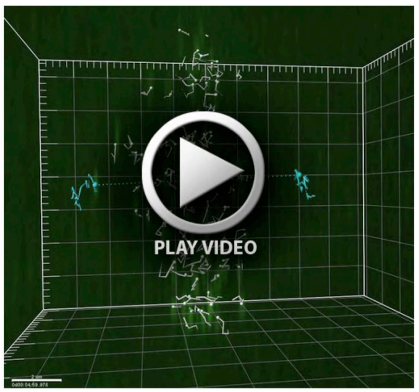

Movie 3. 3D kinetochore and spindle pole tracking. An example of a tracking experiment. Rapamycin-treated mCherry-TACC3 (control) TACC3-depleted HeLa cell stably expressing CENP-A-GFP and Centrin-GFP. Automated tracking of kinetochores (white) and spindle poles (cyan), outlier kinetochores that were rejected are shown in red. Relates to Fig. 8.

7 Bibliography

Akiyoshi, B., Sarangapani, K.K., Powers, A.F., Nelson, C.R., Reichow, S.L., Arellano-Santoyo, H., Gonen, T., Ranish, J.A., Asbury, C.L., and Biggins, S. (2010). Tension directly stabilizes reconstituted kinetochore-microtubule attachments. *Nature* **468**, 576-U255.

Albee, A.J., and Wiese, C. (2008). *Xenopus* TACC3/maskin is not required for microtubule stability but is required for anchoring microtubules at the centrosome. *Molecular Biology of the Cell* **19**, 3347-3356.

Argani, P., Lui, M.Y., Couturier, J., Bouvier, R., Fournet, J.C., and Ladanyi, M. (2003). A novel CLTC-TFE3 gene fusion in pediatric renal adenocarcinoma with t(x;17)(p11.2;q23). *Oncogene* **22**, 5374-5378.

Arrio-Dupont, M., Foucault, G., Vacher, M., Devaux, P.F., and Cribier, S. (2000). Translational diffusion of globular proteins in the cytoplasm of cultured muscle cells. *Biophysical Journal* **78**, 901-907.

Avidor-Reiss, T., and Gopalakrishnan, J. (2013). Building a centriole. *Current Opinion in Cell Biology* **25**, 72-77.

Bajer, A.S. (1973). How microtubules pull chromosomes. *The Journal of Cell Biology* **59**, 14-14.

Barr, A.R., and Gergely, F. (2008). MCAK-independent functions of ch-TOG/xMAP215 in microtubule plus-end dynamics. *Molecular and Cellular Biology* **28**, 7199-7211.

Bastmeyer, M., and Fuge, H. (1986). The distribution of intermicrotubular bridges in meiotic spindles of the crane fly. *Chromosoma* **94**, 419-424.

Basto, R., Lau, J., Vinogradova, T., Gardiol, A., Woods, C.G., Khodjakov, A., and Raff, J.W. (2006). Flies without centrioles. *Cell* **125**, 1375-1386.

Binarova, P., Cenklova, V., Hause, B., Kubatova, E., Lysak, M., Dolezel, J., Bogre, L., and Draber, P. (2000). Nuclear gamma-tubulin during acentriolar plant mitosis. *Plant Cell* **12**, 433-442.

Bishop, A.C., Ubersax, J.A., Petsch, D.T., Matheos, D.P., Gray, N.S., Blethrow, J., Shimizu, E., Tsien, J.Z., Schultz, P.G., Rose, M.D., *et al*. (2000). A chemical switch for inhibitor-sensitive alleles of any protein kinase. *Nature* **407**, 395-401.

Blixt, M.K.E., and Royle, S.J. (2011). Clathrin heavy chain gene fusions expressed in human cancers: Analysis of cellular functions. *Traffic* **12**, 754-761.

Bonaccorsi, S., Giansanti, M.G., and Gatti, M. (1998). Spindle self-organization and cytokinesis during male meiosis in asterless mutants of drosophila melanogaster. *The Journal of Cell Biology* **142**, 751-761.

Bonger, Kimberly M., Chen, Ling-chun, Liu, Corey W., and Wandless, Thomas J. (2011). Small-molecule displacement of a cryptic degron causes conditional protein degradation. *Nature Chemical Biology,* **7**, 531-537.

Booth, D.G., Hood, F.E., Prior, I.A., and Royle, S.J. (2011). A TACC3/ch-TOG/clathrin complex stabilises kinetochore fibres by inter-microtubule bridging. *EMBO Journal* **30**, 906-919.

Boveri, T. (1902). Über mehrpolige mitosen als mittel zur analyse des zellkerns. *Verhandlungen der physicalisch-medizinischen Gesselschaft zu Würzburg Neu Folge* **35**, 67-90.

Boveri, T. (1914). Zur frage der entstehung maligner tumoren (Gustav Fischer Verlag, Jena).

Braun, M., Lansky, Z., Fink, G., Ruhnow, F., Diez, S., and Janson, M.E. (2011). Adaptive braking by ase1 prevents overlapping microtubules from sliding completely apart. *Nature Cell Biology* **13**, 1259-1264.

Breuer, M., Kolano, A., Kwon, M., Li, C.-C., Tsai, T.-F., Pellman, D., Brunet, S., and Verlhac, M.-H. (2010). HURP permits MTOC sorting for robust meiotic spindle bipolarity, similar to extra centrosome clustering in cancer cells. *The Journal of Cell Biology* **191**, 1251-1260.

Bridge, J.A., Kanamori, M., Ma, Z.G., Pickering, D., Hill, D.A., Lydiatt, W., Lui, M.Y., Colleoni, G.W.B., Antonescu, C.R., Ladanyi, M.*, et al*. (2001). Fusion of the Alk gene to the clathrin heavy chain gene, CLTC, in inflammatory myofibroblastic tumor. *American Journal of Pathology* **159**, 411-415.

Brust-Mascher, I., and Scholey, J.M. (2011). Mitotic motors and chromosome segregation: The mechanism of anaphase B. *Biochemical Society Transactions* **39**, 1149-1153.

Cai, S., O'Connell, C.B., Khodjakov, A., and Walczak, C.E. (2009a). Chromosome congression in the absence of kinetochore fibres. *Nature Cell Biology* **11**, 832-U118.

Cai, S., Weaver, L.N., Ems-McClung, S.C., and Walczak, C.E. (2009b). Kinesin-14 family proteins HSET/XCTK2 control spindle length by cross-linking and sliding microtubules. *Molecular Biology of the Cell* **20**, 1348-1359.

Canman, J.C., Lewellyn, L., Laband, K., Smerdon, S.J., Desai, A., Bowerman, B., and Oegema, K. (2008). Inhibition of Rac by the GAP activity of centralspindlin is essential for cytokinesis. *Science* **322**, 1543-1546.

Carlton, J.G., and Martin-Serrano, J. (2007). Parallels between cytokinesis and retroviral budding: A role for the ESCRT machinery. *Science* **316**, 1908-1912.

Cassimeris, L., Becker, B., and Carney, B. (2009). TOGp regulates microtubule assembly and density during mitosis and contributes to chromosome directional instability. *Cell Motility and the Cytoskeleton* **66**, 535-545.

Cassimeris, L., and Morabito, J. (2004). TOGp, the human homolog of XMAP215/Dis1, is required for centrosome integrity, spindle pole organization, and bipolar spindle assembly. *Molecular Biology of the Cell* **15**, 1580-1590.

Chan, J., Jensen, C.G., Jensen, L.C.W., Bush, M., and Lloyd, C.W. (1999). The 65-kDa carrot microtubule-associated protein forms regularly arranged filamentous cross-bridges between microtubules. *Proceedings of the National Academy of Sciences* **96**, 14931-14936.

Charlebois, B.D., Kollu, S., Schek, H.T., III, Compton, D.A., and Hunt, A.J. (2011). Spindle pole mechanics studied in mitotic asters: Dynamic distribution of spindle forces through compliant linkages. *Biophysical Journal* **100**, 1756-1764.

Charrasse, S., Mazel, M., Taviaux, S., Berta, P., Chow, T., and Larroque, C. (1995). Characterization of the cDNA and pattern of expression of a new gene over-expressed in human hepatomas and colonic tumors. *European Journal of Biochemistry* **234**, 406-413.

Cheeseman, I.M., Anderson, S., Jwa, M., Green, E.M., Kang, J.-s., Yates, J.R., Chan, C.S.M., Drubin, D.G., and Barnes, G. (2002). Phospho-regulation of kinetochore-microtubule attachments by the Aurora kinase ipl1p. *Cell* **111**, 163-172.

Cheeseman, I.M., and Desai, A. (2008). Molecular architecture of the kinetochore-microtubule interface. *Nature Reviews Molecular Cell Biology* **9**, 33-46.

Cheeseman, I.M., Niessen, S., Anderson, S., Hyndman, F., Yates, J.R., Oegema, K., and Desai, A. (2004). A conserved protein network controls assembly of the outer kinetochore and its ability to sustain tension. *Genes & Development* **18**, 2255-2268.

Cheeseman, L.P., Booth, D.G., Hood, F.E., Prior, I.A., and Royle, S.J. (2011). Aurora A kinase activity is required for localization of TACC3/ch-TOG/clathrin inter-microtubule bridges. *Communicative & Integrative Biology* **4**, 409-412.

Cheeseman, L.P., Harry, E.F., McAinsh, A.D., Prior, I.A., and Royle, S.J. (2013). Specific removal of TACC3-ch-TOG-clathrin at metaphase deregulates kinetochore fiber tension. *Journal of Cell Science* **126**, 2102-2113.

Chen, J., Kanai, Y., Cowan, N.J., and Hirokawa, N. (1992). Projection domains of MAP2 and tau determine spacings between microtubules in dendrites and axons. *Nature* **360**, 674-676.

Chen, R.H., Waters, J.C., Salmon, E.D., and Murray, A.W. (1996). Association of spindle assembly checkpoint component xMad2 with unattached kinetochores. *Science* **274**, 242-246.

Chikatsu, N., Kojima, H., Suzukawa, K., Shinagawa, A., Nagasawa, T., Ozawa, H., Yamashita, Y., and Mori, N. (2003). Alk(+), cd30(-), cd20(-) large b-cell lymphoma containing anaplastic lymphoma kinase (alk) fused to clathrin heavy chain gene (CLTC). *Modern Pathology* **16**, 828-832.

Civelekoglu-Scholey, G., and Scholey, J.M. (2010). Mitotic force generators and chromosome segregation. *Cellular and Molecular Life Sciences* **67**, 2231-2250.

Conte, N., Delaval, B., Ginestier, C., Ferrand, A., Isnardon, D., Larroque, C., Prigent, C., Seraphin, B., Jacquemier, J., and Birnbaum, D. (2003). TACC1-chTOG-Aurora A protein complex in breast cancer. *Oncogene* **22**, 8102-8116.

Cools, J., Wlodarska, I., Somers, R., Mentens, N., Pedeutour, F., Maes, B., De Wolf-Peeters, C., Pauwels, P., Hagemeijer, A., and Marynen, P. (2002). Identification of novel fusion partners of Alk, the anaplastic lymphoma kinase, in anaplastic large-cell lymphoma and inflammatory myofibroblastic tumor. *Gene Chromosomes Cancer* **34**, 354-362.

de Moor, C.H., Meijer, H., and Lissenden, S. (2005). Mechanisms of translational control by the 3' Utr in development and differentiation. *Seminars in Cell & Developmental Biology* **16**, 49-58.

De Paepe, P., Baens, M., van Krieken, H., Verhasselt, B., Stul, M., Simons, A., Poppe, B., Laureys, G., Brons, P., Vandenberghe, P., *et al*. (2003). Alk activation by the CLTC-Alk fusion is a recurrent event in large B-cell lymphoma. *Blood* **102**, 2638-2641.

DeLuca, J.G., Moree, B., Hickey, J.M., Kilmartin, J.V., and Salmon, E.D. (2002). hNuf2 inhibition blocks stable kinetochore-microtubule attachment and induces mitotic cell death in HeLa cells. *The Journal of Cell Biology* **159**, 549-555.

Desai, A., and Mitchison, T.J. (1997). Microtubule polymerization dynamics. *Annual Review of Cell and Developmental Biology* **13**, 83-117.

Ding, R., McDonald, K.L., and McIntosh, J.R. (1993). Three-dimensional reconstruction and analysis of mitotic spindles from the yeast, schizosaccharomyces pombe. *The Journal of Cell Biology* **120**, 141-151.

Dionne, M.A., Howard, L., and Compton, D.A. (1999). NuMA is a component of an insoluble matrix at mitotic spindle poles. *Cell Motility and the Cytoskeleton* **42**, 189-203.

Dumont, S., and Mitchison, T.J. (2009a). Compression regulates mitotic spindle length by a mechanochemical switch at the poles. *Current Biology* **19**, 1086-1095.

Dumont, S., and Mitchison, T.J. (2009b). Force and length in the mitotic spindle. *Current Biology* **19**, R749-R761.

Engelborghs, Y., Heremans, K.A.H., Demaeyer, L.C.M., and Hoebeke, J. (1976). Effect of temperature and pressure on polymerization equilibrium of neuronal microtubules. *Nature* **259**, 686-689.

Evans, T., Rosenthal, E.T., Youngblom, J., Distel, D., and Hunt, T. (1983). Cyclin - a protein specified by maternal messenger-rna in sea-urchin eggs that is destroyed at each cleavage division. *Cell* **33**, 389-396.

Fielding, A.B., Lim, S., Montgomery, K., Dobreva, I., and Dedhar, S. (2011). A critical role of integrin-linked kinase, ch-TOG and TACC3 in centrosome clustering in cancer cells. *Oncogene* **30**, 521-534.

Fielding, A.B., Willox, A.K., Okeke, E., and Royle, S.J. (2012). Clathrin-mediated endocytosis is inhibited during mitosis. *Proceedings of the National Academy of Sciences of the United States of America* **109**, 6572-6577.

Flemming, W. (1882). Zellsubstanz, kern und zelltheilung (Leipzig, Vogel).

Fotin, A., Cheng, Y.F., Sliz, P., Grigorieff, N., Harrison, S.C., Kirchhausen, T., and Walz, T. (2004). Molecular model for a complete clathrin lattice from electron cryomicroscopy. *Nature* **432**, 573-579.

Fu, W., Tao, W., Zheng, P., Fu, J., Bian, M., Jiang, Q., Clarke, P.R., and Zhang, C. (2010). Clathrin recruits phosphorylated TACC3 to spindle poles for bipolar spindle assembly and chromosome alignment. *Journal of Cell Science* **123**, 3645-3651.

Gard, D.L., Becker, B.E., and Romney, S.J. (2004). Mapping the eukaryotic tree of life: Structure, function, and evolution of the MAP215/Dis1 family of microtubule-associated proteins. *International Review of Cytology - a Survey of Cell Biology, Vol 239* **239**, 179-272.

Gard, D.L., and Kirschner, M.W. (1987). A microtubule-associated protein from *Xenopus* eggs that specifically promotes assembly at the plus-end. *The Journal of Cell Biology* **105**, 2203-2215.

Gascoigne, K., and Cheeseman, I. (2013). Cdk-dependent phosphorylation and nuclear exclusion coordinately control kinetochore assembly state. *The Journal of Cell Biology* **201**, 23-32.

Gascoyne, R.D., Lamant, L., Martin-Subero, J.I., Lestou, V.S., Harris, N.L., Muller-Hermelink, H.K., Seymour, J.F., Campbell, L.J., Horsman, D.E., Auvigne, I., *et al*. (2003). Alk-positive diffuse large B-cell lymphoma is associated with clathrin-Alk rearrangements: Report of 6 cases. *Blood* **102**, 2568-2573.

Geda, P., Patury, S., Ma, J., Bharucha, N., Dobry, C.J., Lawson, S.K., Gestwicki, J.E., and Kumar, A. (2008). A small molecule-directed approach to control protein localization and function. *Yeast* **25**, 577-594.

Gergely, F., Draviam, V.M., and Raff, J.W. (2003). The ch-TOG/xMAP215 protein is essential for spindle pole organization in human somatic cells. *Genes & Development* **17**, 336-341.

Gergely, F., Karlsson, C., Still, I., Cowell, J., Kilmartin, J., and Raff, J.W. (2000a). The TACC domain identifies a family of centrosomal proteins that can interact with microtubules. *Proceedings of the National Academy of Sciences of the United States of America* **97**, 14352-14357.

Gergely, F., Kidd, D., Jeffers, K., Wakefield, J.G., and Raff, J.W. (2000b). D-TACC: A novel centrosomal protein required for normal spindle function in the early drosophila embryo. *EMBO Journal* **19**, 241-252.

Gibbons, I.R. (1963). Studies on protein components of cilia from Tetrahymena pyriformis. *Proceedings of the National Academy of Sciences of the United States of America* **50**, 1002.

Gibbons, I.R., and Rowe, A.J. (1965). Dynein - a protein with adenosine triphosphatase activity from cilia. *Science* **149**, 424.

Giet, R., Uzbekov, R., Cubizolles, F., Le Guellec, K., and Prigent, C. (1999). The *Xenopus* laevis Aurora-related protein kinase pEg2 associates with and phosphorylates the kinesin-related protein xlEg5. *Journal of Biological Chemistry* **274**, 15005-15013.

Goldstein, J.L., Brown, M.S., Anderson, R.G.W., Russell, D.W., and Schneider, W.J. (1985). Receptor-mediated endocytosis - concepts emerging from the ldl receptor system. *Annual Review of Cell Biology* **1**, 1-39.

Gorbsky, G., and Ricketts, W. (1993). Differential expression of a phosphoepitope at the kinetochores of moving chromosomes. *The Journal of Cell Biology* **122**, 1311-1321.

Goshima, G., Wollman, R., Stuurman, N., Scholey, J.M., and Vale, R.D. (2005). Length control of the metaphase spindle. *Current Biology* **15**, 1979-1988.

Gotoh, Y., Nishida, E., Matsuda, S., Shiina, N., Kosako, H., Shiokawa, K., Akiyama, T., Ohta, K., and Sakai, H. (1991). In vitro effects on microtubule dynamics of purified *Xenopus* M-phase-activated MAP kinase. *Nature* **349**, 251-254.

Grill, S.W., and Hyman, A.A. (2005). Spindle positioning by cortical pulling forces. *Developmental Cell* **8**, 461-465.

Ha, G.-H., Park, J.-S., and Breuer, E.-K.Y. (2013). TACC3 promotes epithelial-mesenchymal transition (EMT) through the activation of PI3K/AKT and ERK signaling pathways. *Cancer Letters* **332**, 63-73.

Hanahan, D., and Weinberg, R.A. (2011). Hallmarks of cancer: The next generation. *Cell* **144**, 646-674.

Heath, I.B. (1974). Mitosis in fungus thraustotheca-clavata. *The Journal of Cell Biology* **60**, 204-220.

Hepler, P.K., McIntosh, J.R., and Cleland, S. (1970). Intermicrotubule bridges in mitotic spindle apparatus. *The Journal of Cell Biology* **45**, 438-444.

Heuser, J., and Kirchhausen, T. (1985). Deep-etch views of clathrin assemblies. *Journal of Ultrastructural Research* **92**, 1-27.

Hirst, J., Borner, G.H.H., Antrobus, R., Peden, A.A., Hodson, N.A., Sahlender, D.A., and Robinson, M.S. (2012). Distinct and overlapping roles for AP-1 and GGAS revealed by the "Knocksideways" System. *Current Biology* **22**, 1711-1716.

Holland, A.J., Fachinetti, D., Han, J.S., and Cleveland, D.W. (2012). Inducible, reversible system for the rapid and complete degradation of proteins in mammalian cells. *Proceedings of the National Academy of Sciences of the United States of America* **109**, E3350-E3357.

Holmfeldt, P., Stenmark, S., and Gullberg, M. (2004). Differential functional interplay of TOGp/XMAP215 and the kini kinesin MCAK during interphase and mitosis. *EMBO Journal* **23**, 627-637.

Hood, F.E., and Royle, S.J. (2009). Functional equivalence of the clathrin heavy chains CHC17 and CHC22 in endocytosis and mitosis. *Journal of Cell Science* **122**, 2185-2190.

Hood, F.E., Williams, S.J., Burgess, S.G., Richards, M.W., Roth, D., Straube, A., Pfuhl, M., Bayliss, R., Royle, S.J. (2013). Quaternary domain co-ordination enables TACC3–ch-TOG–clathrin mitotic spindle binding. *The Journal of Cell Biology* ***In Press***

Hubner, N.C., Bird, A.W., Cox, J., Splettstoesser, B., Bandilla, P., Poser, I., Hyman, A., and Mann, M. (2010). Quantitative proteomics combined with BAC transgeneomics reveals in vivo protein interactions. *The Journal of Cell Biology* **189**, 739-754.

Indjeian, V.B., Stern, B.M., and Murray, A.W. (2005). The centromeric protein Sgo1 is required to sense lack of tension on mitotic chromosomes. *Science* **307**, 130-133.

Jacobson, K., Derzko, Z., Wu, E.S., Hou, Y., and Poste, G. (1976). Measurement of lateral mobility of cell-surface components in single, living cells by fluorescence recovery after photobleaching. *Journal of Supramolecular Structure* **5**, 565-576.

Jacobson, K., Rajfur, Z., Vitriol, E., and Hahn, K. (2008). Chromophore-assisted laser inactivation in cell biology. *Trends in Cell Biology* **18**, 443-450.

Janson, M.E., Loughlin, R., Loiodice, I., Fu, C., Brunner, D., Nedelec, F.J., and Tran, P.T. (2007). Crosslinkers and motors organize dynamic microtubules to form stable bipolar arrays in fission yeast. *Cell* **128**, 357-368.

Jaqaman, K., King, E.M., Amaro, A.C., Winter, J.R., Dorn, J.F., Elliott, H.L., McHedlishvili, N., McClelland, S.E., Porter, I.M., Posch, M., *et al*. (2010). Kinetochore alignment within the metaphase plate is regulated by centromere stiffness and microtubule depolymerases. *The Journal of Cell Biology* **188**, 665-679.

Jay, D. G. (1988). Selective destruction of protein function by chromophore-assisted laser inactivation. *Proceedings of the National Academy of Sciences of the United States of America* **85**, 5454-5458.

Jensen, C., and Bajer, A. (1973). Kinetochore microtubules of haemanthus endosperm during mitosis. *The Journal of Cell Biology* **59**, A156-A156.

Jiang, W., Jimenez, G., Wells, N.J., Hope, T.J., Wahl, G.M., Hunter, T., and Fukunaga, R. (1998). PRC1: A human mitotic spindle-associated CDK substrate protein required for cytokinesis. *Molecular Cell* **2**, 877-885.

Jin, A.J., and Nossal, R. (2000). Rigidity of triskelion arms and clathrin nets. *Biophysical Journal* **78**, 1183-1194.

Jung, C.K., Jung, J.H., Park, G.S., Lee, A., Kang, C.S., and Lee, K.Y. (2006). Expression of transforming acidic coiled-coil containing protein 3 is a novel independent prognostic marker in non-small cell lung cancer. *Pathology International* **56**, 503-509.

Kakui, Y., Sato, M., Okada, N., Toda, T., and Yamamoto, M. (2013). Microtubules and alp7-alp14 (TACC-TOG) reposition chromosomes before meiotic segregation. *Nature Cell Biology* **advance online publication**.

Kapitein, L.C., Peterman, E.J.G., Kwok, B.H., Kim, J.H., Kapoor, T.M., and Schmidt, C.F. (2005). The bipolar mitotic kinesin Eg5 moves on both microtubules that it crosslinks. *Nature* **435**, 114-118.

Kapoor, T.M., Mayer, T.U., Coughlin, M.L., and Mitchison, T.J. (2000). Probing spindle assembly mechanisms with monastrol, a small molecule inhibitor of the mitotic kinesin, Eg5. *The Journal of Cell Biology* **150**, 975-988.

Kaverina, I., and Straube, A. (2011). Regulation of cell migration by dynamic microtubules. *Seminars in Cell & Developmental Biology* **22**, 968-974.

Keppler, A., and Ellenberg, J. (2009). Chromophore-assisted laser inactivation of alpha- and gamma-tubulin SNAP-tag fusion proteins inside living cells. *ACS Chemical Biology* **4**, 127-138.

Kettenbach, A.N., Schweppe, D.K., Faherty, B.K., Pechenick, D., Pletnev, A.A., and Gerber, S.A. (2011). Quantitative phosphoproteomics identifies substrates and functional modules of Aurora and Polo-like kinase activities in mitotic cells. *Science Signaling* **4**.

Khodjakov, A., Cole, R.W., Oakley, B.R., and Rieder, C.L. (2000). Centrosome-independent mitotic spindle formation in vertebrates. *Current Biology* **10**, 59-67.

Kimura, K., and Hirano, T. (1997). ATP-dependent positive supercoiling of DNA by 13S condensin: A biochemical implication for chromosome condensation. *Cell* **90**, 625-634.

King, J.M., and Nicklas, R.B. (2000). Tension on chromosomes increases the number of kinetochore microtubules but only within limits. *Journal of Cell Science* **113**, 3815-3823.

Kinoshita, K., Arnal, I., Desai, A., Drechsel, D.N., and Hyman, A.A. (2001). Reconstitution of physiological microtubule dynamics using purified components. *Science* **294**, 1340-1343.

Kinoshita, K., Noetzel, T.L., Pelletier, L., Mechtler, K., Drechsel, D.N., Schwager, A., Lee, M., Raff, J.W., and Hyman, A.A. (2005). Aurora A phosphorylation of TACC3/maskin is required for centrosome-dependent microtubule assembly in mitosis. *The Journal of Cell Biology* **170**, 1047-1055.

Kirchhausen, T., and Harrison, S.C. (1981). Protein organization in clathrin trimers. *Cell* **23**, 755-761.

Kirschner, M.W., and Mitchison, T. (1986). Microtubule dynamics. *Nature* **324**, 621-621.

Kitagawa, D., Vakonakis, I., Olieric, N., Hilbert, M., Keller, D., Olieric, V., Bortfeld, M., Erat, M.C., Flueckiger, I., Gonczy, P., *et al*. (2011). Structural basis of the 9-fold symmetry of centrioles. *Cell* **144**, 364-375.

Kitajima, T.S., Ohsugi, M., and Ellenberg, J. (2011). Complete kinetochore tracking reveals error-prone homologous chromosome biorientation in mammalian oocytes. *Cell* **146**, 568-581.

Kiyomitsu, T., and Cheeseman, I.M. (2012). Chromosome- and spindle-pole-derived signals generate an intrinsic code for spindle position and orientation. *Nature Cell Biology* **14**, 311-317.

Kline-Smith, S.L., and Walczak, C.E. (2004). Mitotic spindle assembly and chromosome segregation: Refocusing on microtubule dynamics. *Molecular Cell* **15**, 317-327.

Koffa, M.D., Casanova, C.M., Santarella, R., Kocher, T., Wilm, M., and Mattaj, I.W. (2006). HURP is part of a Ran-dependent complex involved in spindle formation. *Current Biology* **16**, 743-754.

Kops, G., Weaver, B.A.A., and Cleveland, D.W. (2005). On the road to cancer: Aneuploidy and the mitotic checkpoint. *Nature Reviews Cancer* **5**, 773-785.

Kurasawa, Y., Earnshaw, W.C., Mochizuki, Y., Dohmae, N., and Todokoro, K. (2004). Essential roles of KIF4 and its binding partner PRC1 in organized central spindle midzone formation. *EMBO Journal* **23**, 3237-3248.

Kwon, M., Godinho, S.A., Chandhok, N.S., Ganem, N.J., Azioune, A., Thery, M., and Pellman, D. (2008). Mechanisms to suppress multipolar divisions in cancer cells with extra centrosomes. *Genes & Development* **22**, 2189-2203.

Lampert, F., and Westermann, S. (2011). A blueprint for kinetochores - new insights into the molecular mechanics of cell division. *Nature Reviews Molecular Cell Biology* **12**, 407-412.

Lampson, M.A., and Cheeseman, I.M. (2011). Sensing centromere tension: Aurora B and the regulation of kinetochore function. *Trends in Cell Biology* **21**, 133-140.

Lane, H.A., and Nigg, E.A. (1996). Antibody microinjection reveals an essential role for human polo-like kinase 1 (Plk1) in the functional maturation of mitotic centrosomes. *The Journal of Cell Biology* **135**, 1701-1713.

Larijani, B., and Poccia, D.L. (2009). Nuclear envelope formation: Mind the gaps. In *Annual review of biophysics*, pp. 107-124.

Lauffart, B., Vaughan, M.M., Eddy, R., Chervinsky, D., DiCioccio, R.A., Black, J.D., and Still, I.H. (2005). Aberrations of TACC1 and TACC3 are associated with ovarian cancer. *BMC women's health* **5**, 8-8.

Lee, M.J., Gergely, F., Jeffers, K., Peak-Chew, S.Y., and Raff, J.W. (2001). Msps/XMAP215 interacts with the centrosomal protein d-TACC to regulate microtubule behaviour. *Nature Cell Biology* **3**, 643-649.

Lekomtsev, S., Su, K.-C., Pye, V.E., Blight, K., Sundaramoorthy, S., Takaki, T., Collinson, L.M., Cherepanov, P., Divecha, N., and Petronczki, M. (2012). Centralspindlin links the mitotic spindle to the plasma membrane during cytokinesis. *Nature* **492**, 276-+.

Lengauer, C., Kinzler, K.W., and Vogelstein, B. (1997). Genetic instability in colorectal cancers. *Nature* **386**, 623-627.

LeRoy, P.J., Hunter, J.J., Hoar, K.M., Burke, K.E., Shinde, V., Ruan, J., Bowman, D., Galvin, K., and Ecsedy, J.A. (2007). Localization of human TACC3 to mitotic spindles is mediated by phosphorylation on Ser(558) by Aurora A: A novel pharmacodynamic method for measuring Aurora A activity. *Cancer Research* **67**, 5362-5370.

Li, R., and Murray, A.W. (1991). Feedback control of mitosis in budding yeast. *Cell* **66**, 519-531.

Lin, C.-H., Hu, C.-K., and Shih, H.-M. (2010). Clathrin heavy chain mediates TACC3 targeting to mitotic spindles to ensure spindle stability. *The Journal of Cell Biology* **189**, 1097-1105.

Loughlin, R., Heald, R., and Nedelec, F. (2010). A computational model predicts *Xenopus* meiotic spindle organization. *The Journal of Cell Biology* **191**, 1239-1249.

Lydersen, B.K., and Pettijohn, D.E. (1980). Human-specific nuclear-protein that associates with the polar region of the mitotic apparatus - distribution in a human-hamster hybrid cell. *Cell* **22**, 489-499.

Mack, G.J., and Compton, D.A. (2001). Analysis of mitotic microtubule-associated proteins using mass spectrometry identifies astrin, a spindle-associated protein. *Proceedings of the National Academy of Sciences of the United States of America* **98**, 14434-14439.

Maddox, P., Desai, A., Oegema, K., Mitchison, T.J., and Salmon, E.D. (2002). Poleward microtubule flux is a major component of spindle dynamics and anaphase A in mitotic drosophila embryos. *Current Biology* **12**, 1670-1674.

Mahoney, N.M., Goshima, G., Douglass, A.D., and Vale, R.D. (2006). Making microtubules and mitotic spindles in cells without functional centrosomes. *Current Biology* **16**, 564-569.

Maiato, H., Hergert, P.J., Moutinho-Pereira, S., Dong, Y., Vandenbeldt, K.J., Rieder, C.L., and McEwen, B.F. (2006). The ultrastructure of the kinetochore and kinetochore fiber in drosophila somatic cells. *Chromosoma* **115**, 469-480.

Maro, B., Johnson, M.H., Pickering, S.J., and Louvard, D. (1985). Changes in the distribution of membranous organelles during mouse early development. *Journal of Embryology and Experimental Morphology* **90**, 287-309.

Mastronarde, D.N., McDonald, K.L., Ding, R., and McIntosh, J.R. (1993). Interpolar spindle microtubules in Ptk cells. *The Journal of Cell Biology* **123**, 1475-1489.

McAinsh, A., and Meraldi, P. (2011). The ccan complex: Linking centromere specification to control of kinetochore-microtubule dynamics. *Seminars in cell & developmental biology* **22**, 946-952.

McDonald, K.L., O'Toole, E.T., Mastronarde, D.N., and McIntosh, J.R. (1992). Kinetochore microtubules in Ptk cells. *The Journal of Cell Biology* **118**, 369-383.

McEwen, B.F., Heagle, A.B., Cassels, G.O., Buttle, K.F., and Rieder, C.L. (1997). Kinetochore fiber maturation in Ptk1 cells and its implications for the mechanisms of chromosome congression and anaphase onset. *The Journal of Cell Biology* **137**, 1567-1580.

McIntosh, J.R., Cande, W.Z., and Snyder, J.A. (1975). Structure and physiology of the mammalian mitotic spindle. *Society of General Physiologists series* **30**, 31-76.

McIntosh, J.R., Grishchuk, E.L., Morphew, M.K., Efremov, A.K., Zhudenkov, K., Volkov, V.A., Cheeseman, I.M., Desai, A., Mastronarde, D.N., and Ataullakhanov, F.I. (2008). Fibrils connect microtubule tips with kinetochores: A mechanism to couple tubulin dynamics to chromosome motion. *Cell* **135**, 322-333.

McIntosh, J.R., Grishchuk, E.L., and West, R.R. (2002). Chromosome-microtubule interactions during mitosis. *Annual Review of Cell and Developmental Biology* **18**, 193-219.

Mitchison, T., and Kirschner, M. (1984). Dynamic instability of microtubule growth. *Nature* **312**, 237-242.

Mitchison, T.J., and Kirschner, M.W. (1985). Properties of the kinetochore in vitro .2. Microtubule capture and ATP-dependent translocation. *The Journal of Cell Biology* **101**, 766-777.

Moens, P.B. (1976). Spindle and kinetochore morphology of dictyostelium-discoideum. *The Journal of Cell Biology* **68**, 113-122.

Moens, P.B. (1979). Kinetochore microtubule numbers of different sized chromosomes. *The Journal of Cell Biology* **83**, 556-561.

Mollinari, C., Kleman, J.P., Jiang, W., Schoehn, G., Hunter, T., and Margolis, R.L. (2002). PRC1 is a microtubule binding and bundling protein essential to maintain the mitotic spindle midzone. *The Journal of Cell Biology* **157**, 1175-1186.

Mountain, V., Simerly, C., Howard, L., Ando, A., Schatten, G., and Compton, D.A. (1999). The kinesin-related protein, HSET, opposes the activity of Eg5 and cross-links microtubules in the mammalian mitotic spindle. *The Journal of Cell Biology* **147**, 351-365.

Mousavi, S.A., Malerod, L., Berg, T., and Kjeken, R. (2004). Clathrin-dependent endocytosis. *Biochemical Journal* **377**, 1-16.

Mukherjee, S., Ghosh, R.N., and Maxfield, F.R. (1997). Endocytosis. *Physiological Reviews* **77**, 759-803.

Murray, A.W. (2011). Focus on cell cycle and DNA damage a brief history of error. *Nature Cell Biology* **13**, 1178-1182.

Nezi, L., and Musacchio, A. (2009). Sister chromatid tension and the spindle assembly checkpoint. *Current Opinions in Cell Biology* **21**, 785-795.

Nicklas, R.B. (1983). Measurements of the force produced by the mitotic spindle in anaphase. *The Journal of Cell Biology* **97**, 542-548.

Nicklas, R.B., Kubai, D.F., and Hays, T.S. (1982). Spindle microtubules and their mechanical associations after micromanipulation in anaphase. *The Journal of Cell Biology* **95**, 91-104.

Nishimura, K., Fukagawa, T., Takisawa, H., Kakimoto, T., and Kanemaki, M. (2009). An auxin-based degron system for the rapid depletion of proteins in nonplant cells. *Nature Methods* **6**, 917-U978.

Nishino, T., Rago, F., Hori, T., Tomii, K., Cheeseman, I.M., and Fukagawa, T. (2013). CENP-T provides a structural platform for outer kinetochore assembly. *EMBO Journal* **32**, 424-436.

Norbury, C., and Nurse, P. (1992). Animal-cell cycles and their control. *Annual Review of Biochemistry* **61**, 441-470.

Nurse, P. (1975). Genetic-control of cell-size at cell-division in yeast. *Nature* **256**, 547-551.

O'Brien, L.L., Albee, A.J., Liu, L.L., Tao, W., Dobrzyn, P., Lizarraga, S.B., and Wiese, C. (2005). The *Xenopus* TACC homologue, maskin, functions in mitotic spindle assembly. *Molecular Biology of the Cell* **16**, 2836-2847.

Oakley, B.R., and Heath, I.B. (1978). The arrangement of microtubules in serially sectioned spindles of the alga Cryptomonas. *Journal of Cell Science* **31**, 53-70.

Okamoto, C.T., McKinney, J., and Jeng, Y.Y. (2000). Clathrin in mitotic spindles. *American Journal of Physiology-Cell Physiology* **279**, C369-C374.

Ou, G., Stuurman, N., D'Ambrosio, M., and Vale, R. D. (2010). Polarized myosin produces unequal-size daughters during asymmetric cell division. *Science* **330**, 677-680.

Parker, B.C., Annala, M.J., Cogdell, D.E., Granberg, K.J., Sun, Y., Ji, P., Li, X., Gumin, J., Zheng, H., Hu, L., *et al*. (2013). The tumorigenic FGFR3-TACC3 gene fusion escapes Mir-99a regulation in glioblastoma. *Journal of Clinical Investigation* **123**, 855-865.

Paulmurugan, R., and Gambhir, S.S. (2005). Firefly luciferase enzyme fragment complementation for imaging in cells and living animals. *Analytical Chemistry* **77**, 1295-1302.

Perpelescu, M., and Fukagawa, T. (2011). The ABCs of CENPs. *Chromosoma* **120**, 425-446.

Peset, I., Seiler, J., Sardon, T., Bejarano, L.A., Rybina, S., and Vernos, I. (2005). Function and regulation of maskin, a TACC family protein, in microtubule growth during mitosis. *The Journal of Cell Biology* **170**, 1057-1066.

Peset, I., and Vernos, I. (2008). The TACC proteins: TACC-ling microtubule dynamics and centrosome function. *Trends in Cell Biology* **18**, 379-388.

Peterson, J.B., and Ris, H. (1976). Electron-microscopic study of spindle and chromosome movement in yeast saccharomyces-cerevisiae. *Journal of Cell Science* **22**, 219-242.

Pinsky, B.A., Kung, C., Shokat, K.M., and Biggins, S. (2006). The ipl1-Aurora protein kinase activates the spindle checkpoint by creating unattached kinetochores. *Nature Cell Biology* **8**, 78-83.

Popov, A.V., Pozniakovsky, A., Arnal, I., Antony, C., Ashford, A.J., Kinoshita, K., Tournebize, R., Hyman, A.A., and Karsenti, E. (2001). XMAP215 regulates microtubule dynamics through two distinct domains. *EMBO Journal* **20**, 397-410.

Popov, A.V., Severin, F., and Karsenti, E. (2002). XMAP215 is required for the microtubule-nucleating activity of centrosomes. *Current Biology* **12**, 1326-1330.

Prasher, D.C., Eckenrode, V.K., Ward, W.W., Prendergast, F.G., and Cormier, M.J. (1992). Primary structure of the Aequorea victoria green-fluorescent protein. *Gene* **111**, 229-233.

Raemaekers, T., Ribbeck, K., Beaudouin, J., Annaert, W., Van Camp, M., Stockmans, I., Smets, N., Bouillon, R., Ellenberg, J., and Carmeliet, G. (2003). NuSAP, a novel microtubule-associated protein involved in mitotic spindle organization. *The Journal of Cell Biology* **162**, 1017-1029.

Reynolds, E.S. (1963). The use of lead citrate at high pH as an electron-opaque stain in electron microscopy. *The Journal of Cell Biology* **17**, 208-212.

Ribbeck, K., Groen, A.C., Santarella, R., Bohnsack, M.T., Raemaekers, T., Kocher, T., Gentzel, M., Gorlich, D., Wilm, M., Carmeliet, G., *et al*. (2006). NuSAP, a mitotic RanGTP target that stabilizes and cross-links microtubules. *Molecular Biology of the Cell* **17**, 2646-2660.

Ribbeck, K., Raemaekers, T., Carmeliet, G., and Mattaj, I.W. (2007). A role for NuSAP in linking microtubuies to mitotic chromosomes. *Current Biology* **17**, 230-236.

Richardson, H., Okeefe, L.V., Marty, T., and Saint, R. (1995). Ectopic cyclin-E expression induces premature entry into S phase and disrupts pattern-formation in the *Drosophila* eye imaginal disc. *Development* **121**, 3371-3379.

Rieder, C.L. (1982). The formation, structure, and composition of the mammalian kinetochore and kinetochore fiber. *International Review of Cytology-a Survey of Cell Biology* **79**, 1-58.

Rieder, C.L., Schultz, A., Cole, R., and Sluder, G. (1994). Anaphase onset in vertebrate somatic-cells is controlled by a checkpoint that monitors sister kinetochore attachment to the spindle. *The Journal of Cell Biology* **127**, 1301-1310.

Robinson, M.S. (1994). The role of clathrin, adapters and dynamin in endocytosis. *Current Opinion in Cell Biology* **6**, 538-544.

Robinson, M.S., Sahlender, D.A., and Foster, S.D. (2010). Rapid inactivation of proteins by rapamycin-induced rerouting to mitochondria. *Developmental Cell* **18**, 324-331.

Royle, S.J., Bright, N.A., and Lagnado, L. (2005). Clathrin is required for the function of the mitotic spindle. *Nature* **434**, 1152-1157.

Royle, S.J., Granseth, B., Odermatt, B., Derevier, A., and Lagnado, L. (2008). Imaging pHluorin-based probes at hippocampal synapses. *Methods in Molecular Biology* **457**, 293-303.

Royle, S.J., and Lagnado, L. (2006). Trimerisation is important for the function of clathrin at the mitotic spindle. *Journal of Cell Science* **119**, 4071-4078.

Rusan, N.M., and Rogers, G.C. (2009). Centrosome function: Sometimes less is more. *Traffic* **10**, 472-481.

Ryser, U. (1970). Ultrastructure of mitotic nuclei in plasmodia of physarum-polycephalum. *Zeitschrift Fur Zellforschung Und Mikroskopische Anatomie* **110**, 108.

Laplante, Mathieu, and Sabatini, David M. (2012). mTOR Signaling in Growth Control and Disease. *Cell* **149**, 274-293.

Salmon, E.D., Cimini, D., Cameron, L.A., and DeLuca, J.G. (2005). Merotelic kinetochores in mammalian tissue cells. *Philosophical Transactions of the Royal Society B: Biological Sciences* **360**, 553-568.

Santarella, R.A., Koffa, M.D., Tittmann, P., Gross, H., and Hoenger, A. (2007). HURP wraps microtubule ends with an additional tubulin sheet that has a novel conformation of tubulin. *Journal of Molecular Biology* **365**, 1587-1595.

Sato, M., Koonrugsa, N., Toda, T., Vardy, L., Tournier, S., and Millar, J. B. (2003). Deletion of Mia1/Alp7 activates Mad2-dependent spindle assembly checkpoint in fission yeast. *Nature Cell Biology, **5***, 764-766

Sato, M., Vardy, L., Angel Garcia, M., Koonrugsa, N., and Toda, T. (2004). Interdependency of fission yeast Alp14/TOG and coiled coil protein Alp7 in microtubule localization and bipolar spindle formation. *Molecular Biology of the Cell,* **15**, 1609-1622.

Sauer, G., Korner, R., Hanisch, A., Ries, A., Nigg, E.A., and Sillje, H.H. (2005). Proteome analysis of the human mitotic spindle. *Molecular and Cellular Proteomics* **4**, 35-43.

Sawin, K.E., and Mitchison, T.J. (1991). Poleward microtubule flux in mitotic spindles assembled in vitro. *The Journal of Cell Biology* **112**, 941-954.

Saxton, W.M., and Hollenbeck, P.J. (2012). The axonal transport of mitochondria. *Journal of Cell Science* **125**, 2095-2104.

Schek, H.T., III, Gardner, M.K., Cheng, J., Odde, D.J., and Hunt, A.J. (2007). Microtubule assembly dynamics at the nanoscale. *Current Biology* **17**, 1445-1455.

Schmidt, J., Arthanari, H., Boeszoermenyi, A., Dashkevich, N., Wilson-Kubalek, E., Monnier, N., Markus, M., Oberer, M., Milligan, R., Bathe, M., *et al*. (2012). The kinetochore-bound ska1 complex tracks depolymerizing microtubules and binds to curved protofilaments. *Developmental Cell* **23**, 968-980.

Schmidt, S., Schneider, L., Essmann, F., Cirstea, I.C., Kuck, F., Kletke, A., Jaenicke, R.U., Wiek, C., Hanenberg, H., Ahmadian, M.R., *et al*. (2010). The centrosomal protein TACC3 controls paclitaxel sensitivity by modulating a premature senescence program. *Oncogene* **29**, 6184-6192.

Schneider, L., Essmann, F., Kletke, A., Rio, P., Hanenberg, H., Schulze-Osthoff, K., Nuernberg, B., and Piekorz, R.P. (2008). TACC3 depletion sensitizes to paclitaxel-induced cell death and overrides p21(WAF)-mediated cell cycle arrest. *Oncogene* **27**, 116-125.

Schneider, L., Essmann, F., Kletke, A., Rio, P., Hanenberg, H., Wetzel, W., Schulze-Osthoff, K., Nurnberg, B., and Piekorz, R.P. (2007). The transforming acidic coiled

coil 3 protein is essential for spindle-dependent chromosome alignment and mitotic survival. *Journal of Biological Chemistry* **282**, 29273-29283.

Scholey, J.M., Brust-Mascher, I., and Mogilner, A. (2003). Cell division. *Nature* **422**, 746-752.

Sharp, D.J., Yu, K.R., Sisson, J.C., Sullivan, W., and Scholey, J.M. (1999). Antagonistic microtubule-sliding motors position mitotic centrosomes in drosophila early embryos. *Nature Cell Biology* **1**, 51-54.

Sherr, C.J., and Roberts, J.M. (1999). Cdk inhibitors: Positive and negative regulators of G(1)-phase progression. *Genes & Development* **13**, 1501-1512.

Shimamoto, Y., Maeda, Y.T., Ishiwata, S.i., Libchaber, A.J., and Kapoor, T.M. (2011). Insights into the micromechanical properties of the metaphase spindle. *Cell* **145**, 1062-1074.

Silk, A.D., Holland, A.J., and Cleveland, D.W. (2009). Requirements for NuMA in maintenance and establishment of mammalian spindle poles. *The Journal of Cell Biology* **184**, 677-690.

Sillje, H.H.W., Nagel, S., Korner, R., and Nigg, E.A. (2006). HURP is a Ran-importin beta-regulated protein that stabilizes kinetochore microtubules in the vicinity of chromosomes. *Current Biology* **16**, 731-742.

Silvius, J.R., Bhagatji, P., Leventis, R., and Terrone, D. (2006). K-ras4b and prenylated proteins lacking "second signals" associate dynamically with cellular membranes. *Molecular Biology of the Cell* **17**, 192-202.

Singh, D., Chan, J.M., Zoppoli, P., Niola, F., Sullivan, R., Castano, A., Liu, E.M., Reichel, J., Porrati, P., Pellegatta, S., *et al*. (2012). Transforming fusions of FGFR and TACC genes in human glioblastoma. *Science* **337**, 1231-1235.

Skoufias, D.A., Andreassen, P.R., Lacroix, F.B., Wilson, L., and Margolis, R.L. (2001). Mammalian Mad2 and Bub1/BubR1 recognize distinct spindle-attachment

and kinetochore-tension checkpoints. *Proceedings of the National Academy of Sciences of the United States of America* **98**, 4492-4497.

Song, L., and Rape, M. (2010). Regulated degradation of spindle assembly factors by the anaphase-promoting complex. *Molecular Cell* **38**, 369-382.

Spencer, D.M., Graef, I., Austin, D.J., Schreiber, S.L., and Crabtree, G.R. (1995). A general strategy for producing conditional alleles of src-like tyrosine kinases. *Proceedings of the National Academy of Sciences of the United States of America* **92**, 9805-9809.

Spencer, D.M., Wandless, T.J., Schreiber, S.L., and Crabtree, G.R. (1993). Controlling signal-transduction with synthetic ligands. *Science* **262**, 1019-1024.

Srayko, M., Quintin, S., Schwager, A., and Hyman, A. A. (2003). Caenorhabditis elegans TAC-1 and ZYG-9 form a complex that is essential for long astral and spindle microtubules. *Current Biology,* **13**, 1506-1511.

Stehbens, S., and Wittmann, T. (2012). Targeting and transport: How microtubules control focal adhesion dynamics. *The Journal of Cell Biology* **198**, 481-489.

Stern, B.M., and Murray, A.W. (2001). Lack of tension at kinetochores activates the spindle checkpoint in budding yeast. *Current Biology* **11**, 1462-1467.

Still, I.H., Vince, P., and Cowell, J.K. (1999). The third member of the transforming acidic coiled coil-containing gene family, TACC3, maps in 4p16, close to translocation breakpoints in multiple myeloma, and is upregulated in various cancer cell lines. *Genomics* **58**, 165-170.

Tanabe, T., Oyamada, M., Fujita, K., Dai, P., Tanaka, H., and Takamatsu, T. (2005). Multiphoton excitation-evoked chromophore-assisted laser inactivation using green fluorescent protein. *Nature Methods,* **2**, 503-505.

Tang, N. H., Takada, H., Hsu, K. S., and Toda, T. (2013). The internal loop of fission yeast Ndc80 binds Alp7/TACC-Alp14/TOG and ensures proper chromosome attachment. *Molecular Biology of the Cell,* **24,** 1122-1133.

Tilney, L.G., and Porter, K.R. (1967). Studies on microtubules in heliozoa .2. Effect of low temperature on these structures in formation and maintenance of axopodia. *The Journal of Cell Biology* **34**, 327-&.

Toso, A., Winter, J.R., Garrod, A.J., Amaro, A.C., Meraldi, P., and McAinsh, A.D. (2009). Kinetochore-generated pushing forces separate centrosomes during bipolar spindle assembly. *The Journal of Cell Biology* **184**, 365-372.

Tournebize, R., Popov, A., Kinoshita, K., Ashford, A.J., Rybina, S., Pozniakovsky, A., Mayer, T.U., Walczak, C.E., Karsenti, E., and Hyman, A.A. (2000). Control of microtubule dynamics by the antagonistic activities of XMAP215 and xkcm1 in *Xenopus* egg extracts. *Nature Cell Biology* **2**, 13-19.

Tousson, A., Zeng, C., Brinkley, B.R., and Valdivia, M.M. (1991). Centrophilin - a novel mitotic spindle protein involved in microtubule nucleation. *The Journal of Cell Biology* **112**, 427-440.

Uchida, K.S.K., Takagaki, K., Kumada, K., Hirayama, Y., Noda, T., and Hirota, T. (2009). Kinetochore stretching inactivates the spindle assembly checkpoint. *The Journal of Cell Biology* **184**, 383-390.

Uehara, R., and Goshima, G. (2010). Functional central spindle assembly requires de novo microtubule generation in the interchromosomal region during anaphase. *The Journal of Cell Biology* **191**, 259-267.

Uhlmann, F., Lottspeich, F., and Nasmyth, K. (1999). Sister-chromatid separation at anaphase onset is promoted by cleavage of the cohesin subunit SCC1. *Nature* **400**, 37-42.

Vogel, S.K., Raabe, I., Dereli, A., Maghelli, N., and Tolic-Norrelykke, I. (2007). Interphase microtubules determine the initial alignment of the mitotic spindle. *Current Biology* **17**, 438-444.

Walczak, C.E., Verma, S., and Mitchison, T.J. (1997). XCTK2: A kinesin-related protein that promotes mitotic spindle assembly in *Xenopus* laevis egg extracts. *The Journal of Cell Biology* **136**, 859-870.

Wang, W.Y., and Malcolm, B.A. (1999). Two-stage PCR protocol allowing introduction of multiple mutations, deletions and insertions using QuikChange (™) site-directed mutagenesis. *Biotechniques* **26**, 680-682.

Warner, F.D. (1976). Ciliary inter-microtubule bridges. *Journal of Cell Science* **20**, 101-114.

Warren, G. (1993). Membrane partitioning during cell-division. *Annual Review of Biochemistry* **62**, 323-348.

Waters, J.C., Chen, R.H., Murray, A.W., and Salmon, E.D. (1998). Localization of Mad2 to kinetochores depends on microtubule attachment, not tension. *The Journal of Cell Biology* **141**, 1181-1191.

Welburn, J.P.I., Vleugel, M., Liu, D., Yates, J.R., Lampson, M.A., Fukagawa, T., and Cheeseman, I.M. (2010). Aurora B phosphorylates spatially distinct targets to differentially regulate the kinetochore-microtubule interface. *Molecular Cell* **38**, 383-392.

Williams, S.V., Hurst, C.D., and Knowles, M.A. (2013). Oncogenic FGFR3 gene fusions in bladder cancer. *Human Molecular Genetics* **22**, 795-803.

Willox, A.K., and Royle, S.J. (2012). Stonin 2 is a major adaptor protein for clathrin-mediated synaptic vesicle retrieval. *Current Biology* **22**, 1435-1439.

Wilson, H.J. (1969). Arms and bridges on microtubules in the mitotic apparatus. *The Journal of Cell Biology* **40**, 854-859.

Witt, P.L., Ris, H., and Borisy, G.G. (1980). Origin of kinetochore microtubules in chinese-hamster ovary cells. *Chromosoma* **81**, 483-505.

Witt, P.L., Ris, H., and Borisy, G.G. (1981). Structure of kinetochore fibers: Microtubule continuity and inter-microtubule bridges. *Chromosoma* **83**, 523-540.

Wong, J., and Fang, G. (2006). HURP controls spindle dynamics to promote proper interkinetochore tension and efficient kinetochore capture. *The Journal of Cell Biology* **173**, 879-891.

Wu, H.Y., Windmiller, D.A., Wang, L., and Backer, J.M. (2003). YxxM motifs in the PDGF-beta receptor serve dual roles as phosphoinositide 3-kinase binding motifs and tyrosine-based endocytic sorting signals. *Journal of Biological Chemistry* **278**, 40425-40428.

Yao, R., Natsume, Y., Saiki, Y., Shioya, H., Takeuchi, K., Yamori, T., Toki, H., Aoki, I., Saga, T., and Noda, T. (2012). Disruption of TACC3 function leads to in vivo tumor regression. *Oncogene* **31**, 135-148.

Yu, C.T.R., Hsu, J.M., Lee, Y.C.G., Tsou, A.P., Chou, C.K., and Huang, C.Y.F. (2005). Phosphorylation and stabilization of HURP by Aurora-A: Implication of HURP as a transforming target of Aurora-A. *Molecular and Cellular Biology* **25**, 5789-5800.

Zheng, Y.X., Wong, M.L., Alberts, B., and Mitchison, T. (1995). Nucleation of microtubule assembly by a gamma-tubulin-containing ring complex. *Nature* **378**, 578-583.